



Nisar, Jawad Ahmad (2010) *Modelling the interfaces of bondable pultrusions*. PhD thesis.

<http://theses.gla.ac.uk/5794/>

Copyright and moral rights for this thesis are retained by the author

A copy can be downloaded for personal non-commercial research or study, without prior permission or charge

This thesis cannot be reproduced or quoted extensively from without first obtaining permission in writing from the Author

The content must not be changed in any way or sold commercially in any format or medium without the formal permission of the Author

When referring to this work, full bibliographic details including the author, title, awarding institution and date of the thesis must be given

MODELLING THE INTERFACES OF BONDABLE PULTRUSIONS

by

Jawad Ahmad Nisar



Submitted in fulfillment of the requirements for the Degree of
Doctor of Philosophy

Department of Mechanical Engineering
School of Engineering
University of Glasgow

© JA. Nisar
October 2010

All Rights Reserved.
This work may not be reproduced in whole or in part,
by photocopy or other means, without the permission

Author's Declaration

I declare that the work contained in this thesis is that of my own, except where mentioned and acknowledged. This work has not been previously submitted for any other degree or qualification in any university.

Jawad A Nisar
October, 2010

Abstract

The thesis introduces novel techniques to study the effects of moulding materials including different fabric architecture on the strength of pultruded adhesive joints and how to improve it. The overall objectives are (i) to devise laboratory techniques which mimic the pultrusion moulding process using glass fabric and vinyl ester resin and other moulding materials, (ii) to optimise the moulding materials and maximise the level of adhesion of the pultrusion and hence to improve the structural efficiency of the joints and (iii) to determine critical stresses and failure initiation through thickness of the composite laminate using multi-scale modeling.

A laboratory pseudo pultrusion technique was developed here, based on moulding of small laminates (meso-scale). A special moulding jig was designed and manufactured to represent pultrusion close mould conditions. The meso-scale laminates were then sandwiched between aluminum adaptors to form shear and tensile specimens, using purposely designed bonding jigs. The bonded specimens were tested under a monotonic tensile loading, at ambient laboratory conditions. The joint strength, were determined in relation to the fabric organisation for the outer layers.

Both surface and subsurface fracture of laminates were optically examined to determine loci of failure and level of void/micro defects and their impact on failure load. The transverse adhesive stresses/loading governs the initiation of failure near the edge of the joint and then propagates at the fibre-matrix interface, just below the coating layer, especially in the presence of voids. In the case of coated specimens the failure of rovings is deeper beneath the composite surface.

2-D macro, meso and micro-scale numerical models were constructed in ABAQUS. The meso-scale models took into account the multi-through thickness materials i.e. adhesive, coating resin, impregnated glass fabric and interlaminar matrix resin. The focus was on the composite top layer due to determine the peel/transverse stresses. Good agreements in the level of transverse and interlaminar stresses were found between the macro and meso-scale shear models. In addition, micro-scale models based on single filament/matrix interface were analysed to determine a more accurate stress at the interfaces including the effect of voids. Furthermore, a micro-scale model was used to explain the effect of combined

longitudinal/transverse loadings of filament on the level of transverse stress on the composite surface. The findings from these models help to explain the reason for the lack of correlation between the tensile and shear meso-scale models with reference to transverse stress.

This study demonstrated the worthiness of the “pseudo pultrusion” technique to study pultrusion and adhesion. Among various kinds of fabric architecture, the inlaid/random combination mat (IR) produced the best joint strength results and this ought to be considered by pultruders for top layers of fabric instead of more conventional fabrics. The study also showed that the Maximum stress theory provides a good failure prediction tool in relation to composite transverse stress at the composite surface. Micro-scale models are very important in determining the actual failure stresses and they also help to explain the mechanics of filament/resin failure under longitudinal and transverse loadings.

Acknowledgements

I would like to take this opportunity to acknowledge the people who made this research possible. I greatly appreciate their support, effort and love.

Firstly I would like to express my thanks to my supervisor, Dr Safa Hashim. Without his continued support, supervision and encouragement during the whole period, this research would not have been possible.

I give special thanks to the following for their support:-

- Overseas Research Scheme(ORS) and Faculty of Engineering Scholarship(Glasgow)~ finance
- Network of Intelligence on Marine Structures(MARSTRUCT)~materials
- Mr John Hartley, Technical Director, Exel Composites Ltd. UK~ materials
- Huntsman, DSM , MCP, Formax ~ Resin and fibres
- Dr Phil Dobson~ SEM facility
- Kaz Piechowiak, Ian Peden, John Davidson, Brian Robb, Alan Birbeck, , Denis Kearns~ Technicians
- Kenny Stevenson, Ewan Russell, Walter Robinson ~ Computing support
- Jane Livingstone, Elaine McNamara, Mari-Carmen Garcia-Perez, Marilyn Dunlop ~ Secretaries
- Pat Duncan(Advisor), Evelyn Love, John Taylor~ Faculty Office
- Avril MacGregor ~ International Student Advisor
- Mikko Finnila ~PhD colleague
- Isobel Smith~ Cleaning staff

My grateful thanks go to my mother, father, brothers and sisters for their affectionate support and love during this period of studies. Last but not least, I want to Special thanks to my dear friend and his family for their continual and encouraging support. I am truly privileged to have been associated with them. They are truly the people behind the scene. Once again I express my sincere thanks for whatever they have done for me, during my stay in UK.

Table of Contents

| | |
|---|-------------|
| AUTHOR'S DECLARATION..... | ii |
| ABSTRACT..... | iii |
| ACKNOWLEDGEMENTS..... | v |
| TABLE OF CONTENTS..... | vi |
| LIST OF FIGURES..... | x |
| LIST OF TABLES..... | xvi |
| NOMENCLATURE..... | xvii |
| ACRONYMS AND ABBREVIATION..... | xix |
| | |
| Chapter 1..... | 1 |
| INTRODUCTION..... | 1 |
| 1.1: Motivation..... | 1 |
| 1.2: Overview..... | 3 |
| 1.3: Research objectives..... | 6 |
| 1.4: Outline and methodology..... | 7 |
| 1.5: Research management..... | 9 |
| | |
| Chapter 2..... | 10 |
| LITERATURE REVIEW..... | 10 |
| 2.1: Introduction of pultrusion..... | 10 |
| 2.1.1: Process..... | 10 |
| 2.2: Material..... | 14 |
| 2.2.1: Matrix resin..... | 14 |
| 2.2.2: Reinforcement form..... | 15 |
| 2.2.2.1: Roving and mat..... | 16 |
| 2.2.3: Mould release agent..... | 19 |
| 2.2.4: Peel ply..... | 20 |
| 2.2.5: Filler..... | 20 |
| 2.3: Application of pultrusion and adhesive bonding..... | 21 |
| 2.4: Adhesive bonding..... | 26 |

| | |
|---|-----------|
| 2.4.1: Adhesion..... | 26 |
| 2.4.2: Surface preparation..... | 27 |
| 2.5: Joint analysis..... | 30 |
| 2.5.1: Analytical determination of stress distribution..... | 30 |
| 2.5.2: Numerical determination of stress distribution..... | 32 |
| 2.6: Failure in bonded composite joints..... | 35 |
| 2.7: Previous research on pultrusion bonding..... | 40 |
| Chapter 3..... | 45 |
| EXPERIMENTAL PROGRAMME (MATERIAL PROPERTIES)..... | 45 |
| 3.1: Introduction..... | 45 |
| 3.2: Composite..... | 46 |
| 3.2.2: Vinyl ester resin..... | 46 |
| 3.3: Composite properties..... | 47 |
| 3.3.1: Analytical procedure..... | 47 |
| 3.3.1.1: Fibre volume fraction in single E-glass roving laminate..... | 47 |
| 3.3.1.2: Fibre volume fraction in meso-scale laminate..... | 49 |
| 3.3.2: Experimental procedure..... | 53 |
| 3.3.2.1: Longitudinal properties of pultruded GFRP laminate..... | 53 |
| 3.3.2.2: Transverse properties of pultruded GFRP laminate..... | 56 |
| 3.4: Adhesive properties..... | 59 |
| 3.4.1: Adhesive selection..... | 59 |
| 3.4.2: Production and testing of adhesive specimens..... | 60 |
| 3.4.3: Extrapolation of data..... | 65 |
| 3.5: Coating resin properties..... | 66 |
| Chapter 4..... | 67 |
| EXPERIMENTAL PROGRAMME (MESO LAMINATE)..... | 67 |
| 4.1: Introduction..... | 67 |
| 4.2: Production of specimens and set-up..... | 67 |
| 4.2.1: Specification of various fabric organisations..... | 68 |
| 4.2.2: Laminate moulding..... | 69 |

| | |
|--|----------------|
| 4.2.2.1: Design and manufacturing of moulding jig..... | 69 |
| 4.2.2.2: Moulding with various fabric organisations..... | 71 |
| 4.2.3: Laminate coating..... | 75 |
| 4.2.4: Laminate adhesive bonding..... | 78 |
| 4.2.4.1: Design and manufacturing of bonding jig..... | 78 |
| 4.2.4.2: Bonding of laminate..... | 80 |
| 4.3: Experimental testing and results..... | 85 |
| 4.3.1: Experimental testing..... | 85 |
| 4.3.2: Experimental results..... | 89 |
| 4.4: Experimental failure mechanism..... | 93 |
| 4.4.1: Failure of shear specimens..... | 93 |
| 4.4.2: Failure of tensile specimens..... | 97 |
| 4.5: Microscopic investigation..... | 100 |
| 4.6: Macro-scale DLS joint..... | 103 |
| 4.6.1: Production of specimens..... | 103 |
| 4.6.2: Testing and failure examination..... | 105 |
| Chapter 5..... | 108 |
| FINITE ELEMENT ANALYSIS..... | 108 |
| 5.1: Introduction..... | 108 |
| 5.2: Introduction to finite element analysis..... | 108 |
| 5.3: Meso-scale FE model..... | 109 |
| 5.3.1: Shear models..... | 110 |
| 5.3.2: Tensile models..... | 112 |
| 5.3.3: Critical stress locations and failure..... | 116 |
| 5.3.4: Numerical results..... | 120 |
| 5.3.4.1: Shear models..... | 120 |
| 5.3.4.2: Tensile models | 125 |
| 5.4: Macro-scale model..... | 131 |
| 5.4.1: Critical stress location and failure..... | 133 |
| 5.4.2: Numerical results..... | 134 |
| 5.5: Micro-scale FE models..... | 135 |

| | |
|--|------------|
| 5.5.1: Single filament models..... | 136 |
| 5.5.2: Numerical results..... | 138 |
| Chapter 6..... | 141 |
| DISCUSSION..... | 141 |
| 6.1: Properties of materials..... | 141 |
| 6.2: Pseudo pultrusion..... | 142 |
| 6.3: Adhesive bonding..... | 147 |
| 6.4: Test results..... | 148 |
| 6.5: Modes of failures..... | 150 |
| 6.6: Failure criteria..... | 153 |
| 6.7: Meso-scale modelling..... | 154 |
| 6.7.1: Shear models..... | 155 |
| 6.7.2: Tensile models..... | 158 |
| 6.8: Correlation..... | 162 |
| 6.9: Micro-scale modelling..... | 165 |
| Chapter 7..... | 168 |
| CONCLUSIONS AND FUTURE RECCOMENDATIONS..... | 168 |
| 7.1: Conclusions..... | 168 |
| 7.2: Recommendations..... | 170 |
| LIST OF REFERENCES..... | 172 |
| PUBLICATIONS..... | 185 |
| CONTENT OF APPENDICES..... | A-1 |
| LIST OF FIGURES IN APPENDICES..... | A-3 |
| LIST OF TABLES IN APPENDICES..... | A-4 |

List of Figures

| | | |
|---------------------|---|----|
| Figure 1.1: | Concept bonded pultruded planks to replace aluminum decking..... | 2 |
| Figure 1.2: | Principle of multi-scale modelling..... | 3 |
| Figure 1.3: | Load distribution in different joints: a). riveted joint, b). adhesive joint..... | 5 |
| Figure 1.4: | Design concept of a large plank profile with a standard fabric arrangement..... | 6 |
| Figure 2.1: | The pultrusion process..... | 10 |
| Figure 2.2: | Curing process in the mould..... | 12 |
| Figure 2.3: | Side view of a die with heaters fitted..... | 12 |
| Figure 2.4: | Type of rovings: a). uni-directional, b). spun, c). mock..... | 16 |
| Figure 2.5: | Types of mats: a). Uni-directional mat, b). woven mat, c). inlaid mat, d). chopped strand mat (CSM), e). continuous fibre mat (CFM) | 18 |
| Figure 2.6: | A380 Fuselage..... | 21 |
| Figure 2.7: | FPSO vessel and pipelines..... | 22 |
| Figure 2.8: | Pultruded composite bridge..... | 24 |
| Figure 2.9: | Aberfeldy foot bridge in Scotland..... | 24 |
| Figure 2.10: | Train and tram pultruded body parts..... | 25 |
| Figure 2.11: | Strengthen and repair of concrete structures..... | 25 |
| Figure 2.12: | Mechanical Inter-locking..... | 26 |
| Figure 2.13: | Volkerson's shear stress distribution and deformation in a single lap joint..... | 30 |
| Figure 2.14: | Golland and Reissner peel stress distribution and deformation in a single lap joint..... | 31 |
| Figure 2.15: | Stages of delamination failure..... | 37 |
| Figure 3.1: | Microscopic observation of single filament..... | 46 |
| Figure 3.2: | Polished roving showing number of filaments presents..... | 48 |
| Figure 3.3: | Moulding jig showing: a). impregnation, b). clamping of impregnated rovings, c). GFRP pultruded laminate before and after trimming..... | 49 |

| | | |
|---------------------|---|----|
| Figure 3.4: | Composite material section..... | 54 |
| Figure 3.5: | Composite material pre- machining..... | 54 |
| Figure 3.6: | Dimensions of pultruded specimens..... | 54 |
| Figure 3.7: | Stress-strain distribution curve obtained from tensile test result of pultruded GFRP specimen..... | 55 |
| Figure 3.8: | Pultruded tensile test specimens: a). without rupture, b). rupture with static tensile load, c). severe delamination..... | 56 |
| Figure 3.9: | Pultruded transverse specimen: a). pultruded section, b). uniform pultruded laminate bonded between steel straps, c). diagram showing fibre direction Vs loading..... | 57 |
| Figure 3.10: | Transverse strength and failure load of plane pultruded GFRP..... | 57 |
| Figure 3.11: | Transverse pultruded specimen: a). $25 \times 25\text{mm}$ square composite, b). dog bone specimen, c). Failure specimen after test..... | 58 |
| Figure 3.12: | Transverse strength and failure load of dog bone pultruded GFRP..... | 59 |
| Figure 3.13: | Dimension of bulk adhesive tensile test specimen..... | 61 |
| Figure 3.14: | Production of bulk adhesive dog bone specimen..... | 62 |
| Figure 3.15: | Strain gauge mounted dog bone specimen: a). Longitudinal direction, b). transverse direction..... | 62 |
| Figure 3.16: | Araldite 2015 stress-extension curve from bulk dog-bone specimen..... | 63 |
| Figure 3.17: | Steel butt joint..... | 64 |
| Figure 3.18: | Stress strain curves from steel butt joint..... | 64 |
| Figure 3.19: | Stress-strain curves for Araldite 2015..... | 65 |
| Figure 4.1: | a). tensile and b). shear specimen and adaptor..... | 68 |
| Figure 4.2: | Fabric organisation in meso-scale laminates with epoxy coating..... | 69 |
| Figure 4.3: | Jig used to mould small laminates..... | 70 |
| Figure 4.4: | 3600/4800Tex – E-glass roving..... | 72 |
| Figure 4.5: | E-glass roving impregnation..... | 72 |

| | | |
|---------------------|--|----|
| Figure 4.6: | Aspects of laminate moulding: a). moulding jig, b). impregnated rovings in mould, c). 0/90 impregnated rovings in mould, d). roving clamped and compressed with upper mould..... | 73 |
| Figure 4.7: | Cured 0°/90° laminate: a). after moulding b). after trimming..... | 74 |
| Figure 4.8: | Microscopic image of laminate section showing fibre abrasion after cutting..... | 75 |
| Figure 4.9: | GFRP specimens: a). before and after resin coating, b). edge smoothing..... | 77 |
| Figure 4.10: | Load-displacement curve for shear specimen: a). before, b). after the application of epoxy coating..... | 77 |
| Figure 4.11: | Small laminate bonding jig: a). tensile specimens, b). shear specimens..... | 79 |
| Figure 4.12: | Bonding specimen: a). shear, b). tensile..... | 82 |
| Figure 4.13: | Curved bonded specimen in bonding jig: a). tensile specimens, b). shear specimens..... | 84 |
| Figure 4.14: | Bonded specimens showing 20x20mm laminate bonded between adherend jig: a). tensile specimen, b). shear specimen..... | 85 |
| Figure 4.15: | Meso-scale specimen during clamping into testing machine: a). tensile, b).shear specimen..... | 86 |
| Figure 4.16: | Failure load Vs extension curve of LL shear specimen..... | 88 |
| Figure 4.17: | Failure load Vs extension curve of LL tensile specimen..... | 88 |
| Figure 4.18: | Failure strength variation of meso tensile/shear bonded joint with respect to different fibre architecture..... | 92 |
| Figure 4.19: | Intralaminar fracture mode of LL specimen..... | 94 |
| Figure 4.20: | Intralaminar fracture mode of LT specimen..... | 94 |
| Figure 4.21: | Intralaminar fracture mode of RL specimen..... | 95 |
| Figure 4.22: | Interlaminar fracture mode of WR specimen..... | 96 |
| Figure 4.23: | Interlaminar fracture mode of IR specimen..... | 96 |
| Figure 4.24: | Intralaminar fracture mode of LL specimen..... | 97 |
| Figure 4.25: | Intralaminar fracture mode of LT specimen..... | 98 |
| Figure 4.26: | Intralaminar fracture mode of RL specimen..... | 98 |
| Figure 4.27: | Interlaminar fracture mode of WR specimen..... | 99 |

| | | |
|---------------------|---|-----|
| Figure 4.28: | Interlaminar fracture mode of IR specimen..... | 99 |
| Figure 4.29: | Microscopic images: a). before, b). after, the application of epoxy coating, c). air bubbles on coating surface..... | 100 |
| Figure 4.30: | Microscopic image of cross section through the thickness of LL laminate..... | 101 |
| Figure 4.31: | Closer microscopic image of cross section through the thickness of LL laminate..... | 101 |
| Figure 4.32: | Fracture mode within laminate..... | 102 |
| Figure 4.33: | Geometry of DLS hybrid joint..... | 103 |
| Figure 4.34: | Composite material section..... | 103 |
| Figure 4.35: | Composite material pre-machining..... | 103 |
| Figure 4.36: | Aspects of resin coating: a). preparation, b). resin application, c). cured adherend..... | 104 |
| Figure 4.37: | Failure load Vs extension curve of DLS joint..... | 105 |
| Figure 4.38: | Failure of DLS joint..... | 106 |
| Figure 4.39: | Microscopic image of cross sections through the thickness of manufacturer pultrusion..... | 107 |
| Figure 5.1: | Schematic showing the location of fabric arrangements in shear model with detail dimension and boundary conditions..... | 111 |
| Figure 5.2: | Typical FEA transverse stress contour for shear model..... | 112 |
| Figure 5.3: | Schematic showing the location of fabric arrangements in tensile model with detail dimension and boundary conditions..... | 114 |
| Figure 5.4: | Tensile model with quarter FE model showing layers sequences in laminate and symmetrical boundary conditions..... | 115 |
| Figure 5.5: | Typical FEA maximum transverse stress contour for tensile model..... | 116 |
| Figure 5.6: | Shear model: a). FEA meshed model, b). critical stress locations at different interfaces within the laminate..... | 119 |
| Figure 5.7: | Tensile model: a). FEA meshed model, b). critical stress locations at different interfaces within the laminate..... | 119 |
| Figure 5.8: | Load-extension curve of experimental and FEA results of meso-scale LL shear mode..... | 120 |

| | | |
|---------------------|--|-----|
| Figure 5.9: | Stress distributions in LL shear model..... | 121 |
| Figure 5.10: | Stress distributions in LT shear model..... | 122 |
| Figure 5.11: | Stress distributions in RL shear model..... | 122 |
| Figure 5.12: | Stress distributions in WR shear model..... | 123 |
| Figure 5.13: | Stress distributions in IR shear model..... | 123 |
| Figure 5.14: | Stress distributions in LL tensile model..... | 126 |
| Figure 5.15: | Stress distributions in LT tensile model..... | 127 |
| Figure 5.16: | Stress distributions in RL tensile model..... | 127 |
| Figure 5.17: | Stress distributions in WR tensile model..... | 128 |
| Figure 5.18: | Stress distributions in IR tensile model..... | 128 |
| Figure 5.19: | FEA model of DLS joint with all possible dimensions and symmetrical boundary conditions..... | 131 |
| Figure 5.20: | FE quarter meshed model of DLS joint..... | 133 |
| Figure 5.21: | Possible failure initiation location in pultruded DLS joint..... | 134 |
| Figure 5.22: | FEA results of DLS model: transverse (S22) and shear (S12) stresses at critical location..... | 134 |
| Figure 5.23: | Single filament/matrix model under constant transverse loading with symmetric boundary conditions on matrix..... | 137 |
| Figure 5.24: | Single filament/matrix model under constant transverse with varying longitudinal loading..... | 137 |
| Figure 5.25: | Single filament/matrix model: effect of voids size with different fibre diameter on transverse stress..... | 138 |
| Figure 5.26: | Single filament/matrix model: stress distribution in resin under combined tensile and shear loading..... | 140 |
| Figure 6.1: | Micrographs showing surface defects in GFRP laminates..... | 143 |
| Figure 6.2: | Micrographs showing defects in GFRP laminates: a). manufactured pultrusion, b). pseudo pultrusion..... | 144 |
| Figure 6.3: | Image showing air bubbles trapped in resin..... | 146 |
| Figure 6.4: | Image showing uneven fibre distribution..... | 146 |
| Figure 6.5: | Image showing the fibre damage with extra pulling force during moulding..... | 146 |

| | | |
|---------------------|--|-----|
| Figure 6.6: | Upper and lower adherend misalignment: a). shear, b). tensile specimen..... | 147 |
| Figure 6.7: | Weak adhesive interface with aluminum adherend due to oxide layer..... | 148 |
| Figure 6.8: | Uneven adhesive bondline..... | 150 |
| Figure 6.9: | Scanning electron micrographs (SEM) transverse failure in GFRP laminates at different magnification after final rupture..... | 152 |
| Figure 6.10: | FEA shear model: a). model geometry with LL laminate, b). contour plot in shear model showing critical location..... | 155 |
| Figure 6.11: | FEA results of stresses distributions through thickness of shear model..... | 156 |
| Figure 6.12: | FEA tensile model: a). model geometry with LL laminate, b). contour plot in shear model showing critical location..... | 159 |
| Figure 6.13: | FEA results of stresses distributions through thickness of tensile model..... | 159 |
| Figure 6.14: | FEA through thickness stress distribution at different offset 0.05mm and 0.6mm on: a). macro-scale DLS model, b). meso-scale LL model..... | 164 |
| Figure 6.15: | Fibre/matrix interface mechanism..... | 166 |

List of Tables

| | | |
|-------------------|--|-----|
| Table 2.1: | Resin comparison..... | 14 |
| Table 3.1: | Volume and weight fractions of GFRP laminae..... | 50 |
| Table 3.2: | Properties of single glass fibre and resin..... | 51 |
| Table 3.3: | Material properties of GFRP laminae..... | 53 |
| Table 3.4: | Plastic properties of Araldite 2015..... | 66 |
| Table 4.1: | Experimental results of shear specimen..... | 89 |
| Table 4.2: | Experimental results of tensile specimen..... | 89 |
| Table 4.3: | Summary of experimental results of DLS joint..... | 104 |
| Table 5.1: | Materials properties..... | 109 |
| Table 5.2: | Summary of failure loads and maximum stresses in various shear models..... | 124 |
| Table 5.3: | Summary of failure loads and maximum stresses in various tensile models..... | 129 |
| Table 5.4: | FEA results summary of failure loads and maximum stresses in DLS models..... | 135 |
| Table 6.1: | Correlation between macro and meso-scale model..... | 162 |
| Table 6.2: | Transverse Stresses in resin under combined tensile and shear loading..... | 166 |

Nomenclature

| Symbols | Description | Units |
|------------------|---|------------------------|
| E | Young's Modulus | GPa |
| G | Shear Modulus | GPa |
| ν | Poisson's ratio | -- |
| E_1 | Young's Modulus of composite along x-axis | GPa |
| E_2 | Young's Modulus of composite along y-axis | GPa |
| E_3 | Young's Modulus of composite along z-axis | GPa |
| G_{12} | Shear Modulus of composite in 1-2 plane | GPa |
| G_{13} | Shear Modulus of composite in 1-3 plane | GPa |
| G_{23} | Shear Modulus of composite in 2-3 plane | GPa |
| ν_{12} | Poisson's ratio in 1-2 plane | -- |
| ν_{13} | Poisson's ratio in 1-3 plane | -- |
| ν_{23} | Poisson's ratio in 2-3 plane | -- |
| E_c | Young's Modulus of composite | GPa |
| E_f | Young's Modulus of fibre | GPa |
| E_m | Young's Modulus of matrix | GPa |
| G_f | Shear Modulus of fibre | GPa |
| G_m | Shear Modulus of matrix | GPa |
| V_f | Volume fraction of fibre | % |
| V_m | Volume fraction of matrix | % |
| w_f | Weight fraction of fibre | % |
| w_m | Weight fraction of matrix | % |
| ρ_f | Density of fibre | g/cm^3 |
| ρ_m | Density of matrix | g/cm^3 |
| σ_{22} | Transverse stresses | MPa |
| τ_{12} | Shear stress in 1-2 plane | MPa |
| Y_t | Tensile strength in xy-plane | MPa |
| S_t | Shear strength in xy-plane | MPa |
| $\bar{\sigma}_m$ | Volume averaged matrix stress | MPa |

| | | |
|------------------|------------------------------|---------|
| $\bar{\sigma}_f$ | Volume averaged fibre stress | MPa |
| S11 | Tensile stress | MPa |
| S22 | Peel / transverse stress | MPa |
| S12 | Shear stress | MPa |
| X | Longitudinal strength | MPa |
| Y | Transverse strength | MPa |
| S | Shear strength in xy- plane | MPa |
| ϵ | Strain | -- |
| P | Standard force | N |
| u | Displacement | mm |
| θ_p | Principal direction | Degrees |

Acronyms and Abbreviation

| | |
|-------------------------|--|
| ASTM | American Society for Testing Materials |
| BS | British Standard |
| FRP | Fibre reinforced polymer |
| GFRP | Glass fibre reinforced polymer |
| FEA | Finite element analysis |
| DLS | Double lap shear |
| UTS | Ultimate tensile strength |
| Volume fraction | Fraction of fibres per unit of composite |
| rule of mixtures | An analytical technique which gives expressions for the modulus of the composite based on the constituent's mechanical properties |
| Isotropic | The material properties are independent of direction at every point in the body |
| Orthotropic | A material is said to be orthotropic if it has properties /strengths that are different in different orthogonal directions |
| Anisotropic | The properties of the material are different in all directions at a point in the body |
| Thixotropy | The property of some fluids to show a time dependent variation in viscosity; the longer the fluid undergoes shear stress, the lower is its viscosity |
| Adherend | A body that is held together by an adhesive |
| Analytical | Analysis or calculations of a certain topic to gain numerical solutions |
| Curing | To harden an adhesive so that it is at its optimum strength |
| Accelerator | A material that when mixed with a catalyst or resin, speed up the curing process |
| Hardener | A substance missed to a resin to promote curing |
| Cross-Head | The vertical movement of the specimens during tensile testing |
| Meso | A scale of size settled between the macro and mirco level |

| | |
|---------------------|--|
| Mould | The tooling in which the impregnated rovings is placed to give the correct shape to the part |
| Moulding | The process in which the part manufactured in a mould |
| Impregnation | The process of introducing the resin into filament bundles or fabric laid up in a mould |
| PTFE | Polytetrafluoroethylene |
| Roving | A large grouping of carbon fibre filaments packaged together onto a single spool |
| Strand | An untwisted bundle of fibres |
| Mat | A material held fibre together with a binder or by needling |
| CFM | Continuous filament mat |
| CSM | Chopped strand mat |
| Warp | Longitudinal directional fibres in woven fabric |
| Weft | Transverse directional fibres in woven fabric |
| Size | A treatment applied to yarns or fibres to protect their surface and facilitate handing |
| Tex | A unit of linear density equal to the mass in grams of 1000 meters of filament or yarn |
| Tow | A bundle of continuous filaments that are untwisted typically 600-9600 Tex may be either directly spooled or assembled bundles |
| Yarn | A bundle of filaments that have been twisted, generally used for processing into fabric |
| gsm | Grams per square meter |

Chapter 1

Introduction

1.1 Motivation

Glass fibre reinforced plastic (GFRP) has great potential to replace traditional materials used in structures today. The reasons for this include the high strength to weight ratio of FRP composites and excellent corrosion properties to name a few. These properties would provide for a much reduced weight and more efficient performance which are highly desired in several critical fields such as the marine, aerospace, automotive and civil industries. However, as stated, the use of this material requires better understanding into the crack initiation and propagation process for these materials.

This research investigates the possibility of using pultruded composite planks for the manufacture of advanced fast ships, ship decks, bridges and certain aerospace applications. Pultruded composites used in macro-scale structures for modern day applications offer many advantages over conventional materials. The main engineering challenge when designing structures made from composite materials is the joining process. Commercially available pultruded composite planks are generally only available in lengths up to 15m, which makes joining inevitable. However this depends on the suitability for these components to be adhesively bonded end-to-end, in a similar manner as for a double lap shear (DLS) joint, often referred to as butt connection. Figure 1.1 shows the concept of pultrusion application to ship decks. The adhesive butt joint in this case would be the most efficient way to join these planks side-to-side and end-to-end. The latter is more a critical connection which is more or less represents a DLS joint, as illustrated in the figure. Such a concept could be comparative to aluminium extrusions which are currently fabricated by welding in ship constructions. The layers arrangements in this section require optimisation to suit adhesive bonding (joining), in order to be competitive to aluminium extrusions and

their fabrication by welding.

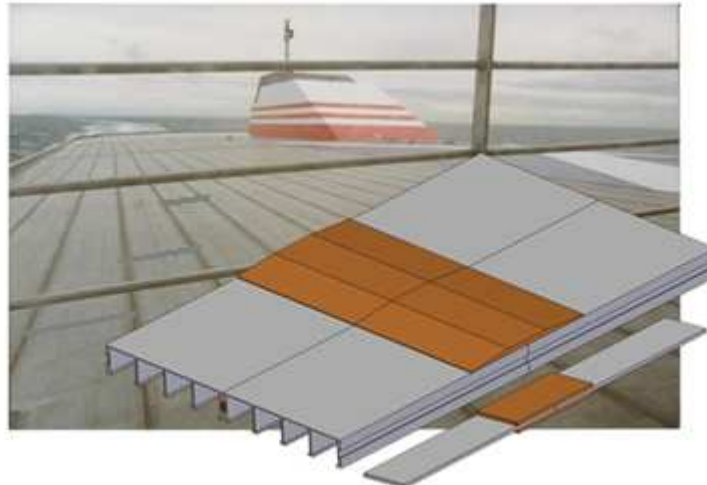


Figure 1.1: Concept bonded pultruded planks to replace aluminum decking [147]

The complex nature of delamination within these bonded joints results in there being a limited understanding of the cause of failure. Therefore, the motivation of this research has arisen from the need to develop meso-scale models which represent critical locations within DLS joints and cater for the variation in architecture of the through thickness materials. This is to enable a better understanding of the failure occurring in macro-scale models, which otherwise could not be examined on a macro-level due to modelling difficulties. When composite structures are assessed on the macro-scale, areas that are likely to raise stress concentrations can be observed, and therefore average failure data can be predicted. However when analysed on the meso-scale, the ability to predict how and why the material failed can be better understood. The schematics below in Figure 1.2 represent models of a DLS joint and its meso-scale equivalent that are to be analysed within this research. It may be assumed that a micro-scale falls into 10s of mm in terms of overlap length, where the meso-scale would be 10mm or less. The micro-scale is governed by the size of different which is about $16\mu\text{m}$.

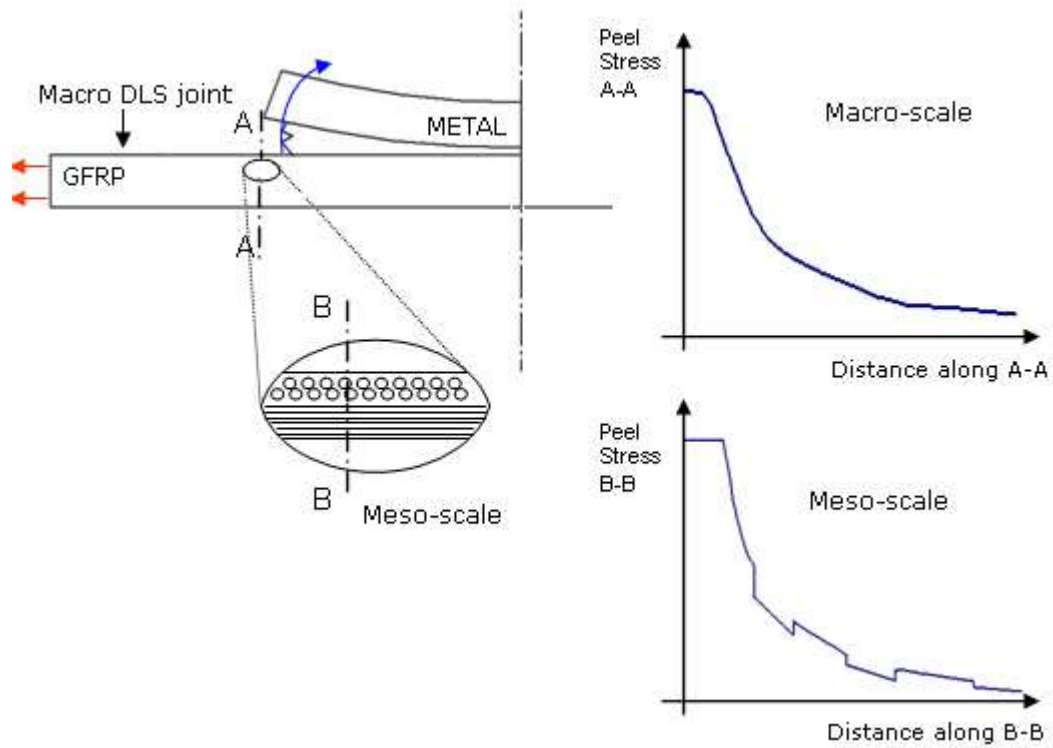


Figure 1.2: Principle of multi-scale modelling

Thus, as can be observed from the figure above, the through thickness stress in the meso-scale model is somewhat different to that found in the macro-scale model and hence failure can be better understood by the ability to examine the stress distribution within each meso layer.

1.2 Overview

The potential of GFRP, based on weak matrix systems such as vinyl ester resin for pultrusions in marine and similar structures, can be realised if the structural efficiency of the adhesive joint for these sections is increased. Efficient methods of joining composite structures are either adhesively bonding or mechanically fastening [1]. The tensile strength capacity of mechanical fastened joints is 50% of the adherend tensile strength. The low capacity is largely due to local stress concentration caused by fasteners. The introduction of holes in the composite leads to high stress concentrations and hence thicker and heavier walls. Such high stress concentrations from the edges of the hole can affect the strength of composite. Mechanical joining is limited by the bearing strength of their substrates. In a

case when one or both of the substrates are composites, resin failure at fastener holes and the difference in stiffness properties between the fastener and composite substrate create bearing stresses and affect the structural integrity at the joint. In addition bolted joints often require heavy straps or clamps which add to the weight of structure. Therefore joining techniques used for metals, such as bolting and riveting are not very suitable for joining composite material and adhesive bonding is the best way forward, enabling designers to take full advantages of their properties. However, this relatively new joining technique is not fully understood for advanced composites, especially pultrusions.

Adhesive joining is the process in which the composites must be joined together with adhesive through surface adherence (adhesion) and internal strength (cohesion). Adhesive bonding does not exhibit high stress concentrations, in the same way for bolted joints as illustrated in Figure 1.3. The quality of adhesive bonding to join dissimilar adherends with minimal stress concentrations has allowed the designers to use composite materials in conjunction with other conventional metals [2]. The tensile strength capacity of adhesively bonded joint has the potential to reach 70% of the adherend tensile strength [3]. This is very significant considering the high longitudinal tensile strength of the pultruded section. It is currently unreasonable to expect better than 40% structural efficiency for basic DLS joints based on commercial GFRP pultrusion. This has been improved to over 50% by introducing a low viscosity resin coating to the bonding surface prior to bonding plus using metallic outer adherends [4]. The low viscosity resin provides good micro-flow on the surface, resulting in a better wettability between the adhesive and the adherend.

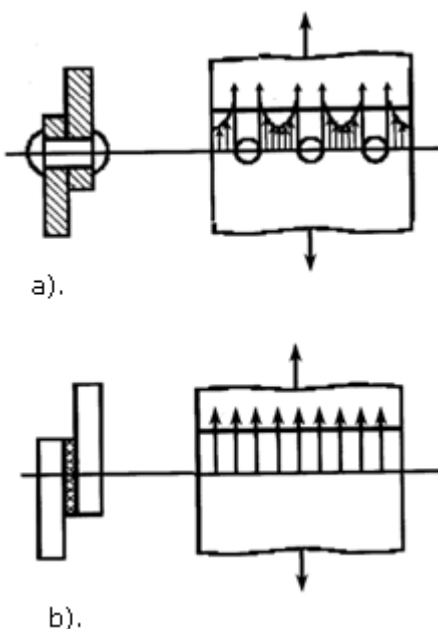


Figure 1.3: Load distribution in different joints:
a). riveted joint, b). adhesive joint [2]

Commercial pultrusion sections often contain uni-directional (UD) reinforcements (rovings) at the centre of the laminate, with the skins based on random/continuous filament mat (CFM). Pultrusions may be based entirely on UD rovings but this is limited to simple narrow sections/strips that are not suitable for structures where transverse loading is expected. Figure 1.4 shows typical fabric layers in connection with a concept plank profile. The bulk of the composite material is unidirectional continuous rovings, sandwiched between random mats and surface veils. The continuous strand mat improves cross fibre strength whereas the surface veil improves the surface finish. A possible replacement for the random skin mat in large and complex profiles such as this plank could be based either on combination mats which incorporate 0/90° inlaid or woven mats on the top of random mat. The latter is currently used by pultruders to enhance stiffness and strength better than the random mat. The architecture of fabric layers is important for adhesion and this is often neglected and dictated by the requirement to balance the stiffness and strength in longitudinal and transverse directions of the pultruded sections.

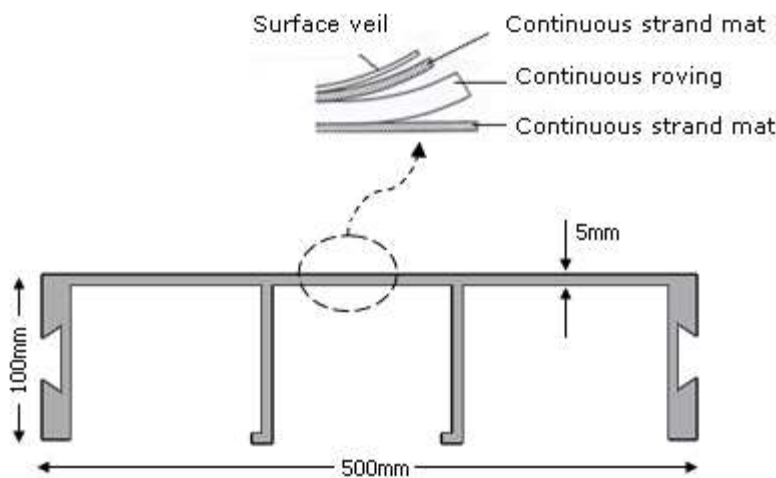


Figure 1.4: Design concept of a large plank profile with a standard fabric arrangement [8]

1.3 Research objectives

The potential of pultruded composite planks in stressed-skin structures for ships, aircrafts and similar constructions is good. This however, depends on the suitability of these long sections to be jointed end to end by adhesive bonding, in the same way as DLS joints. In this case the outer straps could be based on good adhesion materials such as steel or epoxy based composites which will confine the critical stress locations to the inner adherend/pultrusion.

This research is related to commercial pultrusion moulded from glass fibre and vinyl ester resin which represent the inner adherend. The weak resin compromises the through thickness strength of the pultrusion (inner adherend) and hence the joint strength. In order to improve on this, the architecture of the section layers and post processing requirements must be understood and tailored accordingly. Therefore the aim of this research is to develop meso-models representing critical locations within DLS joints, allowing variation in the fabric architecture of through thickness materials. This is to enable a better understanding of failure and behaviour of the materials employed in the pultrusion and its bonding process. Such an understanding may not be achieved on a macro-scale level alone due to moulding and modelling difficulties for the materials concerned.

Previous to this work, pseudo pultrusion 120mm x 120mm x 3mm laminates based on

glass fabric and vinyl ester resin were developed in the laboratory. These were then cut into standard adherend dimensions and bonded into DLS joints including long overlaps. To understand the joint failure and the architecture of the surface fabric layer, it was necessary to produce more laminates more effectively. Therefore an alternative moulding technique was developed here, based on small laminates (meso-scale). These laminates were developed for moulding and adhesive bonding and represent local shear and peel stresses that are expected in DLS joints at specific critical locations.

The research introduces novel techniques to study the effects of moulding materials including fabric architecture on the strength of pultruded joints and how to improve it.

The detailed objectives are:-

- to develop a laboratory technique which mimic the moulding (pseudo pultrusion), based on meso-scale laminates
- to mould the small laminates (10mmx10mmx1.2mm) and characterise their adhesion using shear and tensile adhesive specimens
- to compare and optimise glass fabric architecture for top pultrusion layer
- to compare the level of adhesion of pseudo pultrusion with an equivalent commercial material
- to develop multi-scale numerical models at micro, meso and macro-scale levels to determine critical stresses in bonded composite
- to identify suitable failure criteria of bonded pultruded composites which helps to predict adhesive joint strength.

1.4 Outline and methodology

In the next chapter (Chapter 2), an extensive literature review is presented. This is related to the essential background of joint analysis through numerical methods. The chapter describes the related research carried out on composite materials, adhesives, adhesion, major preparation parameters of adhesive bonding and their failures. The pultrusion process will be explained in detail with regards to all constitutive materials and their relevant literature and applications.

Chapter 3 explains the analytical and experimental procedures on various materials used in this research to obtain essential mechanical properties. rule of mixtures, Tsai and Hahn equations and transversely isotropic material assumptions and experimental testing are used. The composite material was tested in accordance with a BS method. The chapter also describes how the composite and adhesive test specimens were fabricated. Later, the details of experimental testing and their relevant results will follow. Microscopic observations were also performed to further complement this work.

Chapter 4 explains how the meso-scale laminates were moulded with various fabric organisations. It also gives details of the mechanical testing procedures, including tabulated results and graphical figures - based on experimental data which are then compared. Finally the microscopic observations and failure modes are presented. In addition, the bonding, testing and results of macro-scale DLS joints were added for comparison with meso-scale joints.

Chapter 5 deals with the multi-scale modelling of the pultruded joints at macro, meso and micro-scale levels. The main focus, however, is on modelling of the meso-scale bonded laminates taking into account their through thickness materials. This is in order to better understand failure within standard DLS joints, which was supported by limited analysis using both macro and micro-scale models. The macro-scale model is based on a standard DLS joint and the micro-scale model is based on a single filament-matrix resin interface under transverse loading. The micro-model also includes the effects of void/micro defects at the interface and loading mechanism on the filament. The chapter presents and compares all the FEA results.

Chapter 6 goes into the discussion of material properties, moulding, adhesive bonding, test results, numerical modeling and their failure modes. Failure criteria used in this research are also discussed in this chapter. This chapter explains the FEA results of both shear and tensile meso-scale model and the difference between their results. Good correlation is shown during the discussion on macro and meso-scale model comparison. The discussion on micro-scale model explained the reason for failure load difference between shear and tensile meso-scale models.

Finally Chapter 7 presents key conclusions and recommendations for future research.

1.5 Research management

It was crucial to employ a research management technique throughout the research, due to the limited time scale of the task. Not only did this provide a structured and logical path to solving the problem, but it also allowed for the duration of events to be closely monitored.

Each week, two meetings were held with my PhD supervisor which typically lasted for more than one hour. These discussions allowed for the supervisor to monitor the progress of the study and were also provided a good time to communicate any useful ideas or issues that had occurred within the week.

Furthermore a logbook was kept in order to write down any calculations, ideas, or specifications that were integral to the task. Maintaining a well structured logbook was important when compiling results or when referring to specific times of events.

Chapter 2

Literature Review

2.1 Introduction to pultrusion

2.1.1 Process

Traditionally, composite manufacturing methods used to be very labour intensive however breakthroughs in manufacturing development have resulted in automated processes that can produce large quantities of a finished product. One of the most efficient manufacturing techniques developed is that of the pultrusion process. The pultrusion process with all its stages is shown in Figure 2.1.

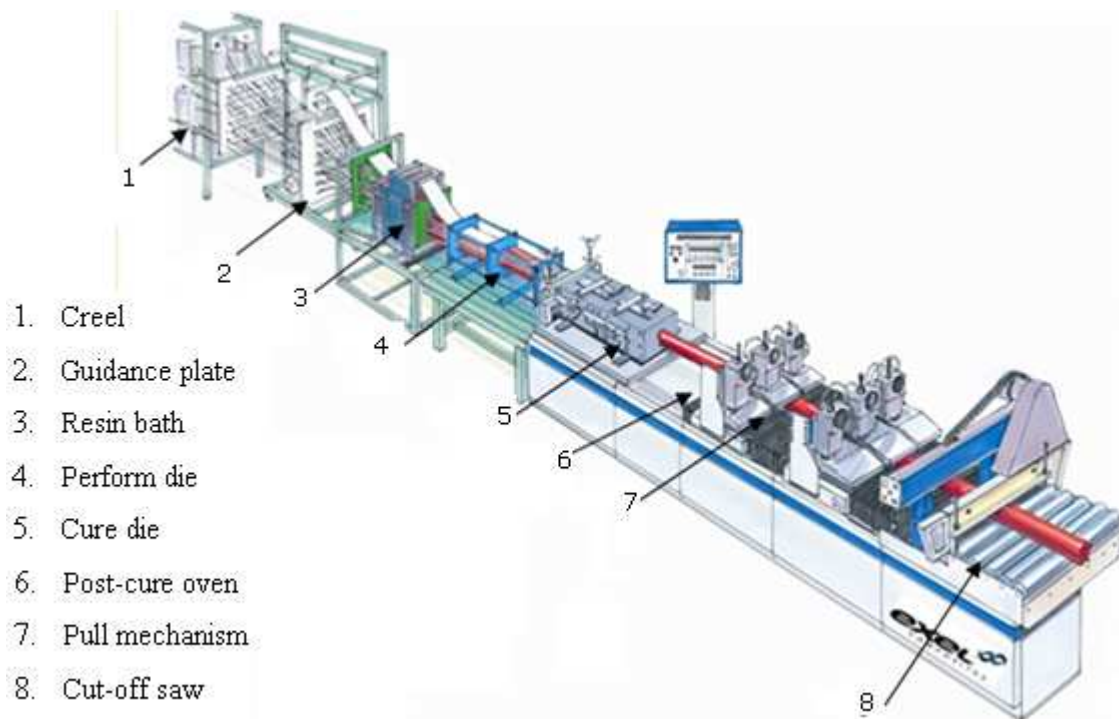


Figure 2.1: The pultrusion process [5]

With pultrusion the continuous rovings, which are wound around spools to conserve valuable floor space, are drawn through an alignment card after leaving the spools. This is to ensure that each roving is straight and separate from one another. After all the fibres have been aligned, they are passed with mat through a resin bath. In order to ensure effective wetting, the strands are passed through a series of rollers which cause the rovings to spread out [6].

This compression action ensures thorough wetting in between each individual fibre. The types of resin used commercially are the same as those types discussed earlier (section 2.2.1). However, property requirements of pultruded components restrict the types of resin available. For example, pultrusion resins must have low viscosity, a long enough ‘pot life’ in order to allow the continuous process to finish, and also a short curing time so that the component holds its final shape after exiting the die. The next stage which is when the fibres enter the die and it is arguably the most important stage in the process. This is because individual fibres coated in resin enter the die and exit as a cured pultruded component. Therefore, the die must undertake a series of important roles if the cured part is to be acceptable. For instance, it must maintain fibre alignment, resist any fibre twisting and compress the fibres into the desired volume fraction. Finally the part must be cured before it leaves the die in a relatively short time period. After exiting the die, the component is mechanically drawn out from the die. This then enables a radial saw, or aligned saw teeth to make a clean and precise cut at pre-set intervals along the pultruded component.

When the impregnated roving enters the mould feed, sections are transversely compressed inside the mould. The exothermic cross-linking reaction (curing) starts as soon as the peroxide (hardener) decomposition temperature is reached and it proceeds from the mould surfaces to the centre of the profile. The resin gels and cures cause high forces of friction along the mould wall and in the case of hollow profiles - along the mandrels too. The continuous roving strands, oriented in a longitudinal direction, absorb the required high take-off forces. Mould release agents are introduced into the matrix in order to reduce friction forces. Cooling sections in the feed zone of the mould are to keep temperatures down in the pultrusion direction so as to avoid premature matrix curing [7] as shown in

Figure 2.2.

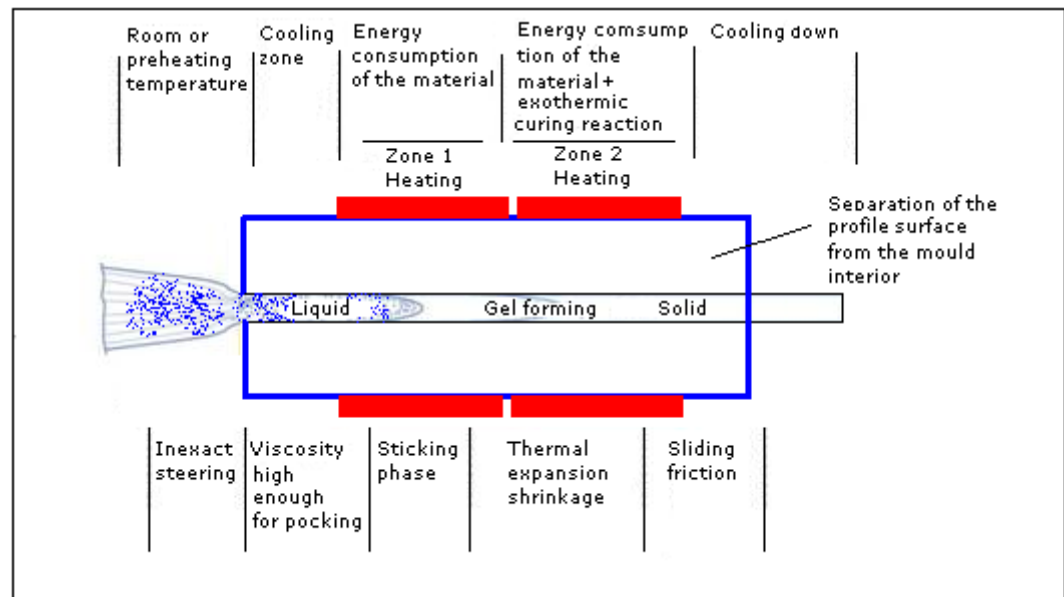


Figure 2.2: Curing process in the mould [7]

The moulds are electrically heated. Sensors, introduced into various different mould sections, afford precise information about the temperature curves in the individual zones [7] (see Figure 2.3).

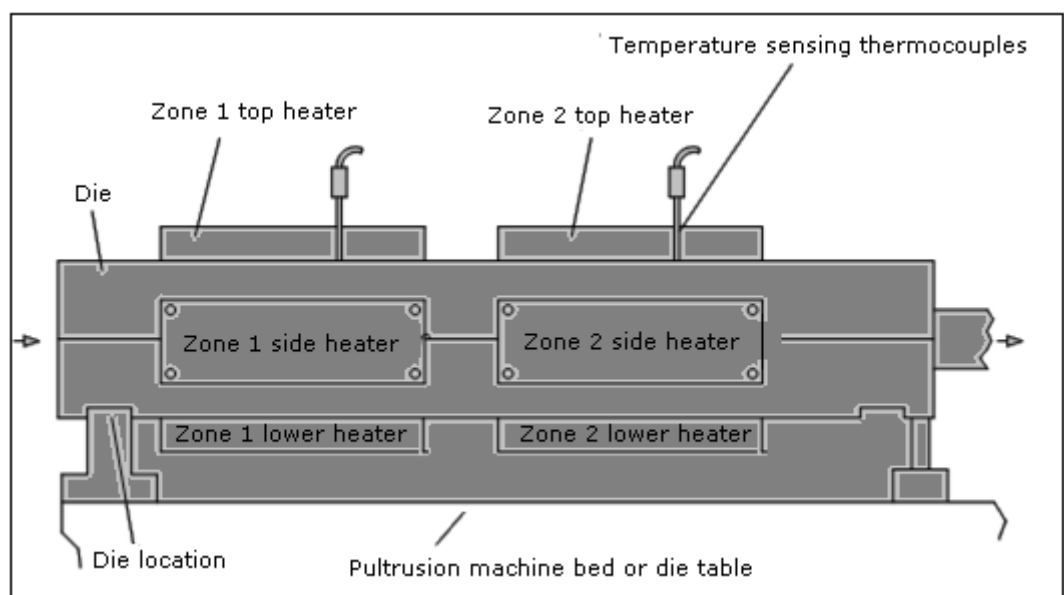


Figure 2.3: Side view of a die with heaters fitted [8]

If the reached temperatures are known, then the take-off speed (production rate) may be optimised between 0.02 and 3m/min. The continuous process is ensured using caterpillar take-off units (pull mechanism) or hydraulic clamps. These may be operated individually, jointly, or in parallel. Take-off forces of 6000kg and more can thus be attained. Process speeds may vary considerably depending on the wall thickness, the reinforcing structure and the complexity of the cross section values between 0.02 and 3m/min may be reached [7]. Although the process is cost effective for a high volume production of composite components, there are some associated disadvantages:

- the chosen resin has to be able to cure in a short period of time and this in itself presents a problem due to the fact that quick curing resin systems generally have lower mechanical properties. Furthermore the process is often run resin-rich to account for any fibre irregularity which again sacrifices strength [9]
- limitations to the length of a pultruded section are the maximum length that can fit in the composite manufacturing plant, and more importantly, the longest plank that can be transported economically. Generally, stocked pultruded composite sections are 6m in length
- a mould release agent is necessary during the production of the composite plank, as it is important that the resin does not stick in the heated die or in the oven. This mould release agent must be removed before adhesive bonding can take place as the adhesive can not adhere properly.

Nevertheless, the pultrusion process offers many advantages such as; a high production rate of up to 5m/min, the ability to recycle any waste, the capability of enforcing high volume fraction ratios which enhance quality and the process itself is generally straight forward. Hence, the process lends itself for manufacturing composite planks for bridges, ship decks and certain aeroplane sections. However, due to their anisotropic and fibrous nature, joining pultruded components end to end remains a challenge. The use of adhesive bonding between composite adherends offers a viable option.

2.2 Materials.

2.2.1 Matrix resin

The polymeric matrix (resin) bonds fibre reinforcement [10]. The constitutive relationship of the resin matrix has been shown to play an important role in the delamination resistance of composite materials by Qriunno et al. [11]. It also offers environmental protection for the fibres. Moreover, when the matrix has reached its cured state, it will also act as a deterrent to crack propagation by providing other routes for the crack to propagate, without the entire material failing. There are a variety of different resins available for different applications, as shown in Table 2.1.

| Material | Specific Gravity | Young's Modulus (GPa) | Poisson's Ratio | Tensile Strength (MPa) | Tensile Failure Strain (%) | Compressive Strength (MPa) | Heat Distortion Temp (°C) |
|-------------|------------------|-----------------------|-----------------|------------------------|----------------------------|----------------------------|---------------------------|
| Polyester | 1.21 | 3.6 | 0.36 | 60 | 2.5 | 130 | 95 |
| Vinyl ester | 1.12 | 3.4 | 0.36 | 83 | 5 | 120 | 110 |
| Epoxy | 1.20 | 3.0 | 0.37 | 85 | 5 | 130 | 110 |
| Phenolic | 1.15 | 3.0 | -- | 50 | 2 | -- | 120 |

Table 2.1: Resin comparison [28]

As shown in Table 2.1, epoxy resin has superior mechanical strength. It is, however, difficult to process and is the most expensive of the resins. Due to its low cost, polyester resin is the most frequently used resin. Vinyl ester resin is better than polyester resin as it allows faster processing speed. Composite materials manufactured from vinyl ester resin can be processed five times faster than composite materials manufactured from epoxy resin. Hence, vinyl ester resin is the obvious choice. The resin system used in this research is vinyl ester (Atlac) resin, which is quite similar to polyesters in that it is cured by radical initiated polymerisation. It is generally tougher than polyesters. It exhibits a range of exceptional properties including excellent chemical resistance, thermal stability, low viscosity, ease of handling and good mechanical strength. A drawback of the vinyl ester resin system is the relatively low fracture toughness that it exhibits. However the vinyl ester resin is derived from the reaction of an epoxy and acrylic or methacrylic acid. This would provide for the production of a range of properties that can be attained by using

different epoxy resins. Another disadvantage in the use of vinyl ester resin is the comparatively high cure shrinkage, which can reach up to 8%. Therefore during manufacturing of the composite, care was taken during cooling by allowing the composite to cure uniformly in the oven, thus reducing the potential of thermal shocks occurring which would damage the structural integrity [10].

Shrinkage of the matrix system upon curing can cause the creation of built in residual stresses, which may cause the early initiation of cracks in the matrix structure upon loading [12]. This factor was taken into account in this research by simply allowing the cured material to gradually decrease in temperature rather than subjecting the material to a sudden temperature change thus risking unacceptable shrinkage of the cured material, compromising mechanical properties.

2.2.2 Reinforcement forms

The main types of fibres used in pultrusions are glass and carbon fibres. The most common type is glass fibre and the most widely used grade of glass fibre is E-glass.

Glass fibres have extra features, which are mentioned below:

- high tensile strength
- low density
- low cost
- high production rates
- non-flammable
- resistant to heat
- good chemical resistance
- relatively insensitive to moisture, able to maintain strength properties over a wide range of conditions
- good electrical insulation [13].

Glass fibres are based on silica with additional oxides of calcium, boron, sodium, iron and aluminium. There are many different classifications of glass fibre, although for this research, the type of fibre used was E-Glass.

2.2.2.1 Roving and mats

As the fibres are very stiff in the longitudinal direction, they have a tendency to fail before the resin. This is especially when the resin has a high strains to failure limit. To help improve the transverse strength of the fibres, they are bundled together in rovings. Roving is properly defined as a number of yarns, strands, or tows which are collected into a parallel bundle with little or no twists [10]. The different roving configurations are available [14], which are illustrated in Figure 2.4.

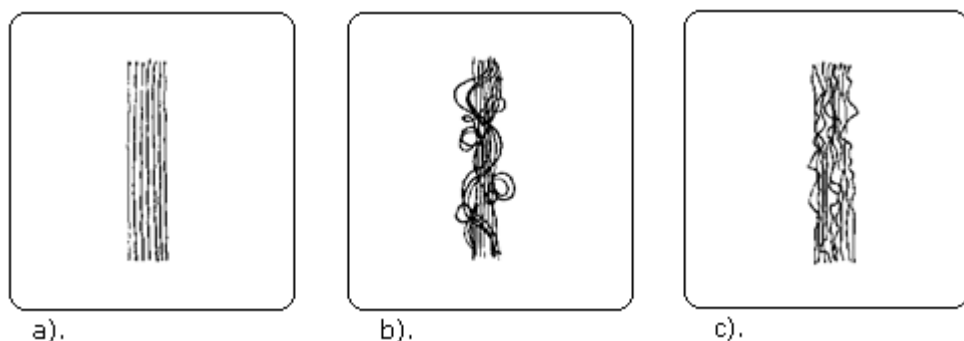


Figure 2.4: Type of rovings: a). uni-directional, b). spun, c). mock [14]

- *Uni-directional mat*

A uni-directional roving is usually combined together by a binder or by needling to make a uni-directional (mat). In uni-directional laminate all the fibres are aligned parallel to one other and only offer high strength in the longitudinal direction (see Figure 2.5a). It is simply the resin that provides mechanical strength in the transverse direction. This fibre orientation is not suitable for uni-axially loaded structures due to poor transverse and peel strength between the laminates. To improve the strength of the composite in the transverse direction, some other fabric/mat can be used as a combination. This gives the composite reduced, but equal strength in the longitudinal and transverse directions.

- *Woven mats*

A woven fabric (see Figure 2.5b) is most common and available in different standard configurations. It contains rovings in which the angle between the warp and weft yarns is 90°. A balanced weave is one in which the number and count of warp and weft yarns are equal. The warp is the longitudinal direction, and the weft is the transverse direction. One disadvantage of this type of roving is that it is very difficult to impregnate resin at the cross-overs, as is often the case; the rovings touch each other as shown in Figure 2.5b.

- *Inlaid mat*

Inlaid fabric contains warp fabric, which are balanced with weft fabric and held together by chain stitching with a fine thread (usually polyester as shown in Figure 2.5c). These are equivalent to a plain weave except that the tows are not crimped. Inlaid fabric is less common than woven fabric with few standard styles, but the abrasion in inlaid fabric is lower than in weaving [10].

- *Chopped strand mat (CSM) and CFM*

A reinforcement mat comprised of randomly dispersed chopped fibres (usually 25-50mm in length) held together with a resinous binder (see Figure 2.5d). CSM is produced in a variety of widths, lengths and weights [15]. CFM is similar to CSM except the fibre is continuous and swirled in a random manner [15] (see Figure 2.5e).

- *Combinational mats*

Combinational fabrics (mat) usually consist of a layer of chopped fibre mat added to any fabric e.g. longitudinal, woven, inlaid fabric by powder bonding, stitching or needling.

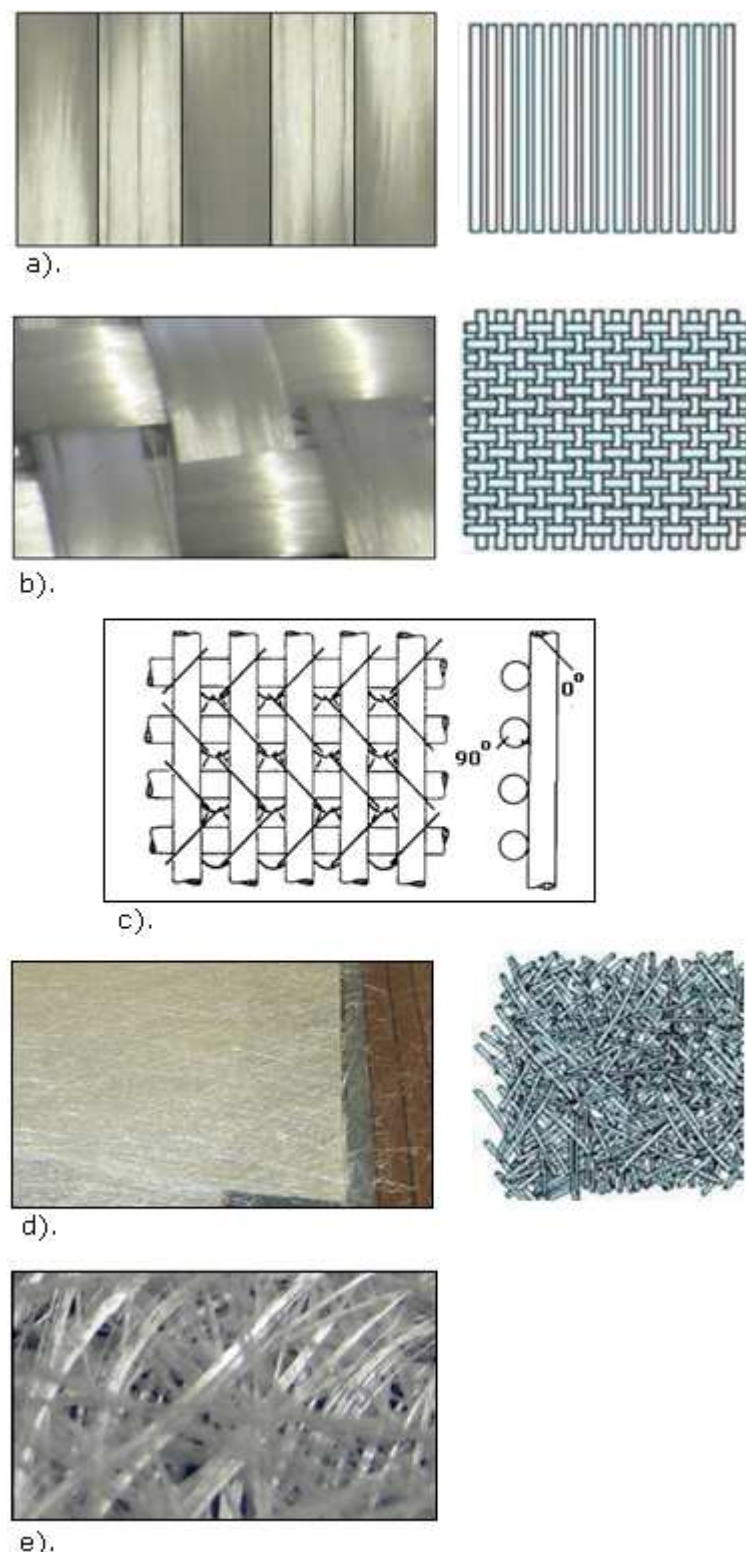


Figure 2.5: Types of mats: a). Uni-directional mat [7], b). woven mat [7], c). inlaid mat [10], d). chopped strand mat (CSM), e). continuous fibre mat (CFM) [7]

2.2.3 Mould release agent

A pultruded section will be cured about 90% at the exit of the die, which has a hard chrome plating to stop wear. A mould release agent has to be mixed with the resin, so that the cured section does not stick to the die. When the section is heated to initiate curing, the release agent migrates to the resin at the surface of the profile and if it is not removed prior to bonding, the efficiency of any adhesive joints can be significantly reduced [16]. The outer surface layer of resin can be removed by abrading. This operation may be achievable in a shipyard but naturally increases manufacturing costs. The abrasion of the pultruded surfaces prior to bonding has shown a modest increase in bond strength in some cases [17]. Concern was expressed however, that this could cause surface fabric damage which compromises bond strength. Abrasion of the surface to remove the release agent rich surface also produces a roughened surface finish, which in itself can improve the bond strength of the material.

A more innovative solution to the problem may be to produce mould release agent free pultrusions. It is known that if a section with a small die contact area is to be pultruded then a mould release agent does not have to be used. The aerospace industry specifies that small pultruded components must be made without a mould release to facilitate satisfactory adhesive joint efficiency. For a larger profile a modified process or use of different materials may make release agent free pultrusion possible:

- it may be possible to produce Teflon coated pultrusion dies [18]. Lack of die wear resistance may render this impractical as pultrusion dies are currently made with a hard chrome plated surface that has to be replaced after every few tens of kilometres of production
- microwave assisted pultrusion allows for a shorter die since cure is initiated prior to the section entering it [18]. It seems reasonable to assume that the pull force required will be reduced, which may also reduce the need for a mould release agent.

2.2.4 Surfacing veil and peel ply

Surface veil is based on fine fabric to form an overlay on profiles, for smooth surface finish and for environmental protection includes UV radiation attack. Peel ply is a very fine surface fabric which may be incorporated in the moulding process. The layer enables efficient adhesive bond of composites, by peeling from the surface prior to applying adhesive. The peel ply keeps all the glass edges down and smooth. When it is removed, there are no sharp points or rough edges left [19].

Cowling et al. [20] have reported a 20% increase in bond strength of polyester/E-glass composite joints that are made with a peel ply surface. The improvement was credited to a flat yet roughened surface finish. The surface finish was achieved without the broken fibres that can often result from alternative roughing techniques such as shot blasting or rotary grinding. Peel ply has the added advantage of ensuring a clean bond surface as it can be removed immediately prior to a joint being made. Interlaminar, rather than adhesive, strength has been shown to limit the joint strength of pultruded polyester adherends in double lap shear tests. It is therefore unclear if using peel ply, to alter the surface topology, would increase the achievable bond strength in this case.

2.2.5 Fillers

Chalk (Calcium based) or clay (Aluminium based) fillers are nearly always added to the matrix resin system for pultrusion processes. Fillers not only reduce costs but also aid die compaction, improve the aesthetics of the surface finish and conduct heat away from the composite once the exothermic cure reaction has been initiated. The addition of filler can change the efficiency of resin impregnation (by altering the resin viscosity) and can change the general processability of the resin [21].

The addition of filler has been shown to improve composite material properties. The tensile stiffness and strength of epoxy resin can increase with the addition of filler as can the short beam shear and 3 point fatigue properties of a composite made with filled resin [22]. Further work from Paciornik et al. [23] has concluded that the addition of filler in composite matrices improves the 3 point bend and short beam shear performance of undamaged material. However it was found that the resistance to damage propagation was

reduced with an increased filler concentration.

Boyd et al. [24] pointed that the filler is employed to reduce the cost of pultruded items by increasing the volume of the resin and reducing the expensive glass reinforcement. They pointed out that filler tends to have a detrimental effect on the mechanical properties of the joint. Binshan et al. [25] investigated a series of pultruded profiles made with vinyl ester/polyester as a resin and glass roving/CFM/woven roving as reinforcement. They concluded that the addition of filler reduced the level of void content in the pultruded composite.

2.3 Applications of pultrusion and adhesive bonding

Pultrusion gives full freedom to engineers to bring their concepts into practise. The use of pultrusion, to be able to make a wide variety of component parts effectively, has seen a steady increase in many industries such as the aerospace, civil, transportation, renewable energy and sports.

Airbus A380 adopts pultruded components in parts of the fuselage sections [26]. Figure 2.6 represents how the use of advanced pultrusion (ADP) is employed in the floor beams of the A380. However joining these pultruded sections end-to-end still remains a challenge in order to achieve satisfactory joint strength.

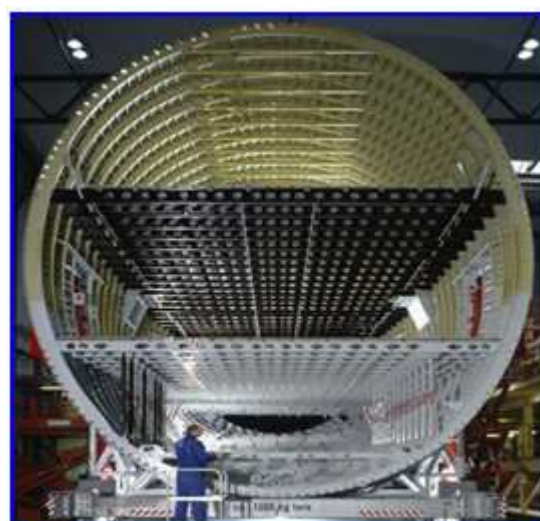


Figure 2.6: A380 Fuselage

This is due to the anisotropic and fibrous nature of the pultruded material, and hence the use of adhesives in such an industry has become increasingly important. In the infrastructures/civil/marine industry, the composite and adhesive bonding includes decks for both pedestrian and vehicle bridges across waterways, railways and roadways, marine plies and fenders, pier decking, railings, pipes and pontoons. Composite reinforcing bars may be used to replace steel in conventional reinforced concrete in order to prevent the internal corrosion of steel reinforcement [1].

The use of adhesive as a structural fastener is successful in marine industry. An exemplar application of where adhesively bonded joints can be used is in the repair of fissures/cracks on marine structures such as FSO (Floating Storage and Offloading) vessels and FPSO (Floating Production Storage and Offloading) vessels [27]. FPSO's receive crude oil through flexible pipelines which connect to the seabed (see Figure 2.7).

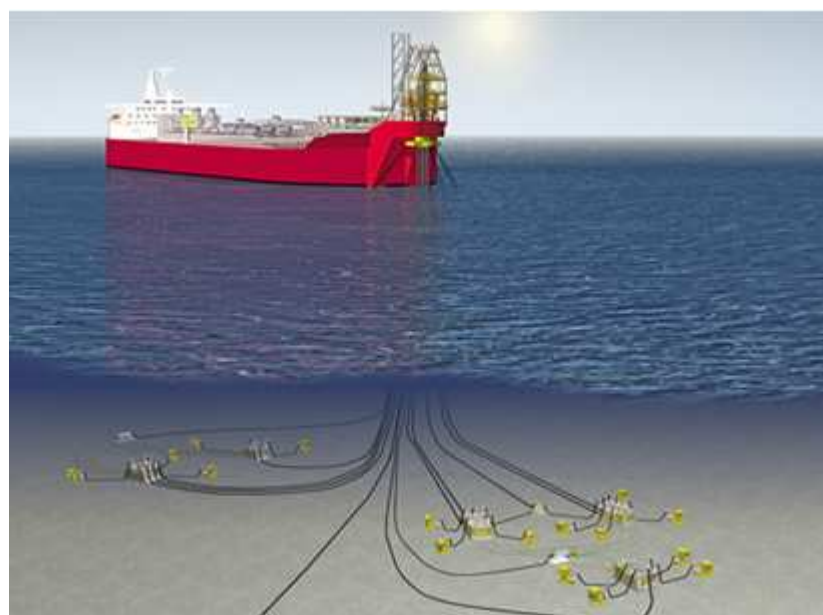


Figure 2.7: FPSO vessel and pipelines [27]

If a crack is discovered on an FPSO production may have to be partially or completely halted to allow the safe repair of the crack through the traditional method of welding. In the oil and gas industry it is obvious to see that this delay, even for a very short period of time, could cause a substantial financial loss to the company. By using an adhesively bonded patch, the repair is much easier and quicker to carry out. Also, a weld repair would

expose the materials being joined to very high temperatures; this could be very dangerous if the area being repaired was, for example, the hull of an oil tanker. Adhesive bonding therefore allows a safer method of repair in such applications. Also, if a composite material is used for the patch instead of steel then there are the added benefits of excellent corrosion resistance, higher strength, lower weight and greater flexibility within manufacture with regard to creating complex shapes and varying thicknesses. Shenoi et al. [28] discussed a practical design of joint, which is suitable for the repair of working structure. They suggest a single butt strap adhesive joint performed well in repair as compared to other lap shear joints with similar metallic adherends such as aluminum, steel, titanium or composite.

Structural pultruded sections have been used successfully in certain engineering applications. A number of composite bridge structures have been built in the U.S [29]. The vehicle bridges in the U.S utilise pultruded girders that span the length of the bridge and a modular Deck system; consisting of interlocking pultruded profiles bonded together with additional face sheets to form a sandwich construction. The weight reductions achieved with the use of composites allows for an increased ‘live’ weight and reduced construction costs. Reduced cost and corrosion resistance has led to increasing numbers of bridges utilising composite components in the U.S.

Figure 2.8 shows a typical example of a pultruded composite bridge. The bridge is 24.5m long and 5m wide and weighs only 12tonnes. This makes the bridge about 30 times lighter than a comparable concrete bridge. The Aberfeldy footbridge [30] was built over ten years ago in Scotland (see Figure 2.9).



Figure 2.8: Pultruded composite bridge [30]

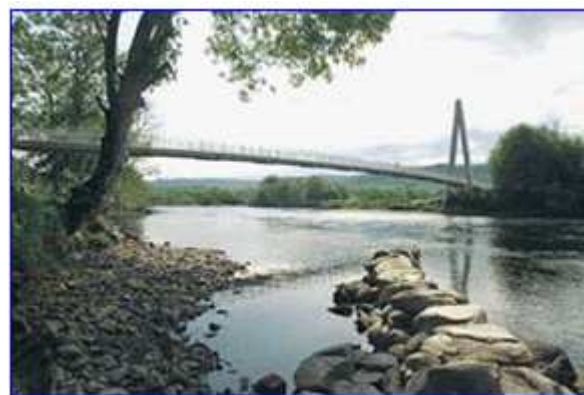


Figure 2.9: Aberfeldy foot bridge in Scotland [31]

In trains and trams large side panels combining constant quality and strength can be pultruded as shown in [30] Figure 2.10.



Figure 2.10: Train and tram pultruded body parts [30]

Carbon fibre laminates (plates) are successfully used to repair and strengthen masonry beams, columns, buildings and other structures. It can usually be embedded or bonded in place by hand without the need for heavy lifting equipment. Such repairs can be carried out much more rapidly than any traditional technique (see Figure 2.11).



Figure 2.11: Strengthen and repair of concrete structures [32]

2.4 Adhesive bonding

Adhesive bonding is desirable in many circumstances because it eliminates the stress concentration factors associated with mechanical means of joining. Introducing holes into a structure, in order to accept mechanical fasteners significantly, reduces the strength of the composite and therefore composite materials are prime candidates for adhesive bonding. In this section the adhesion and properties of adhesives such as wetting and surface preparation are all discussed.

2.4.1 Adhesion

The adhesion in which the adhesive interlock the parts by an interlocking action around the surface roughness of the parts [33] as shown in Figure 2.12.

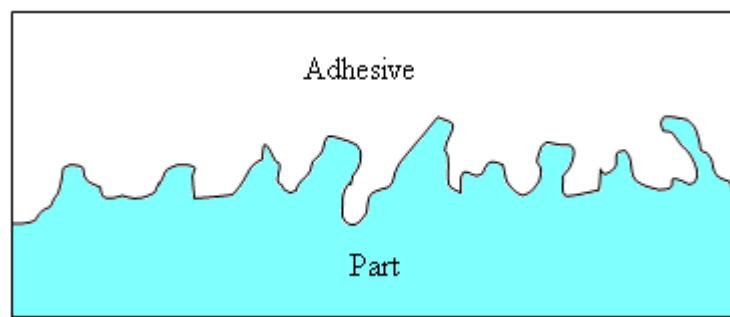


Figure 2.12: Mechanical Inter-locking [34]

The mechanism of adhesion is not fully understood and several theories have been proposed. The main mechanisms have been proposed by Kinloch [34] through absorption theory. This states that the parts are initially joined together by intermolecular contact. This intermolecular contact is achieved through molecular forces on the surface of adhesive and adherend. Kinloch [35] also found that mechanical interlocking and surface irregularities are the main source of adhesion. Bickerman [36] suggests that the mechanical interlocking between the bonded surfaces was sufficient to have strong interface. Voyutskii [37] proposed that the adhesive particles dispersion established the adhesion cross the interface. Deryaguins [38] suggests that the electrical charge layer at the interface formed adhesion. Staverman [39] pointed out that the adherend surface forces, due to chemical

composition at the interface, followed adhesion.

Perhaps the most important factor that can determine the adhesive's strength is the ability of the material to be wetted. Wetting can simply be described as the contact between a fluid and a surface when they are brought into contact. If a surface is said to have high surface energy, then a drop of liquid will be seen to spread over the surface, or wet the surface, effectively. On the other hand, if the surface energy is low then the droplet will remain as a droplet on the surface. Therefore in order to achieve effective wetting, there needs to be strong attractions between the adhesive molecules and the substrate surface [40].

Several authors [41,42] have noticed the wetting behaviour and proposed different hypotheses, which differentiate the wetting features between smooth and rough surfaces. The degree of wetting can be measured by contact angle in which the adhesive drop is plunged on the adherend surface with the assumption that the adhesive drop should not interact with the surface. The size of adhesive drop is in tens of micro litres, measured by a goniometer. Such measurements are based on direction i.e. receding and advancing contact angles. The contact angle hysteresis is obtained under receding and advancing contact angle conditions. Surface roughness and molecular changes in the adherend surface with the interaction of the adhesive are the possible reasons of contact angle hysteresis [41].

2.4.2 Surface preparation

Surface preparation plays an important role in a joint's strength and durability. For the development of a strong bond joint intermolecular contact at the interface is very important. Moreover, thorough surface preparation is also imperative if an acceptable joint strength is to be achieved. Any sort of contaminant can ingress into the adhesive and can have an adverse effect on the overall strength of the joint. However, no amount of preparation will ever completely free a surface of contamination, even if the material surface has been newly machined there may still be a surface film present due to metal oxides, carbon dioxide or water vapour [40]. For instance, in this study the tensile and shear specimens were manufactured from aluminium which forms a spontaneous oxide film on its surface, and although not visible to the naked eye, it may cause interfacial

bonding problems between the surface of the aluminium and the adhesive.

As stated previously the surface needs to be such that high wettability can occur by initiating high surface energies on the surface. This can not occur on smooth surfaces and so the surface of joints often needs to be prepared in order to maximize surface energy and ensure thorough wetting. Some of the methods often used are: mechanical abrasion, sandblasting, acidic etching and solvent degreasing, but some methods are restricted to composite material. All methods change the chemical composition of the surface as reported by Pocius [43]. Boone et al. [44] reported that whichever method is chosen all result in changes in surface tension, surface roughness and surface chemistry, which in turn affect the bond strength. It has been proven that roughening the surfaces prior to adhesion actually enhances the joint strength and the effect of this is that any loose contaminant particles are removed from the surface. This enhances mechanical interlocking with the adhesive [44]. Bakers [45] proposed improved joint strength when the argon ion etching technique is used for surface cleanliness after grit blast.

Wingfield [46] and Brockmann [47] pointed out that the joint bond strength is directly related to proper surface preparation of the parts to be joined. Surface preparation is important for more than one reason, all of which are mentioned below:

- surface roughness improvement
- to change the surface chemistry, this is more or less compatible with the adhesive
- to remove the weak oxide layer from the joint surface.

Sandblasting is unsuitable to prepare a composite surface prior to bonding. This is due to the fact that the extremely harsh abrasion caused by sandblasting would have actually damaged the fibres and therefore the reinforcing nature of the composite material. In the end, this would have reduced the mechanical properties of the composite.

Parkers [48] suggests that in composite adherends, the initial bond strength is directly related to the surface preparation to remove all surface contaminations. Guha et al. [49] conclude that acrylic and urethane adhesives give better strength with only a wipe of the surface. Also epoxy adhesives give good strength with abrasion or flaming the joining

surface.

Wingfield [46] suggests various surface preparation methods for composites, which are as follows:

- dry clean rag wipe: good to remove surface dust only
- solvent wipe: solvent wipe is better than dry cleaning, but still oil /grease exists on the surface after the solvent wipe
- abrasion with emery paper: ideal for GFRP composites
- grit blasting: good for epoxy resin composites
- flame, laser, plasma : good for low surface energy thermoplastic
- peel ply : peel ply is the woven fabric applied on bonding during manufacturing and is removed just before bonding to ensure a clear surface. But there is some conflict in the literature about a contamination free surface with peel ply as the peel ply leaves chemicals on the bonding surface.

The pultrusion process requires internal mould releases and it is essential that the surfaces are properly prepared prior to coating. The mould release agents create a film on the surface of the profile. It can be removed by using several different techniques [50]:

- solvent wiping is the simplest method of surface preparation. Several solvents will attack the mould release films. Some of these include xylene, acetone, or styrene
- abrasion with emery paper is ideal
- sanding will also adequately prepare the surface. However, if the surface is broken, minor imperfections can be exposed and these become quite visible when paint is applied. A sand and fill primer is applied to help this situation
- sand-blasting can be used as a surface preparation technique, but exhibits the same problems as sanding.

In the literature more work about surface preparation of aluminium is available than any other metal. In the case of an oxide layer being present on an aluminium surface, chemical

treatment is not recommended due to cost and surface complexity [51].

2.5 Joint Analysis

2.5.1 Analytical determination of stress distribution

The stress distribution in an adhesive joint is of primary importance for the engineer/designer to minimise stress concentration and assess safety factors. One of the most common adhesively bonded joint designs used in industry, as a quality control test, is the lap shear joint. Initial work on classical theories about the stresses occurring within a lap shear joint was carried out by Volkerson [52] and Golland & Reissner [54]. Their analysis was based on closed form solution of the stresses in single lap adhesive bonded joints. Volkerson's [52] equation took into account the shear induced deformation and combined them with the tensile expansion of the adherends. This results in a more accurate shear stress plot, which demonstrated stress peaks at the free edges of the adhesive with the low stresses between the edges as seen in Figure 2.13.

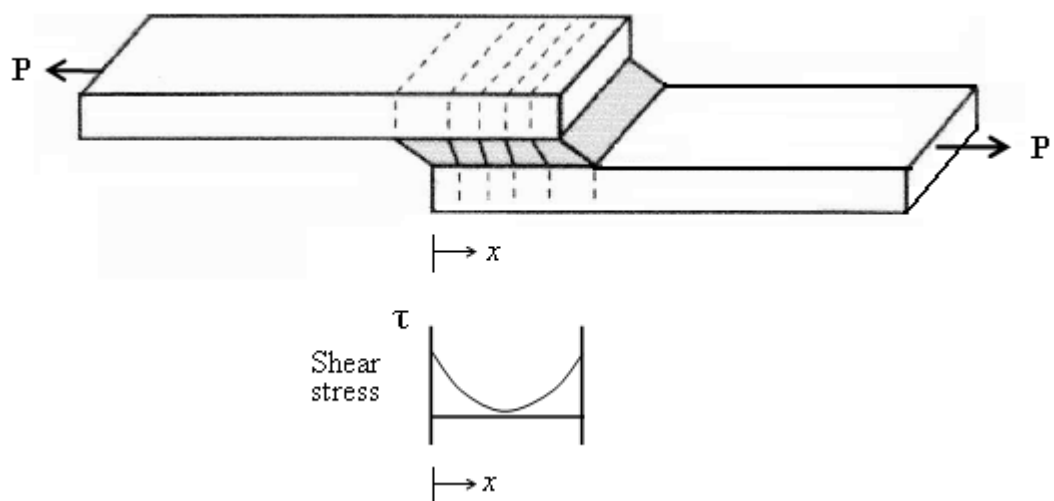


Figure 2.13: Volkerson's shear stress distribution and deformation in a single lap joint [53]

Goland and Reissner [54] extended Volkerson's work by considering the bending moment effect, associated with the bending of the adherend. Figure 2.14 shows that in addition to the peak shear stresses predicted by Volkerson, transverse stresses also peak at both edges of the bond-line. These end zone peak peels and shear stresses govern the strength of the

joint [55].

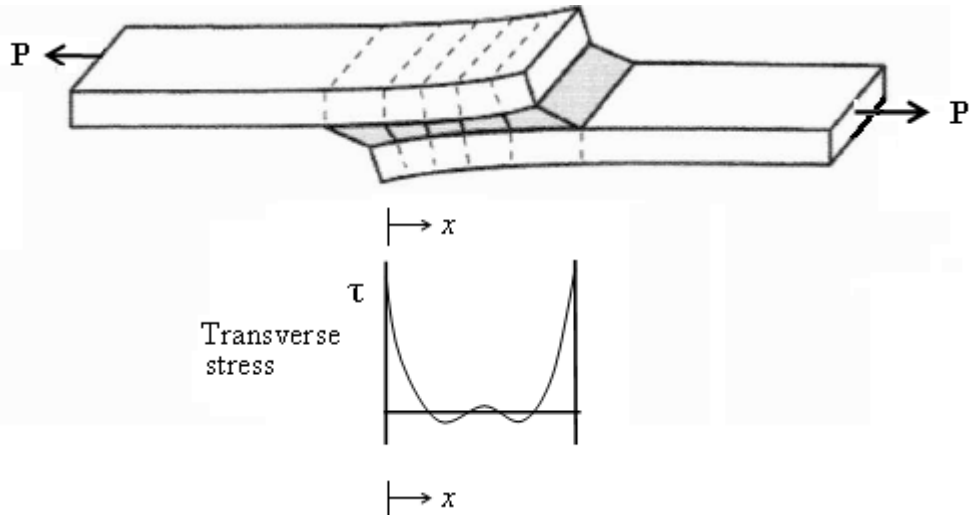


Figure 2.14: Golland and Reissner peel stress distribution and deformation in a single lap joint [53]

Hart-Smith [55] considered the analysis of single lap joints under the Primary Adhesively Bonded Structure Technology (PABST). He took the non-linear behaviour of the adhesives and adherends, including composites, into consideration. He pointed out that the plasticity in the adhesive lead to further improvement into joint strength. His analysis simultaneously determines the edge bending moment and the adhesive stresses while taking into account the effect of large deflection of free adherends, but ignored the effect of large deflection in the overlap. Other factors like failure modes and thermal effects were also considered.

Adam and Mallick [56], Allman [57] and Chen and Cheng [58] considered shear and transverse stress variation through the thickness of the adherend and adhesive, which were ignored by Golland and Reissner. Tsai et al. [59] worked on laminated composite as an adherend by considering the shear stresses varying through the thickness and proved that this method is more compatible with the experimental results than the classical method offered by Volkerson [52], Goland and Reissner, [54]. Renton and Vinson [60] included the variation of stresses in the adherend, but not in the adhesive layer. Adams and Mallicks [56] investigation is based on adhesive elasto-plastic behaviour in single and double lap joints under tensile loading, while subjected to thermal stress. They conclude that through thickness peel stresses are always dominant and the main cause of composite

failure near the interface. Bigwood and Crocombe [61] studied linear analysis and suggested an engineering formula for the design of bonded joints. Wang and Rose [62] worked on triaxial stresses in bonded joints through analytical solutions. Robert [63] presented a two stage analytical solution to measure the shear and transverse stress distribution in various types of adhesive bonded joints.

Analytical methods have their own limitations in pultruded laminated composites due to their complex nature, convoluted boundary conditions and the combined effect of various failure modes. Therefore finite element analysis (FEA) with a suitable failure criterion can be used for predicting the failure behaviour of pultruded composite structures.

2.5.2 Numerical determination of stress distribution

The use of finite element modelling is an extremely useful numerical analysis technique, especially when combined with an experimental programme. Significant studies encourage the use of FEA to observe the behaviour of an adhesive joint. The meshing of the FEA model is always debatable, because it is considered an important factor in two ways, i). for more accurate results, ii). to estimate the simulation time required to run the analysis. There are various techniques which can be used to reduce the simulation time. These include mesh refinement, submodelling, and symmetry boundary conditions. For lap shear joints, the high stress region exists near the end of the free edge and submodelling is normally introduced in such a region [64]. Submodelling is also known as a cut boundary displacement method. Wahab and Ashcroft [65] used submodelling in the centre of an adhesive bondline, which contained all the information about semi-circular crack. Symmetrical modelling in FEA only needs a portion of the full model. Other authors [66] used symmetrical model in the analysis of adhesive bonded joint. As a result of symmetry, the simulation domain reduced, at least, by a factor of two. The reduction in the simulation domain could introduce a finer mesh, resulting in more accurate results.

Tong et al. [67] pointed out that the stress concentration at the edge is mesh dependent in the absence of adhesive fillet. This mesh dependency also exists in non-linear analysis as pointed out by Sheppard et al. [68]. Hattori [69] and Groth [70] noticed that stress concentration is the main cause of failure in bonded joints. Katona and Batterman [71] analysed the adhesive bonded joints through adherend surface roughness. Pradhan [72]

analysed the adhesive bonded joint through finite element analysis. He used a strain energy method to understand the de-bonding in the cracked lap shear joint. Eight interface cracks were suggested at different locations to study their growth along the interface. In addition, different values of elastic modulus, thicknesses of adherend and adhesive, and overlap length were studied.

Liu et al. [73] analysed the single-lap adhesive joints with dissimilar adherends under external bending moments. They pointed out that good correlation was found between analytical and FEA at interface stress distribution. Few important points are concluded in FEA analysis about the strength of the joint and these are as follows:

- the effect of stress singularity is greater at the interface of low Young's modulus adherend
- the adherend length put nominal effect on the stress singularity at the interface
- the joint strength increases with the increase of Young's modulus and thickness of adhesive
- the adherend length put nominal effect on joint strength.

Liu et al. [74] studied the stress distribution in single lap riveted adhesive joint by FEA under the external bending moment. Good agreement is found between FEA and experimental results. Three joints, i). single lap riveted adhesive joints , ii). single lap riveted joints, iii). single lap adhesive joints are used in this study . The following conclusions are made:

- all the joints have comparable strength with thinner adherends
- single lap riveted adhesive joints have the highest joint strength
- single lap riveted joints have low strength with thick adherends.

Mitra et al. [75] presented numerically (FEA) the interfacial stresses and deformation of an adhesive bonded lap joint under tension. It was found that the transverse stresses are more dominant and are the cause of failure. They also suggest a few critical locations for failure initiation in the joint. Wooley et al. [76] presented FEA of single lap joints to examine the

adhesive modulus, overlap length and adhesive bond line thickness effect on the joint strength and found good correlation between FEA and analytical results. Delale et al. [77] proposed a closed form plane strain analysis of adhesively bonded joints. These joints consist of two different orthotropic adherends with constant thicknesses. They also assumed a very thin adhesive without considering the through thickness variation of stresses in the adhesive. They concluded a good correlation between FEA and analytical results. Crocombe and Adams [78,79] performed elasto-plastic investigation of the peel test. They found that the principal tensile stress in the peel test drives the crack towards the thin flexible adherend [80]

Sawa et al. [81] analysed a single lap joint with a dissimilar adherend under tensile load. They found the stress singularity occurs near the edge of interface but it increased with different factors like: i). low modulus adherend, ii). small thickness adherend, iii). small ratio of upper and lower adherend length, iv). very thin adhesive bondline , v). thick adhesive bond line. Good correlation is found between FEA and analytical results.

Representative volume element (RVE) is another alternative approach to virtual testing by a means of computational micromechanics [82,83]. This approach is well suited to measure the mechanical behaviour of composites. This explicitly takes into account the fibres, matrix and their interfaces.

Totry et al. [84] adopted the representative volume element (RVE) approach to compute the failure locus of a composite. The composite used in this study was based on 50% Vol of carbon fibre embedded in an epoxy matrix, which is subjected to transverse compression and out-of-plane shear loading. Through this constitutive model, they focused on the interfacial strength of composite and prediction of failure locus. They proposed this constitutive model presented several advantages over the standard experimental approach, which includes full control of the composite properties without any uncertainty and scatter. They conclude that the dominant failure was interface decohesion rather the matrix plastic deformation. The influence of the weak interfaces on strength was much more severe in shear than in compression. Haj-Ali et al. [85] proposed a 3D micromechanical constitutive models for pultruded fibre reinforced composites. They considered the two alternating layers of roving, continuous filament mat and their fibre/matrix constituents within the

cross section of the pultruded composite.

Fish et al. [86] presented multi-scale damage modelling for composite materials. On the basis of micromechanical scale, they introduced the representative volume element (RVE) to model the damage initiation and growth of microscopic damage and their effect of strength. The RVE is small enough to distinguish the microscopic heterogeneities, but sufficiently large to represent the overall behaviour of the homogeneous medium. González et al. [87] presented multi-scale modelling of fracture in fibre reinforced composites by three point bending of a notched beam. The multi-scale modelling was based on an embedded cell approach. The notched beam was based on two regions: one around the notch tip which contained all the details of composite micro structures separately, like matrix (resin), reinforcement and interfaces. While the other region was surrounding the first region, presenting the composite as an isotropic homogeneous material. This micro-level region around the notch tip controlled the damage by considering the matrix plastic deformation, brittle fibre fracture, voids at fibre/matrix interface and fibre/matrix frictional sliding. These parameters were taken into account in the simulations to assess their influence on the stress-strain curve, failure strength, ductility and the corresponding failure modes. They proposed that this model is ideal for performing parametrical studies of the influence of the constitutive properties on the overall composite properties, which is also impossible to carry out experimentally.

2.6 Failure in bonded composite joints.

It is particularly difficult to identify bonded composite joint failure modes, but the American Standard [168] details a method for their identification and classification. Seven classes of failure are mentioned below:

- adhesive failure: failure occurs to be at the adhesive adherend interface
- cohesive failure: failure occurs within the adhesive
- thin layer cohesive failure: failure occurs very close to the adhesive adherend interface
- fibre tear failure: failure occurs within the fibre reinforced plastic (FRP) matrix

- light fibre tear failure: failure occurs within the adherend near the surface, visible on the adhesive with few or no glass fibres
- stock break failure: failure occurs when the separation is within the adherend but outside the bonded region
- mixed mode failure: failure is the mixture of all failures.

Failure in composite adherends is complex and will be dependent on a variety of factors. With the use of metallic adherends, the situation will be very different due to the isotropic properties of the material. However, due to the anisotropic nature of the material properties of composite materials, the in-plane and through thickness strengths of the material will be different. Delamination failure is generally accepted as the most common mode when failure occurs in the adherend. Experimental tests and theoretical analyses have been carried out for a wide range of composite laminated structures, including glass reinforced polyester, glass reinforced epoxy, carbon reinforced epoxy, etc. These are well documented [23]. The remaining dominant characteristic of adhesive-bonded joints is the peel stress developed in association with the shear stresses. Like the shear stresses, these peak at the ends of the joint. While this phenomenon has long been known for single-lap joints, it is only recently that its impact on inducing laminate failures, in thick double-lap joints, was recognised. The low interlaminar tension strength of composite laminates limits the thickness of the adherends which can be bonded together efficiently by lap joints. The interlaminar splits apart locally due to peel stresses, thereby destroying the shear transfer capacity between the inner and outer plies. This overloads the outer filaments, which break in tension, and the failure progresses as portrayed [88] in Figure 2.15.

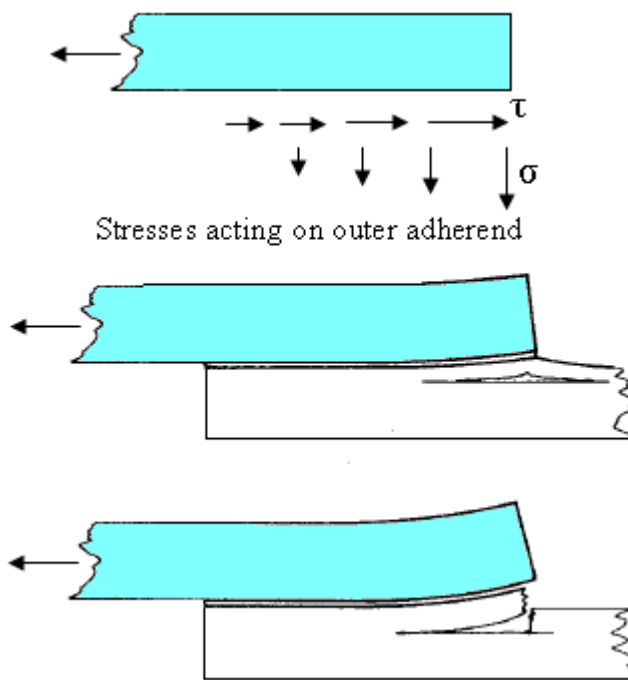


Figure 2.15: Stages of delamination failure [88]

Understanding of failure mechanisms and behaviour in composite bonded joints is important for accurate and reliable failure prediction. Failure prediction requires complete understanding of failure initiation, growth and modes. Analytical methods have their own limitations in pultruded laminated composites due to their complex nature, convoluted boundary conditions and the combined effect of various failure modes. Therefore finite element analysis (FEA) with a suitable failure criterion can be used for predicting the failure initiation of pultruded composite structures. Different failure criteria have been reported for joints are active in literature, e.g. Maximum Stress or Strain criteria, Tsai-Hill, Tsai-Wu and the Hashin failure criteria etc (see Appendix D).

Composite bonded strength depends on many parameters and their influence on the failure prediction and strength was experimentally studied by many researchers [89-94]. Parameters like surface treatments, adhesive fillets, bondline thickness and their variation, surface ply angles, stacking sequences and environmental conditions were considered in these studies. Failure prediction in composite bonded joints was considered by many researchers in previous studies and the majority were based on the failure mode observed during experimental testing [92-97]. This testing points out that the failure prediction

method has two types: (i). stress/strain approach, (ii). fracture mechanics approach. The stress/strain approach uses failure criterion equations, which consider critical stresses and strains in a bonded joint. This approach for failure prediction is quite acceptable as compared to the fracture mechanics approach in bonded joints as this approach is based on initial crack assumption and it's growth depends on a strain energy release rate computed by experiments. Furthermore the fracture mechanics approach is not appropriate for bonded joints as adhesive bonded joints always fail without initial cracking [98].

Many researchers worked on failure prediction and strength improvement of the composite bonded joint in the past but ignored the plastic behaviour of the adhesive material. Adhesive plastic behaviour is quite important because this influences, the stress and strain distribution within the adhesive layer as well as in the composite adherend adjacent to the stress concentration region [99]. Tong L [100] reported that failure often takes place at the fibre/matrix interface, adjacent to the adhesive during the strength measurement of adhesive bonded double lap joints. There is a lack of understanding in failure prediction and strength of adhesively bonded pultruded joints in relation to fabric architecture, at meso level. Keller et al. [101] reported that joint failure was initiated by the combination of through thickness peel and shear stresses in the adhesive fillet and in the outer combinational mat layers of the adherend below the joint edges. In this research the pultruded GFRP profiles are based on uni-directional rovings to the centre and combinational mats towards the outer surface. The combinational mats are based on CSM (chopped strand mat) and woven roving. They concluded that ultimate failure always occurred by delamination in the mat region. They used a new shear-tensile interaction (STI) testing device for combined shear-tensile loadings and introduced the shear-tensile interaction failure criterion for measuring the interlaminar stresses.

Adams et al. [102] pointed out that the cracks propagated easily through the thickness direction between the mat layers, where there is little reinforcement. Final failure occurs when the surface layer delaminates from the adherend in the overlap region through a combined peel and shear stress including the transverse shear in the composite.

Carlos et al. [103] presented all relevant failure criteria for FRP laminates in their studies. Adams and his co-authors [104-106] performed failure analysis of adhesively bonded

joints. Their analysis took into consideration both geometric and material non-linearity in a plane strain condition. They used a maximum principal stress or maximum principal strain failure criterion for the prediction of failure in bonded joints. Other authors [107-110] also used Adam and his co-author's FEA strategy for the prediction of failure in the adhesive. Dvorak et al. [111] assumed that the crack initiates at a localised region due to fibre debonding and matrix cracking. Then this might propagate along the fibre or perpendicular to the fibre axis. They found that the strength is significantly improved by reducing the ply thickness. They also found that the strength of thick plies is initially constant, but it starts decreasing with pre-existing void/damage.

Sheppard et al. [68] used a localised plastic damage zone approach rather than focusing on a singular point at the ends of the joints to predict failure in a DLS composite specimen and reported a reasonable prediction within a 20% error margin. This would be more reliable than the simplistic approach of considering the maximum stresses at a prescribed distance away from the point of singularity. They observe from the literature [112, 113] that the adhesive bonded joints do not inherently have a macroscopic crack and failure could initiate from the material damaged zone. On the basis of these observations, they suggest that fracture mechanics and material based models, which use stress/strain at a singular point, are not valid for the prediction of joint strength. This damage zone approach, introduced by Sheppard et.al is an extension of the singular point approach for composite failure given by Whitney et al. [114]. Other authors [115,116] used the same approach for failure prediction in an out of plane composite adherend.

Clark et al. [117] used the same approach on adhesive failure and suggested the possibility of joint failure when the principal stress over the damage zone exceed the ultimate tensile strength of the adhesive. Similarly John et al. [118] suggest that failure occurs in a bonded joint, when the stresses in adhesive, at specific critical locations, exceeds the shear yield stress.

2.7 Previous research on pultrusion bonding

Boyd et al. [23] pointed that pultruded items have higher probability of interlaminar failure than conventional composite items. They experimentally tested two pultruded planks :

- Plank 1: where the outer surface layer is CFM (Continuous Filament Mat), while the rest of the thickness is made up with the uni-directional fibres.
- Plank 2: where the outer surface layer is needle mat containing woven roving, while the rest of the through thickness arrangements are the same as plank 1.

They pointed out that plank 1 has higher ultimate strength than the plank 2. Perhaps a reason for this is the woven roving providing extra strength with uni-directional fibres near the surface of the needle mat panel. They also concluded that although plank 2 has needle mat providing extra strength, the Plank 1 with CFM gives a stronger joint. Plank 1 was delaminated between the uni-directional fibres, whilst Plank 2's delamination occurred between the woven roving and chopped strand mat surface. Finally they concluded that the needle mat does not increase the butt joint strength of composite materials.

Keller et al. [119] proposed that the joint efficiency could be significantly improved by strengthening the mat with fibres in the through thickness direction. They used a pultruded rectangular section based on uni-directional rovings to the centre and a combinational mat towards the outer surface. The combinational mat was based on CSM (Continuous filament mat) and woven roving. The ultimate failure by delamination observed in their research of approximately 0.5mm offset from the adherend surface. They proposed that such delamination could be significantly improved by reinforcing the mat region with fibre in the through thickness direction. They also concluded the adhesive thickness up to 3mm had small affect on stress distribution.

Zhang et al. [120] tested adhesively bonded joints composed of pultruded GFRP laminates. The layers configuration in such pultruded laminate was based on combinational mat layer consisted on CSM (Continuous filament mat) and woven roving as a surface layer and uni-directional rovings used towards the centre of laminate. They reported the ultimate failure occurred in the outer mat layers of the GFRP pultruded laminate.

Lee et al. [121] present the experimental investigation of adhesively bonded joints. The

joints were made of pultruded GFRP adherends: having the same stiffness as the members that would be used in FRP bridge decks. The pultruded adherends were made of vinyl ester resin and glass fibres with orientations of 0° , 90° , 45° and -45° . Failure within the adherend near the interface was observed in most specimens. They concluded that the peeling effect is the main cause of failure in adhesively bonded joints. They suggest that double lap joints would be more suitable in the FRP bridge deck application.

Lee et al. [122] present the experimental investigation of pultruded GFRP decks under static load. Two types of fabric architecture were used: i). DBT ($45^\circ/90^\circ/-45^\circ$) and ii). LT ($0^\circ/90^\circ$). ABAQUS was used for the verification of experimental results. It was found that the behaviour of all specimens show linearly elastic and brittle fracture. They concluded from the experimental results, that DBT deck exhibits higher stiffness and strength than LT specimen.

Previous research [23,101] on lap-shear joints for pultrusions with random outer mats has shown that failure initiates in the adhesive spew fillet or in the outer mat layers of the pultruded laminate at the joint edge. Cracks then easily propagate between the mat layers (usually random mat) where there is little through thickness reinforcement and an inherent stress concentration. Boyd et al. [23] proposed a finger bonded joint be used, for pultruded materials, to eliminate the load in the through thickness direction. This joint concept was further studied to measure the joint efficiency by using both FEA (finite element analysis) and TSA (thermoplastic stress analysis) [123,124]. The preparation of the finger joint was complicated and time consuming in comparison to that of the butt joint. However, a pultrusion made entirely from glass UD fabric layers has no surface ply as such, so the delamination mechanism detailed above does not take place [4].

Failure occurs a few filaments deep into the composite and hence the strength of this type of material could be superior to the more traditional sandwich lay-up with surface mats. Failure occurs when the surface layer delaminates from the adherend in the overlap region through a combination of through thickness, tensile (transverse) and shear stresses in the composite. Failure may also be initiated at the interlaminar region between the rovings into the overlap region of the composite - the former is believed to be the most critical [125].

Herakovich et al. [126] examined the fibre spacing and resin rich areas in pultruded composites and concluded that significant strength reduction is due to uneven fibre distribution and spacing between them. Pultruded composites show a non-linear response during loading, which is due to the nature of different materials' lay-up but the major impact is due to the voids and micro defects. Wang et al. [127] studied the tensile behaviour of a pultruded I-section beam structure. Void content is relatively high in pultruded composites as compared to the composites made up by other methods. They also showed a large number of voids at different locations of an I-beam which affect strength in both longitudinal and transverse directions. One of the limitations of the pultrusion process is the resin heat transfer problem due to high exothermic curing reactions and low thermal conductivity. Therefore the variation of temperature during the process generates voids and cracks on the pultruded parts quoted by Paciornik et al. [128]. They pointed out these defects and cracks due to improper resin heat transfer during curing, affect the mechanical properties as well as help to moisture absorption. But vinyl ester resin as a matrix with glass fibre performed well to control the heat transfer problem and variation in temperature during pultrusion process.

Binshan et al. [25] tested a number of pultruded profiles to measures their fibre volume fraction and mass density. Such a profile was based on vinyl ester / polyester resin system reinforced with different layers of glass roving, CFM and woven roving. They reported the void content in the pultruded profile to be about 3-5%.

Ganga Rao et al. [129] have published work on the factors that should be considered when designing pultruded adhesive bonded joints e.g., joint efficiency/stiffness, stress concentration, failure mode. Liu's [130] research relating to the pultrusion process, is concerned with the control of the critical process parameter such as die temperature and distribution, pull speed, fibre content and resin kinematics. Hartley [8] highlights the general rules of thumb in a pultrusion overview. In addition Hartley has also pointed out that although vast amounts of research have gone into the pultrusion process it is still described as a trial and error type process. A detailed description of the pultrusion process can be found in Peters [6]. However, none of the above work has taken adhesion into consideration. The pultruded sections are largely joined by fastening methods. Barbero et al. [131] studied the post critical response of pultruded FRP composite under buckling.

The study focused on pultruded columns.

Pyror and Barker [132] performed a finite element analysis of laminated composites. Herakovich [133] analysed cross ply, angle ply and quasi-isotropic laminates to explore the delamination failure. He found that elastic properties mismatch between composite layers, is the main cause of interlaminar stress enhancement, which proceeds to delamination failure. He also concluded that the delamination initiation starts with the combination of both interlaminar shear stress and interlaminar transverse stresses. Pagano et al. [134] presented some fundamental elements in his work, which enhanced the interlaminar strength of composite laminates. Pagano et al. [135] suggested that the composite laminate delaminates due to both interlaminar shear and interlaminar transverse stresses. Good correlation was found with experimental data. Puppo et al. [136] used interlaminar shear stresses, while the effect of interlaminar transverse stresses was totally ignored in their theory of laminated composites.

Amar et al. [137] presented a delaminated mode in composite structures and suggests a few precautionary measures of how to control the delamination and make the structure more damage tolerant. Kairouz et al. [138] performed linear FEA of a single lap joint to see the stacking sequence effect on the overall performance of the joint. They found that the stacking sequence does not have the influence on joint strength but it does have an effect on the failure system [139]. Pradhan et al. [140] presented a parametric study of adhesively bonded composite joints, which includes the different stacking sequence, crack locations and bond length/thickness. The strain energy method was used to observe the trend of interlayer debonding and they concluded that the strain energy method is sensitive to the stacking sequence. Ratwani et al. [141] presented the stacking sequence effect on the damage propagation and failure modes in composite laminates. They found that the damage propagation direction depends on the stacking sequence. Lakshminarayana et al. [142] studied the accuracy of finite element modelling of composite material laminates. Good correlation was found between FEA, analytical and experimental results. Herakovich [143] studied the influence of layer thickness on the strength of angle ply laminates. He concluded that the strength and stiffness of the finite width angle ply laminate is improved with the alternating layer stacking sequences. He pointed out that the strength of the angle ply laminate arrangement can be fold higher than the cluster configuration. Harrison and

Bader [144] presented the influence of the stacking sequence of carbon fibre/epoxy resin laminate. They showed that the stacking sequence with alternating configuration exhibited higher strength than a clustered configuration.

Chapter 3

Experimental Programme (Material Properties)

3.1 Introduction

The reliability of bonded joints depends on the limitations of the material being used and the veracity of joint design. Accurate mechanical properties of all materials used in bonded joints must be taken into consideration. These will require the properties of all constituent materials to be determined .

This chapter explains the analytical and experimental procedures on various materials used in this research to obtain essential mechanical properties. The three main materials and their properties used in this research are GFRP pultruded composite (elastic and orthotropic), epoxy adhesive Araldite 2015 (elasto-plastic) and aluminum (isotropic). The main constituent materials used in the fabrication of GFRP laminates are based glass fibre and vinyl ester resin. Since a composite material is not isotropic, it is impossible to predict exact properties as there are too many variables. It is, however, possible to estimate the properties using the rule of mixtures, Tsai and Hahn equations and transversely isotropic materials assumptions. Another method of determining the mechanical properties of the composite material is to conduct mechanical testing. The composite material was tested in accordance with British Standards [165]. The adhesive properties are another difficult area of investigation. This was based on bulk adhesive casting and testing and a standard steel butt joint. This also required data from manufacturers.

The chapter continues to explain how the composite and adhesive test specimens were constructed with the aid of a mould. Later, the details of experimental testing and their relevant results will follow. Microscopic observations were made to further complement this work.

3.2 Composite

There are different classifications of glass fibre, and it is extremely important to use the correct fibre, so that it may be best suited to the particular application. The main constituent materials used in the fabrication of GFRP composite are based on E-glass fibre roving as a reinforcement and vinyl ester resin as a binder.

3.2.1 E- glass fibre

Glass fibres are the most common type of fibres, used in the pultrusion process, due to their high tensile strength, low density and low cost [13]. The composite provider, (Exel composite Ltd. UK) uses E glass as reinforcement. Two sizes of glass rovings were used in this research, namely 4800Tex and 3600Tex – *a unit of linear density equal to the mass in grams of 1000 meters of filament or yarn.* In addition the mechanical properties and other characteristics of glass fibre were provided by a manufacturer (Formax UK Limited). Typically, E-glass individual filament has a diameter between 8 and 20 μm . Laboratory microscopic observation and manufacturer supplied data proved that individual filament size used in this research were the same (16 μm diameter) as shown in Figure 3.1.

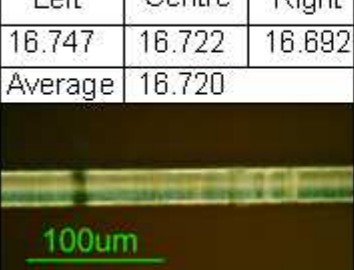
| Specimen A (μm) | | | Specimen B (μm) | | | Specimen C (μm) | | |
|---|--|---|------------------------------|--------|--------|------------------------------|--------|--------|
| Left | Centre | Right | Left | Centre | Right | Left | Centre | Right |
| 16.747 | 16.722 | 16.692 | 16.487 | 16.462 | 16.455 | 16.334 | 16.377 | 16.356 |
| Average | 16.720 | | Average | 16.468 | | Average | 16.355 | |
| | | | | | | | | |
|  |  |  | | | | | | |
| 100 μm | 100 μm | 100 μm | | | | | | |

Figure 3.1: Microscopic observation of single filament

3.2.2 Vinyl ester resin

Vinyl ester resin is commonly used in the pultrusion process for high production rate and to control voids: as voids contents are relatively high in pultruded composites as compared to the composites made up by another method [127]. The variation of temperature during

the pultrusion process generates voids. But vinyl ester resin as a matrix with glass fibre as a reinforcement performs well to control the heat transfer rate [23]. These void/micro defects affect the mechanical properties as well as helping with moisture absorption. Atlac Resin 430 was used as a vinyl ester resin with TRIG C (hardener) and TRIG 21 (Initiator) with the mixing ratio 100:8:8 100 parts resin by weight, 8 parts hardener by weight and 8 parts initiator by weight. This proportion is given by Exel composite Ltd. UK and the resin manufacturer. The resin manufacturer (DSM Composite resin) provided a stress-strain curve (see Appendix A6.2) and technical data sheet (see Appendix A6.1), which included mechanical properties, major applications, processing and other characteristic.

3.3 Composite properties

GFRP composites were produced with E-Glass fibre supplied by Formax in the form of tows or rovings and Atlac 430 resin would normally be mixed with TRIG C (hardener) and TRIG 21 (initiator) supplied by Exel Composites Ltd. UK. In this research, two procedures were adopted for the measurement of composite material properties. These are mentioned below:

- Analytical procedure based on manual method to find the fibre volume fraction of laboratory made laminate.
- Experimental procedure based on manufacturing and testing of pultruded straps provided by the manufacturer (Exel Composite Ltd. UK).

3.3.1 Analytical procedure

The analytical procedure was based on manual calculation of fibre volume fraction in a single glass roving and meso scale laminate and both were impregnated in the laboratory. A difference of 1.8% was found between them. Details are given below:

3.3.1.1 Fibre volume fraction in single E-glass roving laminate

An analytical procedure was adopted to find the fibre volume fraction in order to establish the longitudinal and transverse modulus of a single (impregnated) glass roving which would be needed in the numerical model. The cross section of the roving was examined under the microscope and an image was obtained, as shown in Figure 3.2. E_1 and E_2 were

established by using the rule of mixtures.

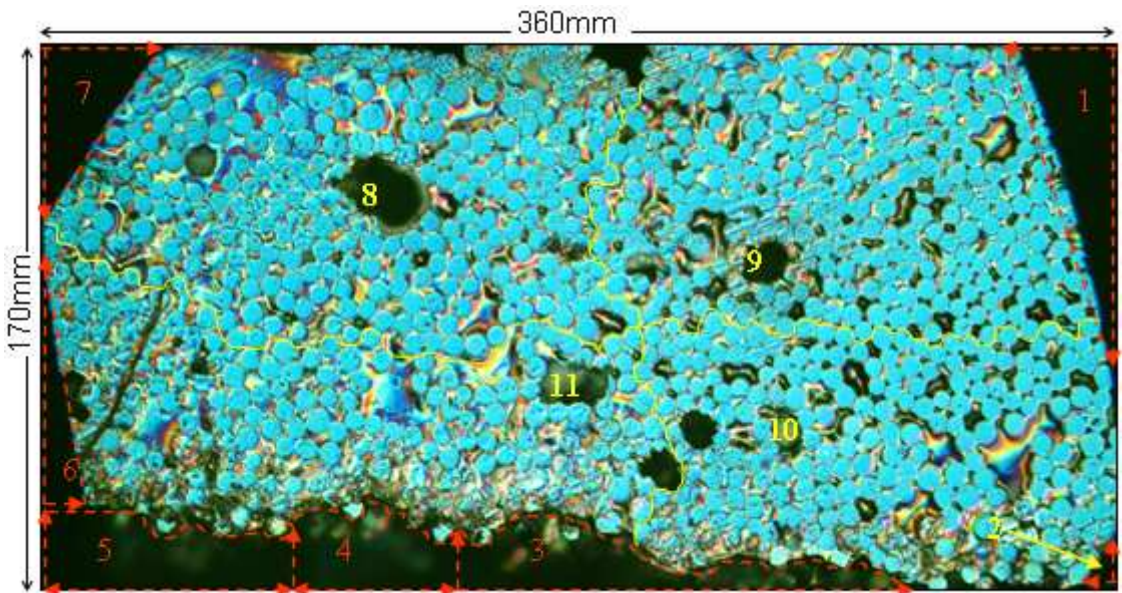


Figure 3.2: Polished roving showing number of filaments presents (image scale)

Calculation of fibre volume fraction in E-glass roving

Average fibre diameter measured = 7mm

| <i>Approx number of fibre in each section:</i> | 1 | 2 | 3 | 4 | 5 | 6 | 7 | 8 | 9 | 10 | 11 |
|--|----|---|---|----|----|----|----|-----|-----|-----|-----|
| | 51 | 4 | 8 | 15 | 24 | 17 | 15 | 254 | 245 | 214 | 165 |

Approx number of fibre in each section:

Total number of fibres counted = Σ of all sections = 1024

$$\begin{aligned} \text{Area of 1 fibre} &= \pi \cdot r^2 \\ &= \underline{0.00003848 \text{m}^2} \end{aligned}$$

$$\text{Total area of fibres within microscopic image} = 1024 * 0.00003848 = \underline{0.039 \text{m}^2}$$

$$\text{Area of image} = 170 * 360 = \underline{0.0612 \text{m}^2}$$

$$\begin{aligned} \text{Therefore, area of matrix material} &= (0.0612 - 0.039) \\ &= \underline{0.0222 \text{m}^2} \end{aligned}$$

$$\text{Fibre Volume Fraction, } V_f = \frac{0.039}{0.0612} * 100\%$$

Fibre volume fraction in single E-glass impregnated roving = 63.7%

Another approach, fibre volume fraction in meso-scale laminate, was also adopted to further verify the results.

3.3.1.2 Fibre volume fraction in meso-scale laminate

The pultruded meso-scale laminate was made up of $0^\circ/0^\circ$ laminae with special jig (see Figure 3.3b) quite close to pultrusion mould conditions. These were then cut into the required size ($20 \times 20\text{mm}$) of small laminate (see Figure 3.3c) using parallel mounted diamond impregnated circular saw blades mounted in a horizontal axis-milling machine. The moulding process will be discussed in details in Chapter 4.

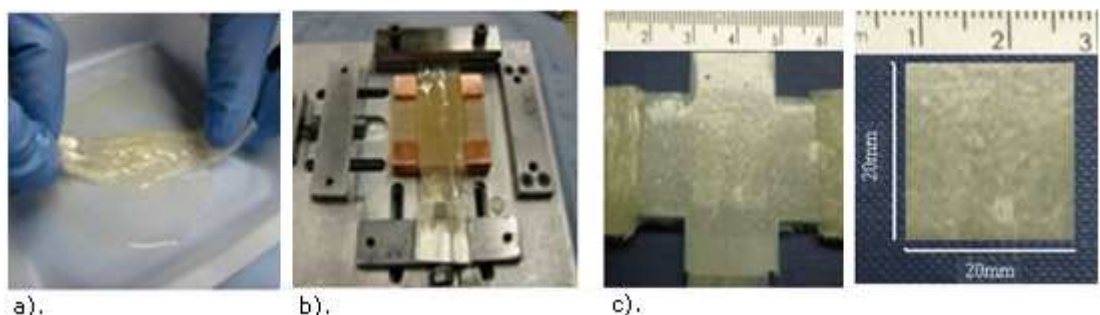


Figure 3.3: Moulding jig showing: a). impregnation, b). clamping of impregnated rovings, c). GFRP pultruded laminate before and after trimming

In order to calculate the fibre and resin weight fraction the ($20 \times 20\text{mm}$) laminae, shown in Figure 3.3c, was weighed before and after impregnation. The mechanical properties of the pultruded composite were obtained using the rule of mixtures, Tsai and Hahn equations and transversely isotropic materials assumption for better estimation. The calculation of fibre volume fraction is shown below:

Calculation of fibre volume fraction in meso-scale laminate

The summary of fibre and matrix weight proportions in the $20 \times 20\text{mm}$ small laminate is

shown below:

Weight of uni-directional roving without resin (1 layer) = 40.05%

Weight of uni-directional roving without resin (2 layer) = 80.1%

Weight of resin = 19.9%

| Material | Weight fraction (%) | Volume Fraction (%) |
|----------|---------------------|---------------------|
| Fibre | 80.1 | 65 |
| Matrix | 19.9 | 35 |

Table 3.1: Volume and weight fractions of GFRP laminae

Most of the composite material calculation is based on the volume fraction of the constituent. Fibre volume fraction is calculated as follows:

$$V_f = \frac{w_f / \rho_f}{w_f / \rho_f + w_m / \rho_m}$$

Where V , w , ρ are the volume fraction, weight fraction and density; subscript f and m represent fibre and matrix respectively. Matrix density $\rho_m = 1.14 \text{ g/cm}^3$ [163] and $\rho_f = 2.54 \text{ g/cm}^3$ [164] were used in fibre volume fraction calculations

Fibre volume fraction of laminate = 65%

The fibre volume fraction obtained from meso-scale laminate is somewhat high but may be acceptable for two reasons:

- the same meso-scale laminate with all materials arrangement was used in the experimental investigation
- the value is comparable with the manufacturer quoted value, (~ 60-65%). The rule of mixtures was used to calculate the composite properties based on this fibre volume fraction. The individual material properties of single glass fibre and resin are tabulated in Table 3.2.

| | Single Glass Fibre | Vinyl Ester Resin |
|---------|--------------------|-------------------|
| E (GPa) | 72 | 3.6 |
| ν | 0.2 | 0.37 |
| p | 2550 | 1210 |

Table 3.2: Properties of single glass fibre and resin

Applying the rule of mixtures:

The laminae properties are obtained using the rule of mixtures as explained below. The rule of mixtures is used for orthotropic material [145] with various notations for different directions:

- 1 represents longitudinal (fibre direction)
- 2 represents transverse direction
- 3 represents through thickness direction

It is suitable if the longitudinal direction was taken along the fibre only for reliable material properties estimations.

- Longitudinal tensile modulus: (E_1)

$$E_1 = E_f V_f + E_m V_m \quad \text{---- (3a)}$$

- Poisson's ratio (ν_{12})

$$\nu_{12} = \nu_f V_f + \nu_m V_m \quad \text{---- (3b)}$$

where

E_f is the modulus of elasticity for the fibres

E_m is the modulus of elasticity for the matrix (resin)

V_f is the volume fraction of the fibres

V_m is the volume fraction of the matrix (resin)

Tsai and Hahn stress portioning parameter [146] is used for better value estimation in transverse directions. These are:

$$E_2 = E_m \frac{V_f + \eta_y V_m}{\eta_y V_m + V_f E_m / E_f} \quad \text{---- (3c)}$$

$$G_{12} = G_m \frac{V_f + \eta_s V_m}{\eta_s V_m + V_f G_m / G_f} \quad \text{---- (3d)}$$

$$G_{23} = G_m \frac{V_f + \eta_G V_m}{\eta_G V_m + V_f G_m / G_f} \quad \text{---- (3e)}$$

Where

- Volume fraction of matrix

$$V_m = 1 - V_f \quad \text{---- (3f)}$$

- Shear modulus of matrix.

$$G_m = E_m / 2(1 + v_m) \quad \text{---- (3g)}$$

- Shear modulus of fibre

$$G_f = E_f / 2(1 + v_f) \quad \text{---- (3h)}$$

Stress partitioning parameters η_y , η_s , and η_G are the additional parameters in the rule of mixtures to measure the accurate transverse properties of laminate introduced by Tsai and Hahn (1980). η_y and η_s are calculated with the experimentally calculated values of E_1 and G_{12} and η_G is calculated through the relation

$$\eta_G = \frac{3 - 4v_m + G_m / G_f}{4(1 - v_m)} \quad \text{---- (3i)}$$

Tsai and Hahn used the assumption of transversely isotropic material for calculating the other transverse properties like $E_2 = E_3$, $v_{13} = v_{12}$, $G_{12} = G_{13}$, and G_{23}, v_{23} is given by the relation.

$$G_{23} = E_2 / 2(1 + v_{23}) \quad \text{---- (3j)}$$

$$v_{23} = E_2 / (2G_{23}) - 1 \quad \text{---- (3k)}$$

The GFRP laminae properties using the rule of mixtures, Tsai and Hahn and transversely isotropic materials assumption, as mentioned above, are tabulated in Table 3.3. The values

in this table are calculated from equations (3a-3k) by using the following material constant $E_f = 72\text{GPa}$, $E_m = 3\text{GPa}$, $v_f = 0.2$, $v_m = 0.36$, $V_f = 65\%$, $V_m = 35\%$, $G_f = 30\text{GPa}$, $G_m = 1.103\text{GPa}$, $\eta_y = \eta_s = 0.5$, $\eta_G = 0.63$.

| Property | Units | GFRP Laminate |
|-----------------------|-------|---------------|
| E_1 | GPa | 47.85 |
| $E_2=E_3$ | GPa | 10.65 |
| $G_{12}=G_{13}$ | GPa | 3.30 |
| G_{23} | GPa | 3.97 |
| $\nu_{12} = \nu_{13}$ | -- | 0.256 |
| ν_{23} | -- | 0.34 |

Table 3.3: Material properties of GFRP laminae

3.3.2 Experimental procedure

Another method of determining the mechanical properties of the composite material is to conduct mechanical testing of pultruded section manufactured at Exel Composite Ltd. UK. The composite material was tested in accordance with British standards [165]. The details of specimen manufacturing, testing and procedures describing how to get mechanical properties through manufacturer provided pultruded section are as follows:

3.3.2.1 Longitudinal properties of pultruded GFRP laminate

A pultruded section manufactured at Exel Composites Ltd. UK used the same E-Glass rovings, which were tested to verify the mechanical properties obtained through an analytical procedure. Firstly, an experiment was conducted on a pultruded composite with longitudinally aligned fibres to determine the UTS as per British Standards [165]. Pultruded composite planks with a dog bone shaped profile, of dimensions 25mm wide and 5 mm thick (see Figure 3.4 and 3.5), were provided by Exel Composites Ltd. UK. These planks were then machined to a uniform thickness; removing the surface veil and continuous strand mat to leave unidirectional fibres. This also removed the mould release agent. The final thickness of the unidirectional composite strips was 3mm. The unidirectional pultrusion strips were then cut to the required length using a parallel mounted diamond impregnated circular saw blade mounted in a horizontal axis-milling machine.

The minimum dimensions for the composite stated in British Standard test method [165] are:-

| | |
|---------------------------------------|------------------|
| A: Overall minimum length | = 200mm |
| B: Length between end-pieces, minimum | = 110mm |
| C: Width of tensile specimen | = 25mm ± 0.5 |
| D: Thickness of material, Min | = 1mm |
| | Max = 10mm |
| E: Length of end pieces, minimum | = 45mm |

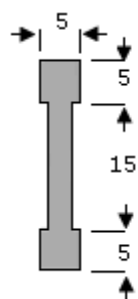


Figure 3.4: Composite material section

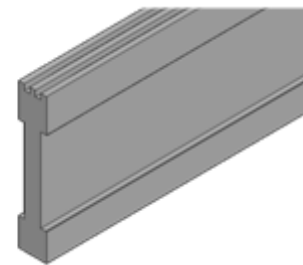


Figure 3.5: Composite material pre-machining

The actual dimensions of the pultruded specimen can be seen in Figure 3.6. The composite material was coated (sealed) with low viscosity epoxy resin Araldite® AY103/HY951 to fill voids, reduce surface roughness and to provide a compatible bonding surface. Steel plates were then adhered to the composite using Araldite® 2015.

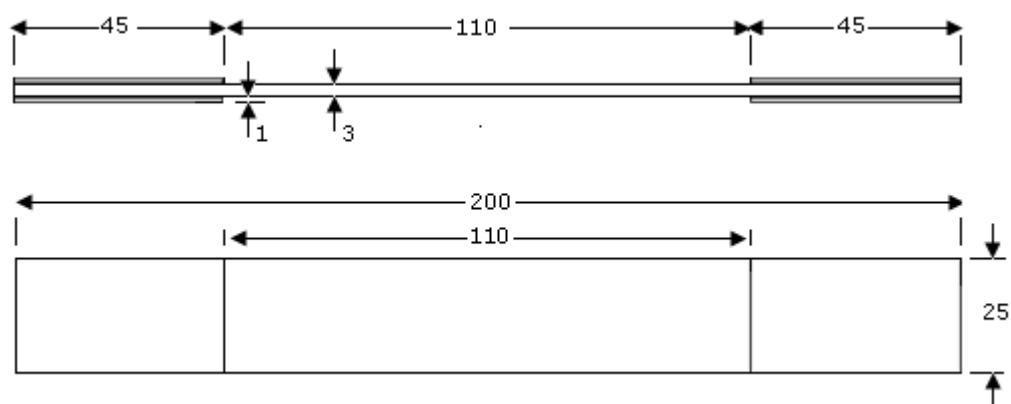


Figure 3.6: Dimensions of pultruded specimens

These were then gripped in the Instron tensile testing rig and pulled at a rate of 0.5mm per minute at ambient temperature conditions, (about 18-22°C). Prior to the test, each test specimen dimension was thoroughly checked. The cross-sectional area calculation of each test specimen gives a rough idea about the failure load of each test specimen. In addition, the thickness and width of each specimen was measured using an electronic micrometer before the experiment. A strain gauge was mounted to the specimen, along the loading direction. The test was performed on an Instron machine at a cross head speed of 0.5min/mm. With the aid of data logger, a stress-strain curve was produced as shown in Figure 3.7.

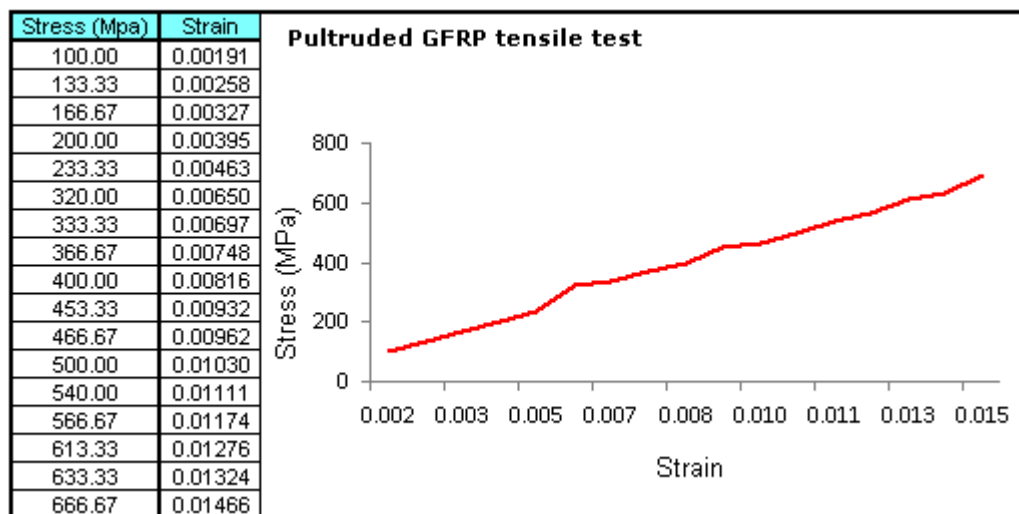


Figure 3.7: Stress-strain distribution curve obtained from tensile test result of pultruded GFRP specimen

Taking the gradient of the elastic region gives the gradient and subsequent Young's Modulus of Elasticity.

$$E_1 = \frac{\sigma_2 - \sigma_1}{\epsilon_2 - \epsilon_1}$$

$$E_1 = \frac{616.33e6 - 366.67e6}{0.01276 - 0.00748}$$

$$E_1 = 47.5 \text{ GPa}$$

The modulus of elasticity of the composite was calculated to be 47.5GPa in the longitudinal direction. Figure 3.8 shows how the pultruded GFRP specimen, before and

after rupture. The figure also shows the delamination of the UD specimen(see Figure 3.8c).

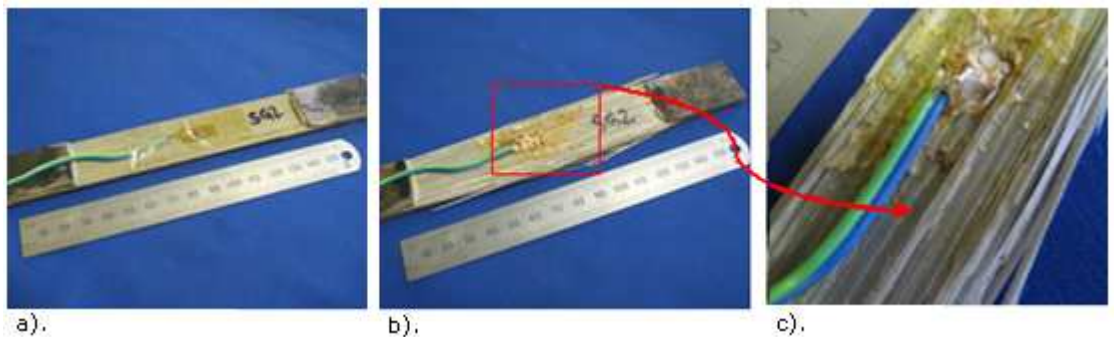


Figure 3.8: Pultruded tensile test specimens: a). without rupture, b). rupture with static tensile load, c). severe delamination

The failure load was 52kN, resulting UTS= 693MPa (Ultimate tensile strength) obtained by using (Stress = Force / Area) and knowing that the specimen was 25mm wide and 3mm thick gives:

$$\sigma = \frac{F}{A}$$

$$\sigma = \frac{52}{0.025 * 0.003}$$

$$\sigma = 693 .3 MPa$$

This is verified in the Fibre force design manual, where the UTS is stated (for ~ 60-65% of fibres volume fraction) as 690N/mm². The tensile modulus, E1 was calculated to be 47.5GPa.

3.3.2.2 Transverse properties of pultruded GFRP laminate

For the unidirectional pultruded GFRP transverse tensile testing, two approaches were adopted. Both approaches were used to investigate the transverse behaviour of pultruded GFRP specimen. Approach 1 applies to the specimen without the dog bone shape and approach 2 with the dog bone shape. Approach 1 is likely to be more expensive and complicated (extra machining and bonding) and the specimens are significantly affected by pre- machining material degradation before testing.

Approach 1:

Pultruded GFRP was cut into a section as shown below in Figure 3.9a. Onward this GFRP cut section was machined to a final uniform thickness up to 3mm and bonded using Araldite® 2015 to steel plates. This was due to the size of the pultruded specimen being too short (see Figure 3.9b). These were then gripped in the Instron Tensile Testing machine at a constant displacement rate of 0.5mm/min. Figure 3.9c shows the fibre direction in specimen; perpendicular to the loading direction. The rest of the procedure was the same as that for the longitudinal tensile test. All major dimensions used in approach 1 transverse tensile test specimen are shown in Appendix A.1.

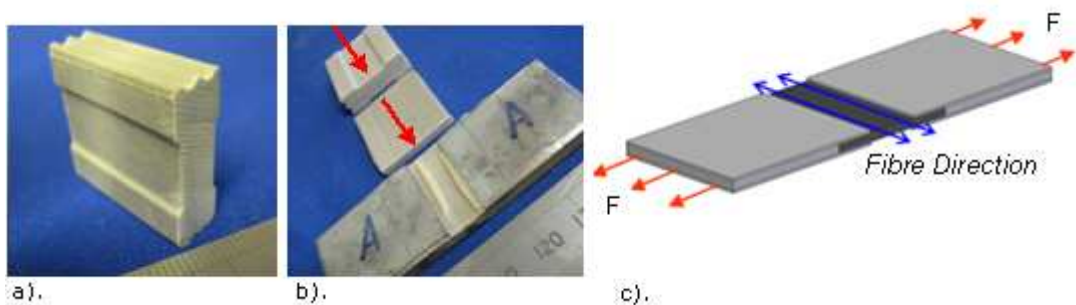


Figure 3.9: Pultruded transverse specimen: a). pultruded section, b). uniform pultruded laminate bonded between steel straps, c). diagram showing fibre direction Vs loading

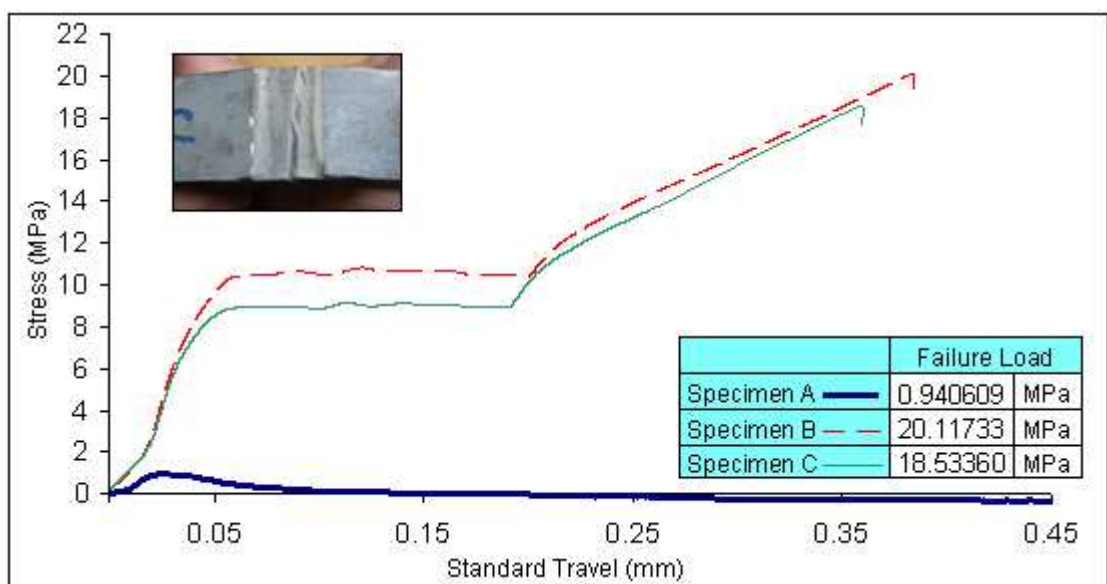


Figure 3.10: Transverse strength and failure load of plane pultruded GFRP

Figure 3.9c displays how the specimens were loaded. Stress Vs displacement curve of three different specimens (A, B and C) are shown in Figure 3.10. Specimen A was discarded due to premature failure. Specimen B and C showed very close correlation in terms of failure load and about 8% deviation was observed between them. A possible reason for this could be misalignment or specimen internal defects.

Approach 2:

In this approach a GFRP pultruded plank of dimensions 100mm long, 25mm wide and 5mm thick by Exel Composite Ltd. UK was cut in 25×25 mm square composites as shown in Figure 3.11a.

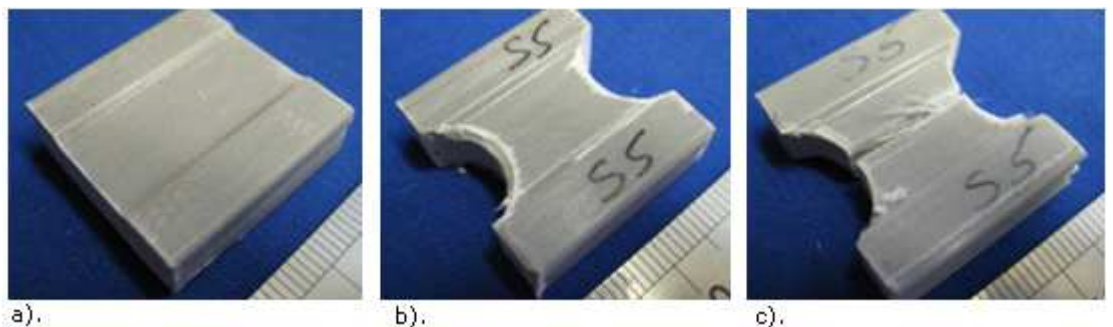


Figure 3.11: Transverse pultruded specimen: a). 25×25 mm square composite, b). dog bone shaped specimen, c). Failure specimen after test

The square composite original thickness (5mm) was kept and extra machining was avoided to overcome the level of pre-material degradation before testing. The square composite was slightly machined to get a dog bone shaped specimen (see Figure 3.11b).

Similar trend stress-displacement curves were generated from five similar configuration dog bone specimens as shown in Figure 3.12. The average failure load obtained through this approach was 20.54MPa, which is quite comparable to approach 1 (Failure load=20.11MPa). In addition the transverse strength of the UD laminates is about 20-22 MPa as claimed by pultrusion manufacturers. The above approaches and strength value (by pultrusion manufacturers) gives a clear indication that the transverse strength cannot exceed 20-23MPa. However the assumption here is that a transverse stress failure within the composite is within the matrix resin rather than the fibres. The resin manufacturer claims a tensile strength value of 90MPa. The main reasons for such a large difference are

the lack of ideal alignment in the transverse direction and interfaces flaws, including voids/micro defects.

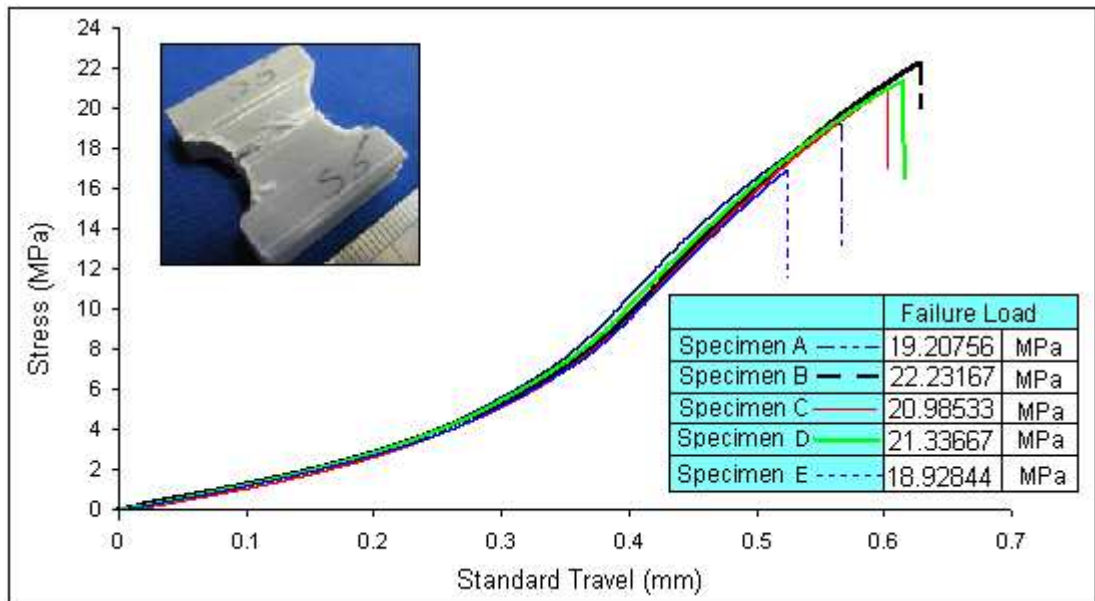


Figure 3.12: Transverse strength and failure load of dog bone pultruded GFRP

3.4 Adhesive properties

In this section selection of adhesive and its properties used in finite element analysis are all discussed. Clearly, the use of proper adhesive has many advantages to offer such as, it allows excellent joint strength, assemblies of similar and dissimilar adherend and they can often result in cost reduction [40]. There is no ‘universal’ adhesive that will bond every substrate together, and so the choice of adhesive is always involved.

3.4.1 Adhesive selection

Araldite® 2015, a two component epoxy paste adhesive was chosen for adhesive bonding in this research. In general, the epoxy based adhesives offer strong bond strength and exhibit good stability. The two part epoxy adhesives are good candidates for the bonding of composites instead of single part adhesives. The choice of Araldite® 2015 was based on the following key properties:

- the adhesive is widely used by many end users for bonding GFRP (Glass fibre reinforced polymers) to itself and many other dissimilar adherends

- it is thixotropic and non-sagging up to level of 10mm thickness
- it offers a resilient bond with high shear and peel strength which are particularly important given the nature of the types of tests performed it has low shrinkage properties
- it has a good shelf life and can be stored at room temperature
- it can either be cured at room temperature or at elevated temperature
- Araldite 2015 exhibits good gap filling properties.

Araldite® 2015 is stored in a refrigerator controlled at the low temperature of 5°C. The recommended temperature set by the manufacturer is 2-8°C. Shelf life established by the manufacturer at this temperature is 2 years and should be replaced within 6 months after being used, prior to the expiry date. The adhesive preparation work requires more care; especially before applying. The adhesive needs to be placed at room temperature from the cold temperature, for at least 30mins. This process is essential to promote effective adherend surface wetting. Araldite® 2015 exhibits good gap filling properties and, so the first thin coat of adhesive was applied by a knife- coating procedure and the rest of the following coats by a normal smooth pressure. Bonding pressure on the joint was applied by using specially designed bonding jigs.

3.4.2 Production and testing of adhesive specimens

Mechanical properties of Araldite® 2015 are required for the finite element analysis, such as Young's modulus, Poisson's ratio and tensile strength. These properties were determined in the laboratory by casting the bulk adhesive into dog bone shaped specimens and testing them after mounting strain gauges (as explained later). The purpose of these tests is to verify the properties provided by manufacturers. The Young's modulus of elasticity provided by the manufacturer (HUNTSMAN) was found to be in line with values derived from these tests. The dimensions of the bulk adhesive specimens were similar to those of British Standard [166] as shown in Figure 3.13 and all other major dimension are mentioned in Appendix A.3 (see Figure A.3.1).

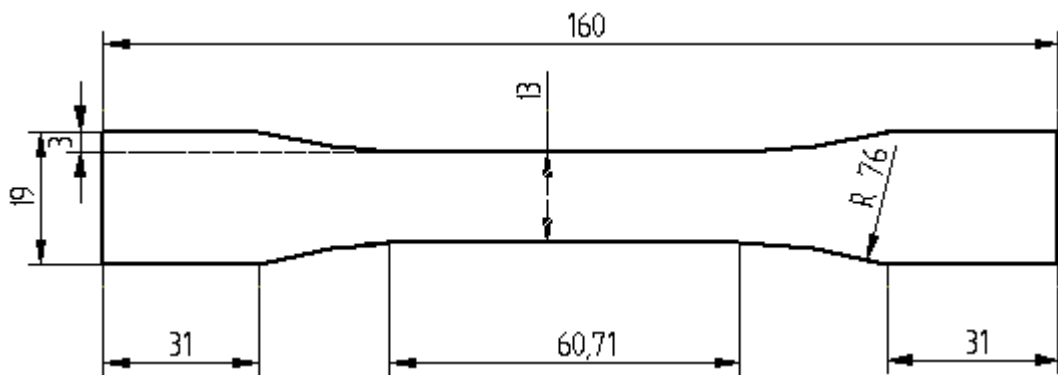


Figure 3.13: Dimension of bulk adhesive tensile test specimen

It was produced using a silicone rubber mould for more accurate dimensions and easy removal of cured specimen without using any mould release spray (see Figure 3.14). The steps involved during the fabrication of a silicone rubber mould are shown in Appendix A.2 and Appendix A.2.1 shows the schematic view of silicone rubber mould fabrication (see Figure A.2.1). The Araldite 2015 bulk specimen fabrication procedure was performed as follows:-

Clean mould thoroughly with LOCTITE 7063 cleaner in order to remove all traces of oil and dirt prior to application of the adhesive

- it was extremely important to make sure that the mould surface and edges are free of air bubbles, pits, sink marks and all type of scratches. Araldite® 2015 was poured into the female mould part using an adhesive gun with mixer nozzle as shown in Figure 3.14a, a spatula was used to spread all adhesive smoothly onto the mould cavity
- the filled mould was then covered with a male mould part (see Figure 3.14b) and clamped at different locations to ensure uniform thickness and smooth surface
- this clamped mould was then placed in a preheated electrical convection oven at 85 °C. After 1 hour of curing, the oven was turned off and the mould was left inside to cool uniformly for 5 hours. This was again aimed at reducing the possibility of thermal shocks occurring to the specimens
- finally, the excess adhesive was carefully trimmed off by using a sanding

adaptor attached to a multi-purpose, high speed rotary tool called the DREMEL®. The final dimension of the cured specimen (see Figure 3.14c) was measured using a micrometer to ensure that final specimen was the right dimension.



Figure 3.14: Production of bulk adhesive dog bone specimen

Rosette type strain gauges (CEA-06-250UW-120 of VISHAY Measurements Group UK Ltd) were used for the strain measurements. A small strain gauge was used to get clear output data because of the limitation of bonding space and to reduce the probability of degradation of the bonded surface. Before bonding a strain gauge, the specimen surface was roughened with fine emery paper. It was cleaned with recommended primers and bonded with the supplier's recommended M-Bond AE-10 Epoxy strain gauge adhesive.

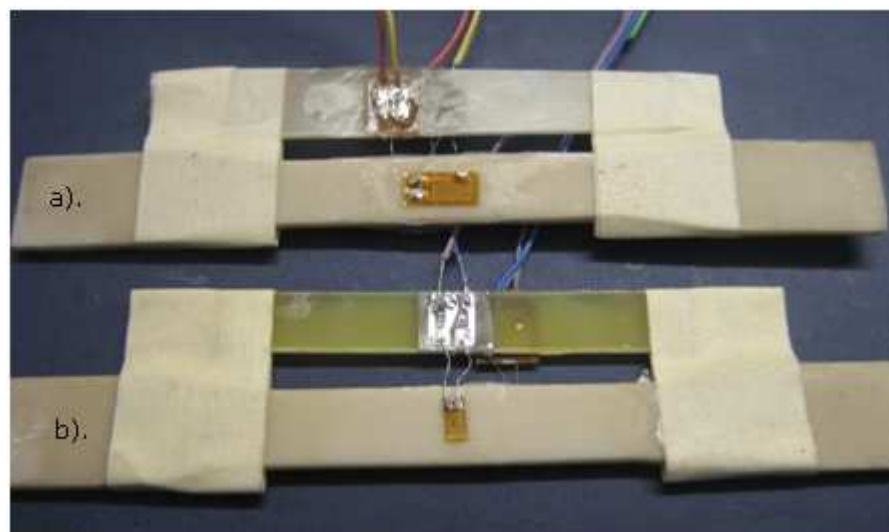


Figure 3.15: Strain gauge mounted dog bone specimen:
a). Longitudinal direction, b). transverse direction

Figure 3.15a represents a strain gauge mounted in a longitudinal direction, while a strain gauge in transverse direction is shown in Figure 3.15b. The best specimens (voids and defect free) were selected and tested under monotonic tensile loading with a Zwick/Roell tensile testing machine at a constant cross head speed of 0.5 mm/min at ambient temperature conditions which are estimated to be about 18-22°C. All specimens were tested to failure and an established stress-extension curve is displayed in Figure 3.16. In addition the stresses are plotted against the corresponding strains in bulk araldite as illustrated in Appendix A.3 (see Figure A.3.3). A Solaritron Schlumberger 3531AD data acquisition system was used for data logging. All associated measuring devices were connected and configured accordingly. The load input from the tensile tester was recorded by the data logger in terms of voltage (10V=5kN). With the application of load, the length of strain gauge arms changes, producing strains that were recorded by the data logger on three selected channels. Output was displayed on the screen of the data logger and simultaneously saved on a floppy disk in the form of a .dat file. This was converted to a .dif file, which was then read and analysed with an Excel spreadsheet, which are tabulated in Appendix A.3 (see Table A.3.1).

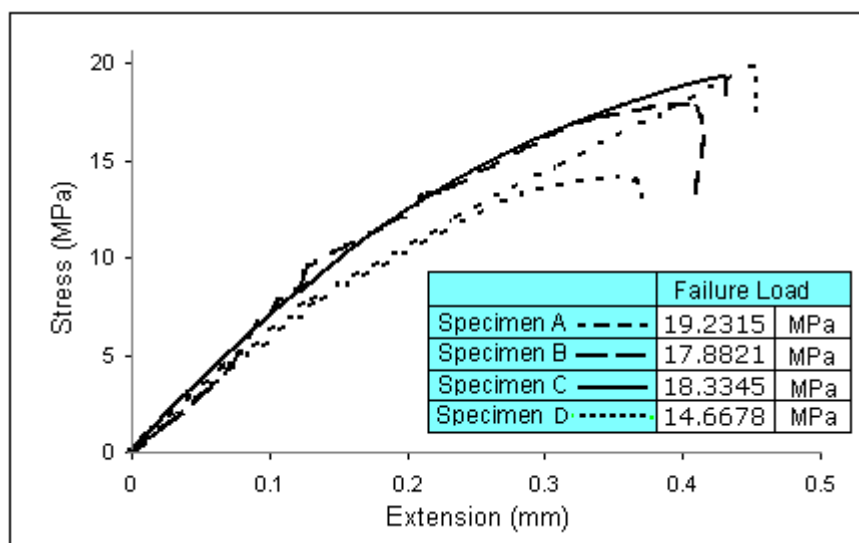


Figure 3.16: Araldite 2015 stress-extension curve from bulk dog bone specimen

The bulk adhesive specimen tested in the laboratory failed at about 19.23MPa as shown in Figure 3.16. This represents only 50% of their maximum expected strength which is 40MPa according to the manufacturer's technical data sheet (see Appendix A.4). The main

reason for this difference is void content at the edges of the specimen as shown in Appendix A.3 (see Figure A.3.2). Therefore, it is important to verify the bulk adhesive results using the steel butt joint as per British Standards [167]. Three butt joint specimens were fabricated and tested (see Figure 3.17).

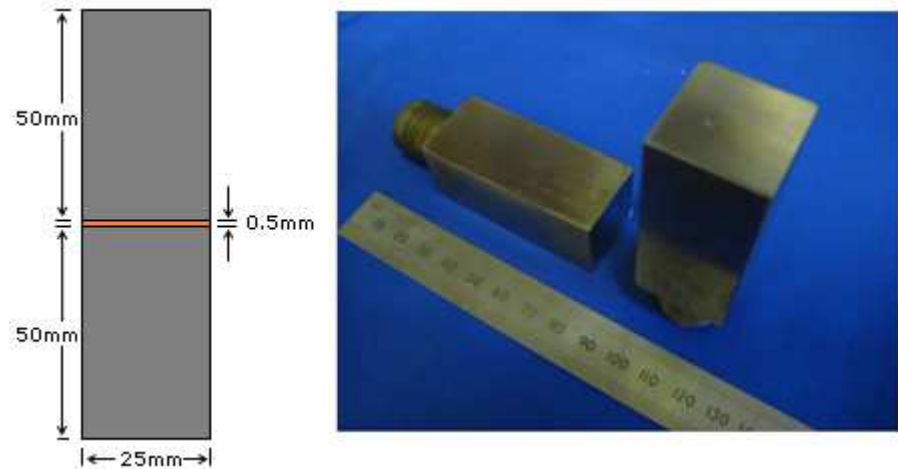


Figure 3.17: Steel butt joint

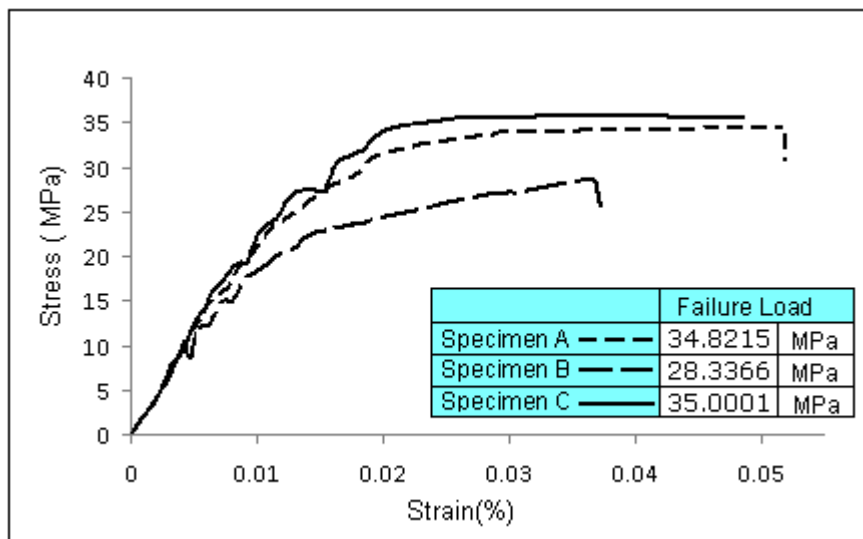


Figure 3.18: Stress strain curves from steel butt joint

These were bonded with Araldite 2015 adhesive with 0.5mm bondline thickness. These were tested under monotonic tensile loading with Zwick/Roell tensile testing machine at a constant cross head speed of 0.5mm/min at ambient temperature. Specimen A and specimen C have comparable and better strength than specimen B as shown in the stress-strain curve of Araldite 2015 (see Figure 3.18). Araldite® 2015 tensile strength using butt

joint gave 35MPa, much closer to the claim by the supplier (up to 42.7MPa).

3.4.3 Extrapolation of data

Since the adhesive displays both the plastic and elastic regions, these properties had to be included in the finite element analysis. Therefore it is necessary to produce elasto-plastic data, based on available test and manufacturer data and relevant engineering assumptions, as shown below:-

The stress-strain curve for Araldite 2015, the small dashed line is the true stress-strain curve from the Huntsman technical data sheet (see Appendix A.4, page A-15 for stress-strain curve). In order to calculate the strain at the adhesive failure load, the true curve is extrapolated to 40MPa. This is the large-dash line. The final point A (from Appendix A) is moved to point B, assuming that the stress-strain curve has the same functional form which gives the large-dash line. The extrapolated true stress-strain curve is then converted to an elastic-plastic stress strain curve: the continuous line (see Figure 3.19 and Table 3.4).

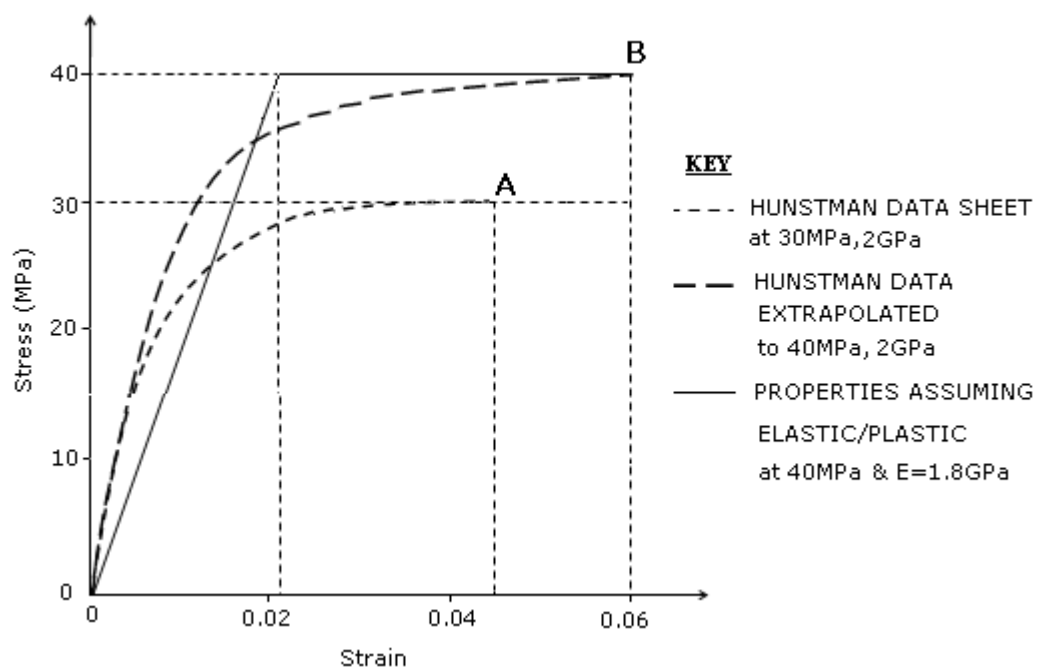


Figure 3.19: Stress-strain curves for Araldite 2015

- At 30MPa, strain is 0.044 (see Appendix A.4-datasheet).
- Properties assuming perfect elastic / perfect plastic at 40MPa & 1.8GPa

$$\epsilon = \frac{\sigma}{E} = \frac{40 \times E 6}{1.8 \times E 9} = 0.022$$

So,

$$\frac{\text{Strain}}{40 \times E 6} = \frac{0.044}{30 \times E 6}$$

$$\text{Strain} = 0.044 \times \frac{40 \times E 6}{30 \times E 6} = 0.06$$

For the elastic plastic model, the adhesive fails at a stress of 40MPa. The adhesive is in the elastic region between a strain of 0 and 0.022. After 0.022 the adhesive is in the plastic region, until 0.06, where it fails. Plastic properties are tabulated in Table 3.4.

| Yield Stress (MPa) | Plastic Strain |
|--------------------|----------------|
| 39.999 | 0.000 |
| 40.000 | 0.022 |
| 40.001 | 0.044 |
| 40.002 | 0.060 |

Table 3.4: Plastic properties of Araldite 2015

The Poisson's ratio, 0.37 was obtained from an adhesive bulk specimen test as tabulated in Appendix A.3 (see Table A.3.1). These adhesive elastic properties are quite comparable to the HUNSTMAN Adhesive data sheet as shown in Appendix A.4.

3.5 Coating resin properties

Araldite® AY103 was used as the resin and HY 951 as the hardener for coating the surface prior to bonding. Using the electronic scales and following the manufacturer's guidelines (see Appendix A.5), the mixing ratio of resin/hardener is 10:0.8, 10parts resin by weight and 0.8parts hardener by weight.

Chapter 4

Experimental Programme (Meso laminate)

4.1 Introduction

To understand failure of DLS joints, based on pultruded composites, it was necessary to produce laminates more effectively with various material arrangements; especially fabric organisations for surface layers. The fabric was based on two sizes of E-glass rovings, namely 4800Tex and 3600Tex and both have the same filament size ($16\mu\text{m}$ diameter). In addition random glass fabric mat of 450gsm was used. The matrix resin is vinyl ester resin. Small laminates (meso-scale) of a size of 20mm x 20mm x 1.2mm were moulded and bonded. These represent local shear and peel stresses that are expected in DLS joints. This chapter explains how the meso-scale laminates were moulded with various fabric organisations. It then goes on to explain coating and bonding with the aid of specially designed jigs. It also gives the details of the testing procedures, including tabulated and graphical figures, based on experimental data which are then discussed. Finally the microscopic observations and failure modes are presented. In addition, the bonding, testing and results of macro-scale DLS model/joints were added for comparison with meso-scale model/joints.

4.2 Production of specimen and set-up

To produce meso-scale laminates with various fabric organisations, special moulding and bonding jigs were designed and manufactured to represent pultrusion close mould conditions. All production processes were carried out according to the manufacturer recommendations including the mixing of resin with hardener, initiator and filler and application of tension/compression on the glass roving (Type 3600/4800Tex from Formax) during impregnation. Figure 4.1 shows the details of the shear and tensile bonded

specimen, which are to be tested (see Figures 5.1 and 5.3 for dimensions). These are not standard test specimen, but are largely based on shear and butt tensile joints in British Standard [166]. The moulding and bonding processes of the meso-scale laminates are described below:

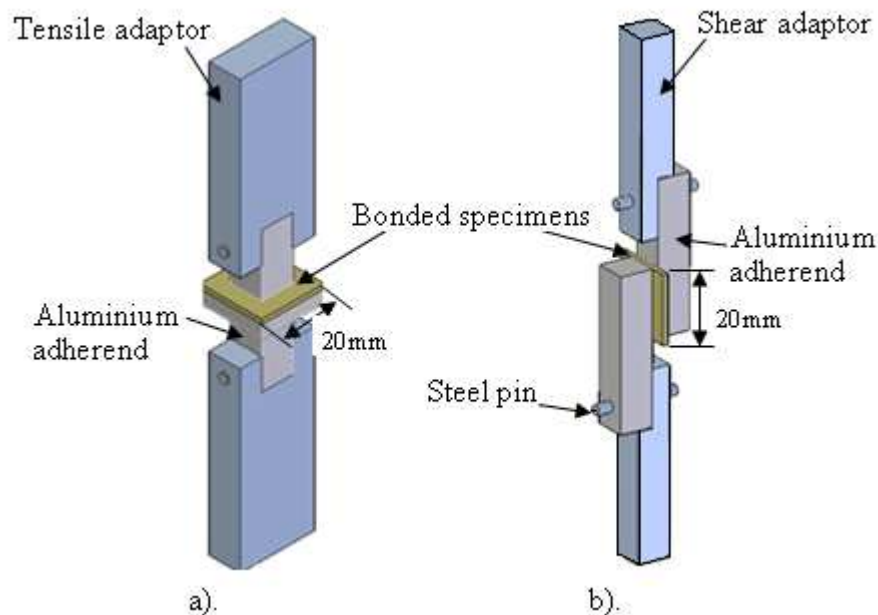


Figure 4.1: a). tensile, b). shear specimen with adaptor

4.2.1 Specification of various fabric organisations

The small laminates were moulded with various fabric organisations (see Figure 4.2), for the surface layers. The organisation of different fabric layers is important for the enhancement of adhesion in adhesive bonded joints and this is often neglected. The pultrusion profiles are dictated by the requirement to balance the stiffness and strength in longitudinal and transverse directions of the pultruded sections. Figure 4.2 shows that the resin impregnated fabric (composite) is separated by thin resin layers to allow interlaminar failure. The outside of the laminates are coated with epoxy resin. The details of fabric organisations used in this research are also shown in Figure 4.2.

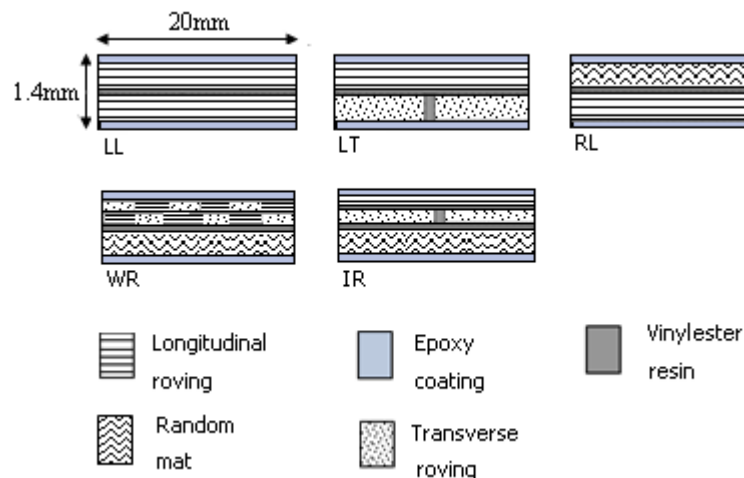


Figure 4.2: Fabric organisation in meso-laminates with epoxy coating

Fabric organisations in meso-laminates with epoxy coating are as follows:-

- LL: - Two UD rovings mats (4800Tex) stacked at 0-direction i.e. along the loading direction (x-axis).
- LT: - Two UD rovings mats stacked at 0/90° bi-direction. Same roving size used in LL (4800Tex).
- RL: - A random mat stacked on the top of UD mat at 0-direction (4800Tex rovings).
- WR: - A 0/90 woven rovings mat (3600Tex) stacked on the top of a random mat.
- IR: - A 0/90 inlaid rovings mat (3600Tex) stacked on the top of a random mat.

The steps of production are described below:

4.2.2 Laminates moulding

4.2.2.1 Design and manufacturing of moulding jig

In order to mould meso-scale laminates with various material arrangements a special moulding jig was designed and manufactured: taking care to ensure perfect alignment of

the roving clamping plates. It also aimed to reduce void content. The moulding jig was based on two main parts:

- The square base plate made of steel.
- The upper and lower detachable copper mould.

The moulding jig was kept as small as possible, to make it portable and easy to use. Steel screw threads and roving clamping plates were screwed on the base plate, while the copper mould was fixed in a detachable slot for resin cleaning as shown in Figure 4.3. An engineering drawing of the moulding jig with details of dimensions is given in Appendix B.1 (see Figure B.1.1 and B.1.2). Further sub parts of moulding jigs are shown in Figure 4.3.

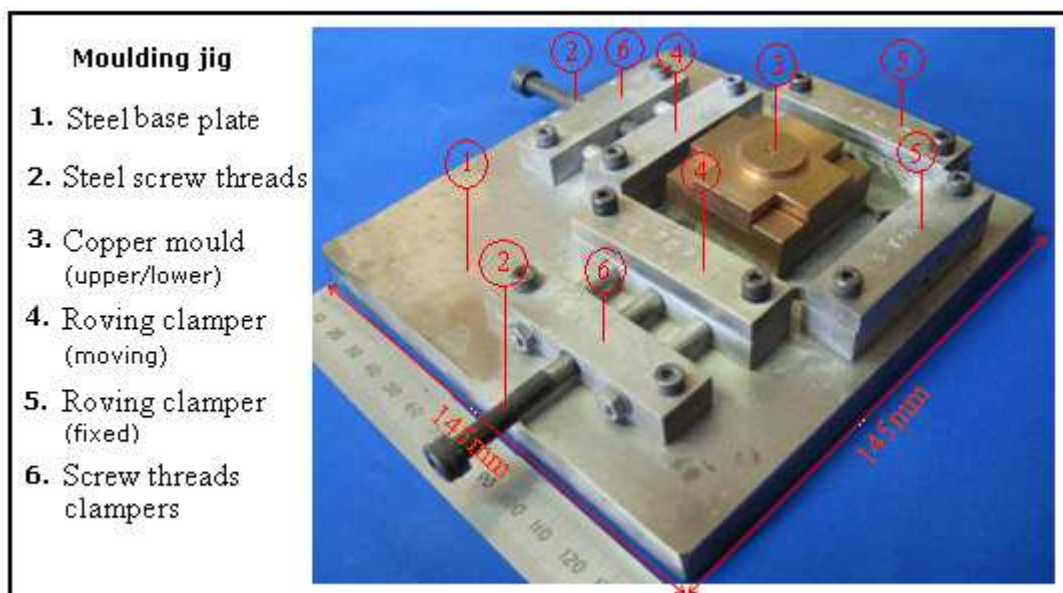


Figure 4.3: Jig used to mould small laminates

The mould is designed to represent pultrusion mould conditions to provide the following loading conditions:

- a tensile load scheme is introduced on the impregnated roving by turning the screw threads in a clockwise direction. This in turn pulls the fibres tightly for proper alignment and reduces the possibility of fibres twisting around one another
- compressive load was applied on the copper mould by 10.5 kg in the form of a

steel block. This was used to apply downward pressure at the top surface of the upper copper mould. This is important as it removes all excessive resin from the mould. The process involves various iterations in consultation with manufacturer (Exel Composite Ltd. UK).

4.2.2.2. Moulding with various fabric organisations

As stated above, the E-glass was supplied by Formax Ltd. in the roving sizes, 4800Tex and 3600Tex. Each individual roving was firstly cut to a 100mm length as shown in Figure 4.4. Four glass rovings were then bound together to make a cross section of 20mm wide. The material included Atlac resin 430 (vinyl ester), TRIG C (hardener), TRIG 21 (Initiator) and other supportive materials like internal mould release agent and calcium based filler powder. Atlac 430 was mixed with the TRIG C and TRIG 21, with the mixing ratio 100:8:8, 100 parts resin by weight, 8 parts hardener by weight and 8 parts initiator by weight. This proportion is given by Exel composite Ltd. UK and resin manufacturer. Resin manufacturer (DSM Composite resin) provided a technical data sheet, which includes mechanical properties, major application, processing and other characteristics, which are mentioned in chapter 3 (See Appendix A.6).The filler powder aims to improve the moulding process and mechanical properties of the composite.

Nisar et al. [147] observed joint strength improvement by about 5% with the addition of filler. Park et al. [148] reported that smaller filler particle size can strengthen the composite. The roving impregnation into the resin mixture is shown in Figure 4.5. It was very important that some preparatory work was carried out on the mould itself before moulding started. Firstly, the jig was cleaned with the industrial cleaner LOCTITE 7063 then PTFE sheet was cut to fit inside the copper section to ensure that the resin and adhesive bits did not bond the copper mould to the steel base plate.

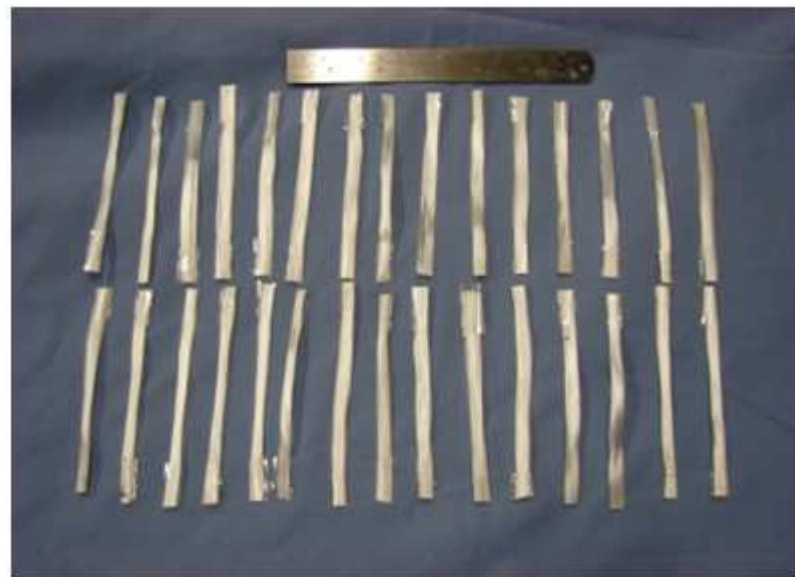


Figure 4.4: 3600/4800Tex – E-glass roving



Figure 4.5: E-glass roving impregnation

Lastly, the entire jig was sprayed with mould release agent of thin polytetrafluoroethylene (PTFE) to guarantee easy release of laminate after the curing process. Figure 4.6 shows the moulding steps of small laminates including rovings impregnation. The details of the moulding jig design are shown in Appendix B.

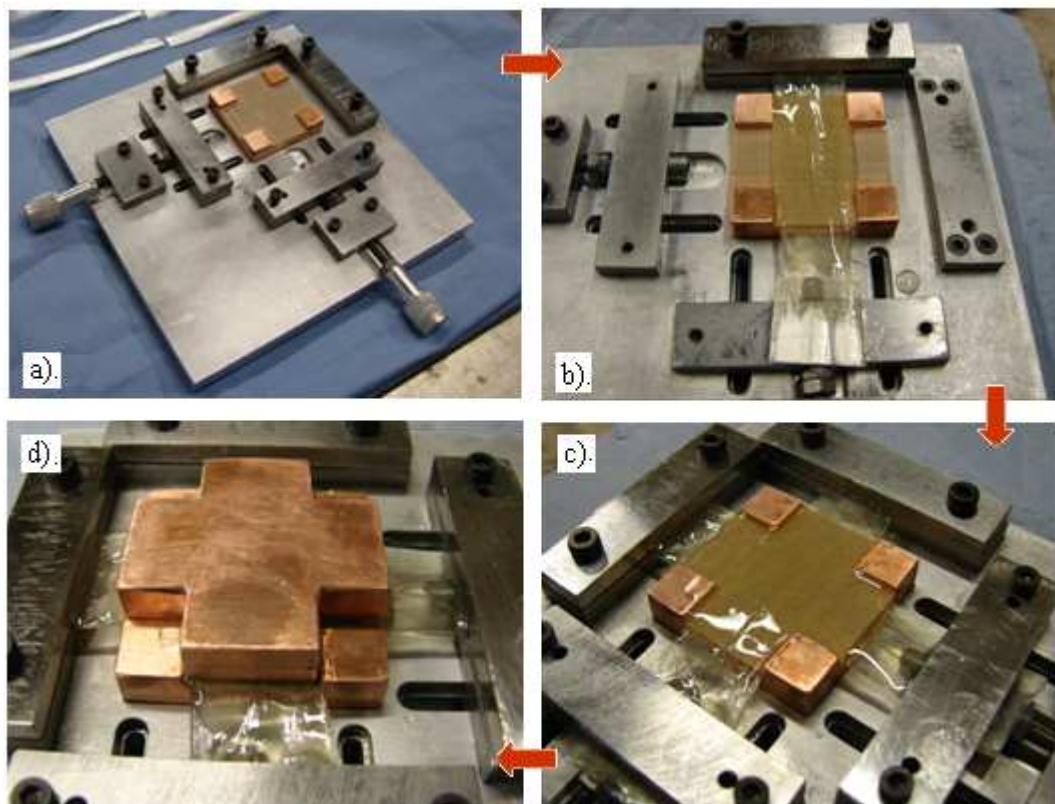


Figure 4.6: Aspects of laminate moulding: a). moulding jig, b). impregnated rovings in mould, c). 0/90 impregnated rovings in mould, d). roving clamped and compressed with upper mould

Two impregnated rovings were placed in a lower copper mould: one perpendicular to the other ($0^\circ/90^\circ$ laminate) and fixed with roving clamps as shown in Figure 4.6c. The screw threads were tightened until the fibres were seen to be almost fully aligned. The copper upper mould was then placed on top of its lower mould counterpart (see Figure 4.6d) and a 10.5kg weight (in the form of steel block) was used to provide downward pressure on the mould. This compressive load is important to control excess resin volume. The composite was cured in the oven for 45mins at 130°C . To reduce the possibility of any thermal shock, the entire assembly was left in the oven for 3-5 hours to cool uniformly; otherwise micro-cracking may have occurred. After curing, the clamps were undone and the composite was

easily removed from the mould as shown in Figure 4.7a.

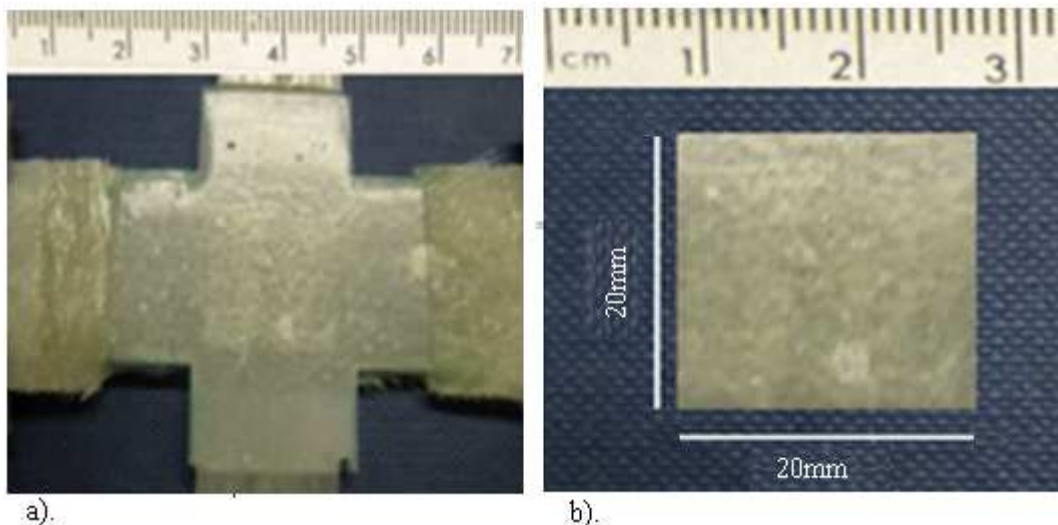


Figure 4.7: Cured $0^\circ/90^\circ$ laminate: a). after moulding, b). after trimming

Excessive edges were trimmed using a diamond cutter to obtain a 20mm x 20mm square laminate (see Figure 4.7b). In total, 10 sets of 10 specimens with various fabric organisations were made in this manner: 5 for the tensile tests and 5 for the shear tests. This was to enable a good average to be obtained. Since the specimens are quite short in length, it was important that when they were cut to size (20mm x 20mm). The edges were smooth with little abrasion to the ends of the fibre; otherwise this may have affected the strength of the final bonded specimens.

GFRP is extremely abrasive when machined [149] and so a special cutting tool was needed. The tool selected was the departmental parallel mounted diamond impregnated circular saw which was mounted in a horizontal axis milling machine. Previous studies indicate that this has proven to be the best method available and due to the quality of the surface finish, all specimens were cut in this manner. The image shown in Figure 4.8 is taken on a microscopic level of the cross section of one of the composites after it was cut to size. Little abrasion at the edges of the laminate was observed as a result of the cutting process as shown in Figure 4.8.



Figure 4.8: Microscopic image of laminate section showing fibre abrasion after cutting

Even so, the composites were still acceptable as the tearing produced was so small that it would not cause any degradation in mechanical strength and would later be covered by the surface coating. Also, since the area of interest was in the centre of the composite, these edges were not of any concern. In order to improve the quality of adhesion between the aluminium and composite, this 20 x 20mm laminate was then coated with an epoxy adhesive, prior to the start of bonding.

It is worth mentioning here that the quality of the laboratory laminates is comparable with those of the manufacturer, in terms of mechanical properties and voids content. This is discussed in detail in Chapter 6.

4.2.3 Laminates coating

To improve the quality of adhesion between adhesive and composite pultrusion, it has been proven that it is beneficial to coat the composite in a low viscosity epoxy resin and then cure, before bonding the two adherend jigs together. This low viscosity coating consolidates the fibres on the surface and subsurface. It also improves wettability by lowering the surface tension and by filling microscopic voids between the fibres. Increasing wettability of the surface increases the area of contact between the adhesive and the adherend as well as promoting molecular adhesion [4]. The coating also sealed in any loose fibres caused by cutting as seen in Figure 4.8.

The method adopted to apply the low viscosity resin was as follows:

A glass bottle was weighed accurately to 0.00005g. The scales were initialised to zero with the bottle remaining on them. Approximately 10g of epoxy resin Araldite AY103 (Huntsman) was poured (very viscous) into the glass jar. (The actual mass was 12.6802g). The scales were initialised again, and then HY 951 hardener was measured to 0.8g. This was carried out by drawing HY 951 into a syringe and gradually adding drop by drop (the actual mass was 0.7983g). The manufacturer's recommended resin / hardener ratio is in between 10:1 and 10:0.8 (see Appendix A.5). The two part epoxy resin was then mixed by a shaking process. The viscosity of the coating was less than 1mps at 25°C. This was then left to rest for 20mins to allow the adhesive to become gel form and to allow the air bubbles to rise to the top of the jar. This ensured that the resin was free from air bubbles. The bubbles could cause problems if directly applied to the composite and cured. The coating process is straight forward, but careful consideration must be taken at all times, otherwise it is difficult to get a smooth coating surface without bubbles. Figure 4.29c shows the air bubbles, which were trapped during the coating process. To remove any loose glass fibres, the composite was abraded with silicon carbide cloth (emery cloth). The composite surface was abraded 10times in one direction and 10times in the cross direction, then against the fibres 10times. This also helps to remove the mould release agent used in the moulding process.

The composite specimens were then cleaned with LOCTITE 7063, which is a general purpose industrial solvent for cleaning and degreasing surfaces. This removed graphite pencil marks and human finger prints, which contain oil. One side of the composite was coated with the epoxy resin using a paint brush. This coated surface was then placed wet side down onto Teflon coated steel plate to allow the resin to pool out and to ensure a consistent even coating. The coated specimens were then placed in the oven to cure at 100°C for 20mins after which the oven was turned off and the specimens were left to cool for 5hrs. This was again aimed at reducing the possibility of thermal shock to the specimens.

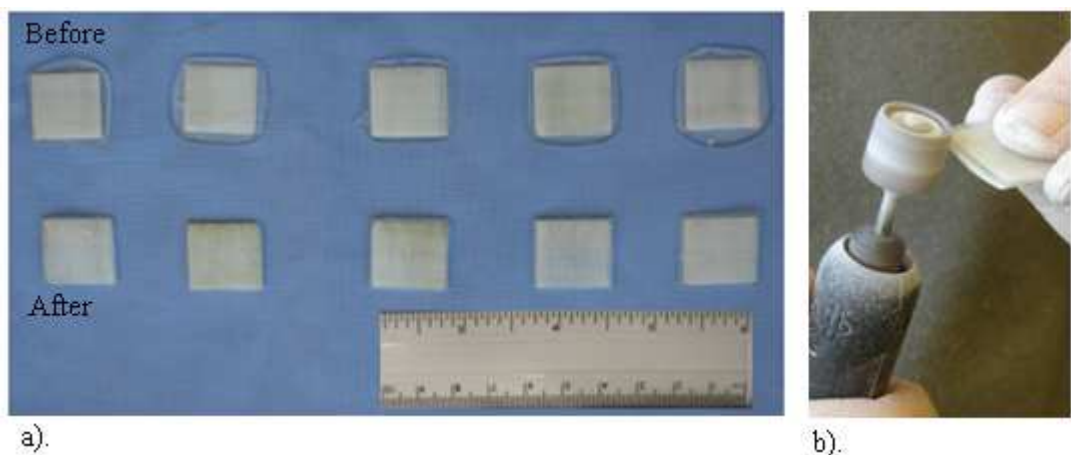


Figure 4.9: GFRP specimens: a). before and after resin coating, b). edge smoothing

This procedure was repeated for the other side of the composite. Finally the excess epoxy resin, that was a result of the resin pooling, was machined off using a small rotary sanding tool called the DREMEL® as shown in Figure 4.9a, b. Special care was taken not to damage the composite/coating and ensured that the tool vibrations were minimal. The thickness of the composite was measured before and after coating and the average thickness of coating was 0.162mm with a standard deviation of 0.035mm. To assess the quality and effect of coating, the shear specimens were tested in the same manner, detailed in section 4.3.1.

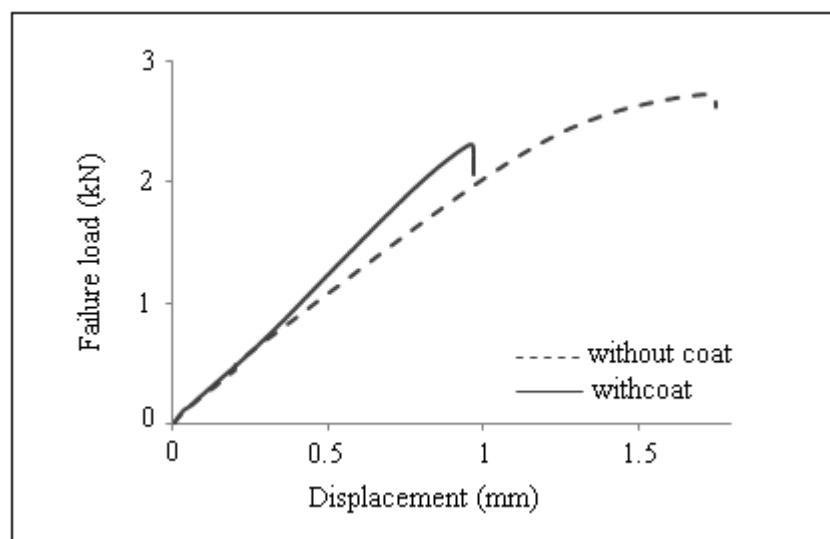


Figure 4.10: Load-displacement curve for shear specimen:
a). before, b). after the application of epoxy coating (also see Figure 4.1)

Figure 4.10 shows the load-displacement curves for coated and uncoated surface joints. This clearly indicates the effectiveness of coating prior to bonding.

4.2.4 Laminates adhesive bonding

4.2.4.1 Design and manufacturing of bonding jig

For the bonding of small laminates, there was always the issue of eccentric alignment between the upper and lower adherend of both shear and tensile specimen. C-clamp and macro jigs (for big joint bonding) were employed in early fabrication to achieve perfect eccentricity alignment but significant variation between results was found using the same configuration specimens with these bonding jigs. Appendix B.2 illustrates the meso-scale bonding jigs, where as Figure B.2.1 shows the bonding of tensile specimens and Figure B.2.2 shows the bonding of shear specimens with C-clamp jig in Appendix B.2.1. Similarly Appendix B.2.2 illustrates the macro jig (See Figure B.2.3). Bonding through these jigs is difficult due to the size of the joint and so help is always required. During the tightening process continuous help was needed to adjust the specimens by using a spatula to correct any slippage. This made it very hard to get perfect alignment. After several trial and error the alignment issue was fixed by designing jig shown in Figure 4.11. Figure 4.11a shows the tensile bonding jig whilst Figure 4.11b shows the shear bonding jig. The engineering drawing with all major dimensions of both jigs is explained in Appendix B.2.3 (See Figure B.2.3.1, B.2.3.2 for tensile and Figure B.2.3.3, B.2.3.4 for shear bonding jig). These jigs are necessary to achieve accurate alignment of adhesive joints and uniform adhesive bondline thickness. Further sub parts of both tensile and shear bonding jigs are shown in Figure 4.11.

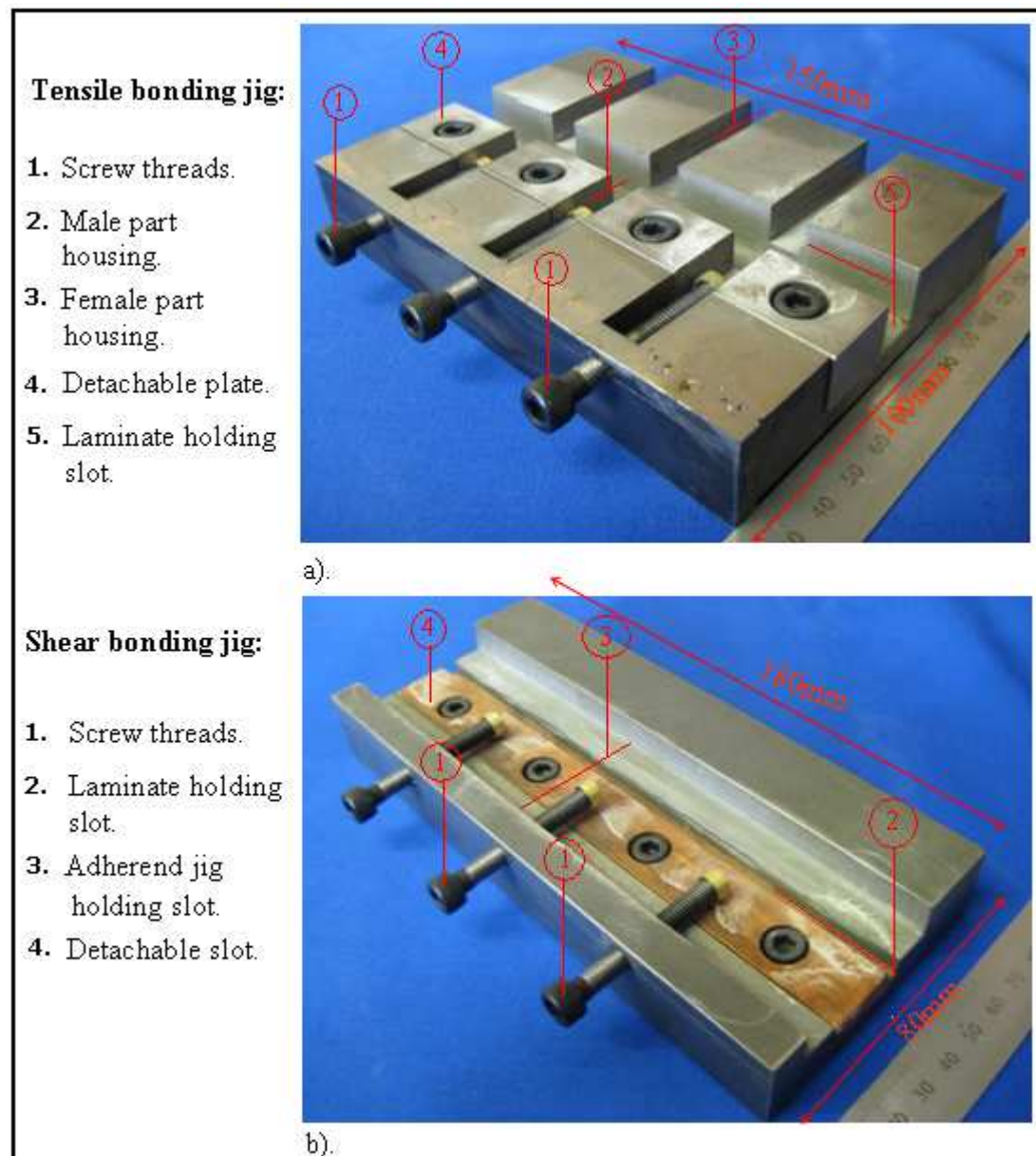


Figure 4.11: Small laminate bonding jig: a). tensile specimens, b). shear specimens

4.2.4.2 Bonding of laminate

This section explains the adhesive bonding of the laminates to the aluminium adherends. This involves sandwiching the thin laminates between two aluminium adherends to form shear or tensile adhesive bonded specimens (see Figure 4.1). The bonding process involved surface preparation, adhesive application, clamping and curing. Surface preparation was carried out to British Standards [150]. The standard states that aluminium is required for proper cleaning prior to bonding. Aluminium has a very thin oxide surface layer that would firstly need to be removed otherwise there may be interfacial problems between the adhesive and the aluminium. In addition, Huntsman [151] provided a general guide about the surface preparation procedure.

The main reasons for surface preparation are as follows:

- to remove and prevent any weak boundary layer on adherend (oxidising layer, grease/oil)
- to maximise the close molecular contact between the adhesive and the adherend during bonding
- to provide the plane surface, that is microscopically rough.

The shear and tensile aluminum adherends were lightly sand blasted and the composite was light abraded prior to bonding. Degreasing the surfaces before and after blasting was done to avoid the contamination of blasting agent, aiming to improve blasting efficiency [152]. Grit size 30/40 mesh was used. A Guyson blast cabinet was used for specimen grit blasting. A blast pressure of 80N/cm^2 was applied through the blast gun. The average distance between the blast gun and adherend surface was about 50-70mm from the gun perpendicular to the blast surface. Blasted adherend surfaces were cleaned using compressed air to ensure the removal of all loose particles. Finally the adherend surfaces were degreased with LOCTITE 7063 cleaner. The edges of the composite were then marked to aid alignment when bringing the bond surfaces together. The aluminum adherends were specially designed to ensure the load transfer directly to the centre of the composite. Minimum alignment effort was required between adherend and composite during bonding. The details of the adherend can be located in Appendix B.4 (see Figure

B.4.1) for shear and for tensile (see Figure B.4.2). The tensile or shear configurations were bonded to the GFRP specimens using the adhesive Araldite® 2015.

The adhesive was mixed by the means of a mixing nozzle attached to the cartridge and then, through a specially designed adhesive gun, the adhesive was squeezed from the cartridges into a plastic mixing tray. To confirm the adhesive was well mixed, a wooden spatula was used. The adhesive was then generously applied using a spatula to both faces of the laminate. One side of upper aluminium adherend and lower aluminum adherend were then placed, and primarily aligned, with the upper adherend using the help of a marked point made at the edges of the GFRP laminate. The schematic details of the shear and tensile specimens are shown in Figure 4.12a, b. thin polytetrafluoroethylene (PTFE) sheeting was applied to one of the aluminum adherends. This was to ensure that the bond area was 10 x 10mm as shown in the figure.

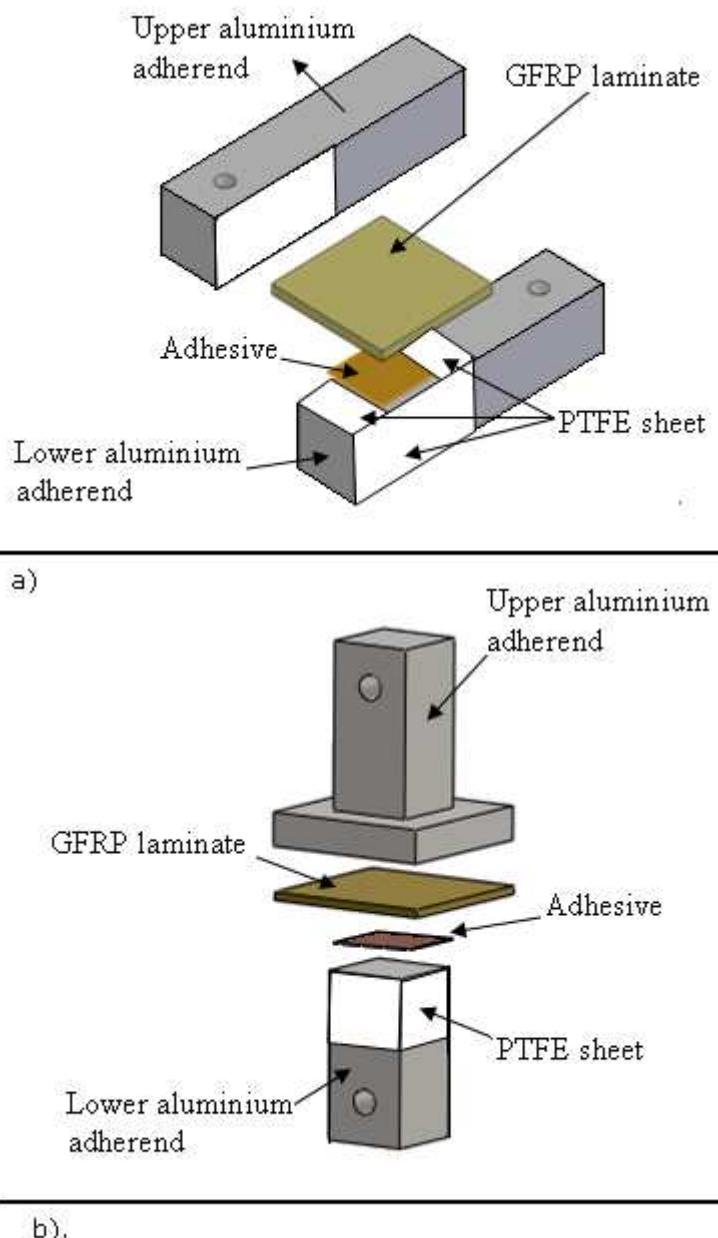
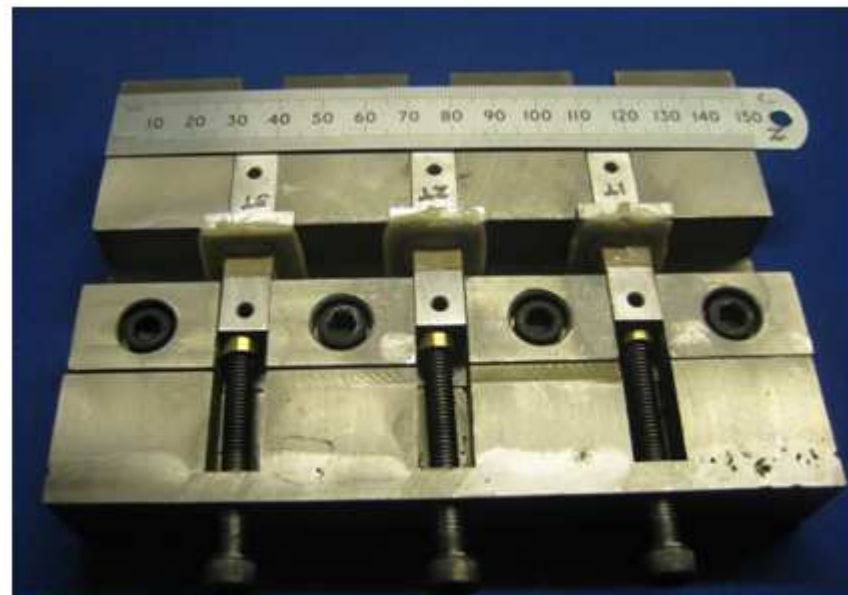


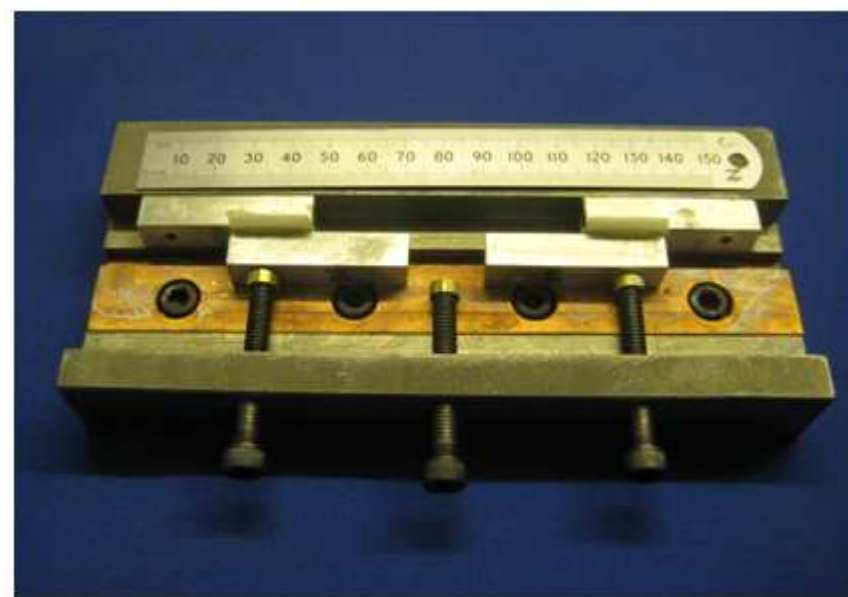
Figure 4.12: Bonding specimen: a). shear, b). tensile

The adhesive thickness was physically controlled by the thickness of the PTFE sheet, which is 0.15mm. This resulted in a normal bondline thickness of 0.2mm. Finally after the application of adhesive and the primary attachment of adherend jigs with the laminate was complete the space between the top surface of the upper adherend and the lower surface of the lower adherend was measured with a depth micrometer to make sure the adhesive bondline had even thickness. It was important to ensure that the adhesive was applied effectively at the edges to ensure good adhesion, where high stresses were likely to occur. The joint was then assembled in the bonding jig.

A modest clamping force was applied to the test specimens. This ensured the adhesive was distributed evenly and at a constant thickness. The joints were already eccentrically aligned by using a specially designed bonding jig as shown in Figure 4.13. Once sufficient force was applied through screw threads, the clamping jig was placed into an oven at 85°C for 1hr. This was to ensure the specimen temperature in the bondline was about 80°C. After 1hr, the oven door was left open and was allowed to cool naturally for at least 5hrs. This was in order to reduce the risk of residual stresses caused by rapid cooling. Due to tightening the jig, excess adhesive had spewed out the sides of the specimens, particularly on the upper adherend (see Figure 4.14). It was important to remove this excess adhesive as it would have caused localised stiffening around the edges and affect the results. The DREMEL® grinding tool was used to remove the excess adhesive, especially from the edges of the shear specimens.



a).



b).

Figure 4.13: Curved bonded specimen in bonding jig:
a). tensile specimens, b). shear specimens



Figure 4.14: Bonded specimens showing 20 x 20mm laminate bonded between adherend jig: a). tensile specimen, b). shear specimen

4.3 Experimental testing and results

4.3.1. Experimental testing

The shear and tensile specimens were tested under monotonic tensile loading with the Zwick/Roell tensile testing machine. This is a constant rate displacement machine. All experimental tests were performed at a constant cross head speed of 0.5mm/min at ambient temperature. Figures 4.15a, b show the tensile and shear specimens with clamping and alignment adaptors during testing. The clamping adaptors were used to ensure the specimens were more effectively held in the tensile testing machine. Details of shear and tensile clamping adopters are shown in Appendix B.3 (see Figure B.3.1 and B.3.2). As discussed earlier the alignment issue was overcome to some extent by proper design of shear and tensile aluminum adherends. Further alignment was controlled through an alignment adapter used, when inserting new specimens after the end of each test. The

details of the alignment adaptor are shown in Appendix B.3.3 (see Figure B.3.3). To secure the bonded specimens during clamping to the adaptors, two high strength steel pins were used instead of screws. This reduced the possibility of a twisting affect on the bonded laminate, which would occur during the tightening of screws. Steel pins were chosen on the basis that high shear stresses would manifest around the holes and therefore it was important to ensure that the pins were stronger than the specimens in order to guarantee that they did not yield at any point during the test.

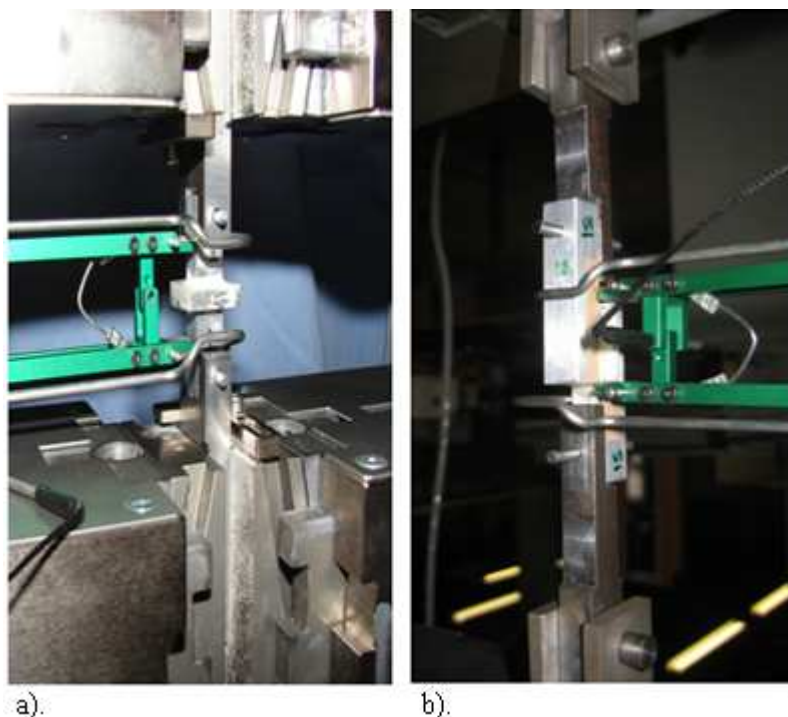


Figure 4.15: Meso-scale specimen during clamping into testing machine:
a). tensile, b). shear specimen

An external extensometer was attached along the joint overlap (see Figure 4.15) for displacement measurement. Besides the external extensometer, there was also a cross-head extensometer in the testing machine. Slight deviation in reading was found between both extensometers, so the reading obtained from built-in extensometer was ignored. The steps of test procedure are as follows:

- the experiments were conducted at room temperature (about 18-22°C). All dimensions of testing specimen were checked and necessary calculations done prior to the start of testing to avoid unusual disturbance. The calculation of the

cross-sectional area of each specimen, prior to testing, helps to get a rough idea about yield load

- prior to the start of the test, the width and thickness of each specimen was measured, as this data is used as an input into the testing machine software
- to ensure thorough visual inspection that the central axis of both test specimens and testing machine grips are aligned
- the machine grips were tightened uniformly to avoid slippage between grip and specimen
- all devices, including software installed PC, were checked and calibrated accordingly
- the cross head speed was set at 0.5mm/min.

Typical graphs for shear and tensile LL specimens are shown in Figure 4.16 and 4.17. Both graphs show the force–displacement curve of three out of five specimens. In addition the average failure load is also mentioned in figures. Graphs for other test specimens are shown in Appendix B.6. Figure B.6.1.1 to B.6.1.4 for shear (see Appendix B.6.1) and Figures B.6.2.1 to B.6.2.4 for tensile specimens (see Appendix B.6.2).

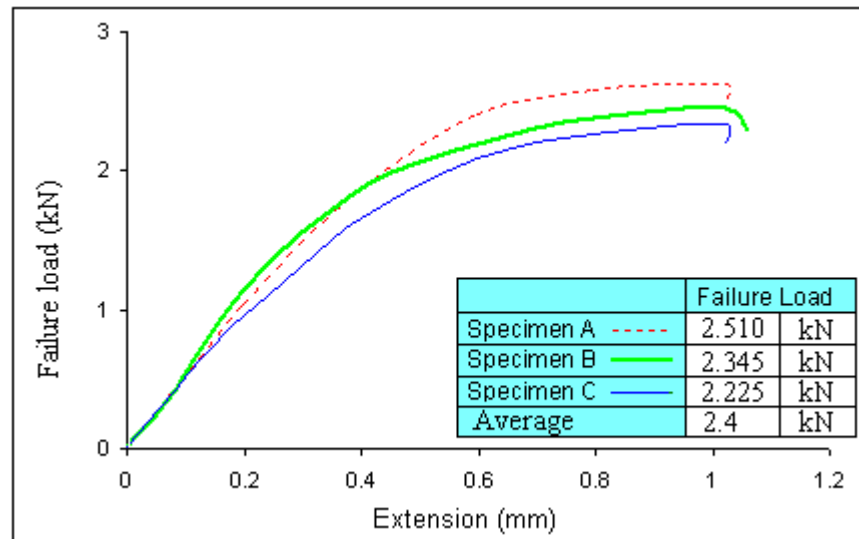


Figure 4.16: Failure load Vs extension curve of LL shear specimen

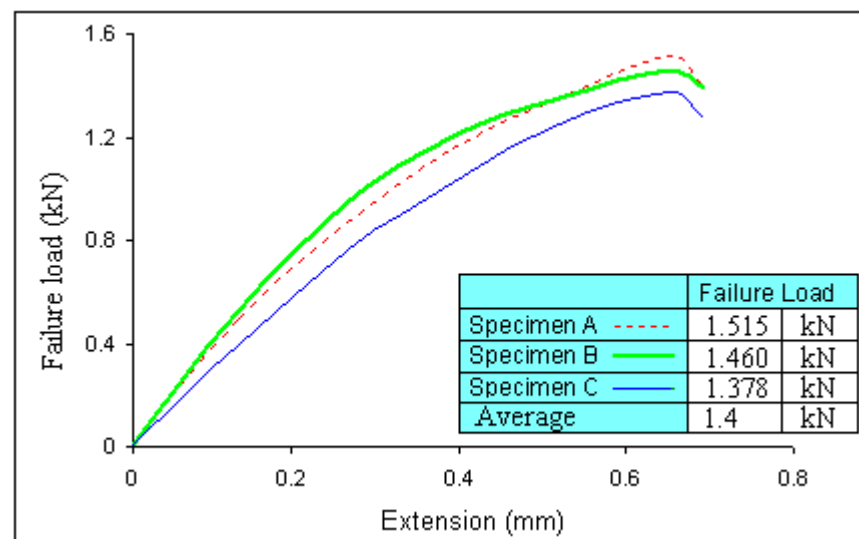


Figure 4.17: Failure load Vs extension curve of LL tensile specimen

4.3.2. Experimental results

Table 4.1, Table 4.2 and Figure 4.18 summarise the results of experimental testing of both shear and tensile specimens.

| | Specimen type | | | | | |
|------------------------------------|----------------------|-------|------|-------|------|-------|
| | Units | LL | LT | RL | WR | IR |
| Laminate thickness without coating | mm | 1.07 | 1.06 | 1.05 | 1.06 | 1.06 |
| Laminate thickness with coating | mm | 1.39 | 1.38 | 1.38 | 1.38 | 1.39 |
| Thickness of coating (one side) | mm | 0.16 | 0.16 | 0.165 | 0.16 | 0.165 |
| Thickness of adhesive | mm | 0.23 | 0.21 | 0.20 | 0.23 | 0.22 |
| Failure load | kN | 2.4 | 2.06 | 1.6 | 2.2 | 2.6 |
| Maximum extension | mm | 1.04 | 0.98 | 0.79 | 1.03 | 1.05 |
| Standard deviation | kN | 0.2 | 0.27 | 0.15 | 0.1 | 0.1 |
| Average strength | MPa | 24 | 20 | 19 | 22 | 26 |
| Fibre content | UD (Uni-directional) | % vol | 65 | 65 | 65 | 65 |
| | Random | % vol | -- | -- | 63 | 63 |

Table 4.1: Experimental results of shear specimen

| | Specimen type | | | | | |
|------------------------------------|----------------------|-------|-------|-------|------|------|
| | Units | LL | LT | RL | WR | IR |
| Laminate thickness without coating | mm | 1.07 | 1.05 | 1.06 | 1.06 | 1.07 |
| Laminate thickness with coating | mm | 1.39 | 1.38 | 1.39 | 1.38 | 1.38 |
| Thickness of coating (one side) | mm | 0.16 | 0.165 | 0.165 | 0.16 | 0.16 |
| Thickness of adhesive | mm | 0.20 | 0.23 | 0.20 | 0.21 | 0.20 |
| Failure load | kN | 1.4 | 1.4 | 1.0 | 1.4 | 1.8 |
| Maximum extension | mm | 0.69 | 0.64 | 0.41 | 0.57 | 0.73 |
| Standard deviation | kN | 0.15 | 0.19 | 0.24 | 0.1 | 0.1 |
| Average strength | MPa | 14 | 14 | 10 | 14 | 18 |
| Fibre content | UD (Uni-directional) | % vol | 65 | 65 | 65 | 65 |
| | Random | % vol | -- | -- | 63 | 63 |

Table 4.2: Experimental results of tensile specimen

The following remarks are relevant:

- all the values used in tables and figures were taken as average values of three out of five specimens
- consistency in adhesive thickness in all specimens was achieved with the help of the bonding jig. The thickness varied between 0.01-0.03mm
- different configurations laminates were achieved after trial and error with less variation in thicknesses with the help of a moulding jig, balanced pulling and compressive force on the roving. The thickness varied between 0.03-0.04mm
- the results clearly demonstrate that the LL configuration have a higher failure load in both shear and tensile specimens than LT and RL. Most like the LL specimen have double strength in a longitudinal direction. Other reasons are given in the discussion chapter
- the RL configuration have significantly lower failure loads than others in both shear and tensile specimens. A possible reason is the poor longitudinal and transverse strength of random fabric. Further details are given in the discussion chapter
- the IR specimens exhibited the highest strength for both the tensile and shear specimens
- the shear strength improvement of the IR model over RL, LL, LT and WR are about 62%, 10%, 26% and 18% respectively. Perhaps using smaller Tex rovings, as well as having UD fabric along the loading direction in the case of IR, is the reason for this improvement
- the tensile strength improvement of IR over RL, LL, LT and WR is about 28% and the improvement of IR over RL is about 44%. The tensile failure is possibly less sensitive to the roving orientation but more so for the random fabric
- a significant difference in failure load was found between shear and tensile testing results, because the tensile specimen is more sensitive to testing than the shear specimen. Shear specimen has combined shear and transverse loading,

which suppress transverse stresses in composite, but the tensile specimen is dominated by transverse loading only

- another possibility for this difference is the issue of voids that were evident from the microscopic examination. Voids are perhaps more critical to failure in tension than in shear loading. When the composites were subjected to shear loading, some areas of the specimens would actually be under compression. These compressive forces would close up any voids and hence the specimens would be more resilient to failure
- although the standard deviations are relatively small for many specimens (see Figure 4.18) they were discarded due to poor moulding at an early stage
- the causes for the results deviations are likely to be the effects of voids and possible misalignments of specimens
- IR and WR specimens exhibit less failure load deviation than LL, LT, RL specimens (see Figure 4.18). A likely reason is that LL, LT, RL specimens used higher Tex roving (4800Tex) and IR and WR specimens are based on smaller Tex roving (3600Tex)
- higher Tex roving had a higher population of voids than smaller Tex. This conclusion was made after several microscopic observations
- the average tensile and shear strength in the laminates are obtained from dividing the failure load by the bond area or the delamination area beneath it.

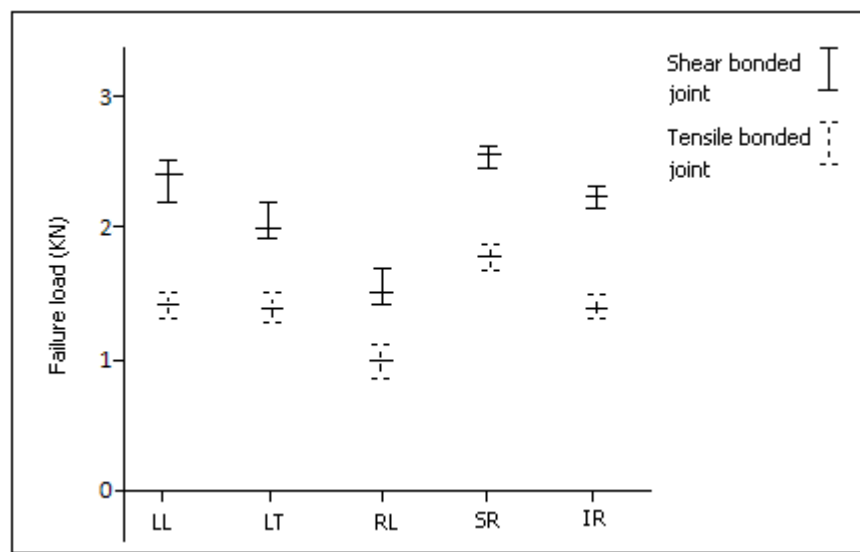


Figure 4.18: Failure strength variation of meso tensile/shear bonded joint with respect to different fibre architecture

4.4 Failure mechanism

The joints were designed and produced to ensure that failure initiates at specific locations, nearer the edge of the joints. However, it is extremely difficult to determine the exact locus of failure because this often happens in a brittle and sudden manner. Examination of fracture surfaces of the specimens suggests three types of failure, which are as follows:-

- intralaminar - transverse (out-of-plane or peel) failure within the laminate surface just below the coating resin layer. This is referred to as transverse failure
- interlaminar - transverse and shear failure at the resin separating the two layers/plies. These is referred to as interlaminar failure
- longitudinal - tensile failure along the laminate. This is may be limited to WR and RL shear specimens.

4.4.1. Failure of shear specimens

As mentioned previously, in the experimental set-up, PTFE tape was used on one of the aluminium adherends so that the bond area of the composite was restricted to 10 x 10mm. This appeared to be successful for most of the specimens which showed a failure occurring only within this restricted area. Figures 4.19-4.23 show the failure surfaces of different shear specimens . Therefore edge effects were assumed to be minimised in that respect. The images below show all fracture modes (intralaminar, interlaminar and mixed). The shear joints were designed to ensure that failure initiates at the edge of the joints, as indicated on the figures. Due to the adhesive coating strong interface, failure proceeds below the coating layer and then propagates deeper into filaments of the composite upper ply. This is perhaps due to voids/micro defects or fibre/matrix interface failure. The LL specimen failed in intralaminar mode at the surface level as shown in Figure 4.19. Some specimens delaminated by the intralaminar fracture as shown in Figure 4.20 for LT specimens. In LT, the longitudinal roving as a surface roving, takes a high proportion of the loading as compared to the transverse rovings beneath it.

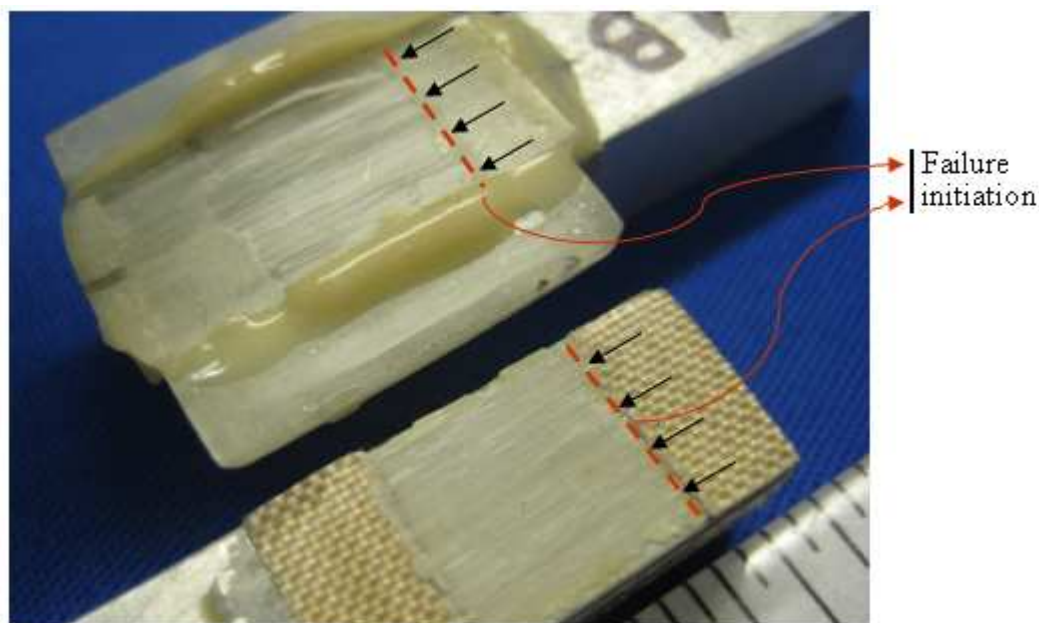


Figure 4.19: Intralaminar fracture mode of LL specimen

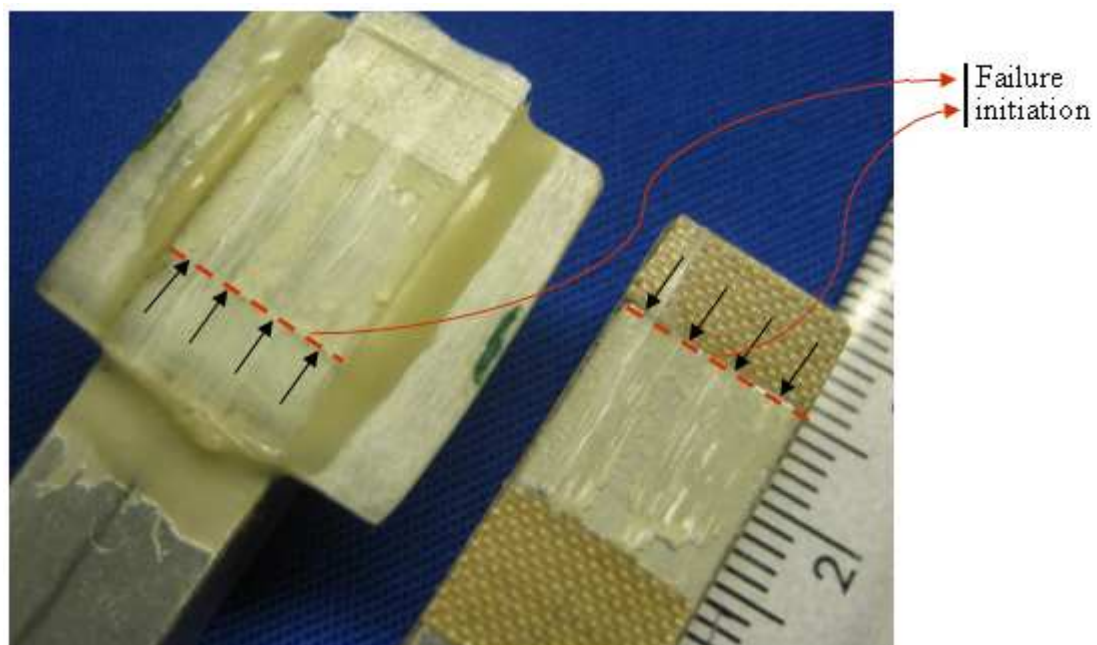


Figure 4.20: Intralaminar fracture mode of LT specimen

The RL specimen showed an intralaminar failure mode (see Figure 4.21) and this is likely due to the random fabric being quite weak in transverse directions. This, along with many other factors (see discussion), was more than likely the cause of the specimen failing at such a low load. Interlaminar failure modes were observed in IR and WR specimens as shown in Figure 4.22 and 4.23.

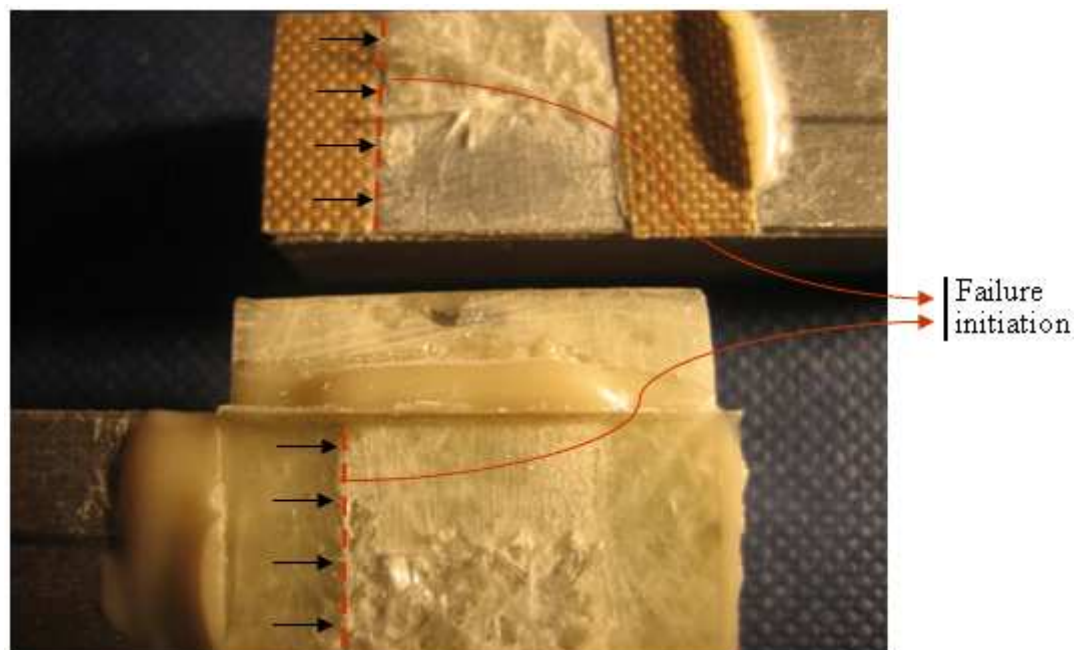


Figure 4.21: Intralaminar fracture mode of RL specimen

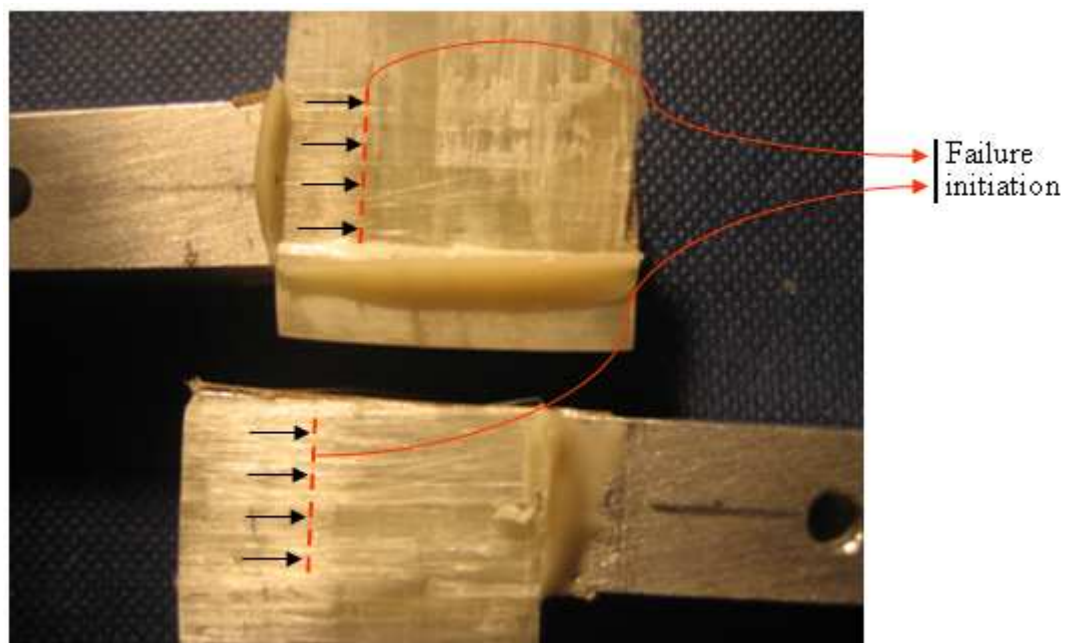


Figure 4.22: Interlaminar fracture mode of WR specimen

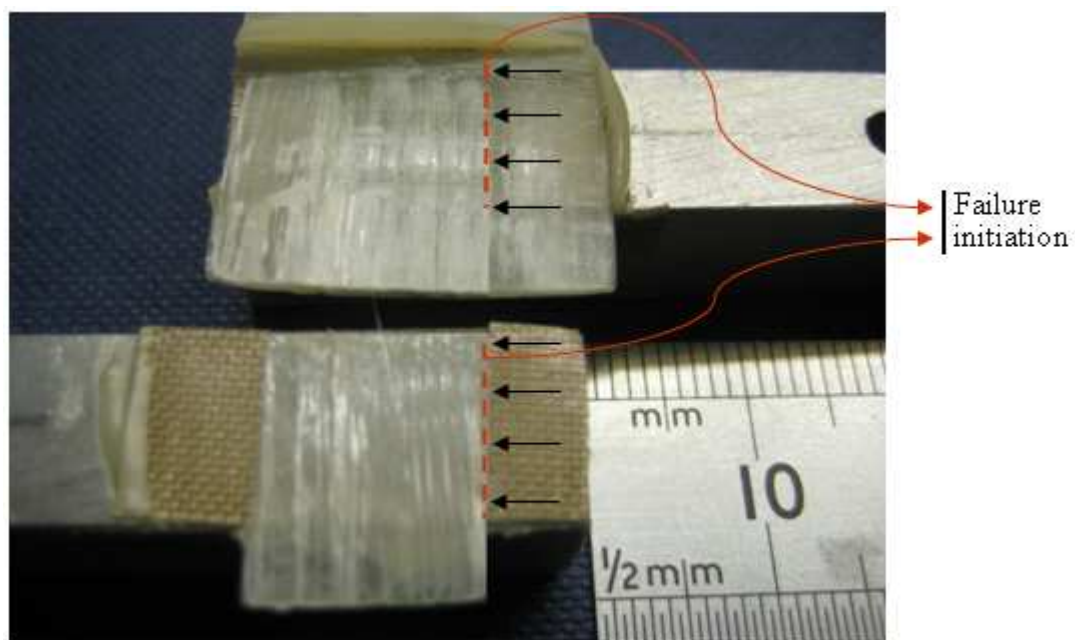


Figure 4.23: Interlaminar fracture mode of IR specimen

4.4.2. Failure of tensile specimens

The failure surfaces for the tensile specimens are shown in Figures 4.24-4.28. Again most of these specimens showed intralaminar failure in LL, LT, RL (see Figure 4.24, 4.25, 4.26). The WR and IR specimens seem to have failed by mixed mode, perhaps mostly interlaminar (see Figure 4.27, 4.28). Delamination was limited to the 10x10mm area. This was achieved by reducing the edge effect in the tensile specimens. Even though the failure mode in the tensile specimens was similar to shear specimens, the failure load in the tensile specimens was significantly lower than shear specimens. As seen from Table 4.2 the failure loads of the five fabric organisations had some variation. A likely reason, as discussed previously, is that tensile specimens are more sensitive to testing than shear specimens. The shear specimens have combined shear and transverse loading, which reduce the effect of transverse stresses on composite, whilst tensile specimens are dominated by transverse loading only.



Figure 4.24: Intralaminar fracture mode of LL specimen

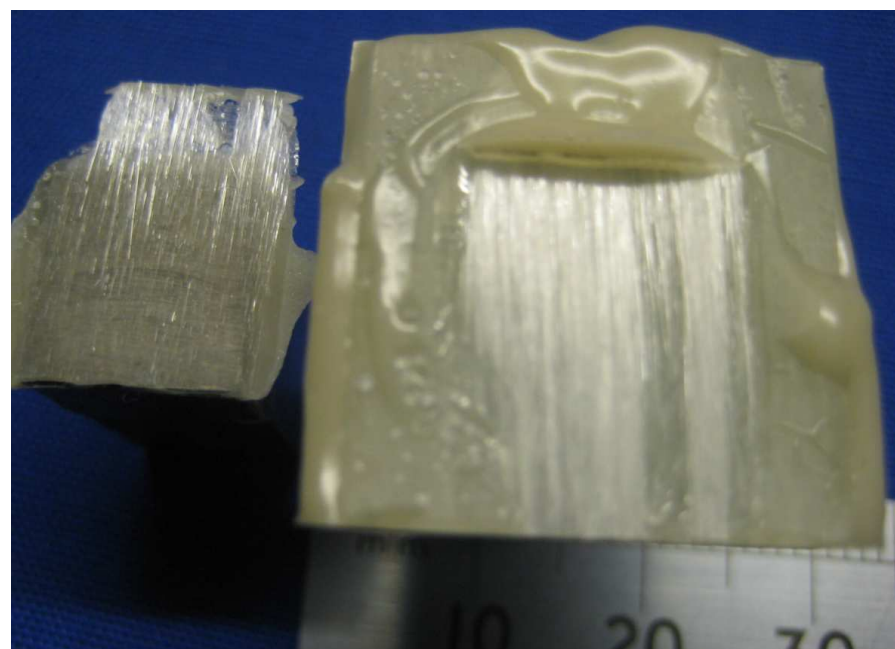


Figure 4.25: Intralaminar fracture mode of LT specimen

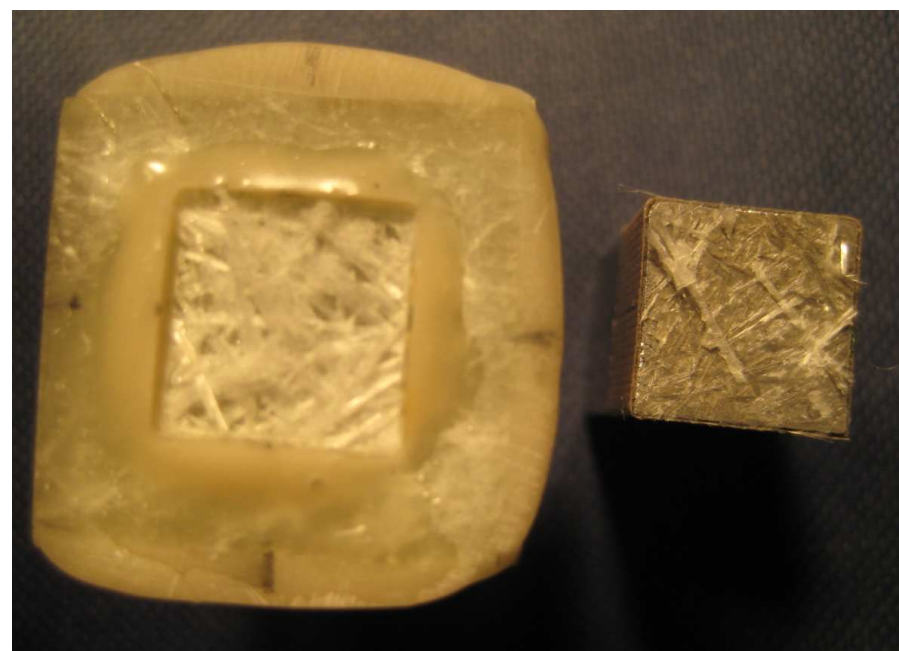


Figure 4.26: Intralaminar fracture mode of RL specimen

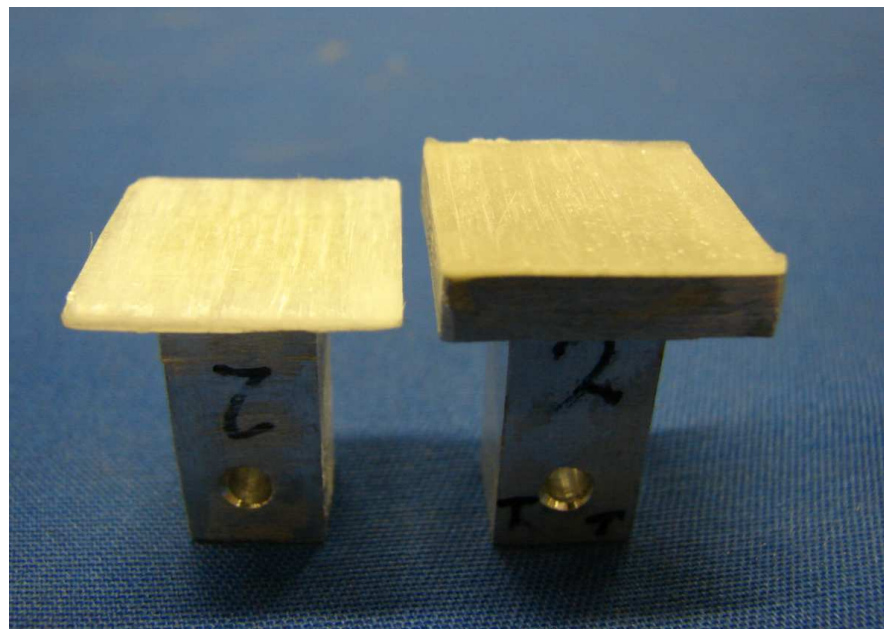


Figure 4.27: Interlaminar fracture mode of WR specimen



Figure 4.28: Interlaminar fracture mode of IR tensile specimen

4.5 Microscopic investigation

Following on from the experimental work, microscopic investigations were utilised to gain a better understanding of how the specimens failed. They aimed to examine the possibility of any voids or any other defect that may have caused premature failure in some of the specimens.

Firstly the surface topology of the coated specimens was examined in order to see if it had filled in any surface flaws on the GFRP specimens. The images in Figure 4.29 show the effects of the surface coating. As seen from the figure, the coated specimen is homogenous and the surface topology is smooth. However Figure 4.29c shows small air bubbles trapped on the surface.

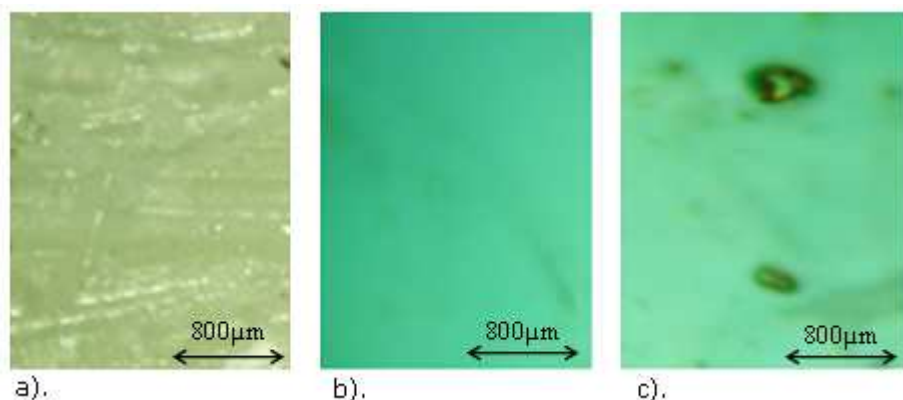


Figure 4.29: Microscopic images: a). before, b) after the application of epoxy coating, c). air bubbles on coating surface

On the other hand, although the coating was aimed at filling any surface flaws, there was no doubt that each GFRP specimen would not be free of sub-surface flaws which may have a more damaging affect. As a consequence, it was important to examine both the cured laminate and the fractured samples under the microscope. This helped to investigate to what extent these sub-surface flaws have contributed to the brittle fracture of the specimens.

The microscopic image shown in Figure 4.30 is the polished section cut from the cured LL laminate before fracture. The figure shows the presence of voids/micro-defects in pseudo GFRP composites. The highlighted circle indicates void, rectangles are resin rich areas and

ovals are defects. It can be deduced that the sizes of these voids are quite significant when compared to the size of a single filament. In addition, there are resin rich areas which signify irregular packing of the fibres. The oval in Figure 4.31 indicates another kind of voids around the fibres. Figure 4.32 shows typical failure in laminate. These failure modes are influenced by voids/micro defects within the fibre/matrix interface as shown in Figure 4.31.

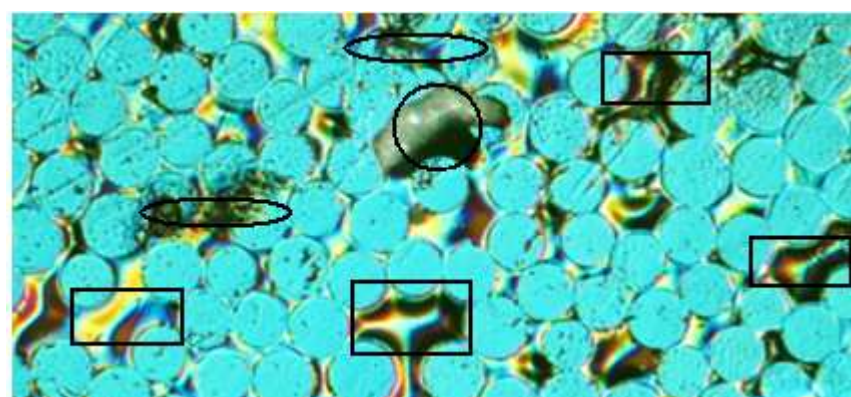


Figure 4.30: Microscopic image of cross section through the thickness of LL laminate

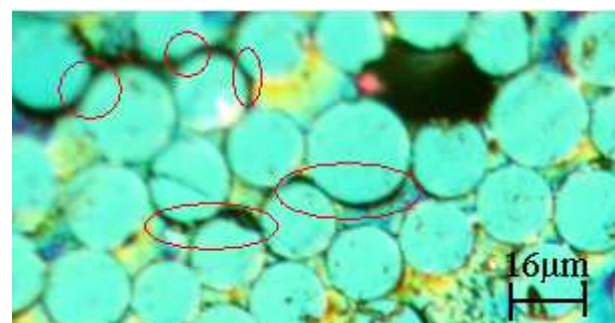


Figure 4.31: Closer microscopic image of cross section through the thickness of LL laminate

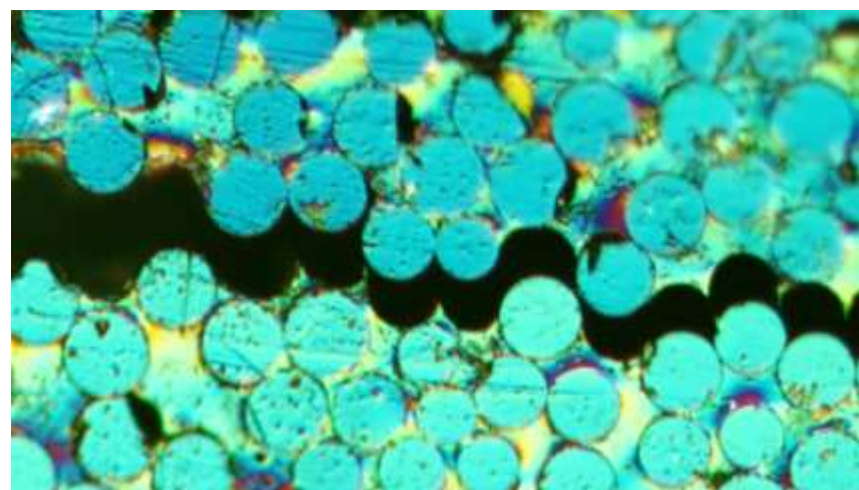


Figure 4.32: Fracture mode within laminate

4.6 Macro-scale DLS joints

4.6.1 Production of specimens

A DLS joint was bonded and tested. Figure 4.33 shows the details of the joint. The inner adherend is based on pultrusion provided by Exel Composite Ltd.

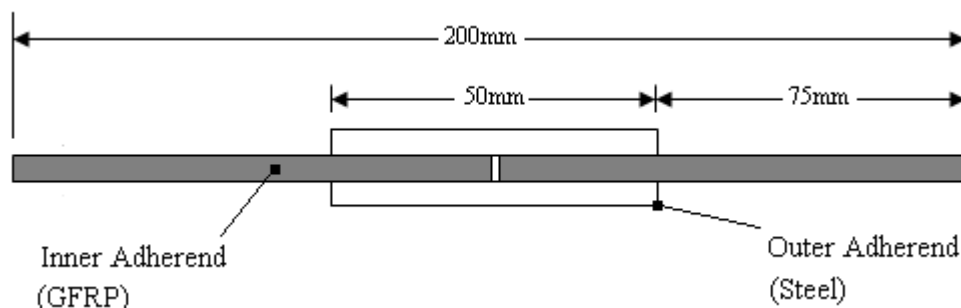


Figure 4.33: Geometry of DLS hybrid joint

A composite section with a 'dog bone shape' profile, of dimension 25mm wide and 5mm thick (see Figure 4.34 and 4.35) was provided by the manufacturer. These sections were then machined to a uniform thickness, removing the surface veil and continuous strand mat to leave unidirectional fibres. This also removed the mould release agent.

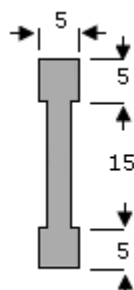


Figure 4.34: Composite material section

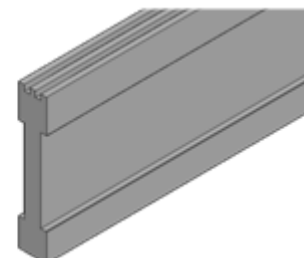


Figure 4.35: Composite material pre-machining

The final thickness of the uni-directional composite strips was 3mm. The uni-directional GFRP adherends were then cut to the required length using a parallel mounted diamond impregnated circular saw blade mounted in a horizontal axis-milling machine. The method adopted for coating the macro-scale joint was the same, as the method used for the meso-scale joint (see section 4.2.3). Aspects of the coating are shown in Figure 4.36. The thickness of the composite was measured before and after coating, and the average

thickness of coating was 0.144mm with a standard deviation of 0.035mm. The exact thickness of each specimen is tabulated in Table 4.3.

| Outer adherend | | Average thickness | | | | Average failure load | Standard deviation | Fibre content |
|----------------|---|-------------------|---------|-------|----------|----------------------|--------------------|---------------|
| | | Composite | Coating | Steel | Adhesive | | | |
| Units | | mm | mm | mm | mm | kN | kN | (%wt) |
| 50 | A | 3.05 | 0.125 | 3.01 | 0.25 | 19.94 | 0.403 | 65 |
| | B | 3.11 | 0.170 | 3.00 | 0.22 | | | |
| | C | 3.07 | 0.150 | 3.01 | 0.20 | | | |
| | D | 3.08 | 0.130 | 3.02 | 0.26 | | | |

Table 4.3: Summary of experimental results of DLS joint

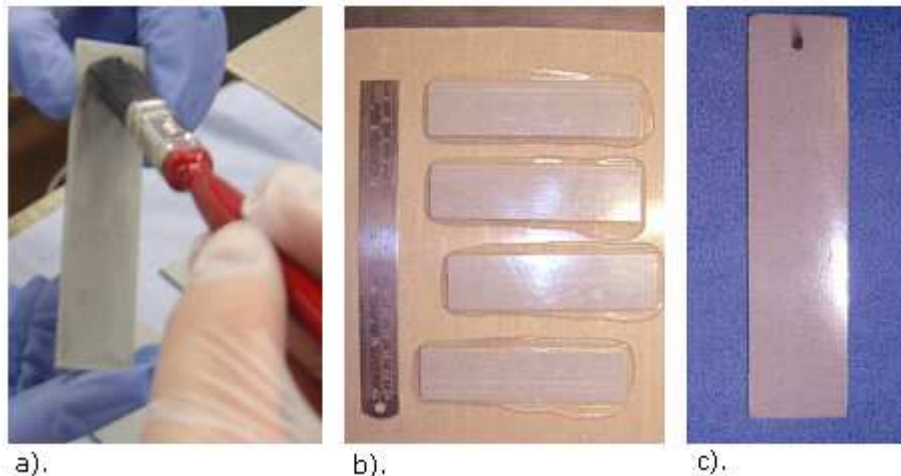


Figure 4.36: Aspects of resin coating: a) preparation, b) resin application, c). cured adherend

The adhesive bonding procedure of the macro-scale DLS joint was exactly the same as the meso-scale joint. The surface preparation procedure was well explained in section 4.2.4.2. The steel surface was prepared by grit blasting and degreasing. Following the application of the adhesive, the joints were assembled in a specially designed jig, namely macro bonding jig, in Appendix B.5 (See Appendix B.5.1), taking care to ensure good alignment. A clamping force was applied to four test specimens. This ensured the adhesive was distributed evenly and at a constant thickness. The joints were continually realigned during this clamping procedure.

4.6.2. Testing and failure examination

The mechanical testing was carried out using a Zwick/Roell Z250 tensile testing machine under a constant cross head speed of 0.5mm/min at ambient temperature. Figure 4.37 shows the test results for four specimens, with small variation in failure load. The average failure load is about 20kN. The examination of the failure surface in Figure 4.38 indicates adherend failure at subsurface the (just below the coating) – similar to failure in LL meso-scale shear joints in section 4.4.

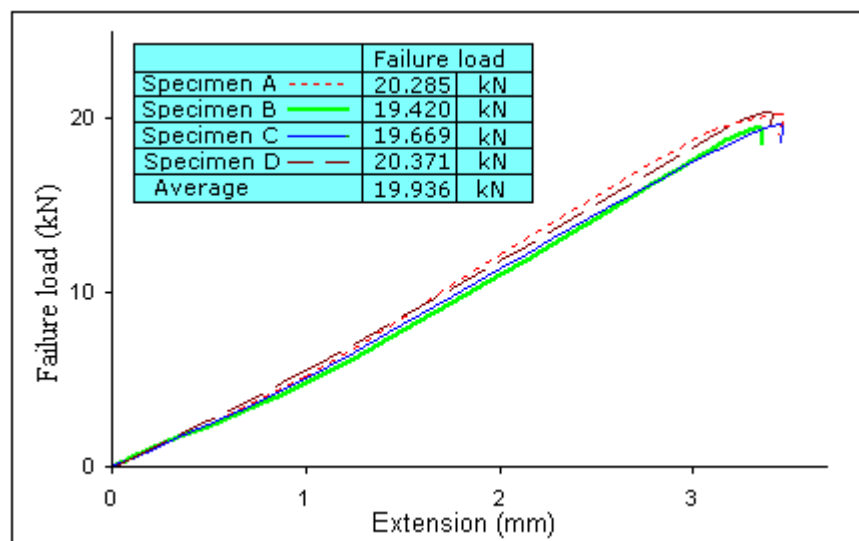


Figure 4.37: Failure load Vs extension curve of DLS joint

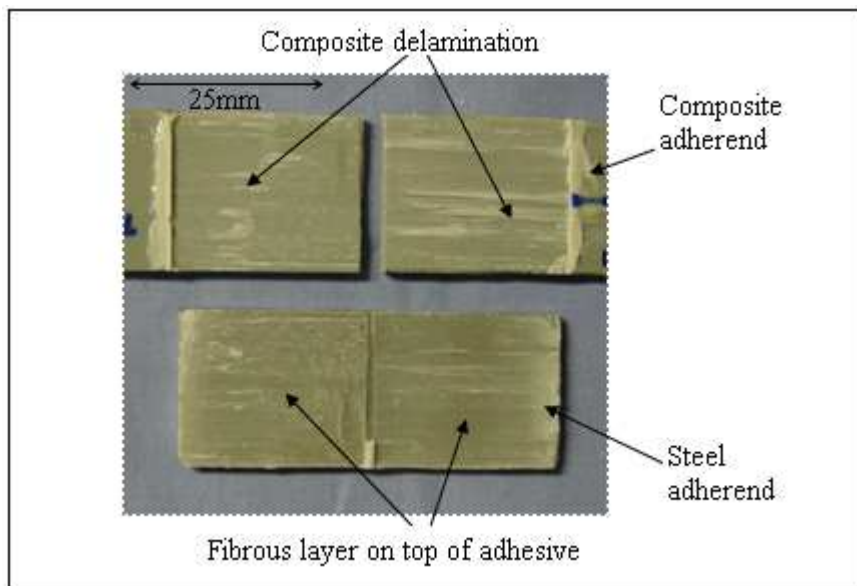


Figure 4.38: Failure of DLS joint

Figure 4.39 shows the microscopic images of polished sections cut from the manufacturer pultruded composite. These show defects and their level including voids (highlighted in circle), resin rich areas (highlighted in ovals) and defects in rectangles. It can be deduced from the figure that the level of voids/micro defects is comparable with the pseudo pultruded composite made in a laboratory.

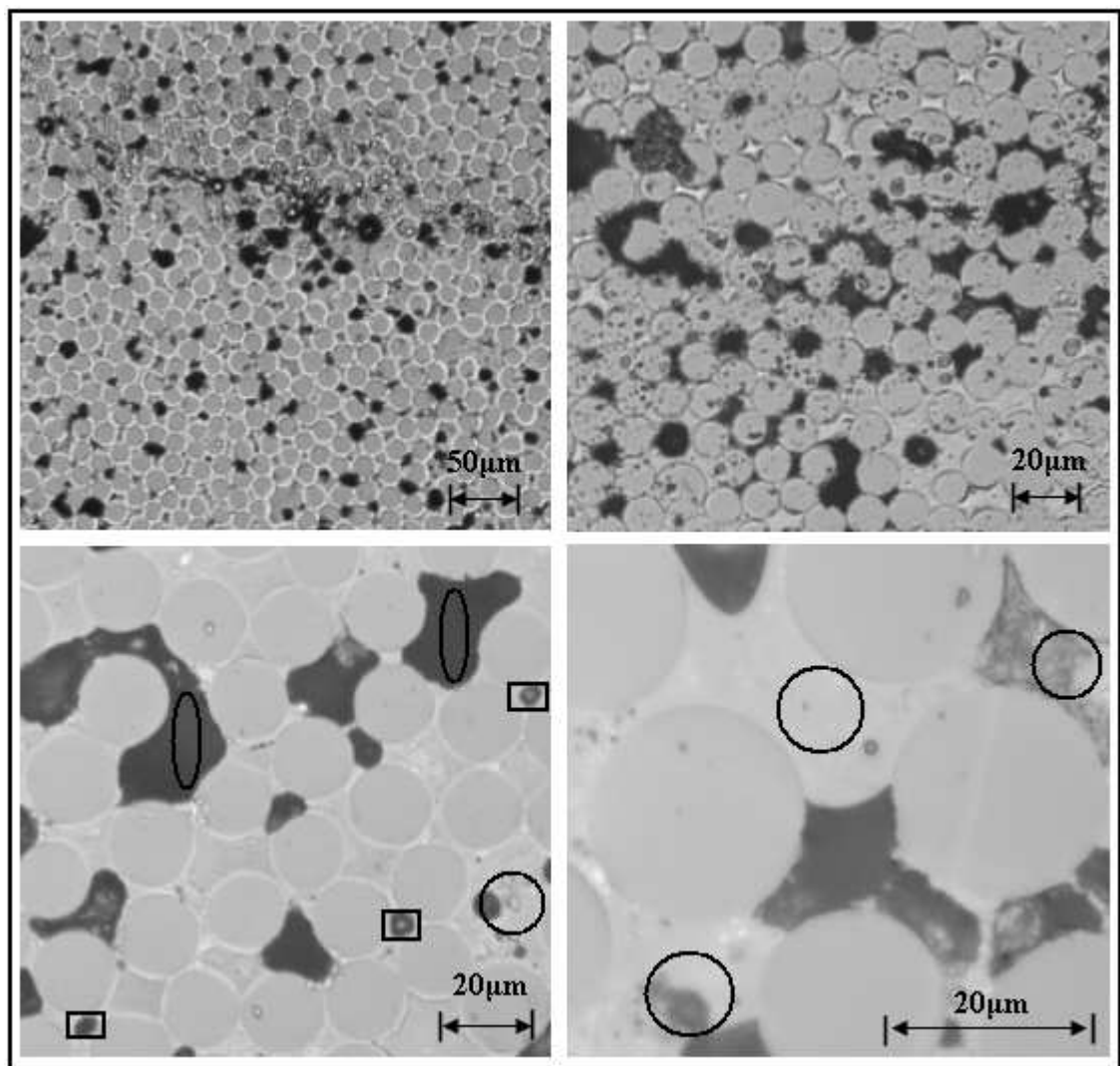


Figure 4.39: Microscopic images of cross sections through the thickness of manufacturer pultrusion

Chapter 5

Finite Element Analysis

5.1 Introduction

The chapter deals with the multi-scale modelling of pultruded joints at macro, meso and micro-scale levels. The main focus, however, is on modelling of the meso-scale bonded laminates discussed in the previous chapter taking into account their through thickness materials i.e. adhesive, coating resin, impregnated glass fabric and interlaminar matrix resin. The main aim of the modelling is to determine the critical stresses, especially transverse/peel at meso-scale level under tensile and shear failure loads. This is in order to better understand failure within standard DLS joints, which was supported by limited analysis using both macro and micro-scale models. The macro-scale model is based on a standard DLS joint and the micro-scale model is based on a single filament - matrix resin interface under transverse loading. The micro-model also includes the effects of void/micro defects at the interface and loading mechanism on the filament. The chapter presents and compares all the FEA results.

5.2 Introduction to finite element analysis

Finite element analysis (FEA) is an excellent way to determine the stress distributions and failure in adhesive joints. Significant studies [153-156] on adhesive joints encourage the use of FEA to observe the behaviour of adhesive joints and compared with the results, which are obtained experimentally or analytically. In this research FEA models were constructed in Abaqus/CAE Version 6.7-1. The descriptions of Abaqus/CAE application are given in Appendix C.

5.3 Meso-scale models

This section will introduce the modelling of the meso-scale laminate and joints by considering the various fabric organisations through laminate thickness to determine local failure stresses that are expected in DLS joints. The properties of these materials are given in Table 5.1, which includes data from manufacturers, mechanical testing and calculation methods. Details are in Chapter 3.

| PROPERTY | Units | Glass fibre | Vinyl ester | UD GFRP | Random GFRP | Araldite 2015 | Coating resin | Aluminium | Steel |
|----------------------------|-------|-------------|-------------|---------|-------------|---------------|---------------|-----------|-------|
| Young's modulus | GPa | 72 | 3 | 48 | 14.87 | 2 | 3 | 72 | 210 |
| Poisson's ratio | -- | 0.2 | 0.36 | 0.26 | 0.23 | 0.36 | 0.37 | 0.3 | 0.3 |
| Tensile strength | MPa | -- | 90 | 600 | -- | 40 | 50 | 180 | 300 |
| Transverse strength | MPa | -- | -- | 20 | -- | -- | -- | -- | -- |

Table 5.1: Materials properties

The FEA models assumed orthotropic properties for the GFRP, elastic-full plastic properties for the adhesive and elastic properties for the brittle vinyl ester and epoxy resins. As discussed earlier, the small laminates were modeled with various fabric organisations namely LL, LT, RL, WR and IR. Brief descriptions (again) of these fabric arrangements are as follows:

- LL: - Two UD rovings mat (4800Tex) stacked at 0-direction i.e. along the loading direction (x-axis)
- LT: - Two UD rovings mat stacked at 0/90° bi-direction. Same roving size used in LL (4800Tex)
- RL: - A random mat stacked on the top of UD mat at 0-direction (4800Tex rovings)
- WR: - A 0/90 woven rovings mat (3600Tex) stacked on the top of a random

mat

- IR: - A 0/90 inlaid (non-crimp) rovings mat (3600Tex) stacked on the top of a random mat.

5.3.1 Shear models

The shear models (and specimens) are based on the thick adherend shear test (TAST) configuration as shown in Figure 5.1. The figure highlights the details of the five shear models as well as the dimensions of multi-layers in the meso-scale laminate, along with the assigned boundary conditions.

The 2-D models include the through thickness materials i.e. adhesive, coating resin, matrix resin, and impregnated roving. The impregnated roving was based on a vinyl ester resin system, reinforced with E-glass rovings and mat (see Table 5.1). The load was taken to be the failure load which was obtained experimentally. There was no symmetry in the shear models, so the boundary conditions were applied on the full shear models (see Figure 5.1). The boundary conditions at the edges signify the clamping mechanisms, restraining the aluminium from displacing in the 'y' direction. Also Figure 5.1 shows the location of the PTFE sheet that was applied in the experimental analysis. This is simply modelled as a gap with the corresponding thickness of the sheet. As aforementioned, this was to prevent any adhesion occurring around the edges of the laminate and to ensure adhesion only occurred in the designated 10 x 10mm area.

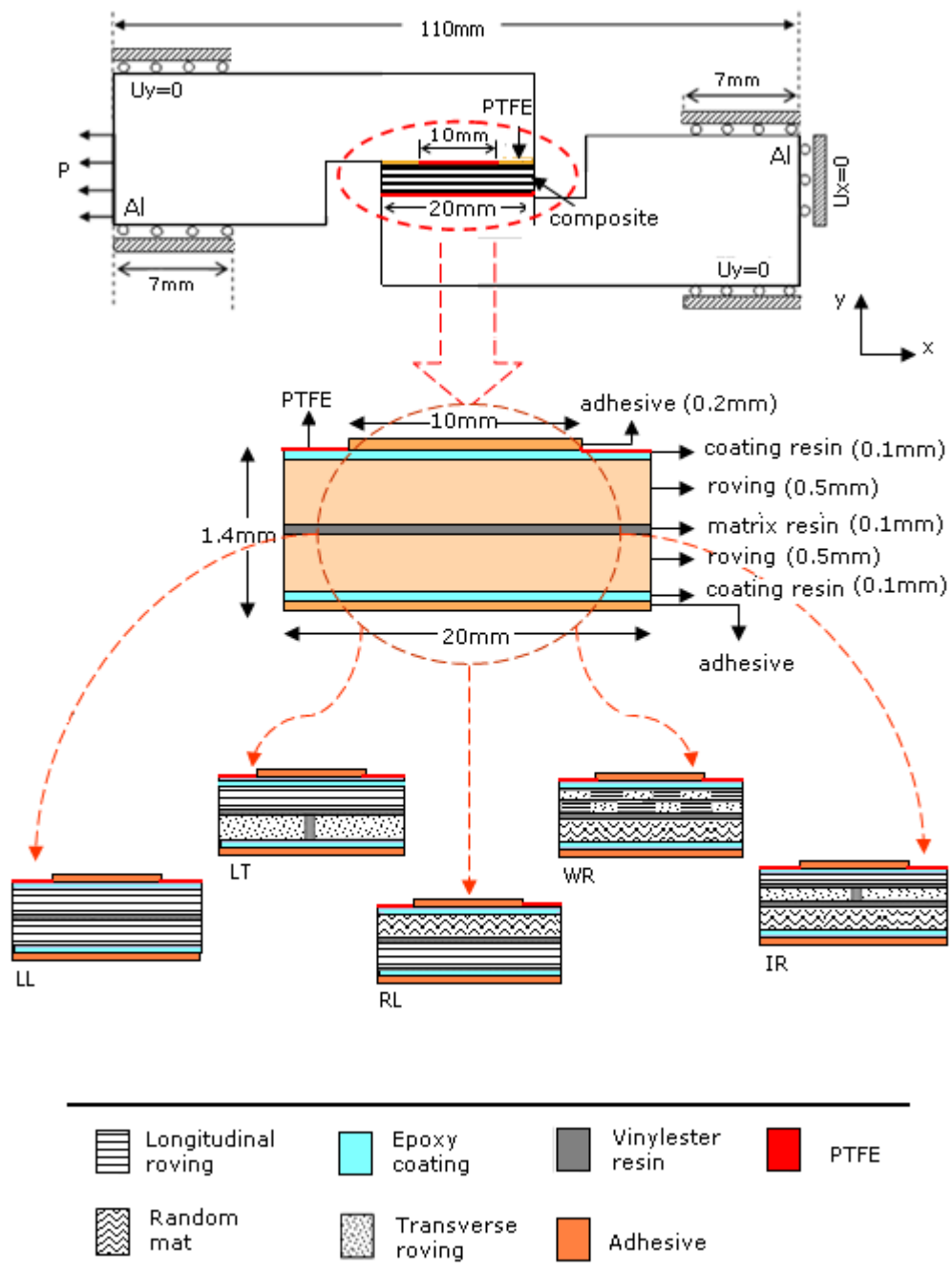


Figure 5.1: Schematic showing the location of fabric arrangements in shear model with detail dimension and boundary conditions (not to scale)

Figure 5.2 shows contours of transverse stress S22 produced from the analysis of a shear model and highlights that adhesion only occurred in the designated 10 x 10mm area. This also shows absence of any edge effects in the laminate, as intended in the experiments.

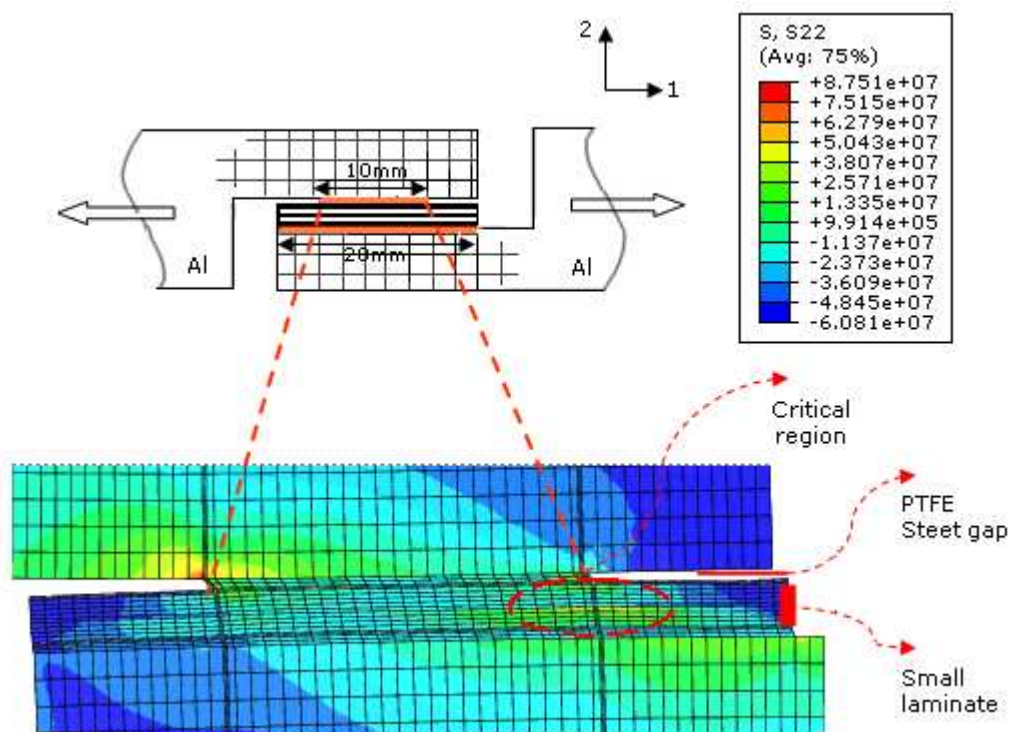


Figure 5.2: Typical FEA transverse stress contour for shear model

The adhesive bondline thickness was modelled at 0.2mm and the coating resin was modelled at 0.1mm. The adhesive and the resin were divided into two elements to allow for determination of through thickness stresses. Mesh sizing is quite important in FEA and the optimisation was obtained when no significant difference was noticed in the load-displacement curve with progressive load of the models. Element aspect ratio of 1:10 to 1:2 were considered for the mesh nearer the model edges. The final mesh was based on a minimum ratio of 1:5.

5.3.2 Tensile models

This section aims to discuss the tensile models, which was aimed at simulating the tensile test performed in section 4.3 (see Chapter 4). The details of the tensile models are the same of those used in the shear models except for loading and boundary conditions. Figure 5.3

gives the basic dimensions of the models, along with the assigned boundary conditions. The figure also shows the various fabric configurations that were considered as a surface layer. These are used to examine the effects of altering the fabric arrangements on through thickness failure stresses. The classification of each layer is mentioned in section 5.3. The dimensions and materials' properties of the tensile FEA models are the same ones which were used in the shear models. The 2-D models used 8-node plane strain quadrilateral, reduced integration element type CPE8R. Each node has two degrees of freedom in the x and y directions.

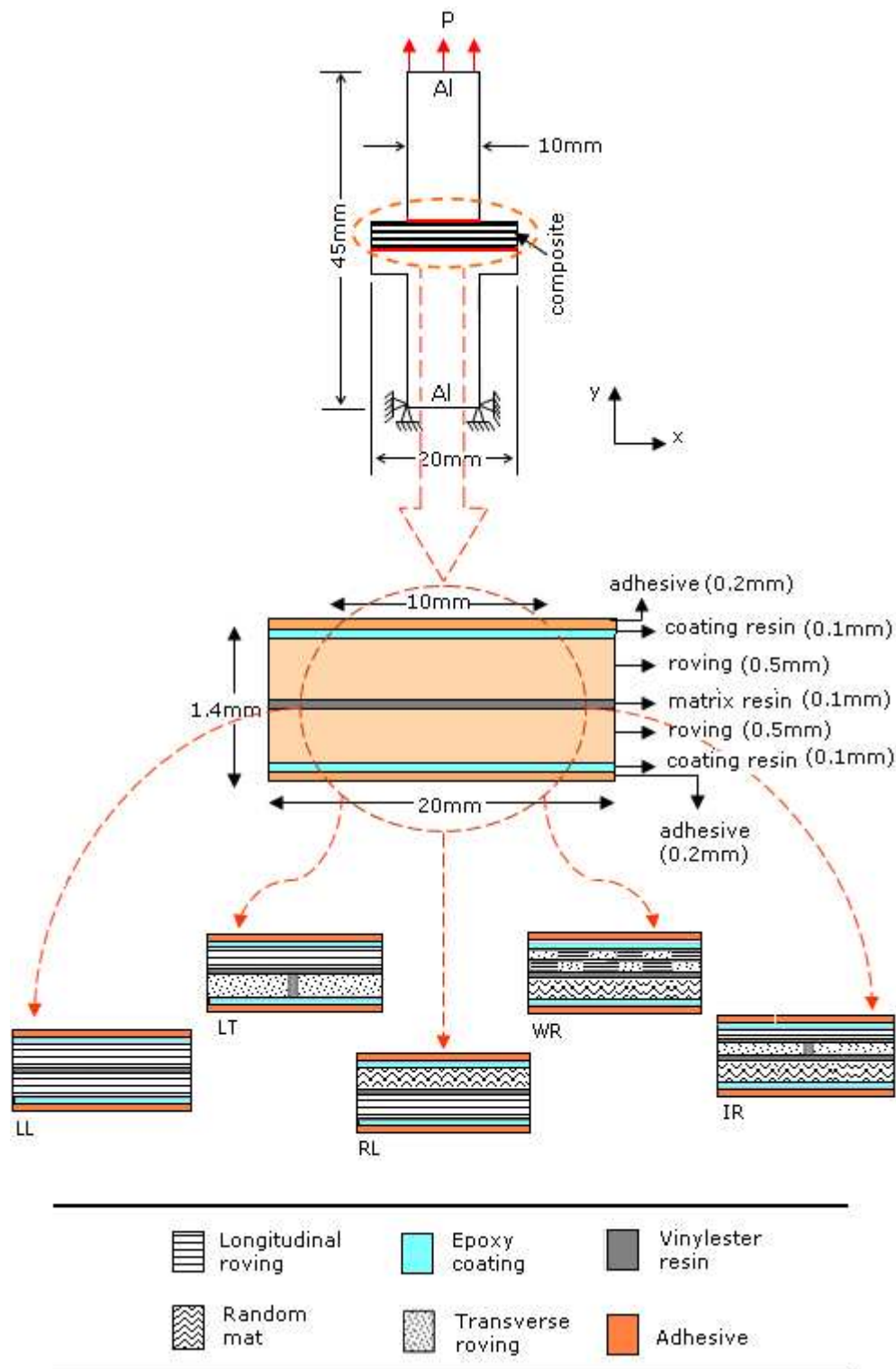


Figure 5.3: Schematic showing the location of fabric arrangements in tensile model with detail dimension and boundary conditions (not to scale)

For further details on the tensile model, Figure 5.4 shows a quarter of the tensile model with the boundary conditions applied. The boundary conditions applied along section C-C imply that this bottom edge was constrained in the X-Y plane. This was designed to simulate the effect of the clamping within the jaws on the Zwick testing machine. The boundary conditions applied along section A-A to restrict any movement in the x- direction which ensured that the analysis was purely tensile. As stated previously, the different failure loads were obtained with various fabric arrangements tensile models through the experimental testing. Such loads were applied on these numerical models to examine how the stresses varied throughout each of the above constituent layers.

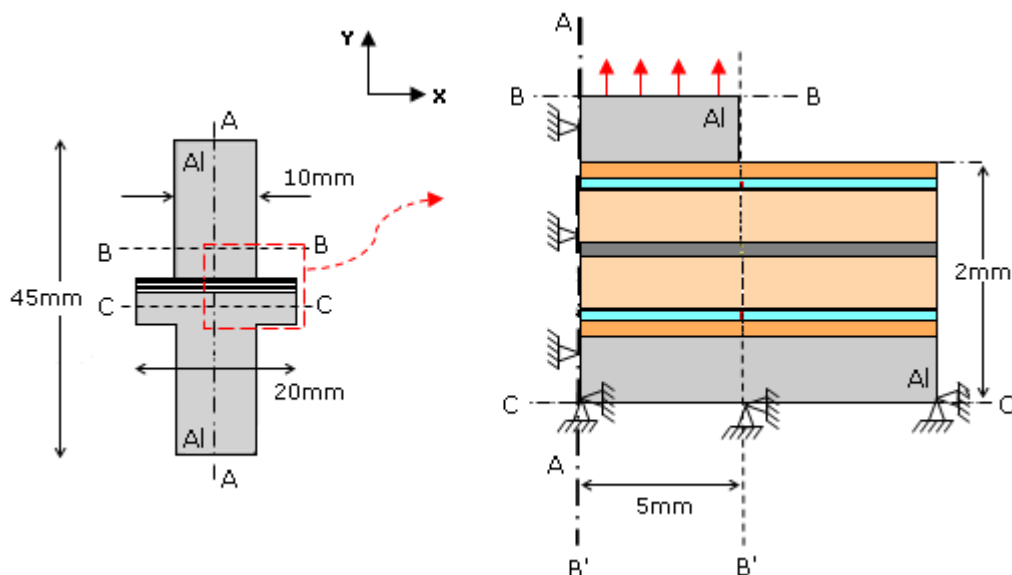


Figure 5.4: Tensile model with quarter FE model showing layers sequences in laminate and symmetrical boundary conditions (not to scale)

The adhesive bondline thickness was modelled at 0.2mm and the coating resin was modelled at 0.1mm whilst the thickness of the impregnated roving was modelled at 0.5mm. The adhesive and the resin were divided into two elements and the roving into four elements to allow determination of through thickness stresses as illustrated in Figure 5.6. Figure 5.5, shows typical FEA contours of transverse stress of a tensile model, which shows a critical stress region. Again, the figure shows absence of any edge effects in the laminate, as intended in the experiments.

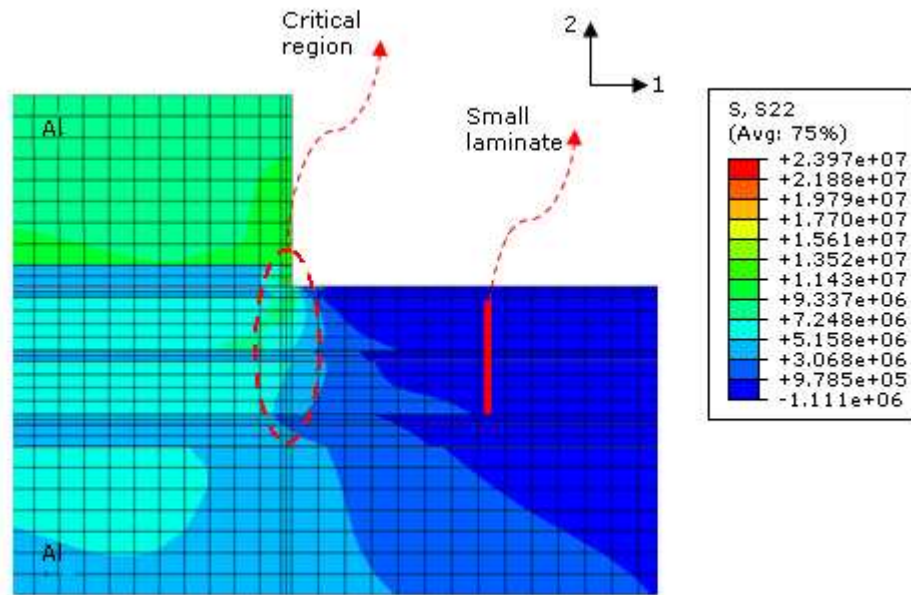


Figure 5.5: Typical FEA maximum transverse stress contour for tensile model

The figure highlights transverse stress regions where the load was applied through the upper aluminium adherend. Hence the FEA contours validate the expectations of high transverse and shear stresses at the edges of the bonding joint (not to the edges of composite). In addition, the layers immediately adjacent to this region will obviously be highly affected and delamination would be highly possible. In the tensile models, both left and right, edges behave in a similar manner, so failure can initiate at either edge. These contours show that the transverse stresses are being distributed evenly throughout each layer and failure would be likely to occur within this region. In general since the FEA contours do not provide a complete understanding of failure initiation all layers were checked individually especially in multi layered materials.

5.3.3 Critical stress locations and failure

Figures 5.6 and 5.7 show critical stress locations for failure initiation for the shear and tensile models, respectively. These locations are as follows:

- location 1: interface of the adhesive with the resin coating
- location 2: laminate top surface; within the top 0.05mm just below the epoxy coating

- location 3: interlaminar location at about 0.6 mm below the surface, i.e. in the matrix resin between the two composite layers.

Locations 2 and 3 are considered more critical after microscopic examination of fracture specimens.

The fracture surfaces of the laminates within the bonded specimens suggest three possibilities of failure modes, which are as follows:-

- intralaminar transverse (out-of-plane or peel) failure within the laminate surface/immediate subsurface just below the coating resin layer. This is referred to as transverse failure
- interlaminar transverse and shear failure at the resin separating the two layers/plies. This is referred to as interlaminar failure
- longitudinal tensile failure along the laminate. This is may be limited to WR and RL shear specimens.

The stresses are taken at a prescribed distance of 0.05mm from the point of singularity, especially for adhesive at location 1. This nominal distance is used for both the meso and macro-scale model to obtain comparative stress values. The designations of stresses are as follows:

- S11 presents the longitudinal stresses, along X-axis (Abaqus coordinate 1)
- S22 presents the transverse stresses, along Y-axis. (Abaqus coordinate 2)
- S12 presents the shear stresses, in the X-Y plane (Abaqus plane 1-2).

These stresses will be used in conjunction with the locations 1, 2 and 3, for examples as follows:-

- S22/1 refers to peel/transverse stress in location 1 (adhesive)
- S12/2 refers to shear stress in location 2 (near composite surface)

- S_{22/3} refers to transverse (peel) stress in location 3 interlaminar within the composite at matrix resin.

The failure criteria for the laminates are based either on Maximum Stress Theory or criteria for failure initiation. These are explained in section 6.3. Therefore two indices are considered here and as follows:-

- index 1 is based on the Maximum Stress criterion for tension, using this equation

$$|\sigma_{22}| \geq Y_t \quad (1)$$

Y_t is taken to be 20MPa based on transverse strength of laminate (see Table 5.1). σ_{22} corresponds to transverse stresses S_{22} at composite surface/subsurface near to interface.

For example for LL model (see Table 5.2)

$$\text{Index 1} = \frac{25}{20} = 1.25$$

- index 2 is based on the Hashin failure criterion for matrix failure in tension, using this equation;

$$\left(\frac{\sigma_{22}}{Y_t}\right)^2 + \left(\frac{\tau_{12}}{S}\right)^2 = 1.0 \quad (2)$$

Similarly Y_t is taken to be 20MPa based on transverse strength of laminate (see Table 5.1) and S is 26MPa based on shear strength of laminate. σ_{22} and τ_{12} corresponds to transverse and shear stresses within composite at matrix resin.

For example for LL shear model (see Table 5.2)

$$\text{Index 2} = \left(\frac{12.4}{20}\right)^2 + \left(\frac{15.3}{24}\right)^2 = 1.12$$

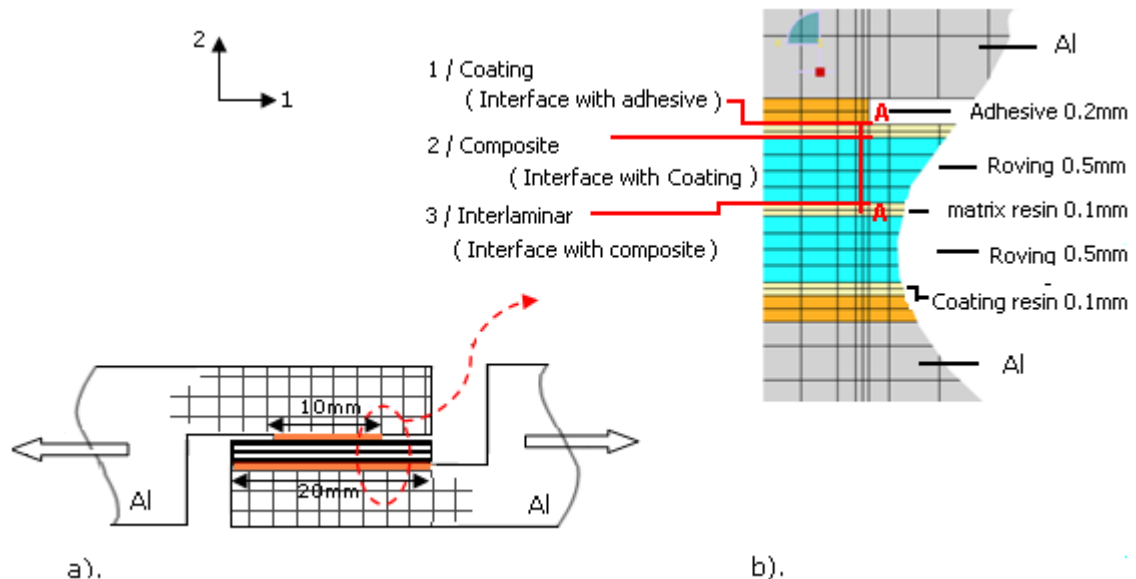


Figure 5.6: Shear model: a), FEA meshed model, b). critical stress locations at different interfaces within the laminate

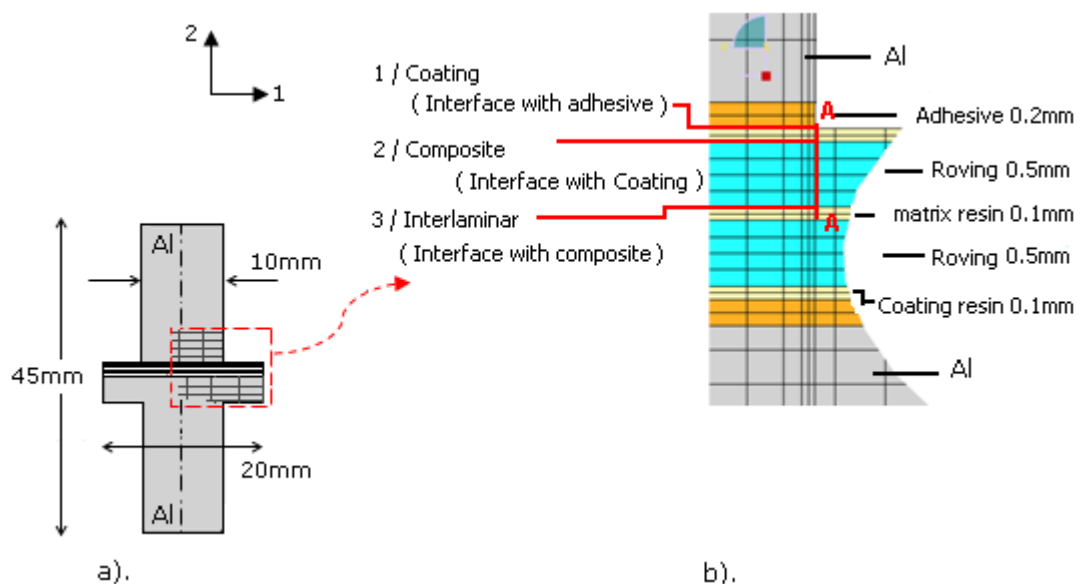


Figure 5.7: Tensile model: a), FEA meshed model, b). critical stress locations at different interfaces within the laminate

5.3.4 Numerical results

Numerical results of both shear and tensile FEA models are presented in this section. As discussed in last section, five different fabric organisations namely LL, LT, RL, WR and IR were used in both shear and tensile models. Significant variations in failure loads were observed between the shear and tensile models. The next two sections give the details of the stresses through the thickness of the laminates at failure load for all shear and tensile models. Good correlation was found between FEA and experimental results for the LL shear model/specimen. Figure 5.8 shows a good agreement between FEA and experimental load-displacement curves. The FEA curve seems to have the same load extension relation with the experimental up to displacement of 0.8mm. A difference in displacement to failure is about 20%.

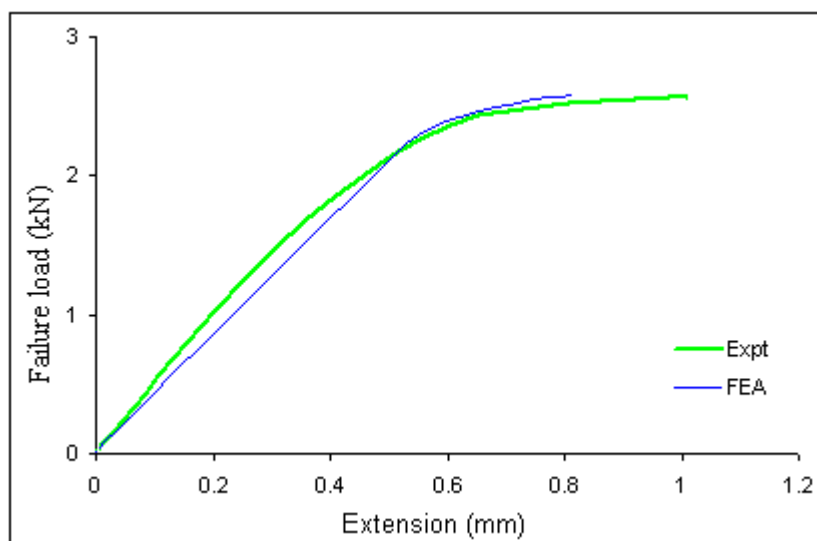


Figure 5.8: Load-extension curve of experimental and FEA results of meso-scale LL shear model

5.3.4.1 Shear models results

The shear models were designed to show the effect of combined shear and tensile loading on through thickness failure stresses in small laminate. The aluminium adherends sandwiching the laminate are actually moving in opposite directions. This creates a bending moment as well as shear traction loading at the right free edge of the joint as illustrated in Figure 5.2. These combined loadings cause through thickness failure stresses in the laminate. The stress distributions in shear models for the five fabric arrangements

are shown in Figures 5.9-5.13. The various stresses correspond to failure load (from experiments of the joints) are given along the joint/laminate. The max transverse (S22/2) stresses in the composite nearer the edge of the joint, especially at location 2, seem to be the most critical values in relation to the strength of the composite. The transverse stresses (S22/1), in adhesive, are consistently high for all models (LL, LT, RL, WR and IR). However, the adhesive failure could not occur because stress values are within the elastic limit of the adhesive (40MPa). Also the shear stresses (S12/2, S12/3) at locations 2 and 3 are low and considerably safe as compared to the corresponding transverse stresses.

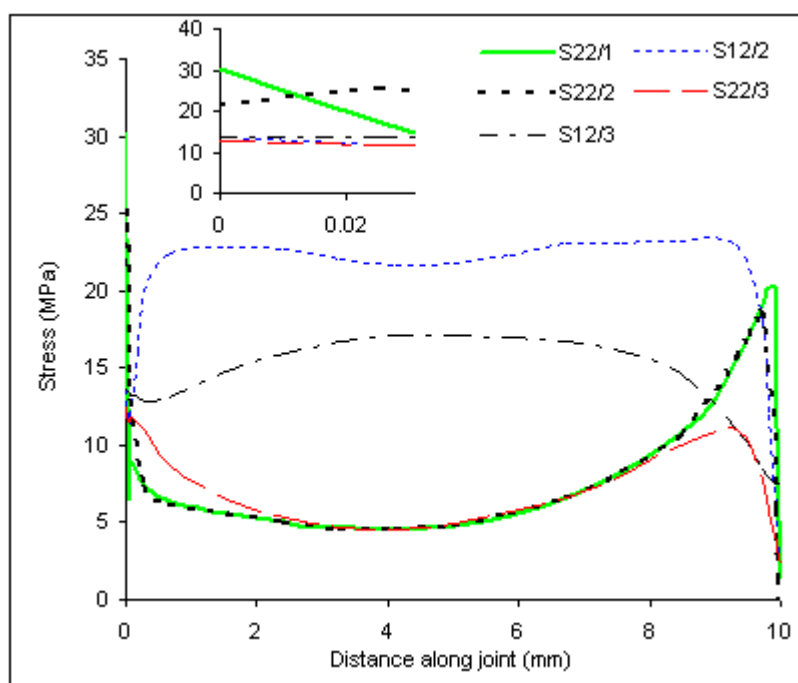


Figure 5.9: Stress distributions in LL shear model (see section 5.3.3)

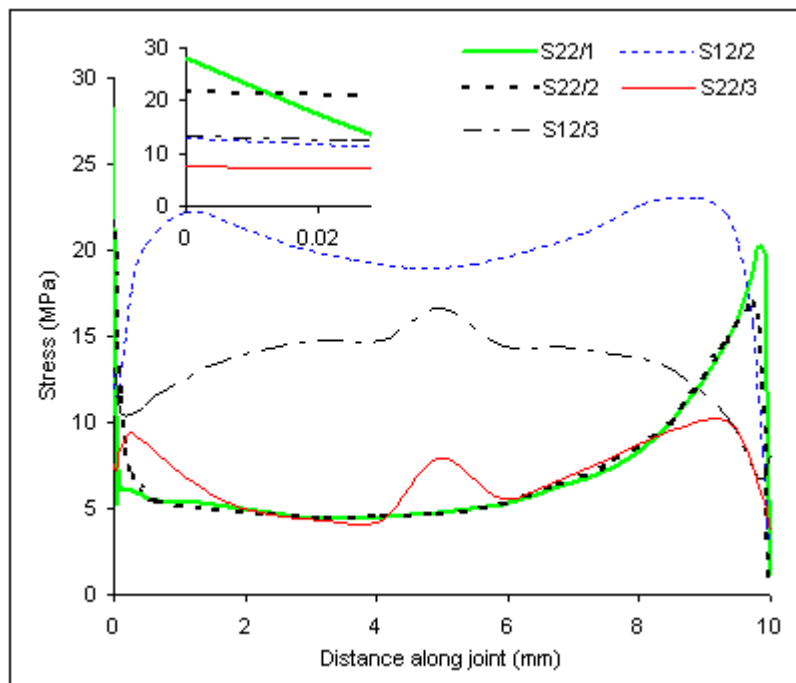


Figure 5.10: Stress distributions in LT shear model (see section 5.3.3)

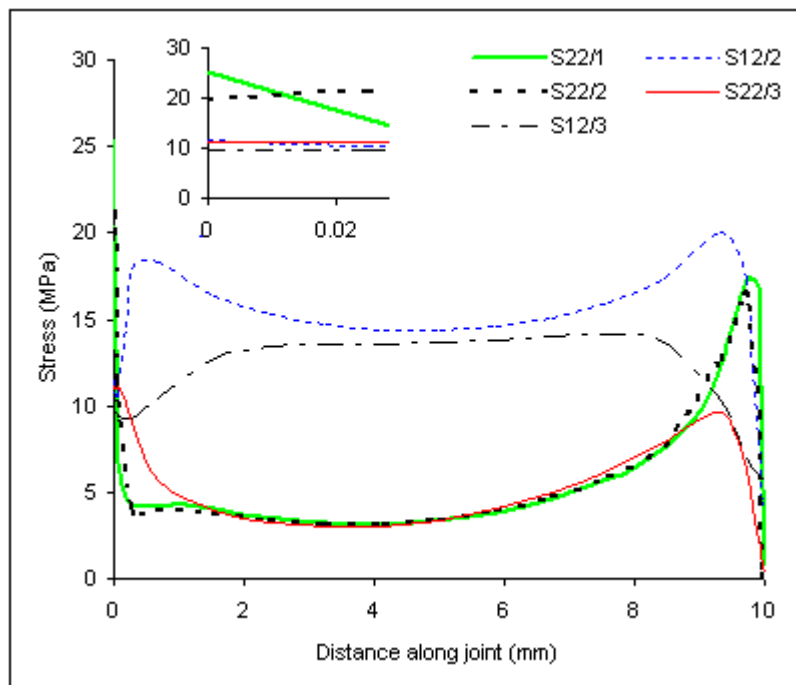


Figure 5.11: Stress distributions in RL shear model (see section 5.3.3)

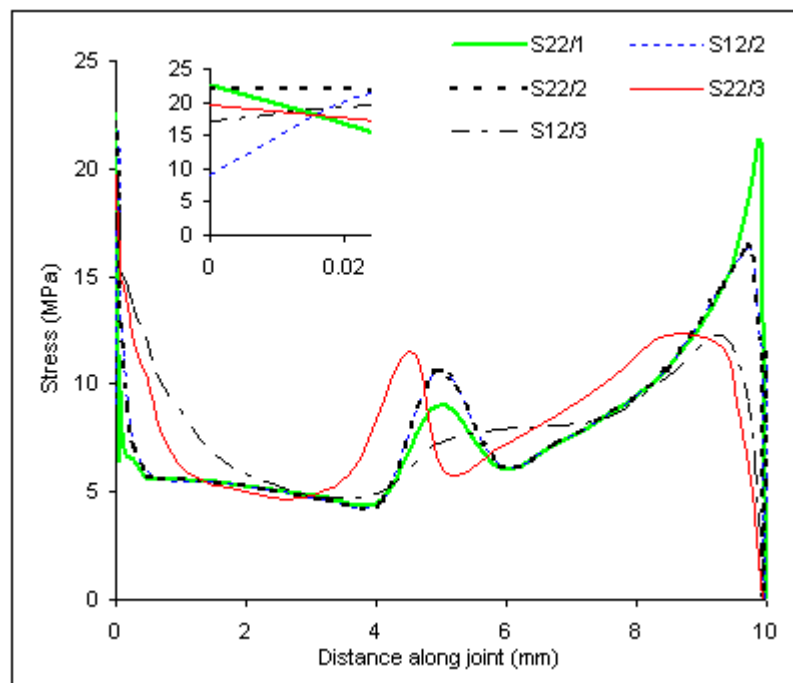


Figure 5.12: Stress distributions in WR shear model (see section 5.3.3)

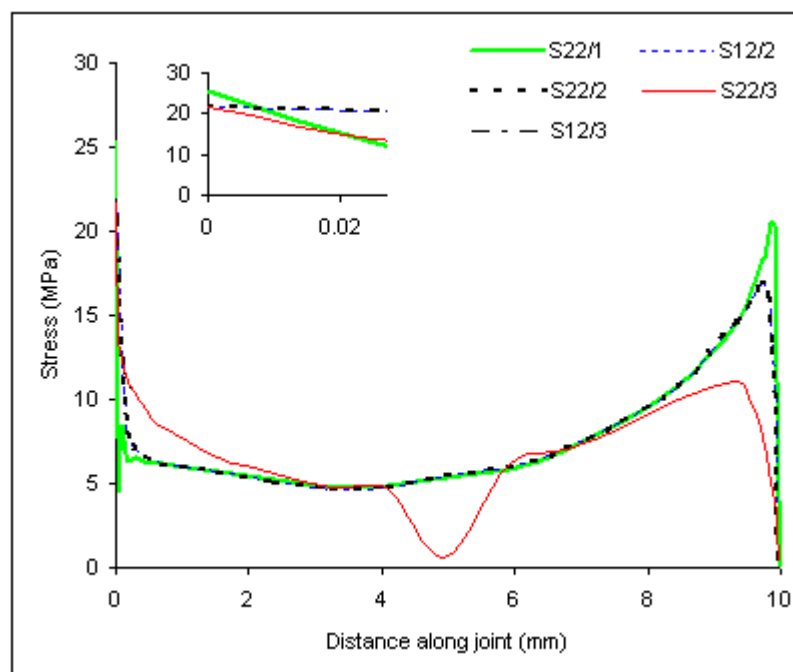


Figure 5.13: Stress distributions in IR shear model (see section 5.3.3)

Summary and failure criteria in shear models

Table 5.2 gives the summary of maximum stresses at critical locations together with failure loads, failure indices and failure modes (see section 5.3.3). The underlined stress values indicate that failure could have taken place as a result of these stresses. The underlined values for the LL model indicate the possibility of either transverse failure (intralaminar at location 2) or interlaminar failure (at location 3). However, the transverse failure could be more dominant. Similarly, due to transverse stresses, the nature of failure in LT model is transverse at a few filaments deep. In addition, the RL model has the possibility of transverse and tensile failure (longitudinal) at location 2. Likely reasons for this are poor transverse and tensile/longitudinal strength of the random mat, as shown in Table 5.2. The WR model shows all the possibilities of failure but the interlaminar failure is likely due to the crimped nature of woven fabric which could compromise the resin strength in location 3. Finally, the IR model has possibility of both transverse and interlaminar failure. Perhaps the interlaminar failure occurs due to higher transverse stresses at location 3 (S22/2). Other details on these results are discussed in Chapter 6.

| Type/Load | Load kN | S22/1 MPa | S11/2 MPa | S12/2 MPa | S22/2 MPa | S12/3 MPa | S22/3 MPa | Index1 (Max theory) | Index2 (Coupled) | Possible failures |
|-----------|---------|-----------|-------------|-----------|-------------|-------------|-------------|---------------------|------------------|---|
| LL | 2.4 | 30.0 | 161.0 | 13.6 | <u>25</u> | <u>15.3</u> | <u>12.4</u> | <u>1.25</u> | 1.12 | ■ Transverse ■ Interlaminar |
| LT | 2.06 | 28.2 | 141.0 | 12.9 | <u>21.0</u> | 14.0 | 7.5 | <u>1.05</u> | 0.83 | ■ Transverse |
| RL | 1.6 | 25.4 | <u>62.0</u> | 11.4 | <u>19.6</u> | 9.7 | 11.2 | <u>0.98</u> | 0.68 | ■ Transverse ■ Tensile |
| WR | 2.2 | 25.6 | <u>76</u> | 13.8 | <u>21.0</u> | <u>12.0</u> | <u>16.3</u> | <u>1.05</u> | 0.93 | ■ Transverse ■ Interlaminar ■ Tensile |
| IR | 2.6 | 22.0 | 223.0 | 14.3 | <u>22.0</u> | <u>14.0</u> | <u>19.7</u> | 1.10 | <u>1.26</u> | ■ Transverse ■ Interlaminar |

Table 5.2: Summary of failure loads and maximum stresses in various shear models
(see section 5.3.3.)

The table shows that failure index 1 seems to give higher values in LL, LT, RL, and WR, which again suggests that failure is largely governed by the transverse stresses in location

2. Failure index 2 seems to give a higher value in IR model, suggesting the possibility of interlaminar failure in location 3, i.e. in the resin between rovings.

Final summary points are as follows:-

- LL provides a higher strength than the LT and RL fabric organisation. LL exhibited double the tensile strength than LT and RL model. LL could even produce a higher joint strength should a thinner roving (smaller Tex) be used
- RL fabric arrangement has significantly lower failure load than other models. The possible reason is the poor longitudinal and transverse strength of random fabric
- strength improvement of IR model over RL, LL, LT and WR are about 62%, 10%, 26% and 18% respectively. The reason for this improvement is the UD roving used as surface layer along the loading direction and it is based on smaller Tex
- LL, LT, RL resulted in a higher strength scatter in comparison to WR and IR fabric arrangements and this is perhaps due to high void defects associated with the higher Tex
- index 1 in LL, LT, RL, WR models seems more dominating for laminates transverse failure and index 2 is dominating in IR model shows interlaminar failure.

5.3.4.2 Tensile models results

The specimen and hence laminates are subjected to pure tension which induces direct tensile/transverse stresses into the laminates, especially nearer the edges of the joint. The stress distributions at the critical locations for the various models are shown in Figures 5.14-5.18. The distance along the joint is taken along the x-axis of the bonded specimen/model, as shown in Figure 5.7a. .The stresses at location 1, 2 and 3 (see section 5.3.3) are taken at the corresponding nodes along the 10mm distance. The node stresses were extracted longitudinally along this region for each layer of the laminate. The transverse stresses ($S_{22}/1$) in the adhesive are the highest for all models, but these are well within the elastic limit of the adhesive (40MPa). However, transverse stresses $S_{22}/2$ and

S22/3 (below the adhesive) remain the most critical and therefore both transverse and interlaminar failure are possible. The shear stresses are negligible. In addition the failure stresses here are considerably lower than the equivalent cases for the shear model. This will be discussed in Chapter 6.

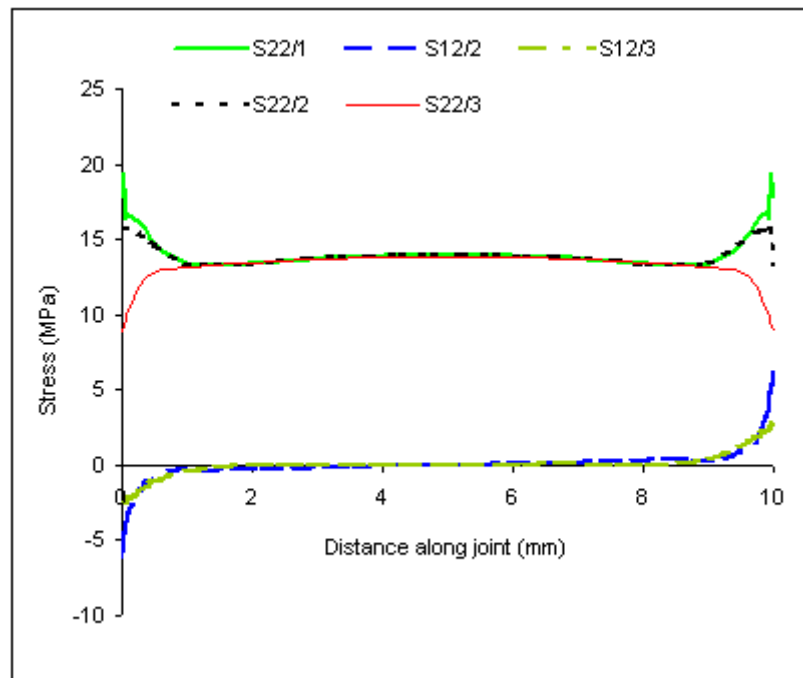


Figure 5.14: Stress distributions in LL tensile model (see section 5.3.3)

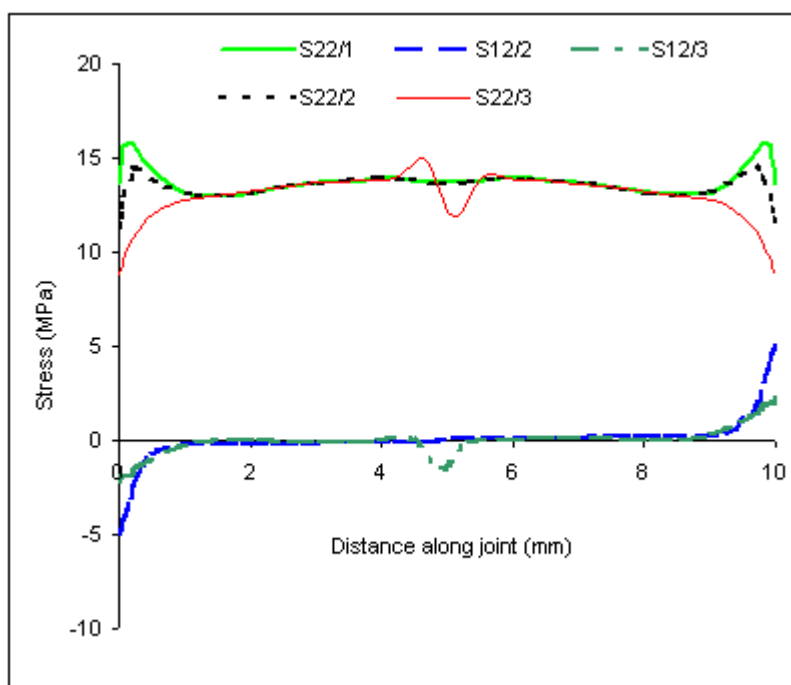


Figure 5.15: Stress distributions in LT tensile model (see section 5.3.3)

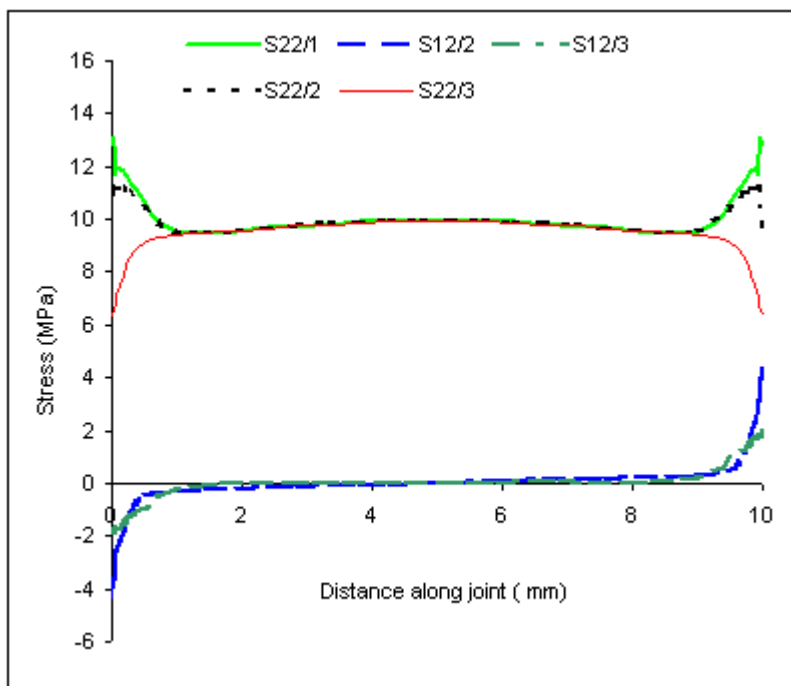


Figure 5.16: Stress distributions in RL tensile model (see section 5.3.3)

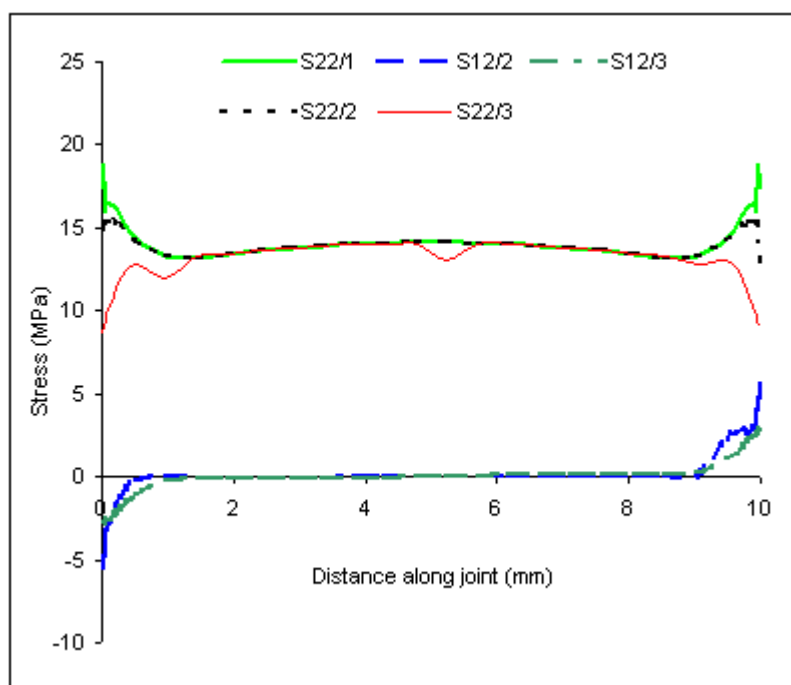


Figure 5.17: Stress distributions in WR tensile model (see section 5.3.3)

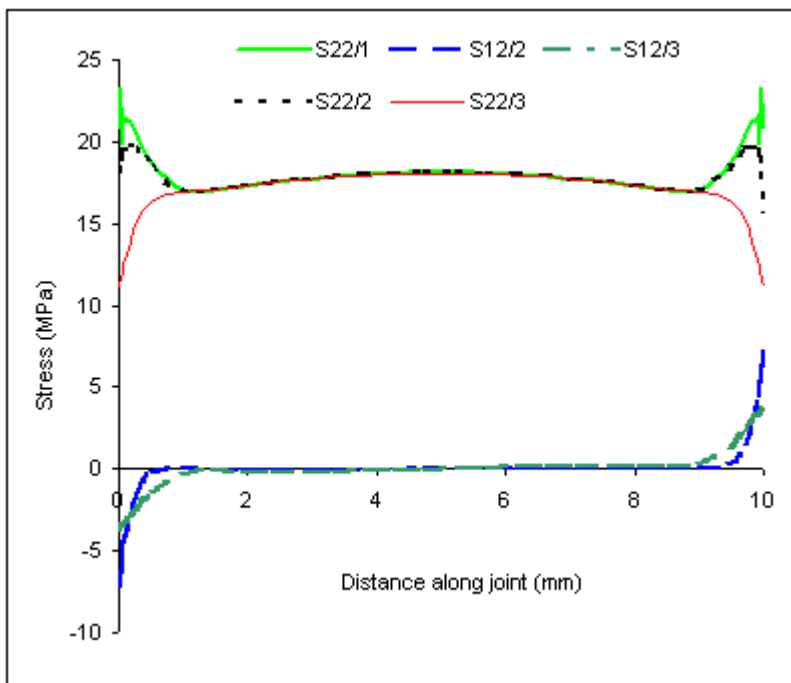


Figure 5.18: Stress distributions in IR tensile model (see section 5.3.3)

Summary and failure criteria for tensile model

Table 5.3 gives the summary of FEA results of the maximum stresses and failure loads for various tensile models. Although the failure initiation and trend at each fabric arrangement in the tensile model are similar to the shear model, failure load was comparatively lower. The details of failure possibilities mentioned in Table 5.3 are given in Section 5.3.3.

| Type/Load | Load kN | S ₂₂ /1 MPa | S ₁₁ /2 MPa | S ₁₂ /2 MPa | S ₂₂ /2 MPa | S ₁₂ /3 MPa | S ₂₂ /3 MPa | Index1 (Max theory) | Index2 (Coupled) | Possible failures |
|-----------|---------|------------------------|------------------------|------------------------|------------------------|------------------------|------------------------|---------------------|------------------|--------------------------------|
| LL | 1.4 | 20.1 | 7.0 | 6.0 | <u>15.7</u> | 2.6 | <u>13.8</u> | <u>0.78</u> | 0.51 | ■ Transverse ■ Interlaminar |
| LT | 1.4 | 15.8 | 5.6 | 5.0 | <u>14.5</u> | 2.1 | 9.8 | <u>0.73</u> | 0.26 | ■ Transverse |
| RL | 1.0 | 13.1 | 2.4 | 4.2 | <u>11.2</u> | 1.9 | 7.3 | <u>0.56</u> | 0.17 | ■ Transverse |
| WR | 1.4 | 18.9 | 5.4 | 5.5 | <u>15.3</u> | 2.8 | <u>14.1</u> | <u>0.77</u> | 0.53 | ■ Transverse ■ Interlaminar |
| IR | 1.8 | 23.3 | 6.9 | 7.2 | <u>18.1</u> | 3.5 | <u>19.2</u> | 0.90 | <u>0.95</u> | ■ Transverse ■ Interlaminar |

Table 5.3: Summary of failure loads and maximum stresses in various tensile models

Again, underlined values represent the critical stress values obtained from FEA at specific locations, which may cause failure. According to these values, the probable nature of failure in LT and RL models was transverse. Similarly there are possibilities of both transverse and interlaminar failure in the LL model. But again the transverse failure could be dominating. The failure load for the RL model was significantly lower than other models and likely reasons for this are the poor longitudinal and transverse strength of the random mat. Other details are given in the discussion chapter.

As mentioned earlier, the tensile model is more sensitive to loading than the shear model and a possible reason for this is the difference in the nature of loading. Shear models have combined shear and transverse loading on laminate, which could suppress the transverse component that appeared at the edge. On the other hand, the tensile model is subjected to pure tension which places the fabric under direct transverse stresses. Further explanation for difference is given in the micro-scale model (see section 5.5.1).

Failure index 1 seems to give higher values for LL, LT, RL and WR models, which may suggest intralaminar failure due to transverse stresses. Whilst the failure index 2 seems to give higher value in the IR model, suggesting that failure might occur at interlaminar location between two composite layers.

Final summary points for the tensile models are as follows:-

- LL provides more strength than the LT and RL fabric arrangements. The LL could even produce a higher joint strength should a thinner roving (smaller Tex) be used
- RL fabric organisation has significantly lower failure load than other models. Possible reasons are poor longitudinal and transverse strength of random fabric. Other possibilities are given in discussion chapter
- IR fabric organisation has higher strength than the woven with random mat WR
- the improvement of IR over LL, LT and WR is about 28% and the improvement of IR over RL is about 44%. The tensile is possibly less sensitive to the roving orientation but more so for the random fabric
- LL, LT and RL resulted in a higher strength scatter in comparison to WR and IR fabric arrangements and this is perhaps due to high void defects associated with the large Tex
- index 1 for LL, LT, RL and WR models seems more dominating and shows Interlaminar failure. Index 2 is dominating in IR model shows laminate interlamine failure.
- the tensile models failed at considerably lower stresses in comparison with the shear equivalent.

5.4 Macro-scale model

Figure 5.19 shows the DLS joint and 2-D FEA model. The figure also gives details of constituent materials. The inner adherend is based on a pultrusion which has the same properties of the LL laminates and the outer adherend is based on mild steel. Both the steel and adhesive were modelled as elasto-plastic isotropic material and the composite was modelled as an orthotropic material. The load was taken to be the failure load which was observed experimentally. The 2-D models used 8-node plane strain quadrilateral, reduced integration element type CPE8R. The element chosen for the mesh enabled a finer mesh to form around deformed edges due to these elements deforming better under bending than other types of elements.

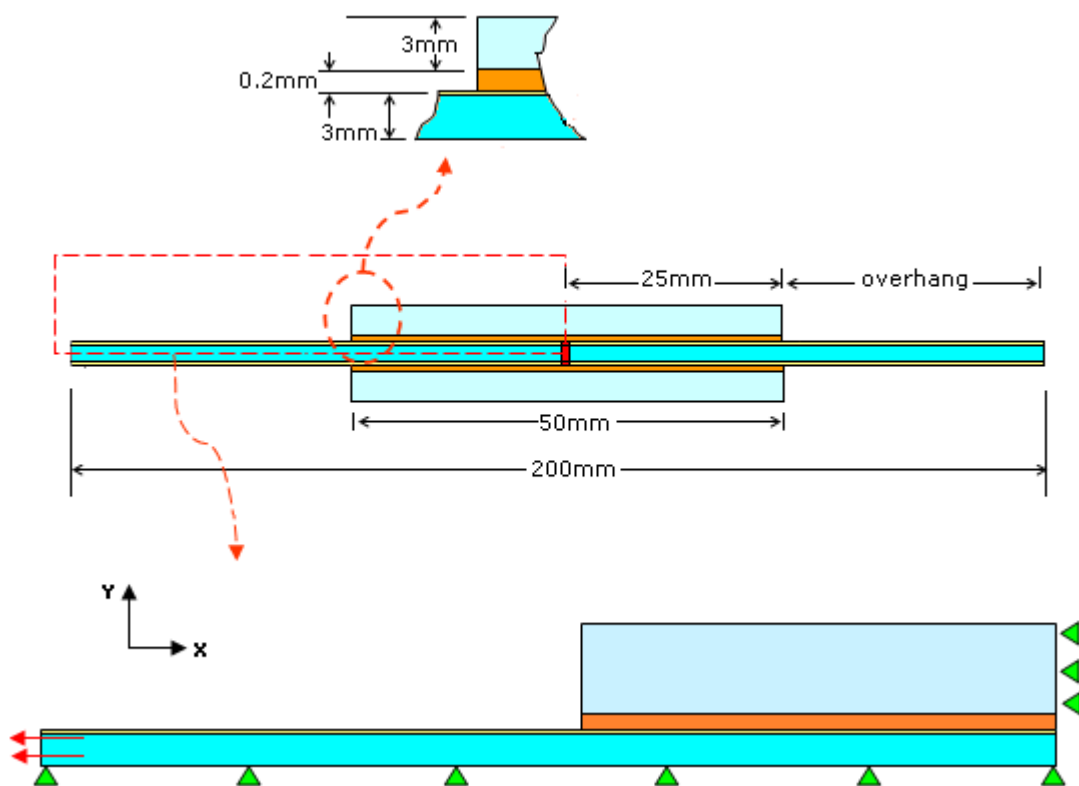


Figure 5.19: FEA model of DLS joint with all possible dimensions and symmetrical boundary conditions (not to scale)

In order to reduce computation time, and to simplify the model, symmetry was used. It is possible to model the double lap strap joint as a quarter model as in Figure 5.19, taking care to set the correct boundary conditions. The tensile load was applied as a stress to the left hand side of the model. The lower edge of the model is constrained in the y-direction, as the composite inner adherend has been split down the middle. The steel outer adherend is fixed in the x-direction to symbolise that it is one continuous piece of steel. The full tensile load should be transmitted through the steel outer adherend. A detailed mesh was assigned to the FEA model. As discussed earlier, failure occurs at the edges of the adherend and high stresses occur in both the adhesive and the composite and this leads to the biased mesh as shown in Figure 5.20.

A fine mesh is important as Abaqus calculates the stresses at Gauss points, and then extrapolates these stresses back to the nodes. It is therefore necessary to have a high density of elements in areas of interest. This gives a much more accurate indication of the actual stresses. A detailed view of the mesh is in Figure 5.20.

The smallest element in Figure 5.20 is 0.1mm. The bias doubles in size from 0.1—0.2—0.4—0.8—1.6—3.2 and then the elements continue at a constant length of 3.2mm for the remainder of the model. In the vertical direction, the outer steel adherend has 4 elements of equal heights, the adhesive has 5 elements of equal heights and the inner composite adherend has an element 0.1mm below the surface, then 0.8mm below the surface. The importance of this mesh is to analyse the stresses in the adhesive and the stresses immediately subsurface in the composite.

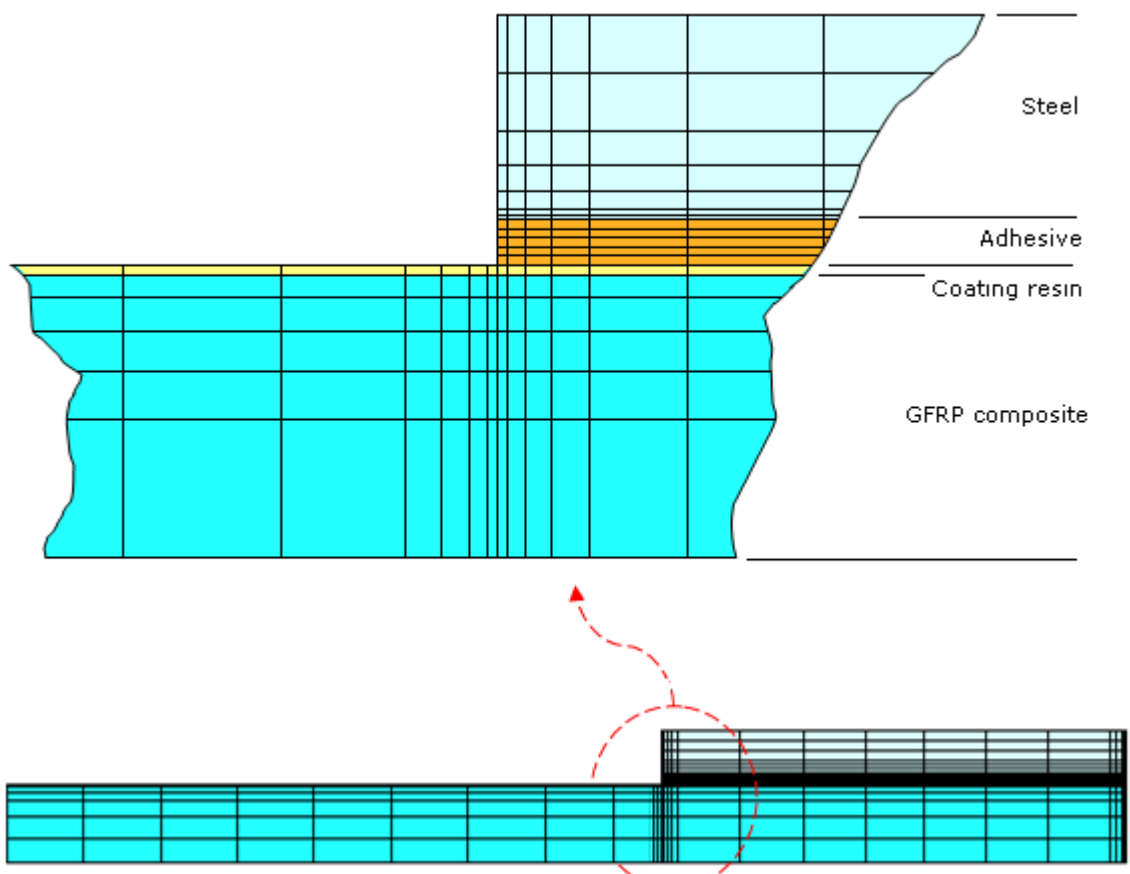


Figure 5.20: FEA quarter meshed model of DLS joint

5.4.1 Critical stress location and failure

Three critical locations named locations 1, 2 and 3 were suggested for the DLS model, just like the meso-scale models. These locations are shown in Figure 5.21 are as follows:

- location 1: interface of adhesive with coating resin
- location 2: laminate top surface; within the top 0.05mm just below the epoxy coating
- location 3: interlaminar location at about 0.6mm below the surface of the composite.

Locations 2 and 3 are considered more critical after microscopic examination of fracture specimens. In addition the modes of failure and failure indices are the same used for the

meso-scale models.

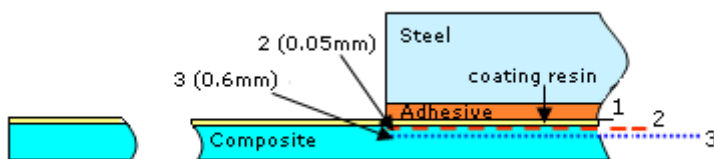


Figure 5.21: Possible failure initiation location in pultruded DLS joint

5.4.2. Numerical results

The DLS model was loaded with its corresponding mechanical failure load. To plot stress vs. displacement curves, every node was selected. This allowed stress and strain data to be taken along paths created at critical stress locations, which are mentioned in Figure 5.21. Both the shear and transverse stresses of the adhesive and composite were examined as these stresses are often the primary cause of the failure in pultruded bonded joints.

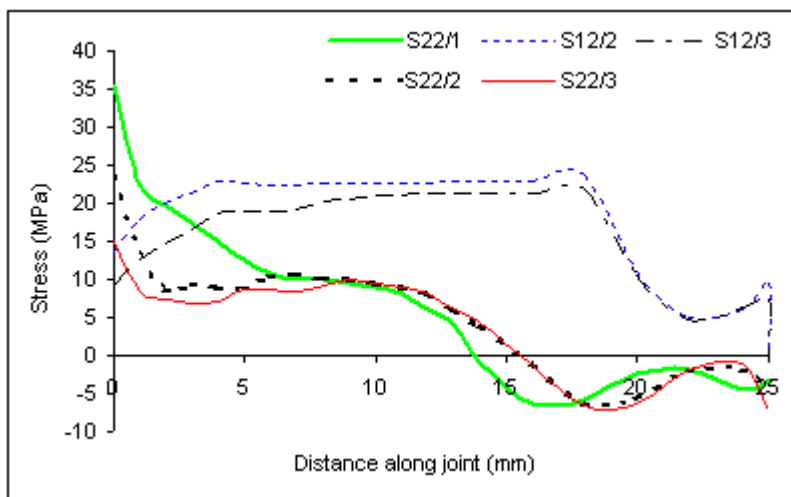


Figure 5.22: FEA results of DLS model:
transverse (S22) and shear (S12) stresses at critical location (see Figure 5.21)

The model has the possibility of both transverse and interlaminar failure as seen in Figure 5.22. However transverse failure at location 2 proceeds further towards final failure, because the transverse stresses (S22/2) at location 2 were higher than (S22/3) at location 3. The microscopic image of the DLS model/joint in chapter 4 (see section 4.6.2 Figure 4.38) shows failure in a DLS joint. Figure 5.22 shows that the transverse stresses (S22/1) in

adhesive were high, but the stress value was in elastic limit of adhesive (40MPa).

Summary and failure criteria for DLS

Table 5.4 gives the summary of FEA results about the maximum stresses and failure loads of the DLS model. The details of failure possibilities mentioned in Table 5.4 are given in section 5.3.3. All the stresses in Table 5.4 were taken at 0.05mm offset from the edge to overcome the stress singularity effect.

| Type/Load | Load kN | S22/1 MPa | S11/2 MPa | S12/2 MPa | S22/2 MPa | S12/3 MPa | S22/3 MPa | Index1 (Max theory) | Index2 (Coupled) | Possible failures |
|---------------------|---------|-----------|-----------|-----------|-------------|-----------|-------------|---------------------|------------------|--|
| 25mm overlap | 20.0 | 35.5 | 358 | 13.3 | <u>23.5</u> | 9.5 | <u>13.8</u> | <u>1.18</u> | 0.56 | <ul style="list-style-type: none"> ■ Transverse ■ Interlaminar |

Table 5.4: FEA results summary of failure loads and maximum stresses in DLS models

Underlined values in Table 5.4 represent the critical stress values. It is probable that the nature of failure in the DLS model was intralaminar, at few filaments deep at top surface/immediate subsurface of composite. The transverse (S22/2) stress is higher than the strength (see Table 5.4). The strong interface at the surface shifts the failure a few filaments deep below the composite surface. Other reasons will be discussed later in Chapter 6. The adhesive was not considered as the transverse stresses were below 40MPa.

Finally, failure index 1 for this model shows a higher value, therefore suggesting that failure would take place at composite subsurface due to transverse stresses. Other possible failure criterion in this case is Tsai-Hill, which will be discussed in Chapter 6.

5.5 Micro-scale models

The macro and meso-scale models help to determine the average failure stresses but they will not be able to quantify an in-depth failure scenario in a single fibre/matrix interface. Based on above observations, mostly macro and meso-scale specimens (shear/tensile) have failed at the composite surface or immediate subsurface a few filaments deep. This failure

occurs for three reasons:

- strong interface with surface coating
- significant voids contents in composite
- fibre/matrix weak interface with voids around the fibre.

To further explore this intralaminar (transverse) failure, the modelling approach was extended to a micro-scale level to determine actual transverse stresses at fibre-matrix interfaces. Two micro-scale FEA models are simulated here to reveal that the failure in the composite adherend is ultimately governed by transverse stresses at filament-matrix interface level.

5.5.1 Single filament models

Two 2-D micro-scale models were constructed in Abaqus as shown in Figures 5.23 and 5.24. The models used an 8-node plane strain quadrilateral, reduced integration (CPE8R) element type. Both models are constructed with a single glass filament (16 μm dia.) and interfacing matrix resin. Different sizes/lengths, voids/defects up to 10 μm were considered, as observed from the microscopic examinations including SEM. The first model applies a constant transverse loading and symmetry boundary conditions on surrounding resin, are shown in Figure 5.23. The load applied at the filament is based on the transverse failure stress of the composite adherend which is about 25MPa. The micro-scale model also allows for the inclusion of cavitations (voids) or a change of filament diameters.

The second model was similarly based on a single filament-matrix interface under combined loading (longitudinal/transverse), rather than single loading (transverse) like in a micro-scale first model as shown in Figure 5.24. This aims to explain the effect of combined longitudinal/transverse loadings of filament on the level of transverse stress in the matrix beneath it. This mechanism represents aspects of the DLS joint's behaviour where UD (LL) top fabric is used. The fibre within the top fabric will be loaded in tension (F1), while the adhesive introduces the transverse forces (F2). A loading range of 0 to 50N was considered for F1 and 0.5-1.5N for F2.

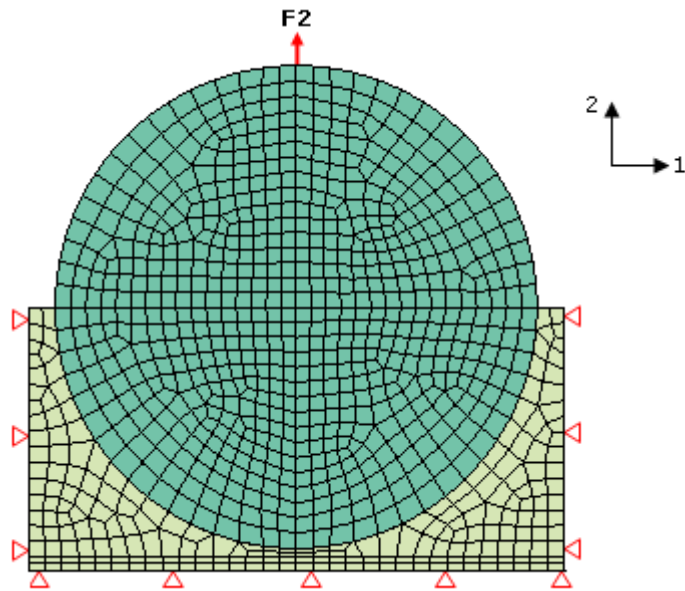


Figure 5.23: Single filament/matrix model under constant transverse loading with symmetric boundary conditions on matrix

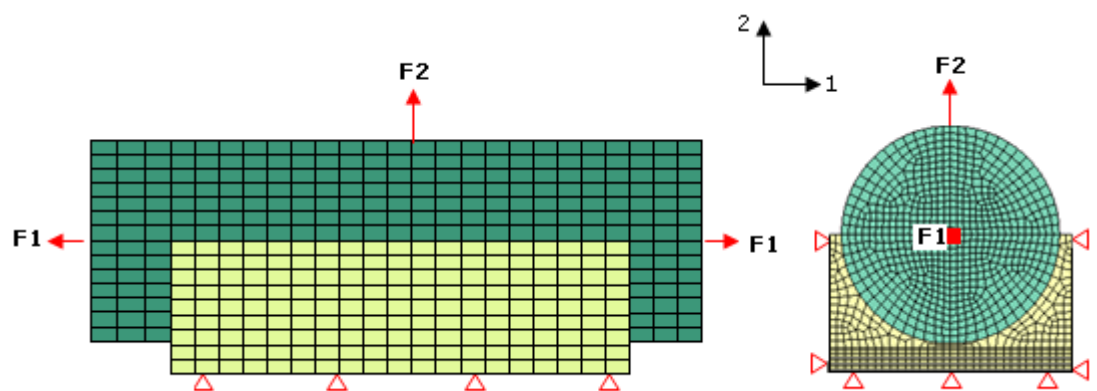


Figure 5.24: Single filament/matrix model under constant transverse with varying longitudinal loading

5.5.2 Numerical results

The resin transverse stresses at the filament-matrix interface are shown in Figures 5.25 and 5.26 for first and second models, respectively. The stresses in first model are much higher than the equivalent stresses in the standard DLS or meso-scale models. The micro-scale model explains why the transverse stresses within the matrix could be very significant and comparable with the manufacturer quoted value for the resin (90MPa), which was mentioned in Section 5.3, Table 5.1. Realistically, the apparent transverse strength of the UD laminates here is about 20-22MPa as quoted by pultrusion manufacturers and obtained from a laboratory test. The main reasons for such a large difference are the lack of ideal alignment in the transverse direction and the fibre/matrix interfaces flaws including voids.

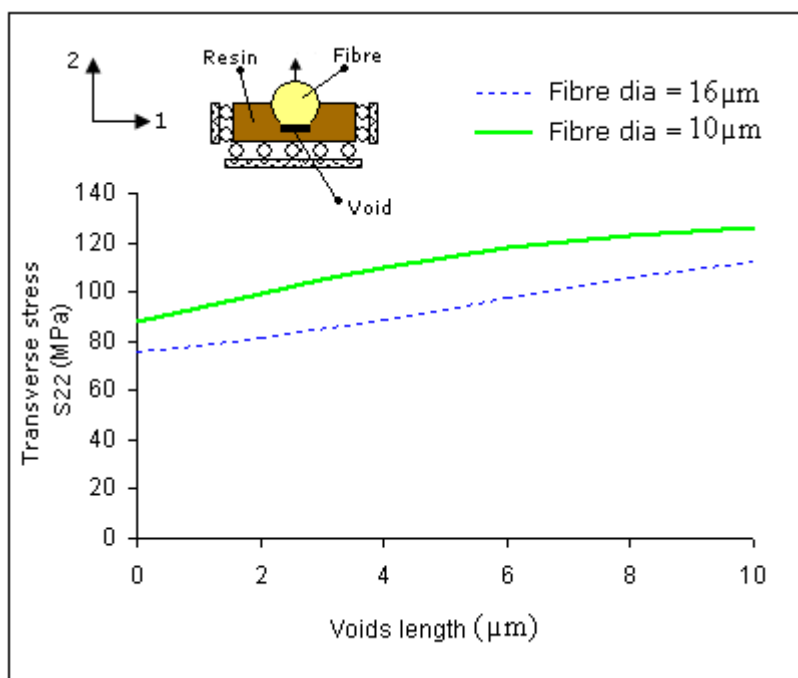


Figure 5.25: Single filament/matrix model: effect of void size with different fibre diameter on transverse stress

So FEA micro-scale models were constructed which included two single filament models with different diameters ($10\mu\text{m}$ and $16\mu\text{m}$) and interfacing matrix resin with the different lengths defects/voids i.e. (up to $10\mu\text{m}$) observed from the microscopic examinations including SEM. The details of the single filament micro-scale models and the effect of different void sizes on transverse stresses around the single fibre are shown in Figure 5.25.

The figure shows the transverse stress as a function of voids length with $16\mu\text{m}$ dia (single filament diameter) and the same trend was observed with $10\mu\text{m}$. Stress level is become high about 15% when single filament diameter trim down from 16 to $10\mu\text{m}$. The load applied at the filament based on transverse failure stress of the composite adherend which is 25MPa in this case. The figure also shows the transverse stress response in composites at micro-scale level at different void sizes at the most critical locations. In fact this explains that the transverse stress within the matrix could be very significant (about 88MPa). This stress is within the bulk vinyl ester strength provided by the manufacturer (90MPa). It is clear that void defect can easily take the relatively low transverse stress (from macro and meso-scale models) into a much higher/actual value. In fact the micro-scale modelling is the way forward to determine the actual failure stress in bonded composite joints and will also enable adhesion improvement.

The second model is based on a single fibre-resin interface where the filament/fibre is subjected to combined tensile and transverse loadings. This aims to explain the effect of combined longitudinal/transverse loadings of filament on the level of transverse stress in the matrix beneath it. This mechanism represents aspects of DLS joints behaviour where LL top fabric is used. The top fabric will be loaded in tension (F1) while the adhesive introduces the peeling forces (F2). A nominal loading range of 0 to 50N was considered for F1 and 0.5-1.5N was considered for F1.

The analysis shows that the F1 forces suppress the transverse stresses/forces, as illustrated in Figure 5.26. This finding helps to explain the reason for the lack of correlation between tension and shear meso-scale models with reference to failure load and transverse stresses at composite surface/immediate surface S22/2 (see Table 5.2 and Table 5.3), especially at LL fabric arrangements. The former does not exhibit significant tensile loading along the top fabric layer.

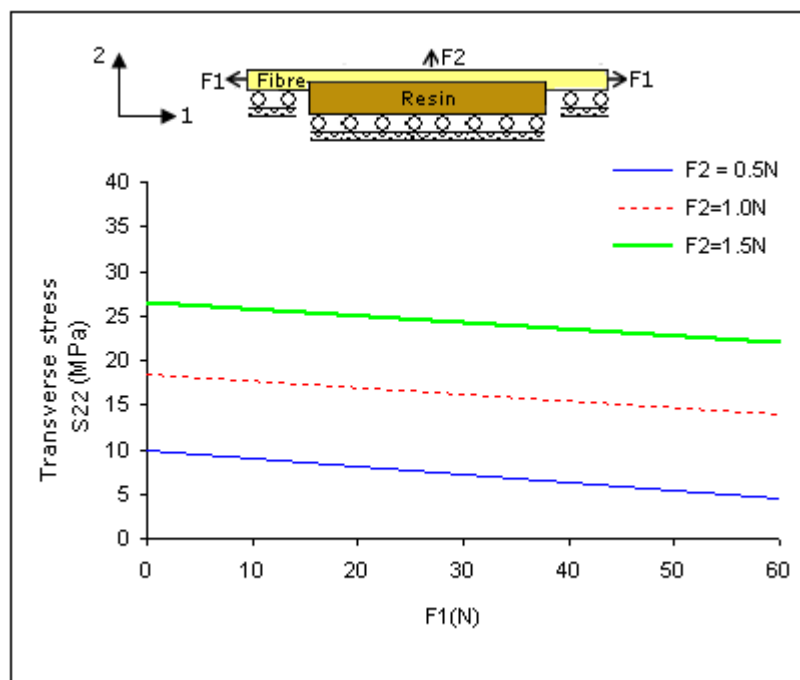


Figure 5.26: Single filament/matrix model: stress distribution in resin under combined tensile and shear loading.

The micro-scale modelling is the way forward to determine the actual failure stresses and their locations in bonded composite joints. This will also enable adhesion improvement by explaining the mechanics of single fibre/resin failure under combined longitudinal and transverse loadings as well as the effect of voids at the interfaces. However, the major challenge here is devising an experimental technique to measure transverse strength at micro-scale level.

Chapter 6

Discussion

6.1 Properties of materials

Several dog bone and butt joint specimens were made for the calculation of Young's modulus and Poisson's ratio of the adhesive. But due to their thixotropic nature, most of the specimens were discarded as air became trapped in many of them. The presence of even tiny air bubbles would cause a difference in results. Five out of ten specimens of bulk adhesive and butt joint specimens were selected for testing, those apparently bubble-free. Some of the results were also discarded due to high bubble contents, as this always compromises the failure strength and strain (see Figure A.3.2). The tests showed that the Young's modulus and Poisson ratio values were in line with the manufacturer's data. The Araldite 2015 is known to have elasto-plastic properties but this was not shown from the tests. This is partially to do with the quality of the cast as well as cure conditions. It is cured at the maximum recommended cure at 80°C rather than usual cure temperatures of 25-40°C. Therefore it was important to produce elasto-plastic properties for the numerical analysis, using supplier data in conjunction with lab tests and engineering assumptions. The adhesive failed at 35MPa obtained from the butt joint lab test. Huntsman quoted 42.5MPa and also mentioned the true failure stress of 30MPa with 0.044 strain. In order to calculate the strain at the adhesive failure load, the true curve was extrapolated to 40MPa. After interpolation in chapter 3 (see Section 3.4.3), the adhesive failure strain was 0.06 at 40MPa. So the adhesive is in the elastic region between a strain of 0 and 0.022. After 0.022 the adhesive is in the plastic region, until 0.06, where it fails. There are still contradictory views about adhesive properties in the literature.

The fibre volume fraction obtained from the analytical approach (see section 3.3.1.2) is somewhat high but is acceptable, as the value is comparable with the manufacturer quoted

value (~ 60-65%). The mechanical properties of the pultruded composite were obtained using rule of mixtures [145], Tsai and Hahn equations [146] and the transversely isotropic materials assumption for better estimation. The mechanical properties obtained from calculations are quite comparable with the value obtained from the mechanical testing of the pultruded composite provided by Exel Composite Ltd. UK.

The transverse strength properties of 20-23MPa, which were from the short test specimens, (see Figure 3.12) are somehow lower than what is normally quoted by the pultruders. They often quote a value of 50MPa but in a private discussion they agreed with the test results from this study. In addition to the transverse strength, shear strength was also estimated from average test results for the shear specimens. This was also assumed to be 20MPa. The properties of the materials, especially the transverse strength of the composite, require a study on their own.

It is common to use a burn off test to determine the fibre fraction of a composite. However in this research a more practical analytical approach was adopted. This was based on manual calculation of a fibre fraction in a single glass roving and meso scale laminate, both were impregnated in the laboratory. A difference of 1.8% was found between them. Details of the calculations are given in chapter 3 (see section 3.3.1).

6.2 Pseudo pultrusion

As discussed earlier, the composite moulding procedure was provided by Exel Composite Ltd. UK and a lot of attempts were made in the laboratory to achieve comparable laminates. The main challenge was to properly apply the materials and moulding conditions which were provided by the manufacturer. Both roving tension and compressive pressure play an important role in controlling the quality of the laminate. Roving tensioning reduces the possibility of fibre twisting and ensures a good alignment. The compressive pressure on rovings or mats (representing a closed-die condition) helps drain out the excess resin from the mould and consolidate the layers. Balanced pressure on roving/mat using an 10.5kg deadweight gave much better results than using a smaller weight (see Figure 3.3.c). This resulted in smooth laminates with almost aligned fibres and minimum resin loss during the moulding operations. The moulding process was however

extremely difficult despite the guidance from the manufacturer. The specially designed mould helped to obtain:-

- proper aligned fibres
- correct fibre content
- properly cured resin
- no broken fibres
- fully wetting of fibres
- minimum voids, defects and areas of pre-delamination.

The fibre volume fraction of up to 65% is somewhat high from a pultrusion point of view. This may be due to error in weighing a small amount of materials. This high proportion of fibre may further reduce the proportion of matrix resin in pultrusion due to pulling and compressive pressure on composite. This matrix resin reduction affects the surface leading to pinhole defects or exposure of fibre. This however, was eliminated by coating the surfaces with low viscosity epoxy resin coating to prompt adhesion. Figure 6.1 shows a laminate surface with a lack of matrix resin.

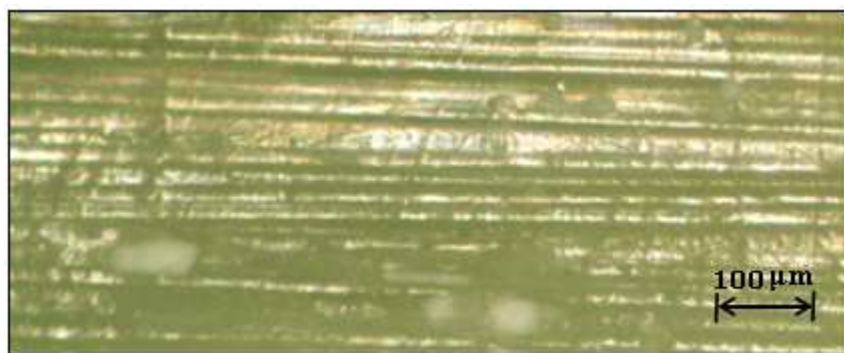


Figure 6.1: Micrographs showing surface defects in GFRP laminate

The microscopic examinations of a “pseudo pultruded” laminate and its equivalent pultruded composite (manufactured by Exel Composites Ltd. UK) show similar levels of micro defects and voids. Both composites have the same constituent materials and mixing ratios. As mentioned earlier, this final pseudo pultrusion was achieved after a trial and error process by following the manufacturer’s guideline. Figure 6.2 shows a close comparison between the manufacturer and pseudo pultrusion. It gives a good indication of

the quality of the laboratory moulded laminates.

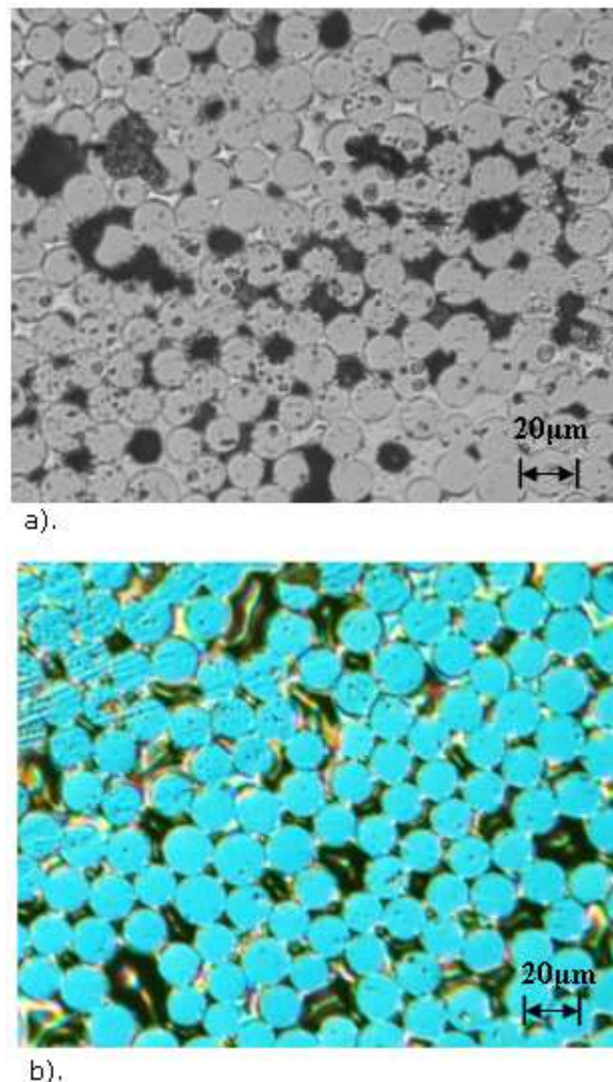


Figure 6.2: Micrographs showing defects in GFRP laminates:
a). manufactured pultrusion, b). pseudo pultrusion

Moulding attempts were made in an early stage and a lot of specimens were discarded due to poor quality, using visual examination. There are a number of reasons for the specimens rejection. These are:

- a large amount of air being trapped in individual roving and also in between resin spaced layer between two rovings
- uneven specimen surfaces and interlayer damage due to sticking to the mould despite the use of PTFE mould release material. If the composite section

sticks to the mould, then it could cause lengthwise inter-layer cracks in the composite. To overcome this problem, the mould was chamfered at the edges to allow it to be separated by gently sliding two screwdrivers between the upper and lower mould

- the thickness of laminate varied from one end to the other
- some areas of cured composite are less translucent , indicating that some fibres have better wetting than others.

As discussed earlier during the moulding process, maintaining the balance between the tensile and compression loading on the roving was quite challenging. Even little variation in such pressure could change the fibre/matrix proportion. Several specimens were discarded during balancing the right proportion between roving pulling and compression. Some important points about moulding pressure on pseudo laminates are as follows:

- less roving pulling will increase the fibre volume fraction in laminate, because of curviness and twisting of fibres
- loose fibre laminate have extra resin between fibres and which catch air bubbles during moulding (see Figure 6.3)
- uneven fibre distribution due to loose fibres in laminate(see Figure 6.4)
- extra pulling of the roving will drain out most of the resin and fibre appears on the laminate's surface (see Figure 6.1). This may be covered with surface coating later on
- extra pulling of the roving could cause delaminating at fibre/matrix interface and resin. This may also cause residual stresses
- there is a high probability of internal fibre damage during extra pulling of the roving (see Figure 6.5).

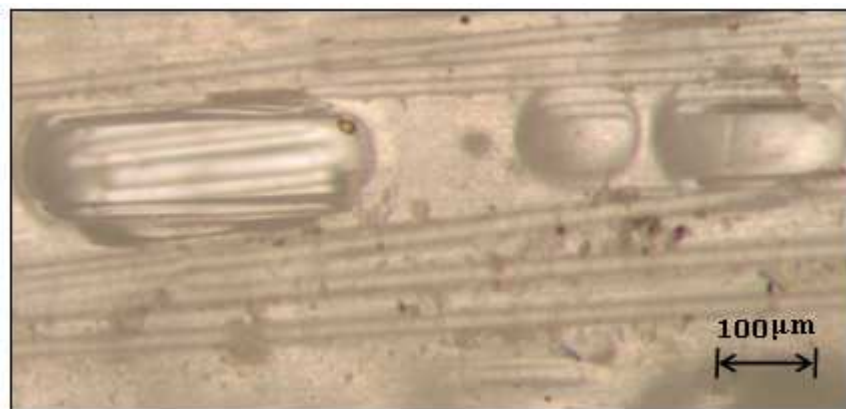


Figure 6.3: Image showing air bubbles trapped in resin

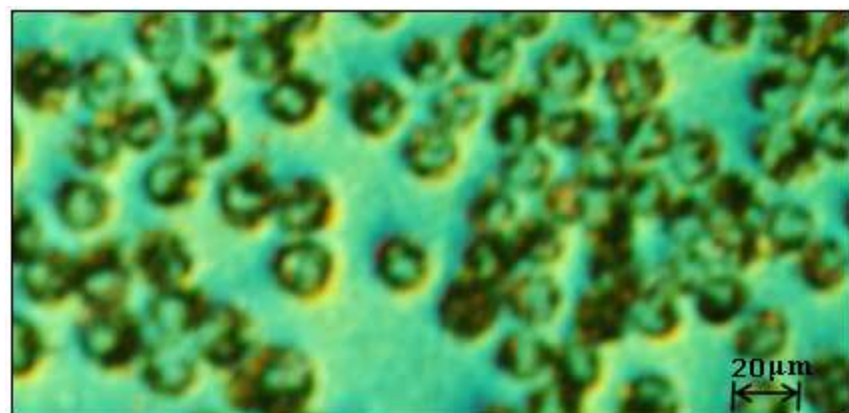


Figure 6.4: Image showing uneven fibre distribution



Figure 6.5: Image showing the fibre damage with extra pulling force during moulding

6.3 Adhesive bonding

Final bonding jigs were designed after the re-designing of early stage jigs for bonding of both macro and meso-scale joints. These jigs ensured proper adherends alignment and consistency of adhesive bondline thickness. These two issues could lead to a premature failure. Early stage bonding jigs required careful realignment during clamping. Figure 6.6 shows defected shear and tensile specimens.

As discussed earlier, shear and tensile bonding adherends were aluminium. Aluminium surfaces are highly reactive leading to the formation of a thin oxide layer. This requires the time between grit-blasting and adhesive bonding to be very short, say less than one hour. The formation of an oxide layer causes adhesive failure as shown in Figure 6.7.

Finally, the effect of coating the laminates with the low viscosity epoxy resin proved to be very effective as shown in Figure 4.10 (see Chapter 4) and this is in-line with the recommendation by Hashim [4].

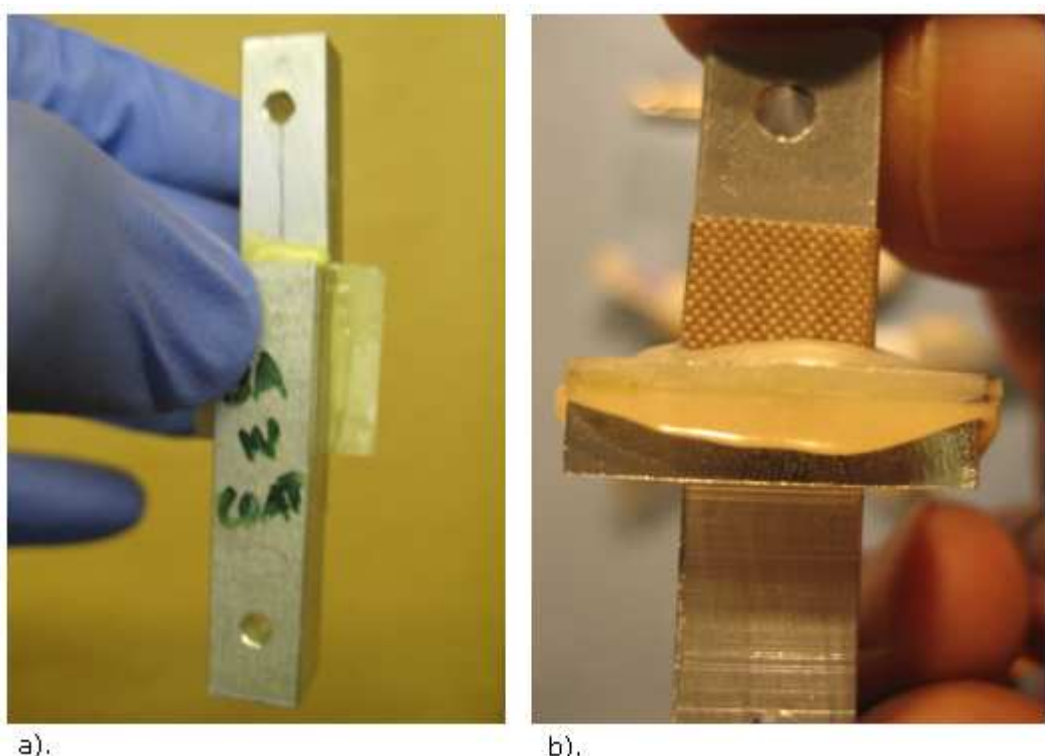


Figure 6.6: Upper and lower adherend misalignment: a). shear, b). tensile specimen

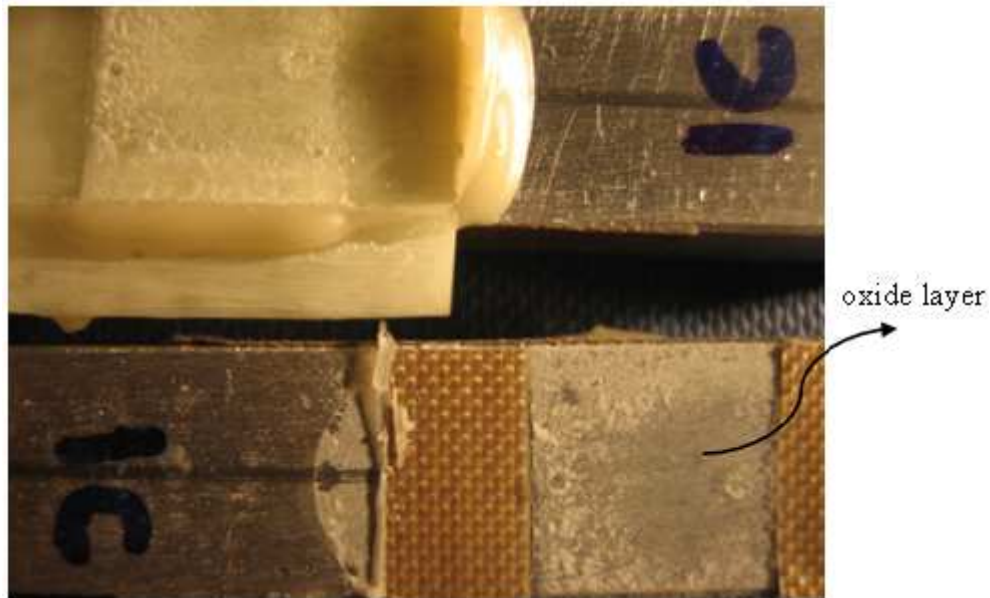


Figure 6.7: Weak adhesive interface with aluminum adherend due to oxide layer

6.4 Test results

Table 4.1 and Figure 4.18 summaries the test results, which were obtained from experimental tests of the shear specimen, are given below:

- the results demonstrate that the IR specimens exhibited the highest strength
- the shear strength improvement of IR over RL, LL, LT and WR are about 62%, 10%, 26% and 18% respectively. Perhaps using smaller Tex rovings as well as having UD fabric along the loading direction, in the case of IR, are the reasons for this improvement
- although the standard deviations of failure load are relatively small, many specimens were discarded due to poor moulding at an early stage
- the average tensile and shear strength in the laminates are obtained from dividing the failure load by the bond area or the delamination area beneath it.

Table 4.2 and Figure 4.18 show the following points, which were obtained from experimental tests of the tensile specimen:

- the results demonstrate that the IR specimens exhibited the highest strength
- the tensile strength improvement of IR over LL, LT and WR is about 28% and the improvement of IR over RL is about 44%. The tensile failure is perhaps less sensitive to the roving orientation but more so for the random fabric
- although the standard deviations of failure load are relatively small, many specimens were discarded due to poor moulding at an early stage.

A significant difference in failure load was found between shear and tensile testing results and possible reasons are as follows:

- the tensile specimens are more sensitive to testing than the shear specimens. In the latter, both longitudinal and transverse combined loadings exist. The longitudinal loading may help to suppress the effect of transverse stresses. These are the main cause for the delamination process. The tensile specimens are dominated by the transverse loading and hence the low strength. This will be discussed further in section 6.9.
- voids are perhaps more critical for tensile specimen than shear specimen. This is because, as stated earlier that when the composites are subjected to shear loading, some areas of the shear specimen would actually be under compression. Compressive forces would actually close up any voids and hence the specimen would be more resilient to failure.

The IR and WR specimens exhibited lower failure load deviations than the LL, LT and RL specimens (see Figure 4.18). A likely reason is that the LL, LT and RL specimens are based on a larger roving (4800Tex) than the IR and WR specimens (3600Tex). The RL exhibited low strength due to the low stiffness of strength of the random fabric.

The tensile LT specimens failed at lower loads than LL specimens. This is perhaps unexpected considering that the through thickness stiffness is the same. However, having two rovings at 90degrees to each other could affect the resin impregnation during

moulding, hence weakening the interface between the two layers.

From visual inspection of fractured specimens, it can be seen that failure (transverse/interlaminar/tensile.... see section 4.4) is taking place within the composite, but this is not always the case. A few specimens with adhesive failure were found and discarded. These specimens failed prematurely. Possible reasons for adhesive failure are as follows:

- weaker interface with the oxide layer on aluminum adherend (see Figure 6.7)
- uneven adhesive bondline (see Figure 6.8).

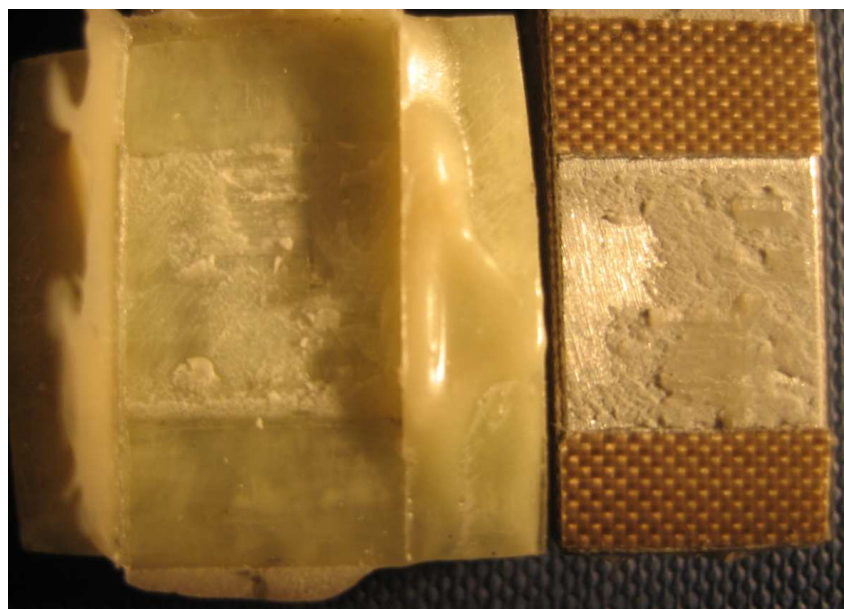


Figure 6.8: Uneven adhesive bondline

6.5 Modes of failure

It is particularly difficult to identify bonded composite joint failure modes, but the American Standard [168] gives the details for their identification and classification. Seven classes of failure are mentioned by the American Standard and these are mentioned in the literature review (see section 2.6). Some of the modes of failure that are likely to be present in this particular research are summarised below:

- fibre tear failure (interlaminar): failure occurs within the fibre reinforced

plastic (FRP) matrix

- light fibre tear failure (intralaminar): failure occurs within the adherend near the surface, visible on the adhesive with few or no glass fibres
- mixed mode failure: failure is the mixture of above both failures

Examination of fracture joints can allow determination of the modes of failure that have occurred, although in some cases there may be evidence of more than one. In these cases, the mechanism of the failure is more difficult to establish. It is possible that more than one mechanism could have occurred simultaneously, but it is more likely that there was an initiating failure mode. The initial failure mode remains more important in this research, due to the use of small specimens.

Limiting the bond area to 10mmx10mm was intended to eliminate laminate edge effects. It is more likely that failure was initiated from the right edge of the shear joint as it was aimed for from the design of the shear specimen. One may assume that the PTFE sheeting to the right-hand side of the joint (see Figure 5.2) forms a crack which contributes to failure, but this may not be the case, due to the relatively thick bond line (0.2mm). In addition, the free end of the upper aluminum adherend is not under load. The failure surfaces for the macro and meso-scale specimens (see Figures 4.38 and 4.19) showed that the transverse adhesive stresses/loading govern the initiation of failure at the fibre-matrix interface, just below the laminate surface/immediate subsurface, especially in the presence of voids.

The microscopic studies of the composite failure surface confirm the multi-defect nature of the bonded laminates, mainly due to the presence of voids and micro cracks (see section 4.5, chapter 4). Figure 6.9 shows an edge view of a fractured shear specimen (LL) at different magnifications using SEM. It shows different loci of failure at micro-scale level and the reasons are:

- failure due to embedded voids/micro defects in the resin
- failure close to or at the fibre matrix interface due to weak interface.

The images in Figure 6.9(a, b, c) indicate that both failures are dominated by resin weakness. Residue of resin particles are left on the fibres as shown in Figure 6.9(d).

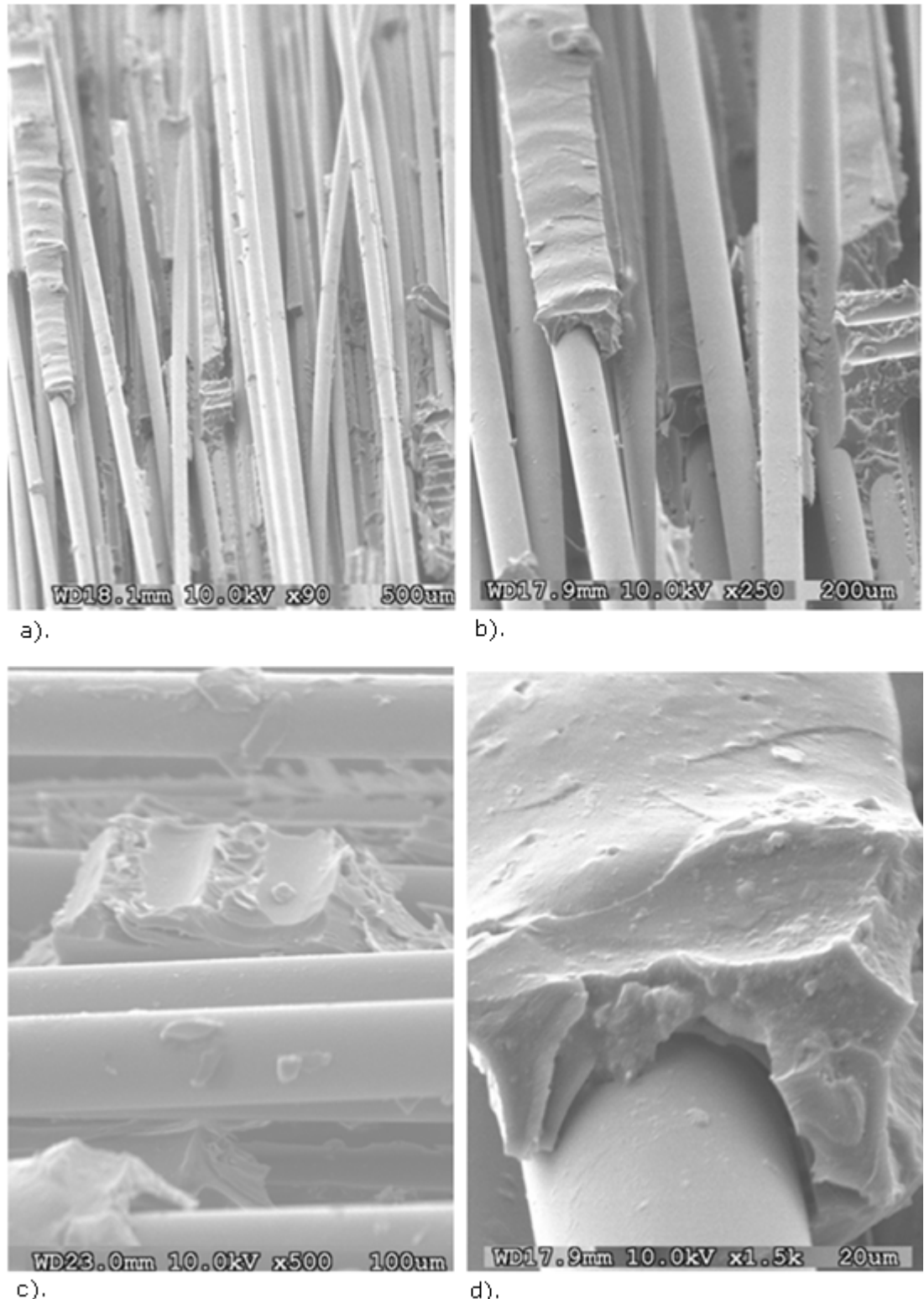


Figure 6.9: Scanning electron micrographs (SEM) transverse failure in GPRP laminates at different magnification after final rupture

6.6 Failure criteria

Failure prediction requires complete understanding of failure initiation, growth and modes. Analytical methods have their own limitations in pultruded laminated composites due to their complex nature, convoluted boundary conditions and the combined effect of various failure modes. Therefore finite element analysis (FEA) with a suitable failure criterion can be used for predicting the failure initiation of pultruded composite structures. Different failure criteria have been reported for joints in literature, e.g. Maximum Stress or Strain criteria, Tsai-Hill, Tsai-Wu and Hashin failure criteria etc (see Appendix D). The Keller-Shear-Tensile interaction failure criterion is used for pultruded composites and this is based on the Hashin quadratic interactive ply-based failure criteria [157]. The problems of carrying out reasonable tests and the lack of reliable experimental data have made it difficult to resolve this issue [158].

Out of all failure criteria which are mentioned above, the Hashin and Maximum stress failure criterion has been recommended for failure initiation through the thickness of pultruded composites. The transverse stresses at the composite surface and immediate subsurface remain critical to composites including pultrusions. Perhaps the Maximum Stress criterion is more relevant. On the other hand, taking the interlaminar stress values, the Hashin criterion for matrix failure could also indicate failure initiation.

Failure indices used in this research were used to examine failure through existing failure criterion. Index 1 is based on the Maximum Stress criteria for tension, using the following equation;

$$|\sigma_{22}| \geq Y_t \text{ or } Y_c \quad (1)$$

Coupled index 2 is based on the Hashin failure criteria for matrix failure in tension, using this equation;

$$\left(\frac{\sigma_{22}}{Y_t}\right)^2 + \left(\frac{\tau_{12}}{S_c}\right)^2 = 1.0 \quad (2)$$

Other possible failure criterion for macro scale DLS joint is Tsai-Hill, which states that failure will occur within uni-directional laminae. Therefore by extracting the maximum S11, S22 and S12 values at location 2 and using them in equation 3 to observe the failure occur in uni-directional laminate.

$$\left(\frac{S_{11}}{X}\right)^2 + \left(\frac{S_{22}}{Y}\right)^2 - \left(\frac{S_{11} \cdot S_{22}}{X^2}\right) + \left(\frac{S_{12}}{S}\right)^2 \geq 1 \quad (3)$$

The maximum stress approach is perhaps most suited for adhesive bonded composites, therefore the failure in the composite may be based on:

- maximum peel stress of the adhesive as an indicator to composite transverse stress
- maximum stress of the composite in a point very near to the point of singularity (material and geometrical singularities)
- maximum stress over a small zone of the composite nearer the joint edge
- the short specimens in this research, where brittle GFRP is used , may justify the maximum stress to compare the various specimens.

6.7 Meso-scale modelling

As discussed earlier the overall aim of these models is to develop a better understanding of the failure of pultruded composites, with reference to various fabric arrangements. Several attempts were made at mesh refinement during the modelling of the 2-D plane strain models, before settling on one meshing level for simulation convergence. Submodelling was not adopted in this research due to the size of model. In addition, a 3-D model approach was also used but this faced convergence problems at failure load. Possible reasons for this are the thin fabric layer and material properties. Extensive experimental work has been done in this research and future work should focus on further FEA analysis, including 3-D modelling of woven and inlaid fabric. This section attempts to give explanations for the different stresses at their corresponding locations for different shear

and tensile models.

6.7.1 Shear models

As mentioned before, the shear specimens/joints were designed to ensure that failure initiates near the right-hand edge of the joints, as shown in Figure 6.10.

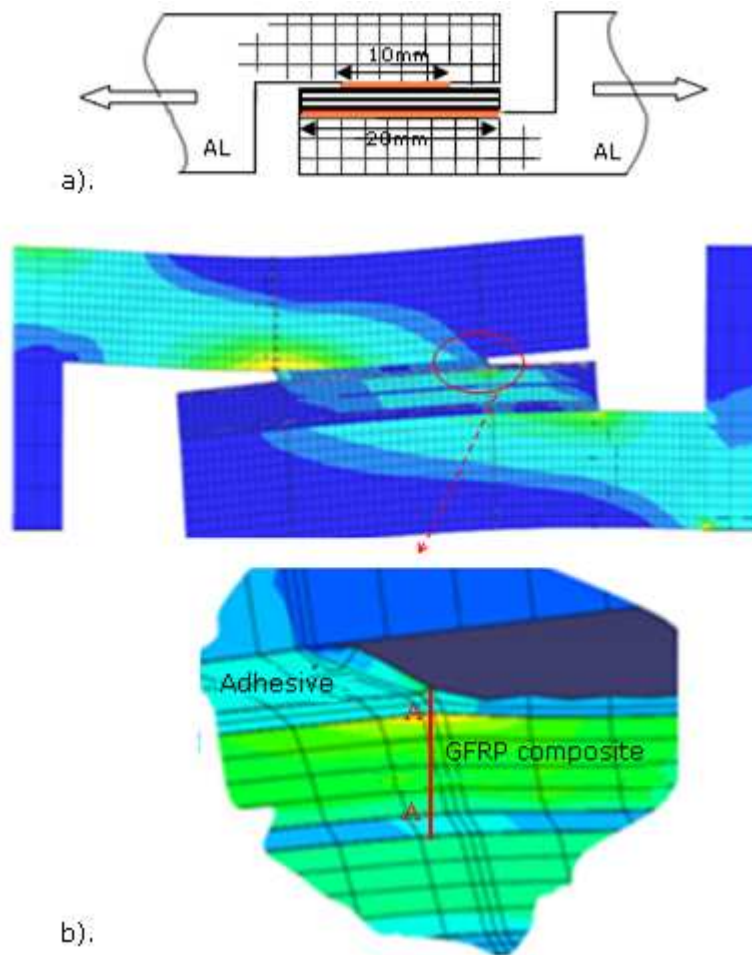


Figure 6.10: FEA shear model: a). model geometry with LL laminate, b). contour plot in shear model showing critical location (transverse stress)

Although high adhesive stresses appeared to the left-hand side, nearer the interface with the aluminum upper adherend, it was just within the strength and strain limits of the adhesive.

The distributions of the shear and transverse stresses through the thickness of laminate section A-A for the shear model/joint are shown in Figure 6.11. The vertical section

includes the upper resin layer (see Figure 6.10b). As mentioned earlier that the transverse stresses was quite high at the resin as shown in Figure 6.11. However, the critical transverse stress is at about 0.05mm at the composite subsurface. This is believed to be the main cause of delamination.

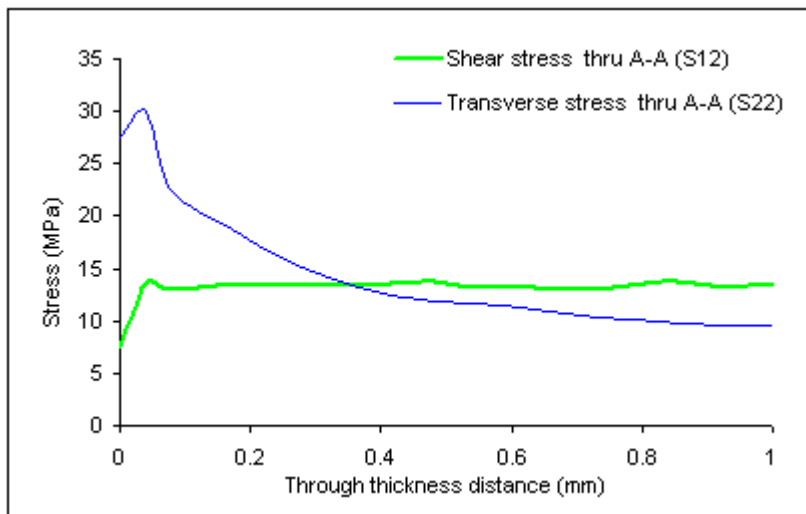


Figure 6.11: FEA results of stresses distributions through thickness of shear model

Table 5.2 summarised the numerical result of shear models with reference to the maximum stresses nearer the edge at different locations. These values were taken at 0.05mm offset from the edge, just to avoid the peak stresses due to material and geometrical singularities. The underlined stress values suggest critical stresses taken through critical stress locations, which were shown in section 5.3.3 (see Figure 5.6). The table also gives the possibilities of joint failure.

From that table, further remarks may be made: -

- the level of transverse adhesive stresses $S_{22}/1$ at joint failure remains within the elastic limit of the adhesive (below 40MPa)
- the transverse composite stresses $S_{22}/2$ at failure for all models at the surface (location 2) are in the range of 20-25MPa
- the shear composite stresses $S_{12}/2$ away from the edges for all models were also high but unlike $S_{22}/2$ were less critical at the surface

- the possibility of both transverse and interlaminar failures exist in LL model. Using a large Tex roving perhaps leads to high voids content
- again transverse failure at location 2 was observed in the LT model. Possible reasons are:
 - the higher transverse stresses (S22/2) at location 2
 - the bi-directional nature of the laminate
 - surface bonded roving based on a large Tex roving. There is also possibility of high population of voids
- the possibilities of all failure modes (transverse/interlaminar/tensile) exist in the RL model, due to the random mat. However, transverse failure was dominating, as seen from the optical image in chapter 4 section 4.4.1 (see Figure 4.21). The reasons are as follows:
 - the transverse stresses at location 2 were high
 - random mat has a poor longitudinal and transverse strength
- the WR model shows all possibilities of failure (transverse/interlaminar/tensile), but mostly interlaminar failure is expected. Although the transverse stresses (S22/2) at location 2 were higher, the failure shifted to the location 3. The crimped nature of woven fabric in terms of weft and wrap directions could be responsible for this. Perhaps this requires 3-D modelling for a better understanding
- the possibility of both (transverse/interlaminar) failure modes exist in IR model but interlaminar failure dominates. Although the transverse stresses (S22/2, S22/3) were almost the same. The possible reasons are as follows:
 - the top surface was made with an inlaid ($0^\circ/90^\circ$) mat, based on small roving size (3600Tex). As discussed previously, low Tex could improve resin impregnation and reduce voids inclusion
 - the small size roving meant that tensile stress S11/2 was high which may have helped to suppress the transverse stresses S22/2

- the content of voids might have been high at location 3, in between two composite layers, rather than top surface
- optical images in chapter 4 section 4.4.1, Figure 4.23 present good picture of failure in an IR model.
- failure index 1 seems to give higher values for LL, LT, RL, and WR, which may suggest, that the transverse failure would take place at location 2. Whilst failure index 2 seems to give a higher value for the IR model. This may suggest that interlaminar failure may occur at location 3 between two composite layers.

6.7.2 Tensile models

In the tensile models, transverse/peel stresses are high at both edges (left and right) just below the adhesive bondline as shown in the stress contour in Figure 6.12. Therefore the joint failure is expected to initiate due to high transverse/peel stress just below the well-consolidated resin coating layer, a few filaments deep below the composite surface at location 2. The damage may also initiate at the interlaminar location between two composite layers, where is a resin-rich matrix layer parting two layers into the overlap region of the composite (location 3). The optical images of the tensile model in Figures 4.24, 4.25 and 4.26, show transverse failure in most of the specimens. The delamination observed was thought to be caused by the weak fibre/matrix interface and presence of voids. Figures 4.27 and 4.28 show interlaminar failure and the delamination observed in matrix layer in between two composite layers due to the matrix strength in transverse direction and the presence of voids.

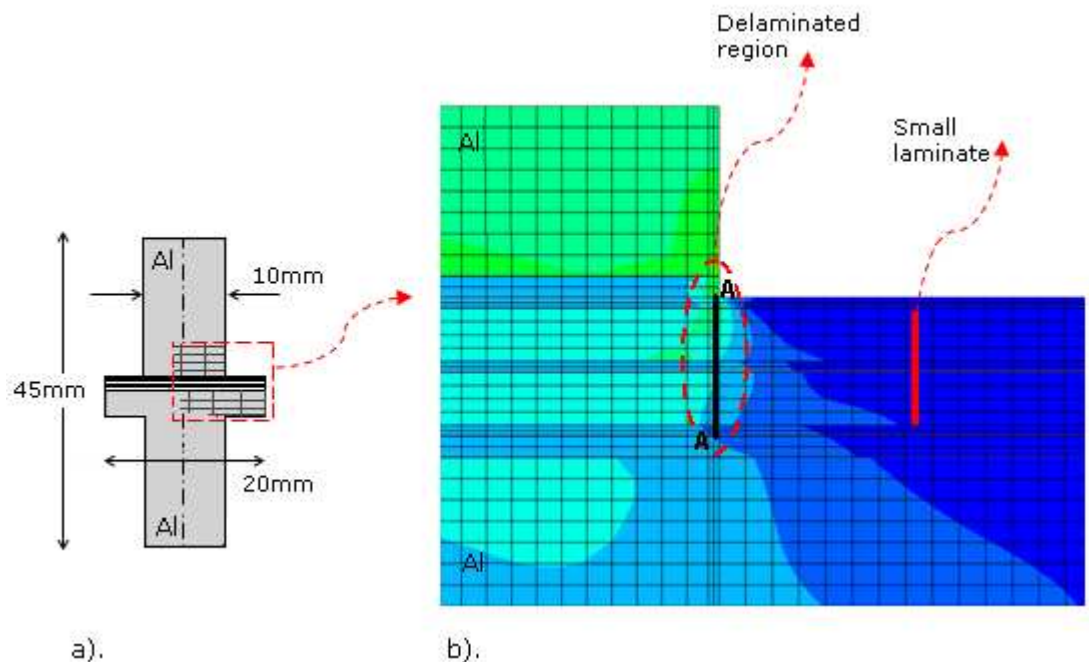


Figure 6.12: FEA tensile model: a). model geometry with LL laminate, b). contour plot in shear model showing critical location (transverse stress)

The distributions of the transverse and shear stresses through the thickness (section A-A Figure 6.12b) for the LL tensile model are shown in Figure 6.13. Again the transverse stresses are quite high near the interfaces, just like in the case of the shear LL model, where the critical location is at about 0.05 mm below the composite surface.

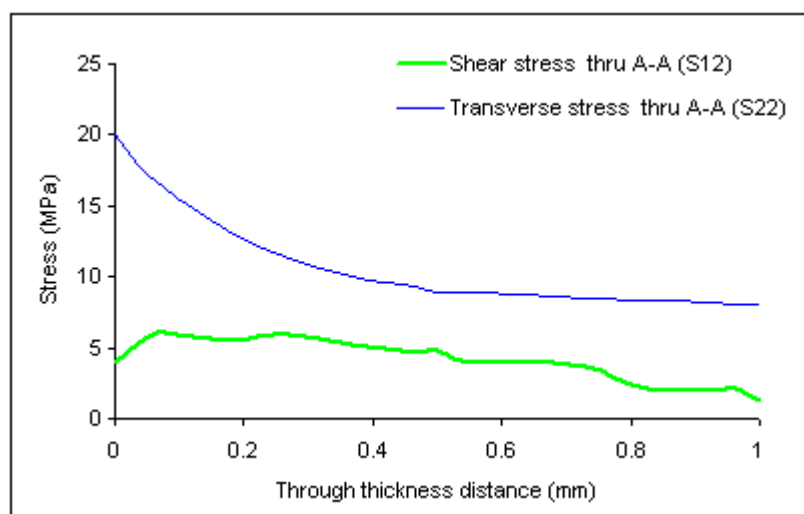


Figure 6.13: FEA results of stresses distributions through thickness of tensile model

However, these stresses are significantly lower than those experienced by the LL shear model (Figure 6.11). The main difference is that the shear model displayed a significant S11/2 tensile stress along the fibres. As indicated before this stress component seems to suppress the transverse stress. This will be discussed in details in Section 6.9.

Table 5.3 summarised the numerical result of tensile models with reference to maximum stresses nearer the edge at different locations. The underlined stress values suggest critical stresses taken through critical stress locations- these are shown in section 5.3.3 (see Figure 5.7). The table also gives the possibilities of joint failure. From the table, the following remarks may be made: -

- the level of transverse adhesive stresses S22/1 at joint failure remains well below the elastic limit of the adhesive (40MPa)
- the transverse composite stresses S22/2 for all models are in the range of 14-18MPa, well below the equivalent stresses in the LL shear model
- S22/2 in the LT model is slightly lower than LL for the same failure load and through thickness stiffness. However, having two bi-directional layers of rovings may cause a difference in Poisson's ratio effects. This is worthy of further investigation
- the RL model seems to have failed at a much lower transverse stress S22/2 than all other models. This suggests that the transverse strength of random fabric is very low and should not be used at a top layer for bondable pultrusions. This requires further material testing
- the WR model shows both possibilities of failure modes (transverse/interlaminar), but mostly interlaminar failure proceeds. Although the transverse stresses (S22/2) at location 2 were higher but the failure shifted to the location 3, due to following reasons:
 - the crimp nature of woven fabric in terms of weft and wrap could be responsible for this. This makes it difficult to fail at sub-surface level and probably shifts the failure between two layers of rovings
 - the surface roving was based on small Tex roving, leading to less

population of voids/micro defects

- the presence of voids/micro defects in the matrix between two layers (location 3).
- The WR, LL and LT models failed at about the same load and produced more or less the same transverse stresses $S_{22}/2$ which seem the main cause of failure. However, WR exhibited a higher interlaminar stress. Perhaps the nature of woven fabric (crimped) requires 3-D models for future work
- the possibility of both transverse/interlaminar failures exists in IR model but interlaminar failure exceeds. Although the transverse stresses ($S_{22}/2$, $S_{22}/3$) were almost the same. Optical images in chapter 4 section 4.4.2 (Figure 4.28) present failure of the IR model. Possible reasons are as follows:
 - the top surface was made with inlaid mat, which was based on smaller Tex roving (3600 Tex) and hence lower voids content
 - the content of voids might be high at location 3

6.8 Correlations

Good agreement was found between the FEA results for macro and meso-scale models, with respect to composite transverse/peel stresses at location 2 and 3. The work demonstrated the importance of having a detailed through thickness model of laminate. This enabled a better understanding of failure and the behaviour of adhesively bonded, pultruded composites. The numerical results are encouraging in terms of failure stress correlation in relation to peel stresses of the composite. A maximum scatter of 20% may be found in the level of failure stress among the meso and macro-scale models, taking both experimental and numerical results into consideration. This is very good considering the complexity of the composite material and delamination stresses. These stress values are also within the range of transverse strength of the composite for both shear and tensile meso-scale models (see Table 5.2 & 5.3). Furthermore, the level of scatter in the experimental results is relatively small. This is because many low strength specimens were discarded due to poor moulding or bonding at an early stage of this study.

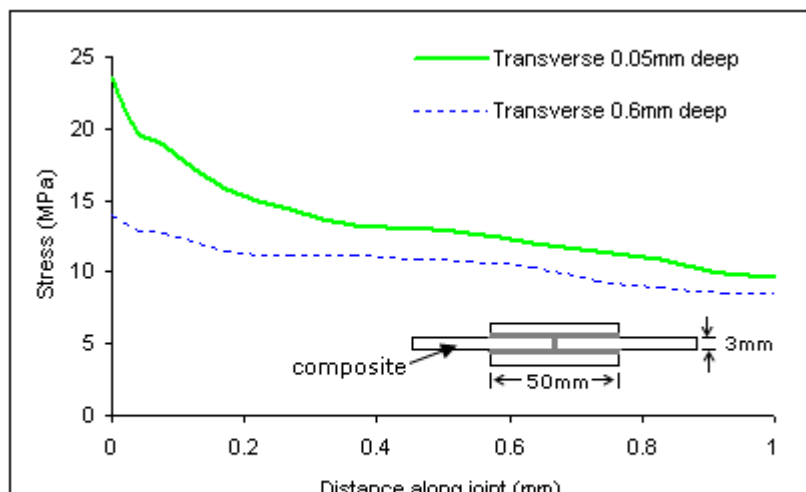
The stresses for the LL/Shear and LL/Tensile models are compared with the DLS macro-scale model which was based entirely on UD rovings of the same volume fibre fraction and materials. Table 6.1 presents the maximum normal and shear stresses in the various locations.

| Type/Load | Load kN | S22/1 MPa | S11/2 MPa | S12/2 MPa | S22/2 MPa | S12/3 MPa | S22/3 MPa |
|------------|------------|--------------|--------------|--------------|--------------|--------------|--------------|
| DLS joint | 20 | 35.5 | 358 | 23.3 | 23.5 | 9.5 | 14.0 |
| LL/Shear | 2.4 | 30.0 | 161.0 | 23.6 | 25 | 15.3 | 12.4 |
| LL/Tensile | 1.4 | 20.1 | 7.0 | 6.0 | 15.7 | 2.6 | 13.8 |

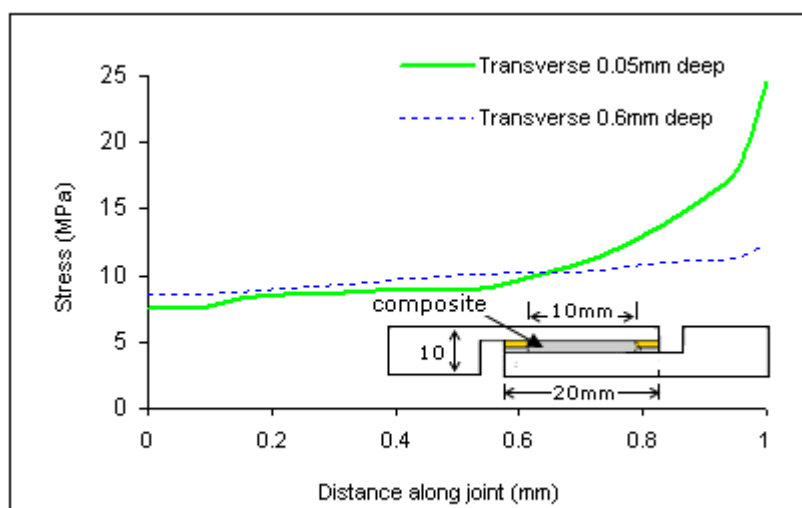
Table 6.1: Correlation between macro and meso-scale model

The table shows that the macro and meso-scale shear models produced similar shear stresses at the composite surface (location 2) – away from the edges. However, the peel adhesive stress is higher for the DLS model. The tensile stress S_{11/2} on the other hand is significantly different between the two models. The value of 358MPa however, is well below the tensile strength of the composite adherend (600MPa). This may suggest that the single lap shear joint used here (TAST) may not be the best representation for double lap joints in pultrusion, some literature referred to this as a butt joint [28].

The most relevant comparison here is the maximum transverse stresses which are shown in Figure 6.14 for the two shear models. The curves of the stress distributions along the joint are at locations 2 and 3. These indicate a close correlation for maximum transverse stresses nearer the edge of the joints/models. These and the table suggest that the difference in the maximum transverse stresses between the two at failure loads is less than 6%. Stresses in location 3 for the two models (0.6mm below the surface) are not that close. Assuming that failure is due to S_{22/2} in both models, it is suggested that the meso-scale model here is a very effective tool to study adhesion in large shear/butt joints.



a).



b).

Figure 6.14: FEA through thickness stress distribution at different offset 0.05mm and 0.6mm on: a). macro-scale DLS model, b). meso-scale LL model

Ideally the correlation should be extended to include other models i.e. LT, RL, WR and IR. In fact the lack of test results for equivalent DLS joints was the main reason to exclude this. The only pultrusion strips which were obtained from the manufacturer for comparisons were the UD strips (equivalent to LL) used for the DLS joints. Considering the excellent performance of the IR model, equivalent materials were requested but this is outside the time of this project. The IR is a type of combination mat which may prove to be the way forward for bondable pultrusions.

However, comparing the two correlated models (LL and DLS) with the LL/Tensile model, gives a difference over 40% in the transverse stresses at failure loads. These clearly do not correlate. This trend seen again in Figures 6.11 and 6.13 for the through thickness shear and transverse stresses. Once again having the tensile specimen with low S11/2 (see Table 6.1) is perhaps the main reason for such a large difference. This suggests that the transverse failure stress requires further investigation and hence a micro-scale model was needed to understand this.

6.9 Micro-scale modelling

In the micro-scale analysis, two models were constructed in Abaqus and further details are given in chapter 5 (see section 5.5.1). The single glass filament of diameter $\sim 16\mu\text{m}$, with matrix resin, is considered as a single filament mode in the first model. Different sizes of voids, up to $10\mu\text{m}$ are considered here to explain their affect on strength.

Figure 5.25 showed the transverse stress response in composites at a micro-scale level at different void sizes at the most critical locations. In fact, this explains that the transverse stress within the matrix could be very significant (about 88MPa). This is well within the bulk vinyl ester strength provided by the manufacturer (90MPa). It is clear that voids/micro defects can easily take the relatively low transverse stress of about 20-22MPa (from macro and meso-scale models) and also provided by the manufacturers. The aim of the second model (see Figure 5.26) is to explain the effect of combined longitudinal/transverse loadings of filament on the level of transverse stress in the matrix beneath it. The mechanism in Figure 6.15 represents aspects of filament /resin interface behaviour within DLS joints and where LL top fabric is used. The top fabric will be loaded in tension

($F_{tensile}$) while the adhesive introduces the peeling force ($F_{transverse}$). The whole mechanism will give a better picture of the difference between shear and tensile models. The diagram shows that $F_{tensile}$ suppresses the transverse stresses resulted from $F_{transverse}$. This combined loading produced another normal component F_{down} , which was added in F_{resin} as shown in equation 1. The analysis shows that the $F_{tensile}$ tend to suppress the transverse stresses, as shown in Table 6.2. This finding helps to explain the reason for the lack of correlation between LL/Tensile and LL/Shear meso-scale models with reference to S22/2 (see table 6.1)

$$F_{transverse} = F_{resin} + F_{down} \quad (1)$$

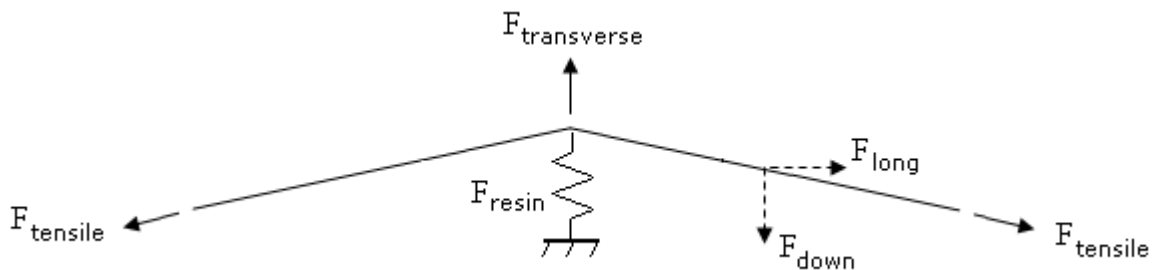


Figure 6.15: Fibre/matrix interface mechanism

| $F_{transverse}$ (0.5N) | | $F_{transverse}$ (1.0N) | | $F_{transverse}$ (1.5N) | |
|----------------------------|-----------------|----------------------------|-----------------|----------------------------|-----------------|
| $F_{tensile}$ | ***S22 (MPa) | $F_{tensile}$ | ***S22 (MPa) | $F_{tensile}$ | ***S22 (MPa) |
| 0 | 9 | 0 | 18.08 | 0 | 27.11 |
| 10 | 7.6 | 10 | 16.81 | 10 | 25.85 |
| 20 | 6.3 | 20 | 15.55 | 20 | 24.59 |
| 30 | 5.2 | 30 | 14.29 | 30 | 23.33 |
| 40 | 3.7 | 40 | 13.03 | 40 | 22.06 |
| 50 | 2.7 | 50 | 11.77 | 50 | 20.8 |

*** Transverse stress

Table 6.2: Transverse Stresses in resin under combined tensile and shear loading

In fact, the tensile micro-scale modelling is the way forward to determine the actual failure stresses in bonded composite joints. This will also enable the study of adhesion characterisation and improvement. The major challenge, however, is devising an experimental technique to perform the test and measure transverse strength at a micro-scale level and this is considered as future work. It is unlikely that an actual interface model is feasible due to the cost associated with micro-mechanics problems of this nature. However, a scale-model might be the way forward and would require dimensional analysis to establish.

Chapter 7

Conclusions and Recommendations

7.1 Conclusions

The “pseudo-pultrusion” has proven to be an effective technique in producing small laminates with different fabric arrangements. Sandwiching these laminates between metallic adherends enables the study of their adhesion in shear and tension. This enabled a good comparison and optimization of the various fabric arrangements. However, more moulding and adhesive bonding parameters need to be considered, including the effects of Tex size, size of filaments, volume fraction and type of adhesives. The effect of moulding conditions in terms of fibre tension and clamping may also have an influence on the adhesion of the laminate, mainly through the changing volume fraction. The mould conditions could lead to residual stresses in the laminate that may affect the adhesion test results. The study demonstrated the validity of the “pseudo-pultrusion” technique in relation to the LL laminates in terms of the level of defects, fibre distribution (see Figure 6.2) and also in term of failure stress correlation (see Figure 6.14). However, the validity of the technique in relation to the IR and other meso-scale laminates requires verification through the moulding of a large scale pultrusion by manufacturers.

The experimental results demonstrated the effectiveness of combining the 0/90° inlaid rovings with random mat (IR). This resulted in a higher strength than the woven equivalent (WR), recently used by pultruders, both in shear and in tension modes. The inlaid fabric would also result in a more uniform surface finish (non-crimp) in comparison with woven or random equivalents.

LL provides a higher longitudinal stiffness than LT and RL due to fibre orientation in

relation to specimens' loading direction. In addition this produced higher strength as shown in Table 5.2 (see Chapter 5). The strength of LL could even produce a higher joint strength should a thinner roving (smaller Tex) be used. However, the LL resulted in a higher strength scatter in comparison to the other fabric arrangements and this is perhaps due to high void defects associated with the large Tex roving. In addition, LL fabric architecture has very limited practical applications.

Due to the geometry, loading and boundary conditions of the meso-scale shear models the composite transverse stress is maximum just below the free edge to the right of the adhesive bondline. Therefore failure is expected to initiate in this region due to high transverse/peel stress just below the well-consolidated resin coating layer, a few filaments deep below the composite surface. This may be referred to as intralaminar failure because of fibre/matrix interface failure or failure due to voids/micro defects. This damage could also initiate at the interlaminar location between the fabric layers (mats), where there is a resin-rich matrix layer parting two layers into the overlap region of the composite.

The determination of the transverse stresses are more challenging in pultruded composites. This is due to the complex nature of the material lay-up. The low aspect ratio of fibre through the thickness of laminate and voids/micro defects puts the major effect on the enhancement of through thickness transverse/peel stresses. Under these situations the Maximum Stress or Hashin failure criteria are recommended for prediction of failure initiation in adhesive bonded pultruded joints. The former is perhaps more accurate.

Finally, the following specific conclusions may be made:

- having detailed through thickness layers in the numerical modeling of composites enables a better understanding of failure and behaviour of adhesively bonded pultruded composites
- the concept of moulding meso-scale laminates is a very worthwhile tool to investigate material parameters without the need to mould large laminates. It also allows detailed through thickness modelling and accounts for failure stresses
- the IR top fabric layer which is based on a relatively small size Tex rovings produced the highest joint strength both in shear and tension joints compared to

other fabrics. The shear IR joints produced a strength improvement of over 50% in comparison to the RL

- a good numerical correlation of failure stresses was obtained using 2-D models for the macro-scale DLS and meso-scale LL/Shear models. A maximum scatter of 20% in level of failure stress is very good, considering the complexity of the composite material and their delamination stresses
- the transverse stresses in the macro and meso-scale models dictate composite failure within bonded joints. It seems that the Maximum Stress failure criterion, with respect to the maximum transverse composite stress, is more relevant to bonded composite joints than other failure criteria
- the micro-scale models are very important in determining the actual failure stresses. These also help to explain the mechanics of filament/resin failure under combined longitudinal and transverse loadings as well as the effect of voids at the interfaces.

7.2 Recommendations

Although the strength of adhesively bonded pultruded joints could already be improved through this research, there are still areas for further research. More experimental and numerical work is recommended to optimize the materials for adhesion and get a better understanding of the behaviour of adhesively bonded pultruded joints. Future work may include the following areas.

- the validity of the “pseudo-pultrusion” technique in relation to the IR requires verification through comparing with large scale pultrusion by the manufacturer
- to measure the structural efficiency of pultrusions based on IR fabric, as top layers taking into consideration joint geometry and dual adhesive system to enhance the joint efficiency
- extensive experimental work has been done in this research and future work should focus on further FEA analysis, including 3-D modelling of woven and

inlaid fabric with different Tex sizes

- further work is needed on the tensile meso-scale and micro-scale modelling to determine the actual failure stresses in bonded composite joints
- to study effects of voids shape, size and location and filament diameters on adhesion
- to devise an experimental technique to measure transverse strength at a micro-scale level. For cost reasons, an up scale-model might be the way forward. This will require dimensional analysis.

List of References

1. Matthews FL., Handbook of polymer composites for engineers, Cambridge, UK, Wood head publishing Limited, 1994.
2. Shahid M., Adhesion characterisation of bonded steel/composite cleavage joints, PhD thesis, University of Glasgow, 1992.
3. Hart-smith LJ., In: Matthews FL., editor. Joining fibre reinforced plastic. London: Elsevier; 1987.
4. Hashim, SA., Strength of resin coated adhesive bonded double lap-shear pultrusion joints at ambient temperature, Int. J. Adhes. Adhes., 2009; Vol.29: pp.294-301.
5. Liberty Pultrusions. 29/10/07.
<http://www.libertypultrusions.com/pulProcess.htm>
6. Peters ST., Handbook for composites. 2nd edition, London: Chapman & Hall; 1998.
7. EPTA, European Pultrusion Technology Association
http://pultruders.com/index.php?option=com_content&task=view&id=15&Itemid=29
8. Hartley J (editor), FibreForce design manual (2002).
www.fibreforce.co.uk.
9. Winona State University, USA. 29/10/07
course1.winona.edu/kdennehy/ENGR390/Topics/pultrusion.ppt
10. Mayer, Rayner M., Design with reinforced plastics, a guide for engineers and designers, London, 1993.
11. Oriunno M., Frediani A., Lazzeri A., Influence of the constitutive characteristic of resin on the composite materials delamination, Eng. Fract. Mech., 1996; Vol.55: pp.1001-1012.
12. Zhao LG., Warrior NA., Long AC., A micromechanical study of residual stress and its effect on transverse failure in polymer-matrix composites, Int. J. Sol. Struc., 2006; Vol.43: pp.5449-5467.

13. Daniel, Isaac M., Engineering mechanics of composite materials, Oxford University Press, 1994.
14. Fibreline composites A/S, 2002: Design manual-revised.
15. Edwards KL., An overview of the technology of fibre reinforced plastic for design purposes, Material and Design, 1998; Vol.19: pp.1-10.
16. McGrath GC, aspect of joining pultrusions.
<http://www.pultron.co.nz/technical.htm>
17. Boyd S., The use of preformed composites for fast marine craft construction, PhD Thesis, 2002, Universities of Glasgow and Strathclyde , Department of Naval Architecture and Marine Engineering.
18. Methvenn JM., Ghaffariyan SR., Microwave assisted pultrusion, Polymeric Materials Science and Engineering, Proceedings of the ACS division of polymeric materials science and engineering, 1992;Vol.66: pp.389-390.
19. <http://www.sierratel.com/jerico/peelply2.html>
20. Cowling MJ., Hashim SA., Smith EM., Winkle IE., Adhesive bonding for marine structural application, Proc. 3rd Int. Conf. on Polymers in a Marine Environment , London, I.Mar.E., October 1991.
21. Lackey E., Vaughan JG., Wasabaugh F., Usifer D., Ubrich P., Effects of fillers on pultrusion processing and pultruded properties, Composite institute, International composites EXPO, 1999.
22. Jeandreau, J., P., Intrinsic mechanical characterisation of structural adhesives, Int. J. Adhes. Adhes. 1991; Vol.6: pp.71-79.
23. Paciornik S., Martinho FM., de Mauricio MHP., d' Ameida JRM, Analysis of the mechanical behaviour and characterisation of pultruded glass fibre resin matrix composites, Compos. Sci. Tech., 2003; Vol.63:pp.295-304.
24. Boyd SW, Winkle IE, Day AH, Bonded butt joints in pultruded GRP panels – an experimental study, Int. J. Adhes. Adhes., 2004; Vol.24: pp.263-275.
25. Binshan SY., Svenson AL., Bank LC., Mass and volume fraction properties of pultruded glass fibre composites, Composites, 1995; Vol.26:pp.725-731.
26. Dr Davies, Curtin University Of Technology, Perth, Australia. 29/10/07
http://mecheng.curtin.edu.au/davies/pdf/Applications_of_composite_materials.pdf

27. MODEC homepage. (2009).
www.modec.com/fps/fpso_fso
28. Shenoi RA., Wellicome JF., Composite materials in maritime structures, Volume 2: Practical consideration, Cambridge Ocean Technology Series 5, Cambridge University Press, 1993.
29. Karbhari VM., Building materials for the renewal of civil infrastructure, Reinforced Plastics, 2005; Vol.49:pp.14-25.
30. Exel Composites Pultrusion.
www.exelcomposites.com
31. Harvey WJ., A reinforced plastic footbridge, Aberfeldy, UK, Structural Engineering International, Vol.3, 2005.
32. Home made composite (HomMaCom).
http://www.composites.ugent.be/home_made_composites/HomMaCom.html
33. Minford JD., In: A.J. Kinloch, Editor, Durability of structural adhesives, Appl. Sci., London, 1983: pp.135.
34. Kinloch AJ., Durability of structural adhesives (ed. AJ. Kinloch), Elsevier Applied Science Publishers, ISBN 0 85334 214 8, chap 1.
35. Kinloch AJ., The science of adhesion part 1. Surface and interfacial aspects, J. Mat. Sci., 1980;Vol.15:pp.2141-2166.
36. Bickerman JJ., The fundamentals of tackiness and adhesion, J. Colloid Sci., 1947; Vol.2:pp.163-175.
37. Voyutskii SS., Autohesion and adhesion of high polymers, John Wiley / Interscience, New Work, 1963.
38. Deryaguins BV., Smilga VP., Adhesion fundamentals and practise, McLaren, London, 1969: pp.152.
39. Staverman AJ., Adhesion and adhesives 1 (ed R. Houwink and G. Salmon), Elsevier, Amsterdam,1965; pp.6.
40. Cagle, Charles V., Handbook of adhesive bonding: wetting, Kingsport Press, USA. , 1973; pp.1-12.
41. Johnson RE., Jr., and Dettre RH., Surface and colloid science. ed., Matijevic E., Wiley-Interscience, New York, 1969.

42. Wenzel RN., Resistance of solid surfaces to wetting by water, *Ind. Eng. Chem.*, 1936; Vol.28: pp.988-994.
43. Pocius AV., *Adhesion and adhesive technology: An Introduction*, Hanser publishers, Munich, 1997.
44. Boone, Michael James., Mechanical testing of epoxy adhesives for naval applications. surface preparation, M.sc Thesis, The university of maine., 1995; pp.7.
45. Baker FS., Effect of ultra clean stainless steel surfaces on the strength of epoxide-stainless steel butt joint, *J. Adhes.*, 1979; Vol.10: pp.107-122.
46. Wingfield JRJ., Treatment of composite surfaces for adhesive bonding, *Int. J. Adhes. Adhes.* , 1993; Vol.13:pp.151-156.
47. Brockmann WG., The importance of surface pre-treatment prior to bonding, *Proc. Conf. IMechE*, 1986; pp.61-70.
48. Parker BM., Adhesive bonding of fibre reinforced composites, *Int. J. Adhes. Adhes.*, 1994; Vol.14:pp.137-143.
49. Guha PK., Epel JN., Adhesives for the bonding of graphite /glass composites, Society of Automotive Engineers, Inc. 790149, 1980: pp.566-572.
50. Pultrex Design Manual, The new and improved pultrex pultrusion global design manual of standard and custom fibre reinforced polymer structural profiles, 2000; Vol.3, Revision 3, Metric Version.
51. Brockmann W., Durability of structural adhesives (ed. AJ. Kinloch), Elsevier Applied Science Publishers, ISBN 0 85334 214 8, Chap 7, 1983.
52. Volkersen, O.Die Niekraftverteilung in Zugbeanspruchten mit Konstanten.
53. Adam RD., Comyn J., Joining using adhesive , *Assembly Automation* 2000; Vol.20: pp.109-117.
54. Goland M. and Reissner E., The stresses in cemented joints. *J. Appl. Mech.*, 1944; Vol.66: pp.17-27.
55. Hart-smith LJ., Adhesive bonded single-lap joints, NASA CR-112235, NASA Langley Research Centre, Hampton, Virginia, USA 1973.
56. Adams RD, Mallick V. Method for the stress analysis of lap joints. *J. Adhes.*, 1992; Vol.38:pp.199-217.

57. Allman DJ., A theory for elastic stresses in adhesive bonded lap joints, *Quart. J. Mech. Appl. Math.*, 1977; Vol.30: pp.415-436.
58. Chen D., Cheng S., An analysis of adhesive-bonded single-lap joints. *ASME J. Appl. Mech.*, 1983; Vol.50:pp.109–115.
59. Tsai MY., Oplinger DW., Morton, J., Improved theoretical solutions for adhesive lap joints. *Int. J. Sol. Struc.*, 1998; Vol.35: pp.1163-1185.
60. Renton WJ., Vinson JR., Analysis of adhesively bonded joints between panels of composite materials, *ASME J. Appl. Mech.*, 1977; pp.101-106.
61. Bigwood A., Crocombe AD., Elastic analysis and engineering design formulae for bonded joints, *Int J. Adhes. Adhes.*, 1989; Vol.9:pp.229-242.
62. Wang CH., Rose LFR., Determination of tri axial stresses in bonded joints, *Int. J. Adhes. Adhes.*, 1997; Vol.17: pp.17-25.
63. Roberts TM., Shear and normal stresses in adhesive joints, *J. Eng. Mech.* 1989; Vol.115:pp.2460-2479.
64. Bogdanovich AE., Kizhakkethara I., Three dimensional finite element analysis of double lap composite adhesive bonded joint using submodelling approach , *Comp. Part B* 1999; Vol.30: pp.537-551.
65. Wahab MMA., Ashcroft LA., Failure prediction using FEA and analytical solutions for adhesively bonded composite beams, *European Adhes. Conf.* 10-10-2002: pp.137-140.
66. Liu J., Sawa T., Strength and finite element analysis of single lap joints with adhesively bonded columns, *J.Adhes. Sci. Tech.*, 2003; Vol.17: pp.1773-1784.
67. Tong L., Steven GP., *Analysis and design of structural bonded joint*, Kulwer Academic Publisher, Massachusetts, USA., 1999.
68. Sheppard A., Kelly DW., Tong L., A damage zone model for the failure analysis of adhesively bonded joints, *Int. J. Adhes. Adhes.*, 1998; Vol.18: pp.385-400.
69. Hattori T., A stress singularity parameter approach for evaluating the adhesive strength of single lap joint, *JSME Int. J. Series I*, 1991; Vol.34: pp.326-331.
70. Groth HL., Stress singularity and fracture at interface corners in bonded joints, *Int. J. Adhes. Adhes.*, 1988; Vol.8: pp.107-113.

71. Katona TR., Batterman SC., Surface roughness effects on the stress analysis of adhesive joints, *Int. J. Adhes. Adhes.*, 1983; Vol.3: pp.85-91.
72. Pradhan SC., Finite element analysis of crack growth in adhesively bonded joints, *Int. J. Adhes. Adhes.*, 1995; Vol.15:pp.33-41 .
73. Liu J., Sawa T., Toratani H., A Two-dimensional stress analysis and strength of single-lap adhesive joints of dissimilar adherends subjected to external bending moments , *J. Adhes.*, 1999; Vol.69: pp.263-291.
74. Liu J., Sawa, T., Stress analysis and strength evaluation of single-lap adhesive joints combined with rivets under external bending moments, *J. Adhes. Sci. Tech.*, 2001; Vol.15: pp.43-61.
75. Mitra AK., Ghosh B., Interfacial stresses and deformations of an adhesive bonded double strap butt joint under tension , *Comp. and Struc.*, 1995; Vol.55: pp.687-694.
76. Wooley GR., Carver DR., Stress concentration factors for bonded lap joints, *J. Aircraft* 8, 1971;Vol.10:pp.817-820:
77. Delale F., Erdogan F., Aydinoglu MN., Stresses in adhesively bonded joints: A closed form solution, *J. Comp. Mat.*, 1981; Vol.15: pp.249-271.
78. Crocombe AD., Adam RD., Influence of the spew fillet and other parameters on the stress distribution in the single lap joint, *J. Adhes.*, 1981; Vol.13:pp.141-155.
79. Crocombe AD., Adam RD., An elastic-plastic investigation of the peel test, *J. Adhes.*, 1982; Vol.13: pp.241-267.
80. Crocombe AD., Adam RD., Peel analysis using finite element analysis, *J. Adhes.*, 1981; Vol.12: pp.127-139.
81. Sawa T, Lin J, Nakano K, Tanaka J., A two-dimensional stress analysis of single lap adhesive joints of dissimilar adherends subjected to tensile loads, *J. Adhes. Sci. Tech.*, 2000; Vol.14: pp.43-66.
82. Segurado J, LLorca J. A computational micromechanics study of the effect of interface decohesion on the mechanical behaviour of compos., *Acta Mater.*, 2005;53:pp.4931-4942.

83. LLorca J., Segurado J., Three-dimensional multi particle cell simulations of deformation and damage in sphere-reinforced composites., Mater. Sci. Eng. A, 2004; Vol.365:pp.267-274.
84. Totry E., Gonza'lez C, LLorca J. Failure locus of fibre reinforced composites under transverse compression and out-of-plane shear, Compos. Sci. Tech., 2008; Vol.68:pp.829-839.
85. Haj Ali RM., Kilic H., Nonlinear constitutive models for pultruded FRP composites, Mech. Mat., 2003; Vol.35: pp.791-801.
86. Fish J., Yu Q., Multiscale damage modelling for composite materials: theory and computational framework, Int. J. Numer. Meth. Engng., 2001; Vol.52:pp.161-191.
87. Gonza'lez C, LLorca J., Multiscale modelling of fracture in fibre reinforcedcomposites. Acta Mater 2006; Vol.54:pp.4171-4181.
88. Hart-smith LJ., Analysis and design of advanced composite bonded joints, NASA contractor report, 1974.
89. Kim KS., Yoo JS., Yi YM., Kim CG., Failure mode and strength of uni-directional composite single lap bonded joints with different bonding methods, Compos. Struc., 2006; Vol.72: pp.477-485.
90. Kairous KC., Matthews FL., Strength and failure modes of bondable single lap joints between cross-ply adherends, Compos.,1993; Vol.24 :pp.475-484.
91. Cheuk PT., Tong L., Failure of adhesive bonded composite lap shear joints with embedded precrack; Compos. Sci. Tech., 2002; Vol.62: pp.1079-1095.
92. Qin M., Dzenis YA., Analysis of single-lap adhesive composite joints with delaminated adherend, Compos. B, 2003; Vol.34:pp.167-173.
93. Kayupov M., Dzenis YA., Stress concentration caused by bond cracks in single lap adhesive composite joints, Compos. Struct., 2001;Vol.54: pp.215-220.
94. Tsai MY., Morton J., The effect of a spew fillet on adhesive stress distributions in laminated composite single-lap joints, Compos. , 1995; Vol.32: pp.123-131.
95. Kim JK., Kim HS., Lee DG., Investigation of optimal surface treatments for carbon/epoxy composite adhesive joints, J. Adhes. Sci. Tech., 2003; Vol.17:pp.339-352.

96. Yang C., Pang SS., Stress-strain analysis of adhesive bonded single lap composite joints under cylindrical bending, Compos., 1993; Vol.3:pp.1051-1063.
97. Kim H., The influence of adhesive bonded thickness imperfections on stresses in composite joints, J. Adhes.,2003; Vol.79:pp.621-642.
98. Kim KS., Yi YM., Cho GR., Kim CG., Failure prediction and strength improvement of uni- directional composite single lap bonded joints. Compos. Struct., 2007; Vol.82: pp.513-520.
99. Petit PH., Waddoups ME., A Method of Predicting the Nonlinear Behaviour of Laminated Composites, J. Compos. Mat., 1969; Vol.3: pp.2-19.
100. Tong L., An assessment of failure criteria to predict the strength of adhesively bonded composite double lap joints, J. Reinforced Plastic & Compos., 1997; Vol.16: pp.698-713.
101. Keller T., Vallee T., Adhesively bonded lap joints from pultruded GFRP profiles. Part II: Joint Strength Prediction, Compos. Part B, 2005; Vol.36:pp.341-350.
102. Adam RD., Comyne J., Wake WC., Structural adhesives in engineering, 2nd ed. London: Chapman & Hall; 1997.
103. Carlos GD., Pedro P., Camanho and Cheryl AR., Failure criteria for FRP laminate, J. Compos. Mat. , 2005; Vol.39: pp.323-345.
104. Harris J., Adams R., Strength prediction of bonded single lap joints by non-linear finite element methods, Int. J. Adhes. Adhes., 1984; Vol.4: pp.65-78.
105. Adam RD., Strength predictions for lap joints, especially with composite adherends. A review, J. Adhes. , 1989; Vol.30: pp.219-242.
106. Adams RD., Harris JA., The influence of local geometry on the strength of adhesive joints, Int. J. Adhes. Adhes. ,1987; Vol.7: pp.69-80.
107. Czarnocki P., Piekarski K., Fracture strength of an adhesive bonded joint, Int. J. Adhes. Adhes., 1986; Vol.6: pp.93-95.
108. Hollaway L., Romhi A., Gunn M., Optimisation of adhesive bonded composite tubular sections, Comp. Struct., 1990; Vol.16: pp.125-170.
109. Lee SJ., Lee DG., Development of a failure model for the adhesively bonded tubular single lap joint, J. Adhes., 1992; Vol.40:pp.1-14.

110. Mori K., Sugibayashi T., Predicting the strength of stepped lap bonded joint with adhesive resin under tensile shear load , JSME, Int. J. Ser. I., 1990; Vol.33: pp.349-355.
111. Dvorak GJ., Laws N., Analysis of progressive matrix cracking in composite laminates: – II First Ply Failure, J. Compos. Mat., 1987; Vol.21: pp.309–329.
112. Papini M., Fernlund G., Spelt JK., Effect of crack-growth mechanism on the prediction of fracture load of adhesive joints, Comp. Sci. Tech., 1994; Vol.52: pp.561-570.
113. Wisnom MR., Shear fracture of unidirectional composites without initial cracks, Comp. Sci. Tech., 1994; Vol.52: pp.9-17.
114. Whitney J., Nusimer R., Stress fracture criteria for laminated composites containing stress concentrations, J. Comp. Mat., 1974; Vol.8:pp.253-265.
115. Brewer J., Lagace P., Quadratic stress criterion for initiation of delamination, J. Comp. Mat., 1988; Vol.22: pp.1141-1155.
116. Joo J., Sun C., A failure criterion for laminates governed by free edge interlaminar shear stress, J. Comp. Mat., 1992; Vol.26: pp.1510-1522.
117. Clark JD., McGregor IJ., Ultimate tensile stress over a zone: a new failure criterion for adhesive joints, J. Adhes., 1993; Vol.42: pp.227-245.
118. John SJ., Kinloch AJ., Matthews FL., Measuring and predicting the durability of bonded carbon fibre-epoxy composites joints, Compos., 1991; Vol.22: pp.121-126.
119. Keller T., Vallee T., Adhesively bonded lap joints from pultruded GFRP profiles. Part I: stress-strain analysis and failure mode, Compos. Part B, 2005; Vol.36:pp.331-340.
120. Zhang Ye., Keller T., Progressive failure process of adhesively bonded joints composed of pultruded GFRP, Compos. Sci. Tech., 2008;Vol.68:pp.461-470.
121. Lee HK., Pyo SH., Kim BR., On joint strengths, peel stresses and failure modes in adhesively bonded double-strap and supported single-lap GFRP joints. Compos. Struc., 2009; Vol.87: pp.44-54.
122. Lee J., Kim Y., Jung J., Kosmatka J., Experimental characterisation of a pultruded GFRP bridge deck for light weight vehicles, Compos. Struc., 2007; Vol.80,pp.141-151.

123. Boyd SW., Dulieu Barton JM., Rumsey L., Stress analysis of finger joints in pultruded GRP materials, *Int. J. Adhes. Adhes.*, 2005; Vol.26:pp.498-510.
124. Boyd SW., Dulieu Barton JM., Thomson OT., Gherardi A., Development of a finite element model for analysis of pultruded structures using thermoelastic data, *Compos. Part A*, 2008; Vol. 39:pp.1311-1321.
125. Kinlock AJ., Blackman BRK., Teo WS., The adhesive bonding of polymeric matrix composites, *Proc ICCM17*, Edinburgh July ; 2009.
126. Herakovich CT., and Mirzadeh F., Properties of pultruded graphite/epoxy, *J. Reinforced Plastic and Compos.*, 1991; Vol.10: pp.2-28.
127. Wang Y., Zureick A., Characterization of the longitudinal tensile behaviour of pultruded I-shape structural members using coupon specimens. *Compos. Struct.*, 1994; Vol.29: pp.463-472.
128. Paciornik S., Martinho FM., de Mauricio MHP., d' Almeida, JRM., Analysis of the mechanical behaviour and characterization of pultruded glass fibre-resin matrix composites. *Compos. Sci. Tech.*, 2003; Vol.63:pp.295-304.
129. GangaRao HVS., Palakamshetty S., Designing for pultruded adhesive bonded joint. *Modern plastic international*, 2001;Vol.31:pp. 79-82.
130. Liu XL., Hillier W., Heat transfer and cure analysis for the pultrusion of a fibre glass- vinlyester beam. *Compos. Struc.*, 1999; Vol.47:pp.581-588.
131. Barbero EJ., Trovillion J., Prediction and measurement of the post critical behaviour of fibre-reinforced composite columns, *Compos. Sci. Tech.*, 1998; Vol.58: pp.1335-1341.
132. Pyror CW., Jr., Barker RM., Finite element analysis of bending extensional coupling in laminated composites, *J. Comp. Mat.*, 1970; Vol.4:pp.549-552.
133. Herakovich CT., Edge effects and delamination failures, *J. Strain Anal.* , 1989; Vol.4:pp.245-252.
134. Pagano NJ., Pipes RB., Some observations on the interlaminar strength of composite laminates, *Int. J. Mech. Sci.*, 1973; Vol.15 : pp.679-888.
135. Pagano N.J., Pipes RB., The influence of stacking sequence on laminate strength, *J. Compos. Mat.*, 1971; Vol.5: pp.50-57.
136. Puppo AH., Evensen HA., Interlaminar shear in laminated composites under generalized plane stress, *J. Compos. Mat.*, 1970; Vol.4: pp.204-220.

137. Amar C., Garg., Delamination a damage mode in composite structures, Engi. Fract. Mech., 1988; Vol.29: pp.557-584.
138. Kairouz KC., Matthew FL., A finite element analysis of the effect of stacking sequence on the failure mode of bonded composite single lap joints, Comp. Mat., Design and Analysis, ed De Wilde, WP., and Blain, WR., Computational Mechanics Publications, Southampton, 1990: pp.549-564
139. Kairouz KC., Matthew FL., Mechanism of failure in bonded CFRP single lap joints with stacking sequences, Conf. Proc. FRC 90, Liverpool, Institution of Mechanical Engineers, UK, 1990: pp.47-59.
140. Pradhan SC., Iyengar NGR., Kishore NN., Parametric study of interfacial debonding in adhesively bonded composite joints, Comp. Struc., 1994; Vol.29: pp.119-125.
141. Ratwani MM., Kan HP., Effect of stacking sequence on damage propagation and failure modes in composite laminates, Damage in Comp. Mat., ASTM STP 775, ed. Reifsnider KL., American society for testing and materials, 1982:pp.211-228.
142. Lakshminarayana HV., Viswanath S., A correlation study of finite element modelling for the stress analysis of composite material laminates, J. Strain Anal., 1978; Vol.13: pp.205-212.
143. Herakovich CT., Influence of layer thickness on the strength of angle-ply laminates, J. Comp. Mater. 1982; Vol.16: pp.216–218.
144. Harrison RP., Bader MG., Damage development in CFRP laminate under monotonic and cyclic stressing, IV National and I International meeting on composite materials, Milan 1980: 19-21. (To be presented in 1981 by Appl. Sci. Pub. Ltd.).
145. Jones RM., Mechanics of composite materials, ^{2nd ed. Taylor & Francis, Inc ;1999.}
146. Tsai SW, Hahn HT, Introduction to composite materials, Pennsylvania: Technomic Publishing Company; 1980.
147. Nisar JA, Hashim SA, Das PK," Pultrusion characteristic for adhesive joints, 2nd International Conference on Analysis and Design of Marine Structures, Lisbon, Portugal, March 2008.

148. Park JY., Zureick Abdul-Hamid, Effect of filler and void content on mechanical properties of pultruded composite materials under shear loading, *Poly Compos.* 2005; Vol. 26: pp.181-192.
149. Davim J.P., Mata, F., New machinability study of glass fibre reinforced plastics using polycrystalline diamond and cemented carbide (K15) tools. *Materials and Design*, Elsevier, 2005; pp.1050-1051.
150. BS 5350-A1: Methods of test for adhesives, Adherends, Adherenpreparation, 1976.
151. Shields, J., *Adhesion handbook*, Butterworth & Co Ltd. ISBN: 0408002107, 1976.
152. Elbing F., Anagreh N., Dorn L., Uhlmann E., Dry ice blasting as a pre-treatment of aluminium surfaces to improve the adhesive strength of aluminium bonding joint, *Int. J. Adhes. Adhes.*, 2005; Vol.23:pp.69-79.
153. Li W., Blunt L., Stout KJ., Stiffness analysis of adhesive bonded Tee- joint, *Int. J. Adhes. Adhes.*, 1999;Vol.19:pp.315-320.
154. Lucas FM., Adams RD., The strength of adhesively bonded T-joints, *Int. J. Adhes. Adhes.*, 2002; Vol.22:pp.311-315.
155. Knox EM., Cowling MJ., Hashim SA., Creep analysis of adhesively bonded connections in GRE pipes including the effect of defects, *Compos. Part A: Applied science and manufacturing*, 2000; Vol.31:pp.583-590.
156. Hu SZ., Jiang L., A finite element simulation of the test procedure of stiffened panels, *Marine structures*, 1998; Vol.11:pp.75-99.
157. Z. Hashin, Failure criteria for unidirectional fibre composites. *J. App. Mech.*, 1980; Vol. 47: pp.329–334.
158. Wisnom MR, S. Yucel, The effect of transverse compressive stresses on tensile failure of glass fibre-epoxy. *Compos. Struct.*, 1995; Vol. 32: pp.621-626.
159. Tsai SW., Wu EM., A general theory of strength for anisotropic materials, *J. Compos. Mater.*, 1971;Vol.5:pp. 58–80.
160. Goswami S., A finite element investigation on progressive failure analysis of composite bolted joints under thermal environment, *J. Reinforced Plastics and Compos.*, 2005; Vol. 24: pp.161-171.

161. Chandler HD., Campbell IMD., Stone MA., An assessment of failure criteria for fibre-reinforced composite laminates, Int. J. Fat., 1995; Vol.17:pp.513-518.
162. Herakovich CT, Mechanics of fibrous composites. New York: Wiley. 1998.
163. ASTM D 792-00, Test methods for density and specific gravity of plastic. In: Annual book of American Society for Testing Materials, 08.01, 2002, pp.156-161.
164. Barbero EJ, Introduction to composite materials design, Philadelphia, PA: Taylor and Francis, Publication, 1999.
165. BS 2782-3: Methods 320A to 320F: Methods of testing plastics: Mechanical properties: Tensile strength, elongation and elastic modulus, 1976.
166. BS EN ISO 527-2: Plastics-Determination of tensile properties - Part2: Test conditions for moulding and extrusion plastics, British standard Institution, 1996
167. BS 5350-C3: Methods of test for adhesives: Determination of bond strength in direct tension, 1989.
168. ASTM D5573-99: Standard Practice for Classifying Failure Modes in Fiber-Reinforced-Plastic (FRP) Joints, 2005.

Publications

Journal publications

- J.A. Nisar, S.A. Hashim, (2010)," **Meso-scale laminate adhesive joints for pultrusions**, Inter. Journal. Adhesion and Adhesives (in press 2010).
- SA. Hashim, JA. Nisar, Tsouvalis & K. Anyfantis, P. Moore ,I. Chirica, C. Berggreen, A. Orsolini & A. Quispitupa, D. McGeorge & B. Hayman, S. Boyd, K. Misirlis, J. Downes & R. Dow, E. Juin, (2010), **Fabrication, testing and analysis of steel/composite DLS adhesive joints**, Journal of Ships and offshore structures, Taylor & Francis (in press 2010)

Conference publications

- Jawad A Nisar, SA Hashim, P. Dobson" **Multi-scale modelling of the interfaces in pultrusion joints**, 14th European Conference on Composite Materials (ECCM 14), Budapest, Hungary 7-10th June 2010.
- Jawad A Nisar, SA Hashim," **Modelling the interfaces of bondable pultrusions**, 5th International ASRANet conference on Integrating Structural Analysis, Risk & Reliability, Edinburgh Grosvenor, Edinburgh, UK, 14-16th June 2010.
- SA Hashim, Jawad A Nisar, ,” **Moulding and modeling of bondable pultrusions** , 2nd Indo-Swiss bonding International Symposium on Bonding, Adhesion & Nano Technology at Sikkim Manipal Institute of Technology, East Sikkim, India, 11-13th February 2010.
- Jawad A Nisar, SA Hashim,” **Experimental and numerical study of meso scale adhesive bondable pultrusions**, ICCM-17 17th International Conference on composite materials, Edinburgh International Convention Centre, Edinburgh (EICC), UK, 27-31th July 2009.
- Jawad A Nisar, SA Hashim, PK. Das,” **Pultrusion characteristic for adhesive**

joints, 2ND International Conference on Analysis and Design of Marine Structures, Lisbon, Portugal, 16-18 March 2009.

- Jawad A Nisar, SA Hashim, Marc Gow," **Meso-Scale models for bondable pultursions**, 10th International Conference on Science & Technology of Adhesion and Adhesives, St Catherine's Oxford, Oxford, Uk, 3-5 September 2008.
- Jawad A Nisar, C. Soutis, Frank R. Jones," **Photoelastic Analysis of stress transfer from matrix to fibre through interphase in compression**, 12th International Conference on AEROSPACE SCIENCES & AVIATION TECHNOLOGY Egypt, 29-31 May 2007.
- Jawad A Nisar, C. Soutis, Frank R. Jones," **Compressive Behaviour of Glass Fibre Reinforced Polymer (GFRP) composite. Effect of Fibre/Matrix Interface/Interphase**, 9th Deformation and Fracture of Composites conference (DFC9) Sheffield University, Sheffield, UK, April 2007.
- Jawad A Nisar, Ahmad S Abdullah , Numan Iqbal "Mass **Optimization of a Small Pressure Vessel Using Metal/FRP (Fiber Reinforced Polymers) Hybrid Structures** ", 3rd International Bhurban Conference on Applied Sciences and Technology, BHURBAN PAKISTAN, June 2004.
- SA. Hashim & JA. Nisar, N. Tsouvalis & K. Anyfantis, P. Moore ,I. Chirica, C. Berggreen, A. Orsolini & A. Quispitupa, D. McGeorge & B. Hayman, S. Boyd, K. Misirlis, J. Downes & R. Dow, E. Juin," **Design and analysis of DLS steel/composite thick adherend adhesive joints**, ICCM-17 17th International Conference on composite materials, Edinburgh International Convention Centre, Edinburgh (EICC), UK, 27-31th July 2009.
- SA Hashim, Jawad A Nisar, Adam smith" **Durability of adhesive joints in wet conditions**", International Conference on Light Weight Marine Structures, Department of Dept. of Naval Architecture & Marine Engineering, Universities of Glasgow & Strathclyde, UK, 6-8 September 2009.

- SA Hashim, Jawad A Nisar” **Adhesive bonding of composites**”, GMRI Event on light weight materials, Sir Charles Wilson Building, Universities of Glasgow, UK, 19th June 2009.
- SA. Hashim & JA. Nisar, N. Tsouvalis & K. Anyfantis, P. Moore ,I. Chirica, C. Berggreen, A. Orsolini & A. Quispitupa, D. McGeorge & B. Hayman, S. Boyd, K. Misirlis, J. Downes & R. Dow, E. Juin,” **Fabrication, testing and analysis of steel/composite DLS adhesive joints**, 2ND International Conference on Analysis and Design of Marine Structures, Lisbon, Portugal, 16-18 March 2009.
- SA Hashim, GM Miller, Jawad A Nisar” **Smart Strap for DLS pultrusion adhesive joints**”, 10th International Conference on Science & Technology of Adhesion and Adhesives, St Catherine’s Oxford, Oxford, UK, 3-5 September 2008

Content of Appendices

| | |
|---|-------------|
| CONTENT OF APPENDICES..... | A-1 |
| LIST OF FIGURES IN APPENDICES..... | A-3 |
| LIST OF TABLES IN APPENDICES..... | A-4 |
| | |
| APPENDIX A..... | A-5 |
| MATERIAL PROPERTIES..... | A-5 |
| A.1: Pultruded transverse tensile specimen..... | A-5 |
| A.2: Silicone rubber mould fabrication..... | A-6 |
| A.2.1: Silicone rubber mould fabrication..... | A-7 |
| A.2.2: MCP SILICONE RUBBER technical data sheet (KE-1300T)..... | A-8 |
| A.3: Adhesive bulk specimen..... | A-9 |
| A.4: HUNSTMAN technical data sheet (Araldite 2015)..... | A-12 |
| A.5: CIBA-GEIGY technical data sheet (AY 103/AY 105)..... | A-16 |
| A.6: DSM composite resin..... | A-19 |
| A.6.1: Technical data sheet (Atlac 430)..... | A-19 |
| A.6.2: Stress-strain curve of Atlac 430..... | A-20 |
| | |
| APPENDIX B..... | B-1 |
| EXPERIMENTAL PROGRAMME..... | B-1 |
| B.1: Engineering Drawings of meso-scale laminate moulding jig..... | B-1 |
| B.2: Meso-scale joint bonding..... | B-3 |
| B.2.1: C-clamp as a bonding jig..... | B-3 |
| B.2.2: Macro bonding jig..... | B-4 |
| B.2.3: Engineering drawing of advance bonding jig..... | B-5 |
| B.2.3.1: Tensile bonding jig..... | B-5 |
| B.2.3.2: Shear bonding jig..... | B-7 |
| B.3: Engineering Drawings of Clamping Adaptor..... | B-9 |
| B.3.1: Tensile clamping adaptor..... | B-9 |
| B.3.2.: Shear clamping adaptor..... | B-10 |

| | |
|---|-------------|
| B.3.3.: Alignment adaptor..... | B-11 |
| B.4: Engineering Drawings of adherend..... | B-12 |
| B.4.1: Shear aluminium adherend..... | B-12 |
| B.4.2: Tensile aluminium adherend..... | B-13 |
| B.5: Macro-scale joint bonding..... | B-14 |
| B.5.1: Macro bonding jig..... | B-14 |
| B.6: Experimental results..... | B-15 |
| B.6.1: Shear specimen..... | B-15 |
| B.6.2: Tensile specimen..... | B-17 |
| APPENDIX C..... | C-1 |
| FINITE ELEMENT ANALYSIS | C-1 |
| APPENDIX D..... | D-1 |
| FAILURE CRITERIA..... | D-1 |

List of Figures in Appendices

| | | |
|------------------------|--|------|
| Figure A.2.1: | Schematic view of silicone rubber mould fabrication..... | A-7 |
| Figure A.3.1: | Adhesive bulk tensile test specimen..... | A-9 |
| Figure A.3.2: | Adhesive dog bone specimen with trap air bubble in circle..... | A-10 |
| Figure A.3.2: | Stress-strain curve obtained from bulk adhesive dog-bone specimen..... | A-11 |
| Figure B.1.1: | Meso-scale moulding jig (Full assembly)..... | B-1 |
| Figure B.1.2: | Meso-scale moulding jig (Exploded view)..... | B-2 |
| Figure B.2.1: | Tensile specimen bonding..... | B-3 |
| Figure B.2.2: | Shear specimen bonding..... | B-3 |
| Figure B.2.3: | Macro bonding jig..... | B-4 |
| Figure B.2.3.1: | Tensile bonding jig (Exploded view)..... | B-5 |
| Figure B.2.3.2: | Tensile bonding jig (Full assembly)..... | B-6 |
| Figure B.2.3.3: | Shear bonding jig (Exploded view)..... | B-7 |
| Figure B.2.3.4: | Shear bonding jig (Full assembly)..... | B-8 |
| Figure B.3.1: | Tensile clamping adaptor..... | B-9 |
| Figure B.3.2: | Shear clamping adaptor..... | B-10 |
| Figure B.3.3: | Shear-tensile adaptor..... | B-11 |
| Figure B.4.1: | Shear adherend jig..... | B-12 |
| Figure B.4.2: | Tensile adherend jig..... | B-13 |
| Figure B.5.1: | Macro bonding jig..... | B-14 |
| Figure B.6.1.1: | Failure load Vs extension curve of LT shear specimen..... | B-15 |
| Figure B.6.1.2: | Failure load Vs extension curve of RL shear specimen..... | B-15 |
| Figure B.6.1.3: | Failure load Vs extension curve of WR shear specimen..... | B-16 |
| Figure B.6.1.4: | Failure load Vs extension curve of IR shear specimen..... | B-16 |
| Figure B.6.2.1: | Failure load Vs extension curve of LT tensile specimen..... | B-17 |
| Figure B.6.2.2: | Failure load Vs extension curve of RL tensile specimen..... | B-17 |
| Figure B.6.2.3: | Failure load Vs extension curve of WR tensile specimen..... | B-18 |
| Figure B.6.2.4: | Failure load Vs extension curve of IR tensile specimen..... | B-18 |
| Figure 5.1: | Three stages in finite element analysis..... | C-1 |
| Figure 5.2 : | ABAQUS file environment..... | C-2 |

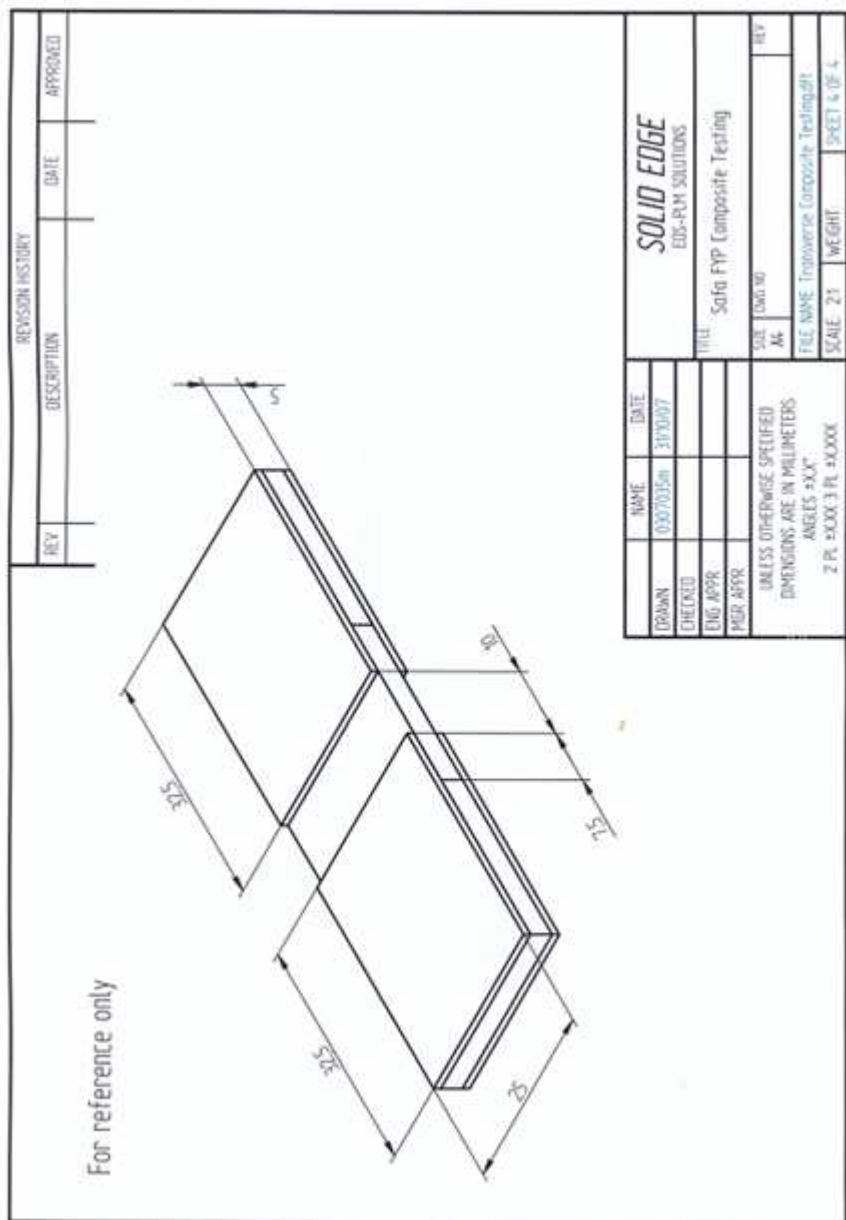
List of Tables in Appendices

Table A.3.1: Data measured from bulk adhesive specimen..... A-11

Appendix A

Material properties

A.1 Pultruded transverse tensile specimen



A.2 Silicone rubber mould fabrication

The following steps followed during the fabrication of silicon rubber mould and their schematic views are shown in Figure A.1.1.

- a). Moulding gate glued with aluminium dumbbell shaped specimen.
- b). Placed all glued specimen with equal space in wooden box.
- c). Manual mixing of MCP SILICONE RUBBER (TYPE KE-1300T) and catalyst of mixing ratio by weight is 10:1 in jar at least 8-10min until get homogeneous mixture.
- d). Mixture jar in vacuum oven to remove all air.
- e). Poured all mixture in wooden box and put again in Vacuum oven to remove all remaining air.
- f). Wooden box in vacuum oven.
- g). Finally cured in oven at 80°C for 2hrs.

A.2.1 Silicone rubber mould fabrication



Figure A.2.1: Schematic view of silicone rubber mould fabrication

A.2.2 MCP SILICONE RUBBER technical data sheet (KE-1300T)



MCP SILICONE RUBBER
DATA SHEET: TYPE KE-1300T

| | | |
|------------------------|---------------------|-------------|
| TYPE | | KE-1300T |
| COLOUR | | TRANSPARENT |
| MIXING RATIO | By weight | 10 : 1 |
| POT LIFE | Mixed (25°C) | 120 mins |
| VISCOSITY | Poise (25°C) | 1000 |
| CURING TIME | Hours (25°C) | 24 |
| SPECIFIC GRAVITY | 25°C, cured | 1.08 |
| HARDNESS (JIS 'A') | 25°C | 40 |
| TENSILE STRENGTH | Kgf/cm ² | 45 |
| ELONGATION AT FRACTURE | % | 300 |
| TEAR STRENGTH | Kgf/cm ² | 17 |
| LINEAR SHRINKAGE | % | |

* Cured @ 80°C for 2hrs

A.3 Adhesive bulk specimen

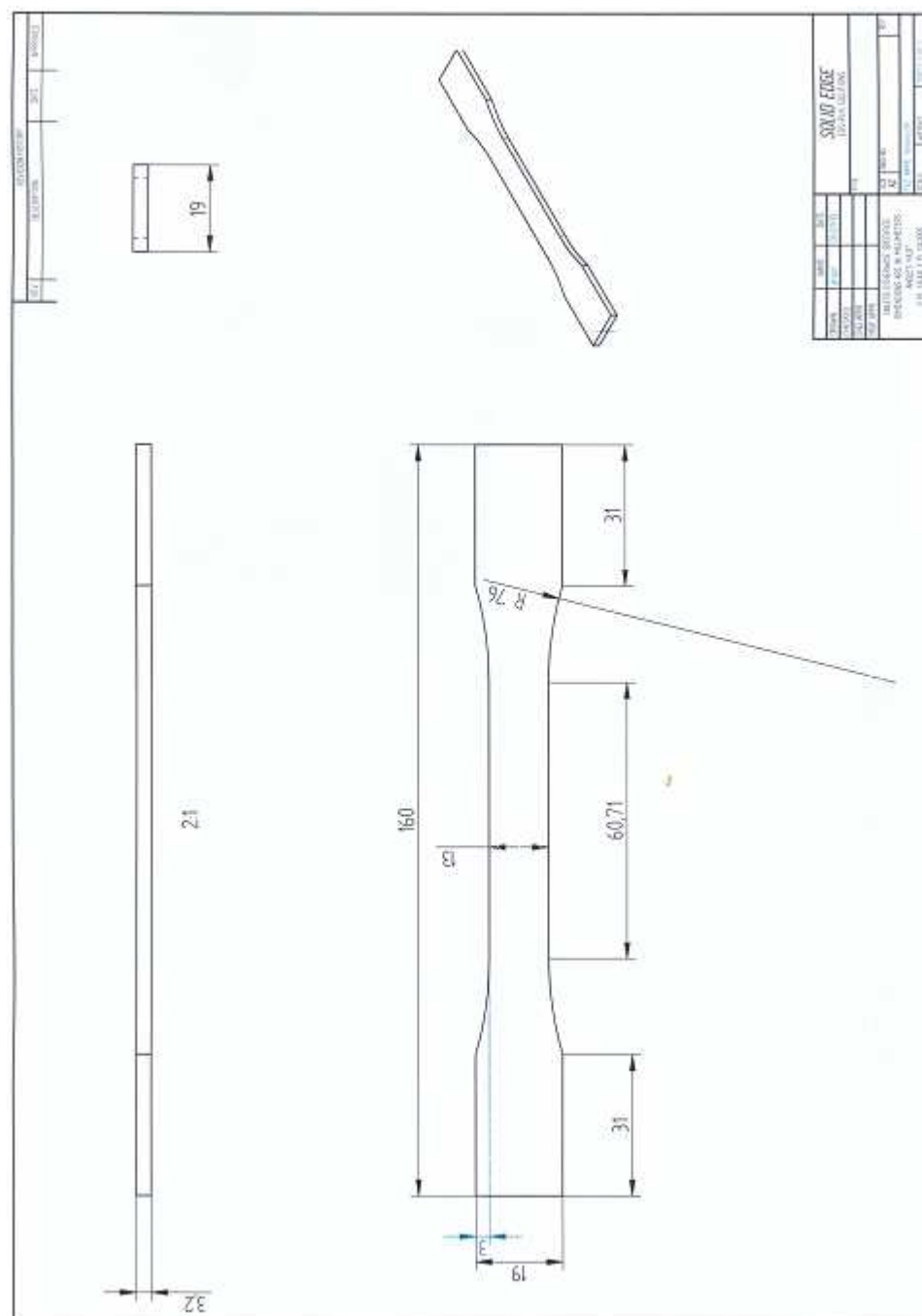


Figure A.3.1: Adhesive bulk tensile test specimen

The ratio of strains measured normal and parallel to the load directions was taken as Poisson's ratio and ratio of stress and axial strain gives Young's modulus. The average calculated by Young's modulus and Poisson's ratio as tabulated in Table A.3.1 is in line with the value reported by adhesive supplier. Figure A.3.2 illustrates linear stress-strain curve obtained from bulk Araldite® 2015.

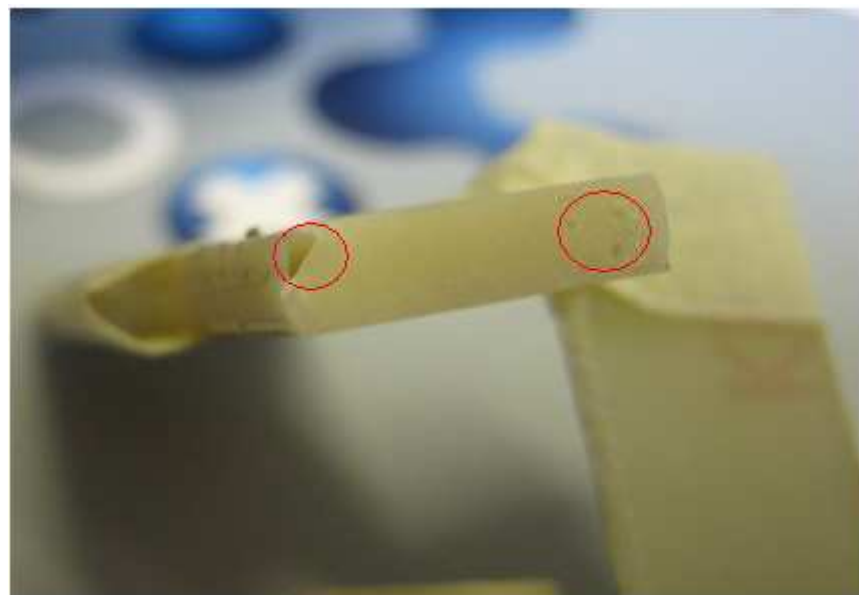
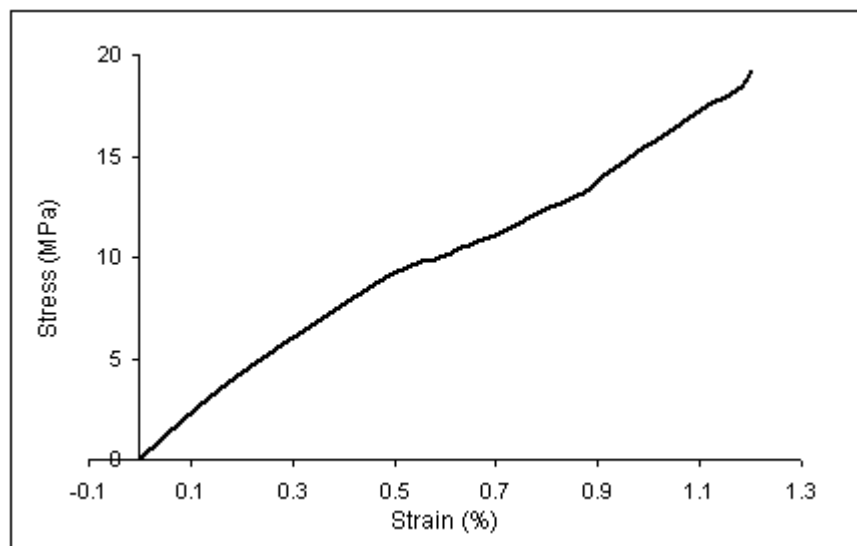


Figure A.3.2: Adhesive dog bone specimen with trap air bubble in circle

| Load (N) | Axial Strain (%) | Trans Strain (%) | Poisson Ratio | Stress(MPa) | E(Gpa) |
|----------|------------------|------------------|---------------|-------------|--------|
| 0 | 0.0002 | 0.00025 | 1.25 | 0 | 0.0 |
| 100 | 0.0846 | 0.0252 | 0.30 | 2.02 | 2.4 |
| 200 | 0.1878 | 0.0561 | 0.30 | 4.05 | 2.2 |
| 300 | 0.3017 | 0.0856 | 0.28 | 6.07 | 2.0 |
| 450 | 0.49 | 0.1183 | 0.24 | 9.11 | 1.9 |
| 500 | 0.6005 | 0.1498 | 0.25 | 10.12 | 1.7 |
| 520 | 0.6295 | 0.1502 | 0.24 | 10.53 | 1.7 |
| 550 | 0.6983 | 0.1763 | 0.25 | 11.13 | 1.6 |
| 600 | 0.7821 | 0.2171 | 0.28 | 12.15 | 1.6 |
| 650 | 0.8711 | 0.2475 | 0.28 | 13.16 | 1.5 |
| 680 | 0.9 | 0.2567 | 0.29 | 13.77 | 1.5 |
| 700 | 0.92 | 0.2726 | 0.30 | 14.17 | 1.5 |
| 850 | 1.0999 | 0.3593 | 0.33 | 17.21 | 1.6 |
| 900 | 1.1715 | 0.4045 | 0.35 | 18.22 | 1.6 |
| 950 | 1.2005 | 0.4609 | 0.38 | 19.23 | 1.6 |

Table A.3.1: Data measured from bulk adhesive specimen**Figure A.3.3: Stress-strain curve obtained from bulk adhesive dog-bone specimen**

A.4 HUNSTMAN technical data sheet (Araldite 2015)

HUNTSMAN

Structural Adhesives

Araldite® 2015 (AV 5308 / HV 5309-1)
Two component epoxy paste adhesive

| Key properties | <ul style="list-style-type: none"> • Thixotropic • Toughened adhesive • Gap filling, non sagging up to 10mm thickness • Suitable for SMC and GRP bonding • High shear and peel strength | | | | | | | | | | | | | | | | | | | | | | |
|-----------------------------|---|--------------------|-----------------|-----------|------------------|--------------------|------------------|-----------------|---------------|-----------------|---------------|------------------|-----|-----|-----|-------------------------|-------------|-------------|-------------|---------------------------|---|---|-----------------|
| Description | Araldite 2015 is a two component, room temperature curing paste adhesive giving a resilient bond. It is thixotropic and non sagging up to 10mm thickness. It is particularly suitable for SMC and GRP bonding. | | | | | | | | | | | | | | | | | | | | | | |
| Typical product data | <table border="1" style="width: 100%; border-collapse: collapse;"> <thead> <tr> <th style="text-align: left;">Property</th> <th style="text-align: left;">2015 A (AV 5308)</th> <th style="text-align: left;">2015 B (HV 5309-1)</th> <th style="text-align: left;">Mixed Adhesive</th> </tr> </thead> <tbody> <tr> <td>Colour (visual)</td> <td>neutral paste</td> <td>neutral paste</td> <td>neutral paste</td> </tr> <tr> <td>Specific gravity</td> <td>1.4</td> <td>1.4</td> <td>1.4</td> </tr> <tr> <td>Viscosity at 25°C (Pas)</td> <td>thixotropic</td> <td>thixotropic</td> <td>thixotropic</td> </tr> <tr> <td>Pot Life (100 gm at 25°C)</td> <td>-</td> <td>-</td> <td>30 - 40 minutes</td> </tr> </tbody> </table> | | | Property | 2015 A (AV 5308) | 2015 B (HV 5309-1) | Mixed Adhesive | Colour (visual) | neutral paste | neutral paste | neutral paste | Specific gravity | 1.4 | 1.4 | 1.4 | Viscosity at 25°C (Pas) | thixotropic | thixotropic | thixotropic | Pot Life (100 gm at 25°C) | - | - | 30 - 40 minutes |
| Property | 2015 A (AV 5308) | 2015 B (HV 5309-1) | Mixed Adhesive | | | | | | | | | | | | | | | | | | | | |
| Colour (visual) | neutral paste | neutral paste | neutral paste | | | | | | | | | | | | | | | | | | | | |
| Specific gravity | 1.4 | 1.4 | 1.4 | | | | | | | | | | | | | | | | | | | | |
| Viscosity at 25°C (Pas) | thixotropic | thixotropic | thixotropic | | | | | | | | | | | | | | | | | | | | |
| Pot Life (100 gm at 25°C) | - | - | 30 - 40 minutes | | | | | | | | | | | | | | | | | | | | |
| Processing | <p>Pretreatment The strength and durability of a bonded joint are dependent on proper treatment of the surfaces to be bonded. At the very least, joint surfaces should be cleaned with a good degreasing agent such as acetone, iso-propanol (for plastics) or other proprietary degreasers in order to remove all traces of oil, grease and dirt. Low grade alcohol, gasoline (petrol) or paint thinners should never be used. The strongest and most durable joints are obtained by either mechanically abrading or chemically etching ("picking") the degreased surfaces. Abrading should be followed by a second degreasing treatment.</p> <table border="1" style="margin-top: 10px; width: 100%; border-collapse: collapse;"> <thead> <tr> <th style="text-align: left;">Mix ratio</th> <th style="text-align: left;">Parts by weight</th> <th style="text-align: left;">Parts by volume</th> </tr> </thead> <tbody> <tr> <td>Araldite 2015 A,</td> <td>100</td> <td>100</td> </tr> <tr> <td>Araldite 2015 B</td> <td>100</td> <td>100</td> </tr> </tbody> </table> <p>The resin and hardener should be blended until they form a homogeneous mix.</p> <p>Resin and hardener are also available in cartridges incorporating mixers and can be applied as ready to use adhesive with the aid of the tool recommended by Huntsman Advanced Materials.</p> <p>Application of adhesive The resin/hardener mix is applied with a spatula, to the pretreated and dry joint surfaces. A layer of adhesive 0.05 to 0.10mm thick will normally impart the greatest lap shear strength to the joint. The joint components should be assembled and clamped as soon as the adhesive has been applied. An even contact pressure throughout the joint area will ensure optimum cure.</p> | | | Mix ratio | Parts by weight | Parts by volume | Araldite 2015 A, | 100 | 100 | Araldite 2015 B | 100 | 100 | | | | | | | | | | | |
| Mix ratio | Parts by weight | Parts by volume | | | | | | | | | | | | | | | | | | | | | |
| Araldite 2015 A, | 100 | 100 | | | | | | | | | | | | | | | | | | | | | |
| Araldite 2015 B | 100 | 100 | | | | | | | | | | | | | | | | | | | | | |

June 2004
Publication No. A 234 a GB
Page 1 of 4

Mechanical processing

Specialist firms have developed metering, mixing and spreading equipment that enables the bulk processing of adhesive. We will be pleased to advise customers on the choice of equipment for their particular needs.

Equipment maintenance

All tools should be cleaned with hot water and soap before adhesives residues have had time to cure. The removal of cured residues is a difficult and time-consuming operation.

If solvents such as acetone are used for cleaning, operatives should take the appropriate precautions and, in addition, avoid skin and eye contact.

Times to minimum shear strength

| Temperature | °C | 10 | 15 | 23 | 40 | 60 | 100 |
|---|---------|----|-----|----|----|----|-----|
| Cure time to reach LSS > 1 N/mm ² | hours | 12 | 7.5 | 4 | 1 | - | - |
| LSS > 10 N/mm ² | minutes | - | - | - | - | 17 | 5 |
| Cure time to reach LSS > 10 N/mm ² | hours | 21 | 13 | 6 | 2 | - | - |
| LSS > 10 N/mm ² | minutes | - | - | - | - | 35 | 7 |

LSS = Lap shear strength.

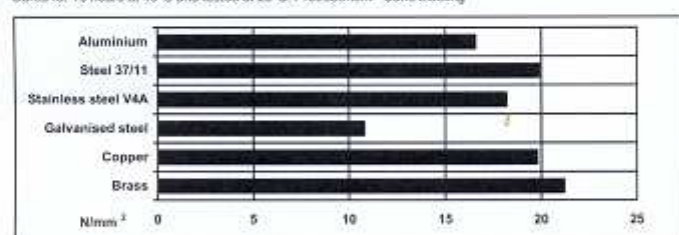
Typical cured properties

Unless otherwise stated, the figures given below were all determined by testing standard specimens made by lap-jointing 170 x 25 x 1.5 mm strips of aluminium alloy. The joint area was 12.5 x 25 mm in each case. The figures were determined with typical production batches using standard testing methods. They are provided solely as technical information and do not constitute a product specification.

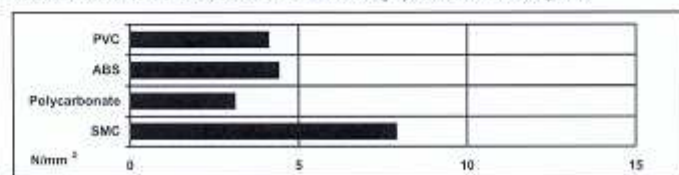
Note: The data in this edition is based on recent testing of the product.

Average lap shear strengths of typical metal-to-metal joints (ISO 4587)

Cured for 16 hours at 40°C and tested at 23°C. Pretreatment - Sand blasting

**Average lap shear strengths of typical plastic-to-plastic joints (ISO 4587)**

Cured for 1 hour at 80°C and tested at 23°C. Pretreatment - Lightly abrade and alcohol degrease.



Tensile strength at 23°C (ISO 527) : 30 MPa

Tensile modulus : 2 Gpa

Elongation at break : 4.4 %

Lap shear strength versus heat ageing.
Cure: 16 hours at 40°C

| Condition | Value (N/mm ²) |
|------------------|----------------------------|
| As-made value | ~20 |
| 30 days/70°C | ~20 |
| 60 days/70°C | ~20 |
| 90 days/70°C | ~20 |
| Thermal cycling* | ~20 |

*25 cycles -30°C to +70°C

Shear modulus (DIN 53445)
Cure: 1 hour at 80°C

| Temperature | G' (GPa) | A |
|-------------|----------|------|
| 0°C | 1.0 Gpa | 0.25 |
| 25°C | 0.9 Gpa | 0.25 |
| 50°C | 0.8 Gpa | 0.35 |
| 75°C | 0.2 Gpa | 1.9 |
| 100°C | 2 MPa | 0.5 |

Flexural Properties (ISO 178) Cure 16 hours/ 40°C tested at 23°C

Flexural Strength: 42.7 MPa
Flexural Modulus: 1813.6 MPa

Resistance to fatigue (40 Hz at 23°C) (quoted as cycles to failure)

| Maximum applied load | Sandblasted aluminium | Chromate pickled aluminium |
|----------------------------|-----------------------|----------------------------|
| 20% of static failing load | >10 ⁷ | >10 ⁷ |
| 25% of static failing load | >10 ⁷ | 10 ⁷ |
| 30% of static failing load | 3 x 10 ⁶ | 5 x 10 ⁵ |

(Static failing load 10 N/mm²)

Storage Araldite 2015 A and B may be stored for up to 3 years at room temperature provided the components are stored in sealed containers. The expiry date is indicated on the label.

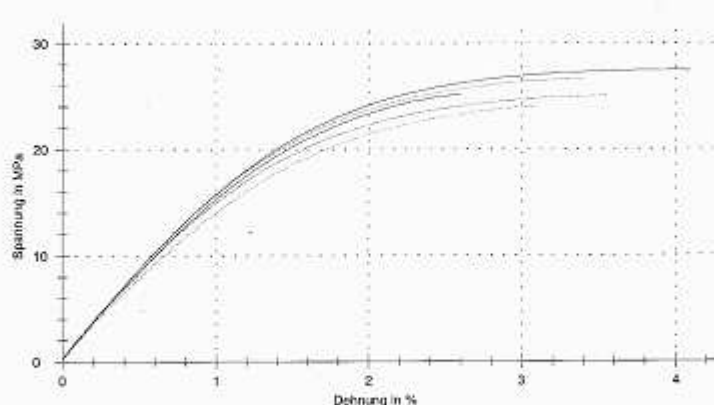
Handling precautions Caution
Our products are generally quite harmless to handle provided that certain precautions normally taken when handling chemicals are observed. The uncured materials must not, for instance, be allowed to come into contact with foodstuffs or food utensils, and measures should be taken to prevent the uncured materials from coming in contact with the skin, since people with particularly sensitive skin may be affected. The wearing of impervious rubber or plastic gloves will normally be necessary. Likewise the use of eye protection. The skin should be thoroughly cleansed at the end of each working period by washing with soap and warm water. The use of solvents is to be avoided. Disposable paper - not cloth towels - should be used to dry the skin. Adequate ventilation of the working area is recommended. These precautions are described in greater detail in the Material Safety Data sheets for the individual products and should be referred to for fuller information.

Huntsman Advanced Materials All recommendations for the use of our products, whether given by us in writing, verbally, or to be implied from the results of tests carried out by us, are based on the current state of our knowledge. Notwithstanding any such recommendations the Buyer shall remain responsible for satisfying himself that the products as supplied by us are suitable for his intended process or purpose. Since we cannot control the application, use or processing of the products, we cannot accept responsibility therefor. The Buyer shall ensure that the intended use of the products will not infringe any third party's intellectual property rights. We warrant that our products are free from defects in accordance with and subject to our general conditions of supply.

Duxford, Cambridge
England CB2 4QA
Tel: +44 (0) 1223 852121
Fax: +44 (0) 1223 493322
www.araldite.com

© 2004 Huntsman Advanced Materials (Switzerland) GmbH
®Araldite is a registered trademark of Huntsman LLC or an affiliate thereof in one or more, but not all, countries.

June 2004 Publication No. A 234 e GB Page 4 of 4

| HUNTSMAN Advanced Materials Material Testing K-401.P.24 CH-4057 Basel Tel.: ++41 61 966 33 59 | PRÜFBERICHT  S SCHWEIZERISCHER PRÜFSTELLENDIENST SERVIZO SUISSA DI PROVA SERVIZIO DI PROVA IN SVIZZERA SWISS TESTAG SERVICE | | | | | | | | | | | | | | | | | | | | | | | | | | | | | | | | | | | | | | | | | | | | | | | | | | | | | | | | | | | | | | | | | | | | |
|--|--|------------------------|------------------------|----------------------|-----------------------------------|--------------------------------|--------------------------------|-------------|--------------|----------------|-------------|------------------------|------------------------|----------------------|-----------------------------------|--------------------------------|--------------------------------|-------------|--------------|-----------|--------|-------|------|-------|------|-------|------|------|------|---|--------|-------|------|---|---|-------|------|------|------|---|--------|-------|-------|---|---|-------|-------|------|------|---|--------|-------|------|---|---|-------|------|------|------|---|--------|-------|------|-------|------|-------|------|------|------|
| Akkreditierungs-Nr. STS 440 Zertifikats-Nr.: 07001074 | | | | | | | | | | | | | | | | | | | | | | | | | | | | | | | | | | | | | | | | | | | | | | | | | | | | | | | | | | | | | | | | | | | | | |
| Zugversuch | | | | | | | | | | | | | | | | | | | | | | | | | | | | | | | | | | | | | | | | | | | | | | | | | | | | | | | | | | | | | | | | | | | | | |
| Prüfdatum : 21.05.07 Norm : ISO 527T2/93 Auftraggeber : CHOUVET,L. Mat.-Typ : GHG Adresse : K-411.9.04 Pk-Typ : PK-TYP 5A Autr.-Nr. : 7000986 Prüf-Temp. : 23°C Mag.-Nr. : 183125 Prüfer : bivalal Lagerung : ---- Muster : ARALDITE 2015 Kraftaufnehmer: 10kN Aushärtung : 16h/40°C Maßlänge L0 : 20 mm | | | | | | | | | | | | | | | | | | | | | | | | | | | | | | | | | | | | | | | | | | | | | | | | | | | | | | | | | | | | | | | | | | | | | |
| Ergebnisse: | | | | | | | | | | | | | | | | | | | | | | | | | | | | | | | | | | | | | | | | | | | | | | | | | | | | | | | | | | | | | | | | | | | | | |
| <table border="1" style="width: 100%; border-collapse: collapse;"> <thead> <tr> <th>Nr</th> <th>EMod MPa</th> <th>σ_{\max} MPa</th> <th>ϵ_{\max} %</th> <th>σ_{-S} MPa</th> <th>ϵ bei σ_{-S} %</th> <th>σ_{Bruch} MPa</th> <th>ϵ_{Bruch} %</th> <th>Dicke mm</th> <th>Breite mm</th> </tr> </thead> <tbody> <tr> <td>1</td> <td>1684,5</td> <td>25,09</td> <td>2,60</td> <td>-</td> <td>-</td> <td>25,09</td> <td>2,60</td> <td>5,50</td> <td>3,93</td> </tr> <tr> <td>2</td> <td>1703,3</td> <td>25,02</td> <td>3,51</td> <td>-</td> <td>-</td> <td>25,01</td> <td>3,58</td> <td>5,43</td> <td>3,90</td> </tr> <tr> <td>3</td> <td>1802,3</td> <td>26,83</td> <td>3,40</td> <td>-</td> <td>-</td> <td>26,62</td> <td>3,42</td> <td>5,48</td> <td>3,96</td> </tr> <tr> <td>4</td> <td>1578,9</td> <td>24,05</td> <td>3,08</td> <td>-</td> <td>-</td> <td>24,03</td> <td>3,12</td> <td>5,52</td> <td>4,02</td> </tr> <tr> <td>5</td> <td>1731,1</td> <td>27,44</td> <td>3,96</td> <td>27,44</td> <td>3,98</td> <td>27,32</td> <td>4,10</td> <td>5,52</td> <td>3,94</td> </tr> </tbody> </table> | | | | | | | | | | Nr | EMod MPa | σ_{\max} MPa | ϵ_{\max} % | σ_{-S} MPa | ϵ bei σ_{-S} % | σ_{Bruch} MPa | ϵ_{Bruch} % | Dicke mm | Breite mm | 1 | 1684,5 | 25,09 | 2,60 | - | - | 25,09 | 2,60 | 5,50 | 3,93 | 2 | 1703,3 | 25,02 | 3,51 | - | - | 25,01 | 3,58 | 5,43 | 3,90 | 3 | 1802,3 | 26,83 | 3,40 | - | - | 26,62 | 3,42 | 5,48 | 3,96 | 4 | 1578,9 | 24,05 | 3,08 | - | - | 24,03 | 3,12 | 5,52 | 4,02 | 5 | 1731,1 | 27,44 | 3,96 | 27,44 | 3,98 | 27,32 | 4,10 | 5,52 | 3,94 |
| Nr | EMod MPa | σ_{\max} MPa | ϵ_{\max} % | σ_{-S} MPa | ϵ bei σ_{-S} % | σ_{Bruch} MPa | ϵ_{Bruch} % | Dicke mm | Breite mm | | | | | | | | | | | | | | | | | | | | | | | | | | | | | | | | | | | | | | | | | | | | | | | | | | | | | | | | | | | | |
| 1 | 1684,5 | 25,09 | 2,60 | - | - | 25,09 | 2,60 | 5,50 | 3,93 | | | | | | | | | | | | | | | | | | | | | | | | | | | | | | | | | | | | | | | | | | | | | | | | | | | | | | | | | | | | |
| 2 | 1703,3 | 25,02 | 3,51 | - | - | 25,01 | 3,58 | 5,43 | 3,90 | | | | | | | | | | | | | | | | | | | | | | | | | | | | | | | | | | | | | | | | | | | | | | | | | | | | | | | | | | | | |
| 3 | 1802,3 | 26,83 | 3,40 | - | - | 26,62 | 3,42 | 5,48 | 3,96 | | | | | | | | | | | | | | | | | | | | | | | | | | | | | | | | | | | | | | | | | | | | | | | | | | | | | | | | | | | | |
| 4 | 1578,9 | 24,05 | 3,08 | - | - | 24,03 | 3,12 | 5,52 | 4,02 | | | | | | | | | | | | | | | | | | | | | | | | | | | | | | | | | | | | | | | | | | | | | | | | | | | | | | | | | | | | |
| 5 | 1731,1 | 27,44 | 3,96 | 27,44 | 3,98 | 27,32 | 4,10 | 5,52 | 3,94 | | | | | | | | | | | | | | | | | | | | | | | | | | | | | | | | | | | | | | | | | | | | | | | | | | | | | | | | | | | | |
| Statistik: <table border="1" style="width: 100%; border-collapse: collapse;"> <thead> <tr> <th>Serie n = 5</th> <th>EMod MPa</th> <th>σ_{\max} MPa</th> <th>ϵ_{\max} %</th> <th>σ_{-S} MPa</th> <th>ϵ bei σ_{-S} %</th> <th>σ_{Bruch} MPa</th> <th>ϵ_{Bruch} %</th> <th>Dicke mm</th> <th>Breite mm</th> </tr> </thead> <tbody> <tr> <td>\bar{x}</td> <td>1700,0</td> <td>25,65</td> <td>3,31</td> <td>27,44</td> <td>3,98</td> <td>26,61</td> <td>3,36</td> <td>5,49</td> <td>3,95</td> </tr> <tr> <td>s</td> <td>81,2</td> <td>1,36</td> <td>0,51</td> <td>-</td> <td>-</td> <td>1,33</td> <td>0,55</td> <td>0,04</td> <td>0,04</td> </tr> <tr> <td>v</td> <td>4,78</td> <td>5,31</td> <td>15,31</td> <td>-</td> <td>-</td> <td>5,18</td> <td>16,48</td> <td>0,68</td> <td>1,13</td> </tr> </tbody> </table> | | | | | | | | | | Serie n = 5 | EMod MPa | σ_{\max} MPa | ϵ_{\max} % | σ_{-S} MPa | ϵ bei σ_{-S} % | σ_{Bruch} MPa | ϵ_{Bruch} % | Dicke mm | Breite mm | \bar{x} | 1700,0 | 25,65 | 3,31 | 27,44 | 3,98 | 26,61 | 3,36 | 5,49 | 3,95 | s | 81,2 | 1,36 | 0,51 | - | - | 1,33 | 0,55 | 0,04 | 0,04 | v | 4,78 | 5,31 | 15,31 | - | - | 5,18 | 16,48 | 0,68 | 1,13 | | | | | | | | | | | | | | | | | | | | |
| Serie n = 5 | EMod MPa | σ_{\max} MPa | ϵ_{\max} % | σ_{-S} MPa | ϵ bei σ_{-S} % | σ_{Bruch} MPa | ϵ_{Bruch} % | Dicke mm | Breite mm | | | | | | | | | | | | | | | | | | | | | | | | | | | | | | | | | | | | | | | | | | | | | | | | | | | | | | | | | | | | |
| \bar{x} | 1700,0 | 25,65 | 3,31 | 27,44 | 3,98 | 26,61 | 3,36 | 5,49 | 3,95 | | | | | | | | | | | | | | | | | | | | | | | | | | | | | | | | | | | | | | | | | | | | | | | | | | | | | | | | | | | | |
| s | 81,2 | 1,36 | 0,51 | - | - | 1,33 | 0,55 | 0,04 | 0,04 | | | | | | | | | | | | | | | | | | | | | | | | | | | | | | | | | | | | | | | | | | | | | | | | | | | | | | | | | | | | |
| v | 4,78 | 5,31 | 15,31 | - | - | 5,18 | 16,48 | 0,68 | 1,13 | | | | | | | | | | | | | | | | | | | | | | | | | | | | | | | | | | | | | | | | | | | | | | | | | | | | | | | | | | | | |
| Bemerkung: z. Beilage: Prüfgeschwindigkeit: 1 mm/min Messplatz-Nr.: 1004 Visum: b/y | | | | | | | | | | | | | | | | | | | | | | | | | | | | | | | | | | | | | | | | | | | | | | | | | | | | | | | | | | | | | | | | | | | | | |
|  <p>The graph plots Stress (in MPa) on the y-axis (0 to 30) against Strain (in %) on the x-axis (0 to 4). Five curves represent different specimens. All curves show a linear elastic region followed by yielding and a non-linear plastic region. Specimens 1, 2, and 3 reach higher peak stresses (around 25-27 MPa) compared to specimens 4 and 5 (around 24 MPa).</p> | | | | | | | | | | | | | | | | | | | | | | | | | | | | | | | | | | | | | | | | | | | | | | | | | | | | | | | | | | | | | | | | | | | | | |
| 202103125.ZSE | | | | | Seite 1/1 | | | | | | | | | | | | | | | | | | | | | | | | | | | | | | | | | | | | | | | | | | | | | | | | | | | | | | | | | | | | | | | | |

A.5 CIBA-GEIGY technical data sheet (AY 103/AY 105)

CIBA-GEIGY
June 1990 Instruction Sheet No. A.26k

STRUCTURAL ADHESIVES

***Araldite AY 103 and AY 105**
with Hardener HY 951 or HY 956

Epoxy resin adhesives

Four solvent-free epoxy resin adhesives of medium viscosity for bonding metals, ceramics, glass, rubber, plastics, etc., can be produced by mixing either of the resins:

Araldite AY 103 – a plasticised liquid epoxy resin
Araldite AY 105 – an unmodified liquid epoxy resin with either of the hardeners:
Hardener HY 951 – a liquid of low viscosity
Hardener HY 956 – a liquid of moderately low viscosity according to mixtures 1, 2, 3, and 4, listed below.

The four adhesives give joints of high mechanical strength which are resistant to chemical attack and provide full electrical insulation.

The essential difference between the two resins – mixed with Hardener HY 951 or HY 956 – is:

Araldite AY 103 develops excellent bond strength when cured at room temperature.
Araldite AY 105 requires heat to achieve a cure, but gives additional strength at elevated temperatures.

Instructions for use

Pretreatment

Degrease the surfaces to be bonded. Certain materials will also require abrasion or chemical etching. Detailed information is given in CIBA-GEIGY Instruction Manual No. A.15 Araldite Bonding – Surface Preparation and Pretreatments.

| Mixtures | Parts by weight | Parts by volume |
|---------------------------------------|-----------------|-----------------|
| 1. Araldite AY 103 Hardener HY 951 | 100 8–10 | 100 9½–12 |
| 2. Araldite AY 103 Hardener HY 956 | 100 16–18 | 100 18–20 |
| 3. Araldite AY 105 Hardener HY 951 | 100 10–12 | 100 12–14 |
| 4. Araldite AY 105 Hardener HY 956 | 100 22–24 | 100 25–27 |

Approvals

Araldite AY 103 with Hardener HY 951 can be released against Procurement Executive, Ministry of Defence Specification DTD 900/4365 for bonding metal to metal. Araldite AY 103 with Hardener HY 951 can also be supplied to conform to the standard of quality agreed by the Directorate of Quality Assurance/Technical Support as defined in Agreed Firm's Schedule AFS 774. Araldite AY 105 with Hardener HY 951 can likewise be supplied to conform to AFS 859. The following products can be supplied individually to conform to Agreed Firm's Schedules:

Araldite AY 105 . . . AFS 1014A
Hardener HY 951 . . . AFS 45B
Hardener HY 956 . . . AFS 122B

Mixing

Mix resin and hardener together at room temperature, stirring thoroughly.

Note In cold weather Araldite AY 105 is viscous and difficult to mix. This is overcome by warming Araldite AY 105 prior to mixing to about 30°C.

Usable life

A 50 gram quantity of resin-hardener mixture has usable life:

| Temperature of mixtures | Araldite AY 103 + HY 951 or HY 956 | Araldite AY 105 + HY 951 or HY 956 |
|-------------------------|------------------------------------|------------------------------------|
| 25°C | 1½–2 hours | 45–60 minutes |
| or 40°C | 35–45 minutes | 20–30 minutes |
| or 60°C | ca. 15 minutes | ca. 10 minutes |

But, owing to the heat generated by the exothermic reaction between resin and hardener, the usable life will be noticeably shortened if more than 250 grams of mixture is allowed to stand in one compact mass – e.g. in a mixing beaker or similar 'bulk' container. To minimise exothermic temperature rise, which is the cause of this shortening of usable life, the heat generated must be rapidly conducted away. The following procedure is suggested when mixing large quantities:

Divide the mixture into several small containers or pour into a shallow container so that the mixture spreads out to a thin layer (5–10 mm). A shallow polythene basin is recommended since this allows hardened resin residues to be removed simply by flexing. Where there is risk of exposure to damp air, containers must be covered – see Moisture Pick-up below. Dividing or spreading out the mixture increases its surface-to-volume ratio so assisting dissipation of heat generated by the resin-hardener reaction.

Since usable life is limited, it is good practice to prepare only the quantity of mixture needed for immediate use – or to use automatic mixing-dispensing equipment.

Application

Spread a thin layer of adhesive by spatula, brush or roller on both the surfaces to be bonded and close the joint preferably as soon as possible – maximum joint assembly time is 1 hour. Keep the joint lightly clamped or otherwise supported while the adhesive cures.

Curing

Cure the adhesive for at least:

| Temperature of curing | Araldite AY 103 + HY 951 or HY 956 | Araldite AY 105 + HY 951 or HY 956 |
|-----------------------|------------------------------------|------------------------------------|
| 25°C | 24 hours | — |
| or 40°C | 8 hours | 12 hours |
| or 60°C | 3 hours | 3 hours |
| or 100°C | 20 minutes | 20 minutes |

Bonds of excellent strength are obtained by curing at room temperature (Araldite AY 103) or at 40°C (Araldite AY 105) but to obtain optimum properties the adhesive should be given a short post-cure at a higher temperature. Allow extra time for the joint assembly to reach the required temperature.

Notes**Moisture pick-up**

Hardeners HY 951 and HY 956 are hygroscopic – they absorb moisture when exposed to damp air. The hardeners and uncured resin-hardener mixtures are in consequence adversely affected by high atmospheric humidity, which, when the mixture is applied as a thin layer, may even prevent curing. Low ambient temperatures, which prolong curing, aggravate this effect. The mixtures should not be prepared or applied in work areas exposed to high atmospheric humidity combined with low ambient temperature. To make the effect of moist air less severe, the mixture should be allowed to stand* in the mixing beaker – covered with lid – so that the resin-hardener reaction is well under way when the mixture is used.

* Standing time for mixture at room temperature:

| | |
|------------------------------------|---------------|
| Araldite AY 103 + HY 951 or HY 956 | 15–20 minutes |
| Araldite AY 105 + HY 951 or HY 956 | 5–10 minutes |

Properties

| Resin-hardener mixture | | Araldite AY 103+ HY 951 | Araldite AY 103+ HY 956 | Araldite AY 105+ HY 951 | Araldite AY 105+ HY 956 |
|---------------------------|-----------|-------------------------------|-------------------------------|-------------------------------|-------------------------------|
| Initial viscosity at 25°C | Pas | 0.5-1.0 | 0.8-1.5 | 1.5-3.0 | 2.0-3.5 |
| Cured adhesive | | | | | |
| Shear strength* at -60°C | MPa | 14.5 | 12.5 | 14.5 | 12.5 |
| Cure: 1 hour at 120°C | | | | | |
| Shear strength* at 20°C | MPa | 17.5 | 17.5 | — | — |
| Cure: 24 hours at 20°C | MPa | 17.5 | 17.5 | 17.5 | 17.5 |
| 12 hours at 40°C | MPa | 19.5 | 19.5 | 19.5 | 19.5 |
| 20 mins. at 100°C | | | | | |
| Shear strength* at 90°C | MPa | 2.0 | 2.0 | 8.5 | 8.5 |
| Cure: 20 mins. at 100°C | MPa | 2.8 | 2.8 | 12.5 | 12.5 |
| 1 hour at 120°C | | | | | |
| Deflection temperature | °C | 45-60 | 45-60 | 85-90† | 85-90† |
| BS 2782 method 121A | | | | | |
| Coefficient of expansion | linear/°C | 90-95 $\times 10^{-6}$ | 95-100 $\times 10^{-6}$ | 65-70 $\times 10^{-6}$ | 65-70 $\times 10^{-6}$ |
| ASTM D 696-70 | | | | | |
| Modulus of elasticity | GPa | 2.7-3.0 | 3.0-3.3 | 3.8-4.2 | 3.3-3.7 |
| BS 2782 method 335A | | | | | |

* Average shear strength of a 0.91 mm BS L152 aluminium alloy lap joint (12.5 mm overlap \times 25 mm wide).

† Average deflection temperature after curing for 3 hours at 60°C. Prolonged curing above 60° will give a deflection temperature approaching 100°C (with HY 956) or above 100°C (with HY 951). For example:

| System | Curing schedule | Deflection temperature |
|-----------------|---|------------------------|
| AY 105 + HY 951 | 16 h at 25°C + ½ h at 120°C 3 h at 60°C + 2 h at 120°C | 95-100°C 125-130°C |
| AY 105 + HY 956 | 16 h at 25°C + ½ h at 120°C 3 h at 60°C + 2 h at 120°C | 95-100°C 95-100°C |

With Araldite AY 103 + HY 951 or HY 956 curing schedules more extensive than 3 hours at 60°C do not substantially improve deflection temperature.

CIBA-GEIGY

All information is based on results gained from experience and tests and is believed to be accurate but is given without acceptance of liability for loss or damage attributable to reliance thereon as conditions of use lie outside our control. No statements shall be incorporated in any contract unless expressly agreed in writing nor construed as recommending the use of any product in conflict of any patent.

No. A.29th JUNE 1990 Replacing No. A.29, Portfolo, 1000
© CIBA-GEIGY registered trademark

Ciba-Geigy Plastics
Duxford Cambridge
England CB2 4QA
Tel: (0223) 832121
Telex: 81101 CIGYPL G
Fax: (0223) 838404



A.6 DSM Composite resin

A.6.1 technical data sheet (Atlac 430)

DSM Composite Resins

Product data **Atlac 430**

Chemical/physical nature
Atlac 430 is a vinylester based on bisphenol A epoxide, dissolved in styrene. Atlac 430 has a medium reactivity and a medium viscosity.

Major applications
Atlac 430 is intended for glass fibre reinforced parts with improved mechanical properties, that require outstanding chemical resistance (tanks, vessels and apparatus, corrosion protection, hydraulic engineering, renovation of sewage systems). Laminates made from Atlac 430 show excellent long-term heat resistance and high resistance to dynamic loads.

Approvals
Cured unreinforced Atlac 430 conforms to type 1310 according to DIN 16946/2 and is classified in group 5 according to DIN 18820/1.

| Properties of the liquid resin (typical values) | | | |
|---|------------|-------------------|------|
| Property | Value | Unit | TM |
| Density, 23°C | appr. 1060 | kg/m ³ | - |
| Refractive index | 1.5675 | - | 2150 |
| Flash point | appr. 33 | °C | 2900 |
| Acid value, as such | 7 | mg KOH/g | 2401 |
| Stability, no init., dark, 25°C | 6 | Max. | - |

| Typical values of cast unfilled resin | | | |
|---------------------------------------|-------|-------------------|-----------|
| Property | Value | Unit | TM |
| Density, 20°C | 1145 | kg/m ³ | - |
| Tensile strength | 95 | MPa | ISO 527-2 |
| Mod. of elasticity in tension | 3.6 | GPa | ISO 527-2 |
| Elongation at break | 6.1 | % | ISO 527-2 |
| Flexural strength | 150 | MPa | ISO 178 |
| Mod. of elasticity in bending | 3.4 | GPa | ISO 178 |
| Elongation in flex | 6.5 | % | ISO 178 |
| Impact res. - unnotched sp. | 28 | kJ/m ² | ISO 178 |
| Heat deflection temp. (HDT) | 105 | °C | ISO 75-A |
| Glass transition temp. (Tg) | 130 | °C | DIN 53455 |

Curing conditions
Cured with 1 ml Butanox LPT (AKZO-Nobel) and 0.5 ml Co-catal. solution (1 % Co in styrene) added to 100 g resin. Cured 24 h at room temperature and 24 h at 80°C. For HDT and Tg post-curing 24 h at 120°C.

Processing
Atlac 430 normally exhibits tack-free cure. However, the surface may not be cured completely. To ensure tack-free curing of surfaces exposed to air, suitable additives (e.g. paraffin solution) should be added. The final state of cure may further be optimised by post-curing at elevated temperatures (e.g. 80 or 100 °C) for several hours. Post-curing is especially recommended if parts made from Atlac 430 are intended for contact with chemicals. Atlac 430 may be cured using MEK-Peroxide with a low content of hydrogen peroxide (e.g. Butanox LPT, AKZO-Nobel; MEKP-LA 3, Peroxid Chemie GmbH), with CHP, and cumene hydroperoxide (e.g. Trigonox 239, AKZO-Nobel; Luperox Cu 60 VE, Elf Atochem).

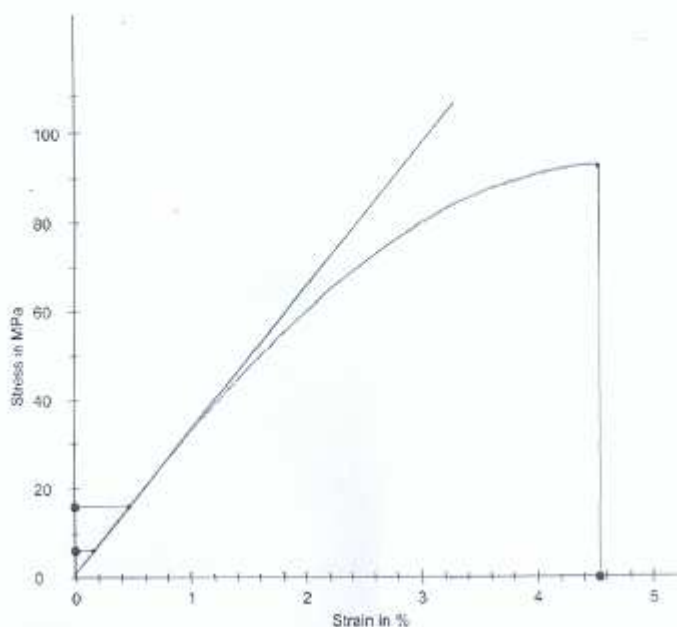
DSM 

Although the facts and suggestions in this publication are based on our own research and our practical experience, we cannot assume any responsibility for performance or results obtained under the use of our products herein described, nor do we accept any liability for loss or damages directly or indirectly caused by our products. The user is held to check the quality, safety and all other properties of our product prior to use. Nothing herein is to be taken as permission, information or recommendation to practice any patented invention without a license.

Version: 0103692.1
Date of issue: September 2000

Head office: DSM Resins bv - P.O. Box 915 - 3000 AP Zwolle - The Netherlands
Tel: (+31) (0)38 - 4586566 - Fax: (+31) (0)38 - 4586600 - Internet site: www.dsmresins.nl

A.6.2 Stress-strain curve of Atlac 430



Atlac 430 casting (060-C-19-03-07) according to ISO 527
Cured with 1 ml Butanox LPT (AKZO-Nobel) and 0.5 ml Co-oct. solution (1 % Co in styrene) added to 100 g resin.
Post cure: 24h 80°C.

Appendix B

Experimental Programme

B.1. Engineering Drawings of meso-scale laminate moulding jig

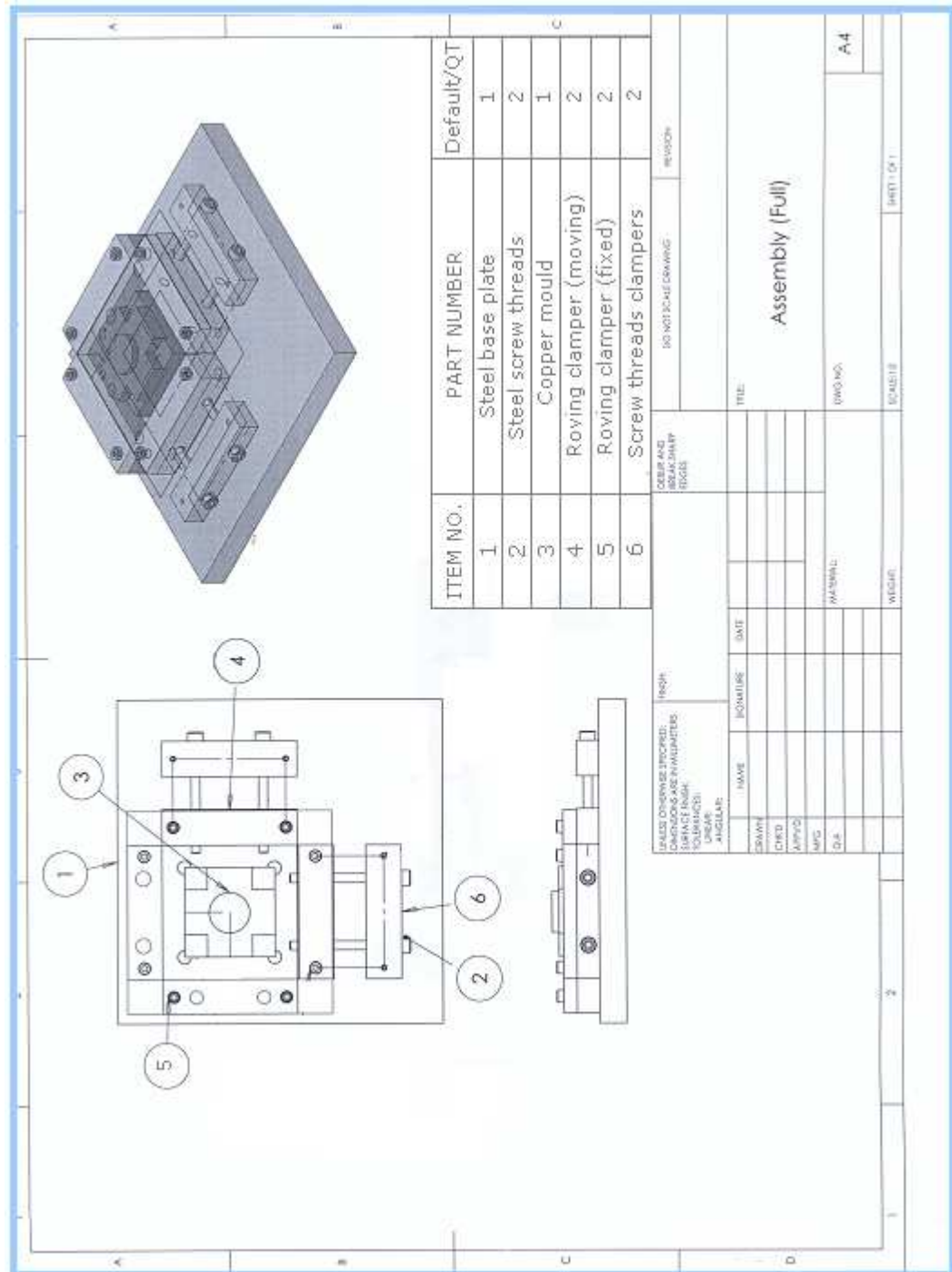
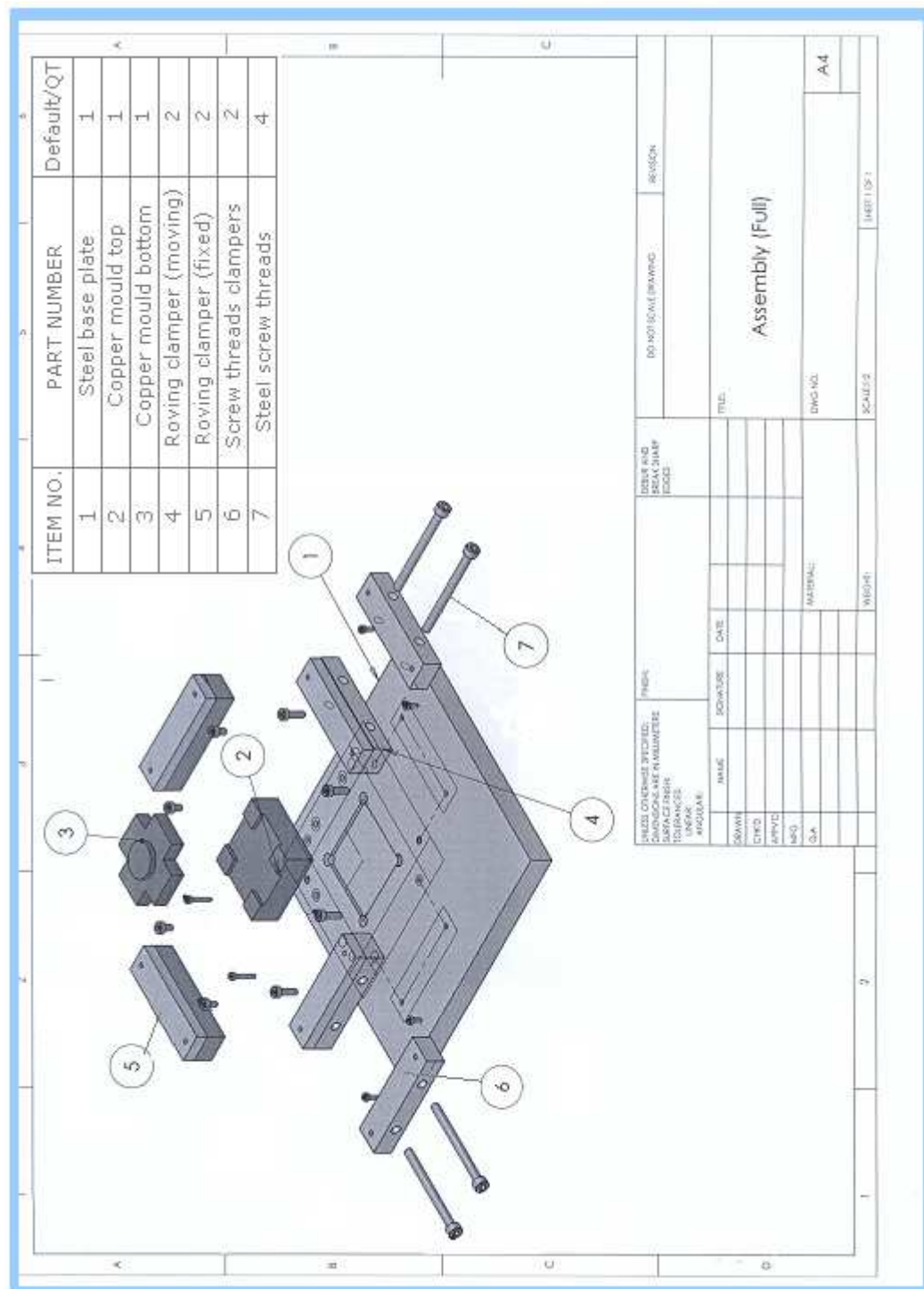


Figure B.1.1: Meso-scale moulding jig (Full Assembly)


Figure B.1.2: Meso-scale moulding jig (Exploded view)

B.2. Meso-scale joint bonding

B.2.1. C-clamp as a bonding jig



Figure B.2.1: Tensile specimen bonding



Figure B.2.2: Shear specimen bonding

B.2.2. Macro bonding jig



Figure B.2.3: Macro bonding jig

B.2.3. Engineering drawing of advance bonding jig

B.2.3.1. Tensile bonding jig

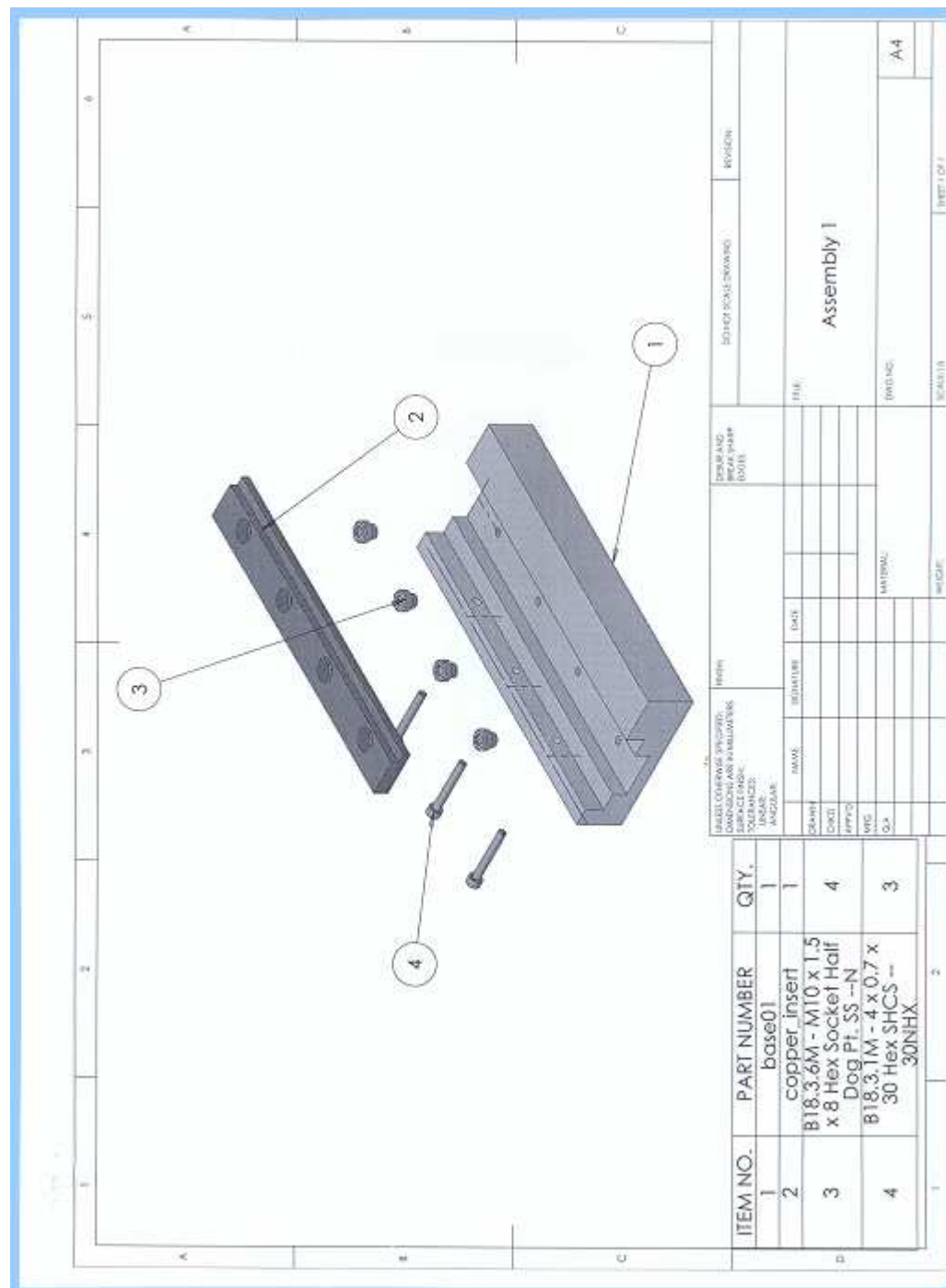


Figure B.2.3.1: Tensile bonding jig (Exploded view)

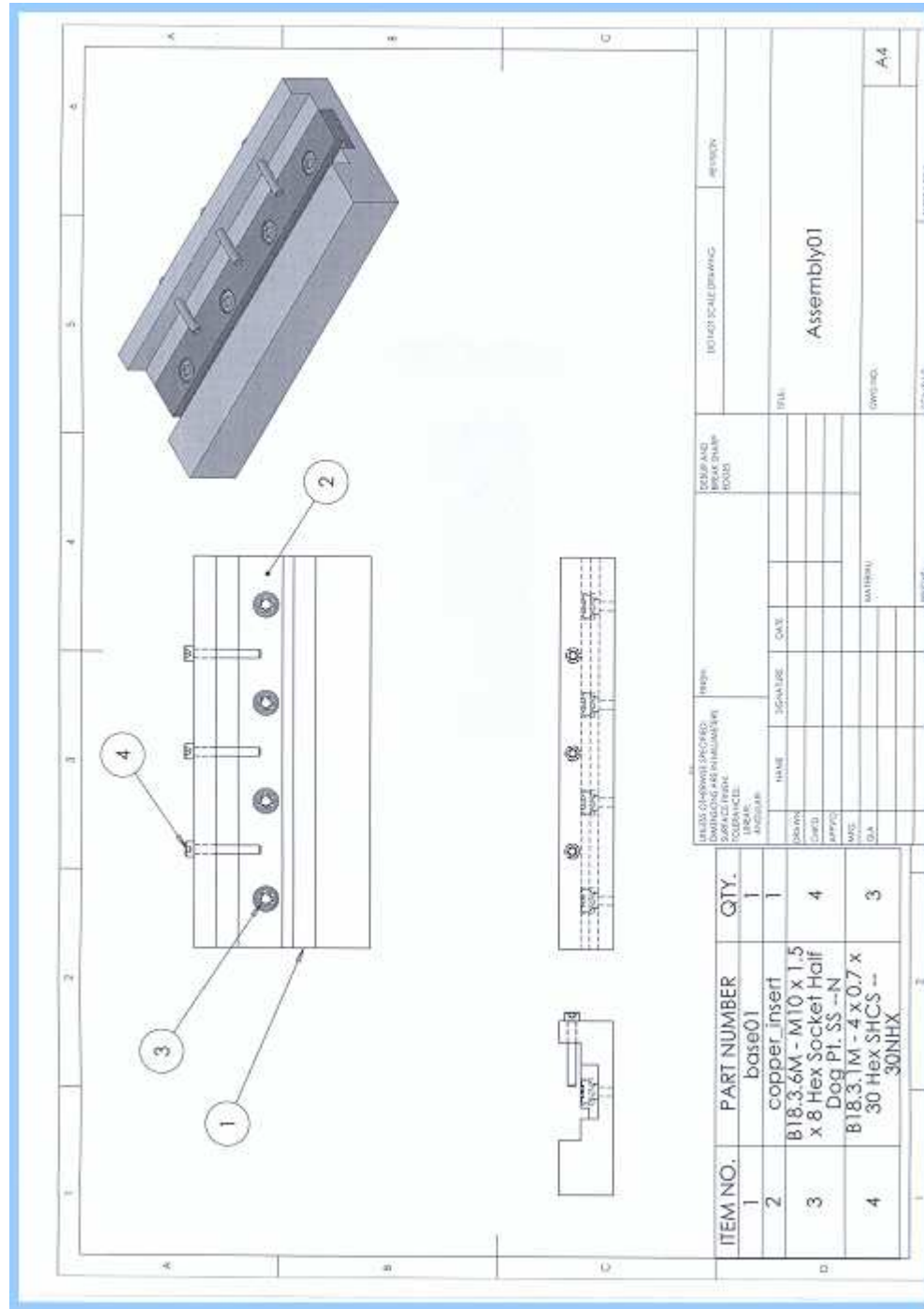


Figure B.2.3.2: Tensile bonding jig (Full assembly)

B.2.3.2. Shear bonding jig

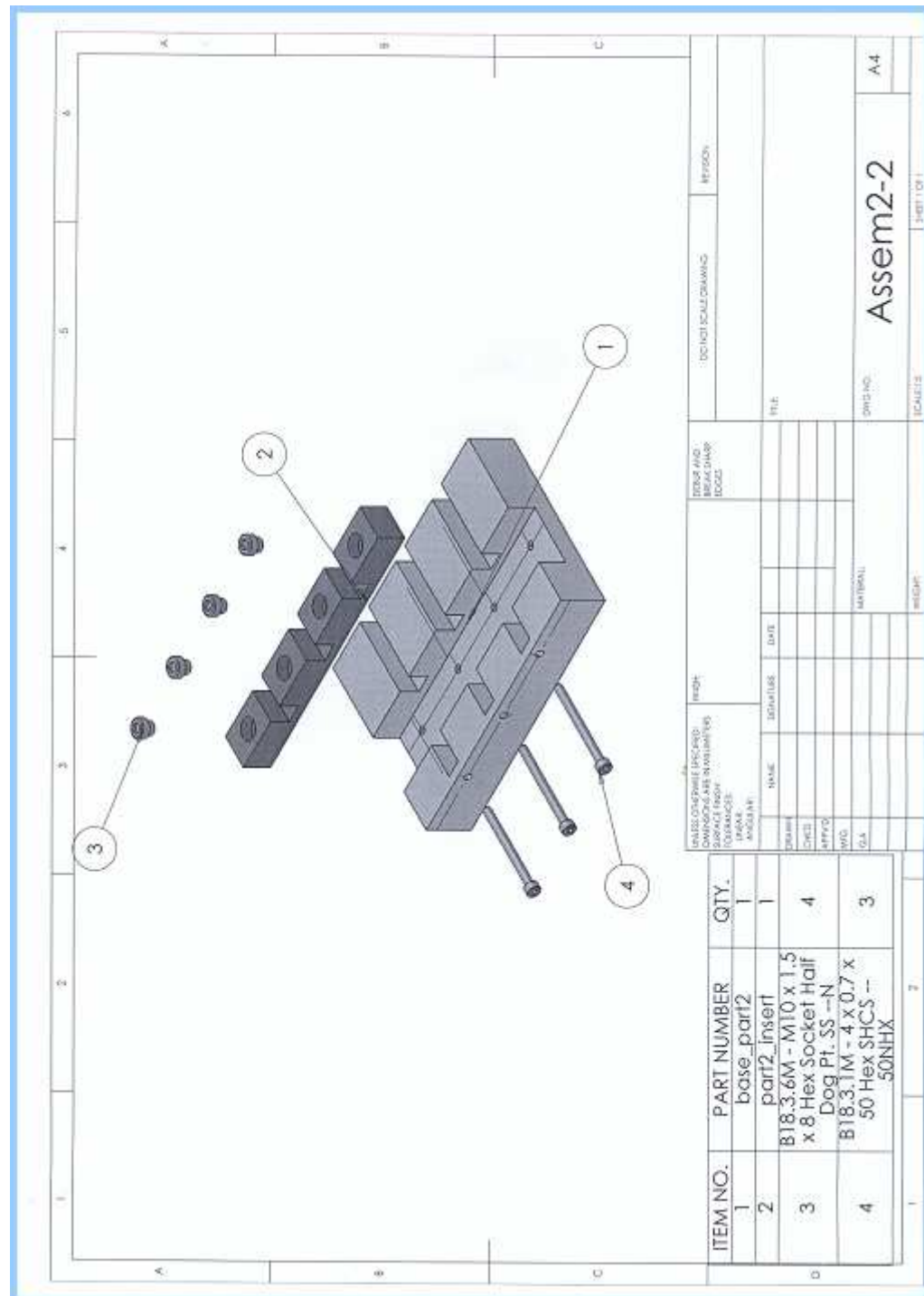


Figure B.2.3.3: Shear bonding jig (Exploded view)

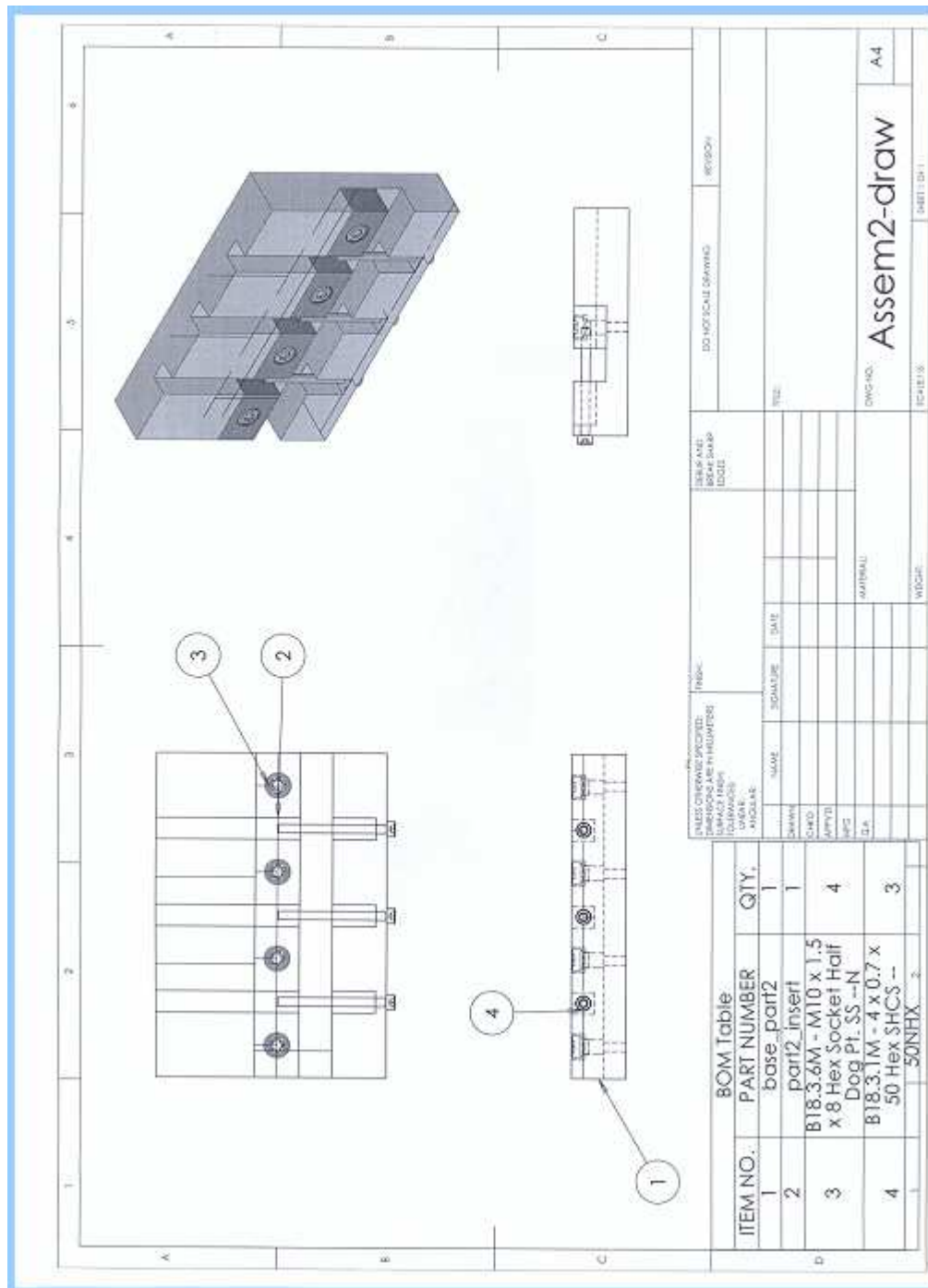


Figure B.2.3.4: Shear bonding jig (Full assembly)

B.3. Engineering Drawings of Clamping Adaptor

B.3.1. Tensile clamping adaptor

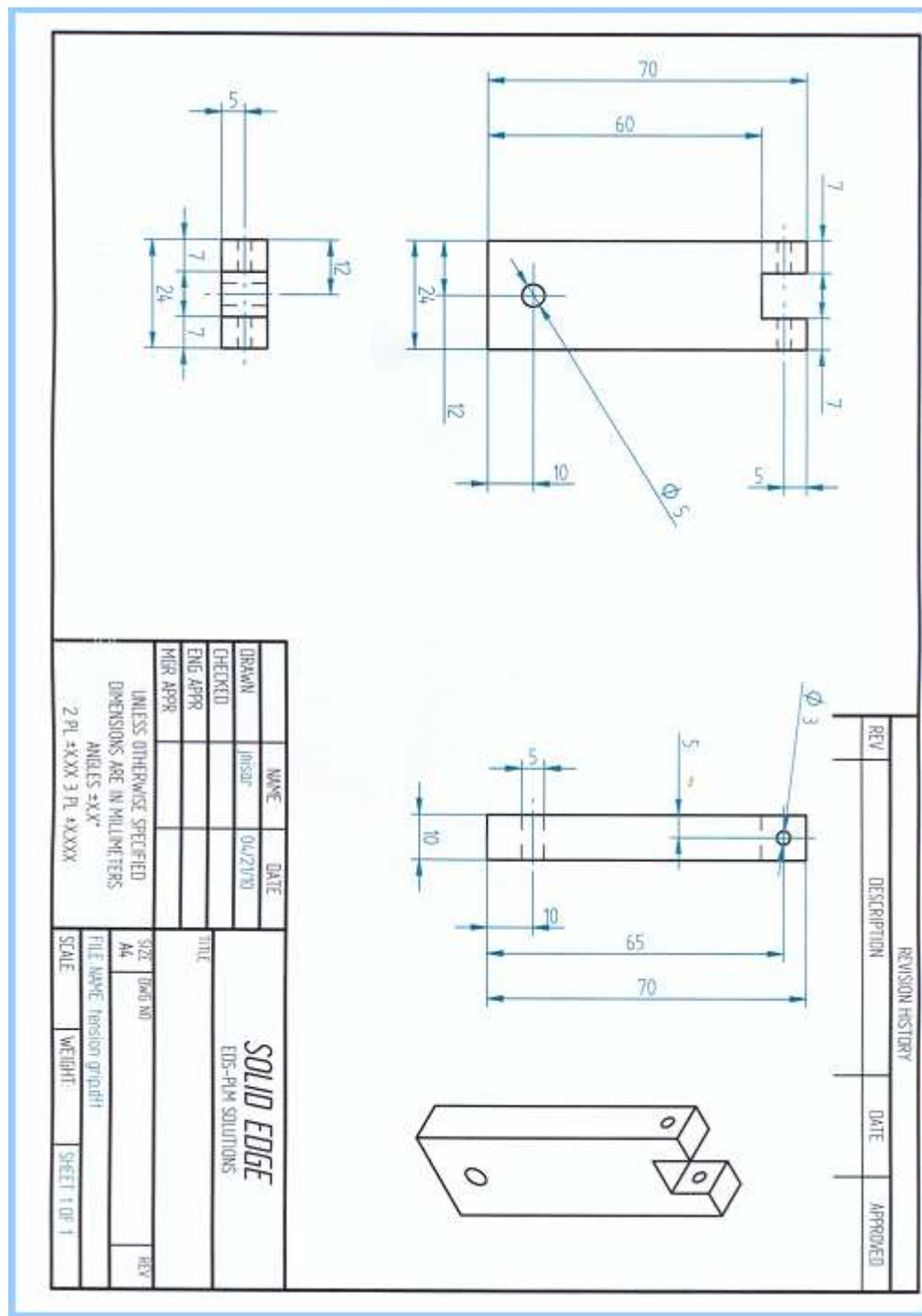


Figure B.3.1: Tensile clamping adaptor

B.3.2. Shear clamping adaptor

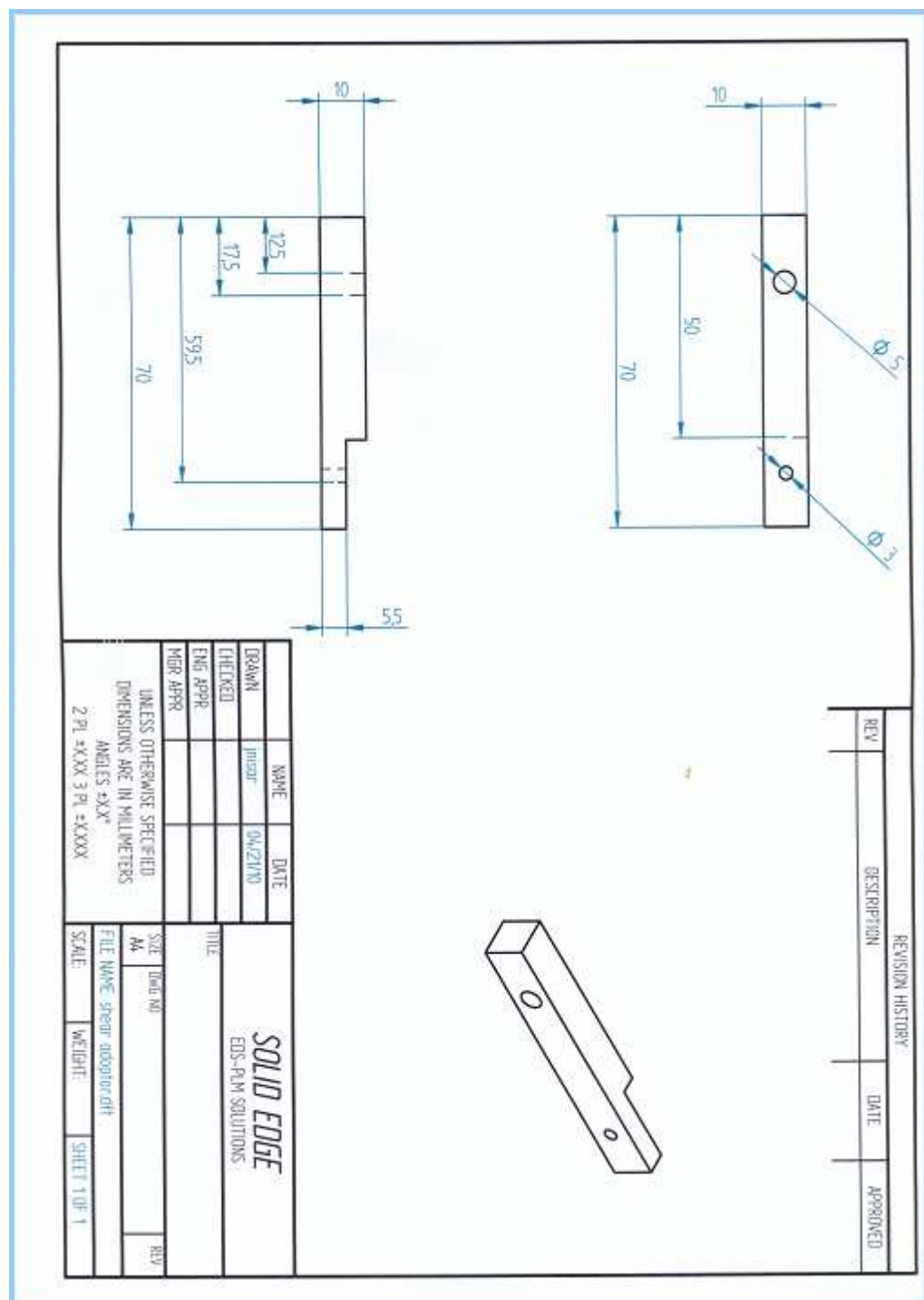


Figure B.3.2: Shear clamping adaptor

B.3.3. Alignment adaptor

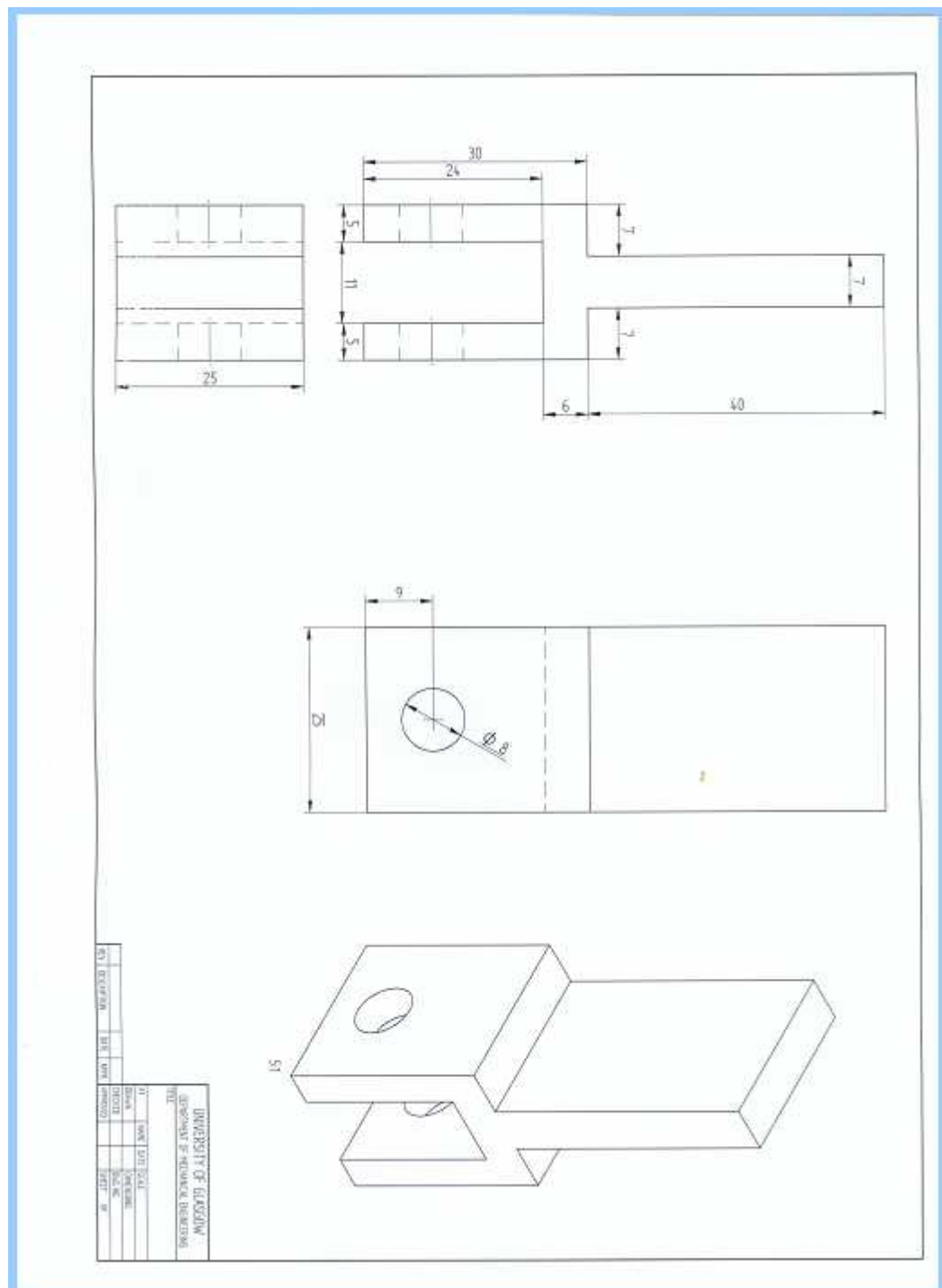


Figure B.3.3: Shear-tensile adaptor

B.4. Engineering Drawings of adherend

B.4.1. Shear aluminium adherend

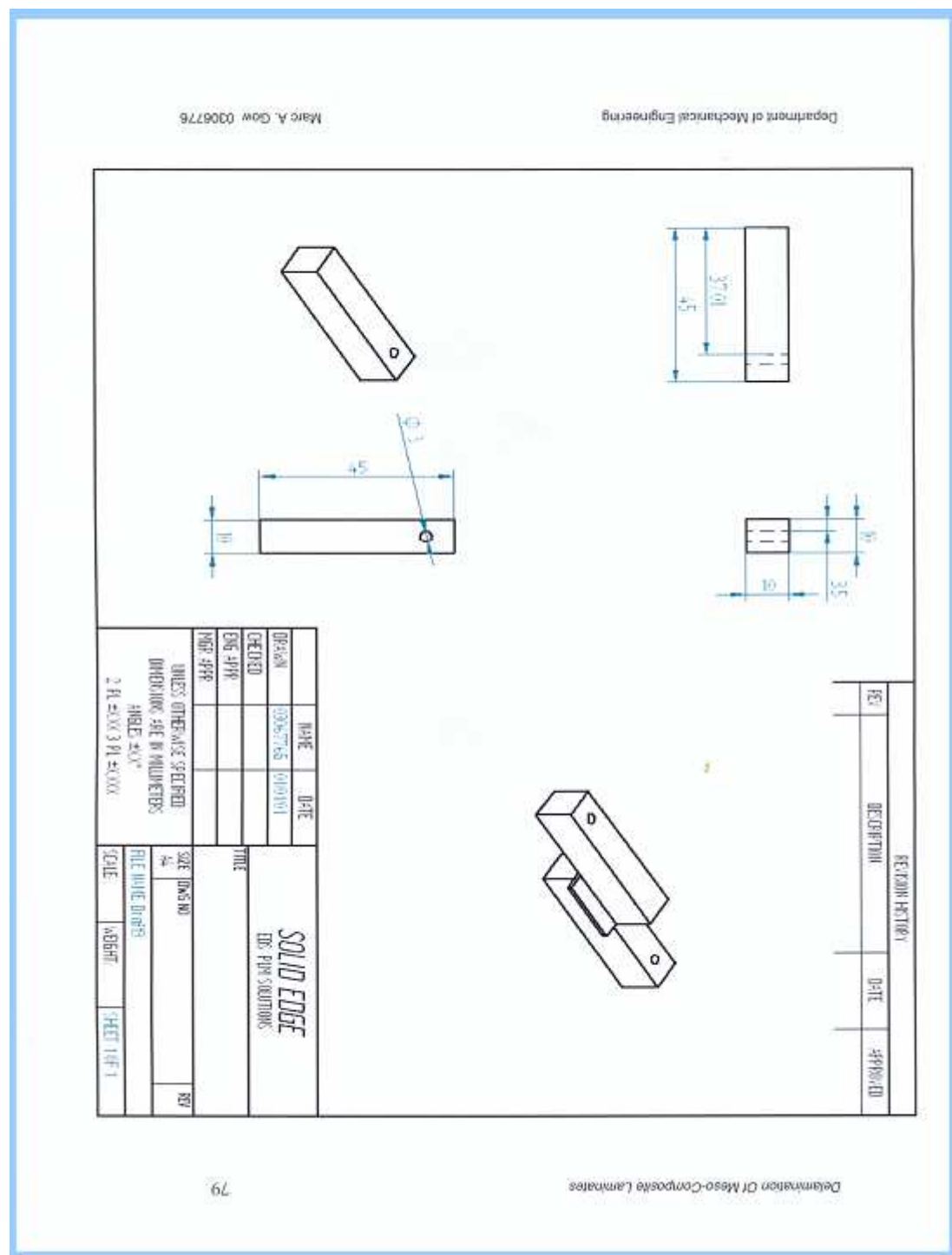


Figure B.4.1: Shear adherend jig

B.4.2. Tensile aluminum adherend

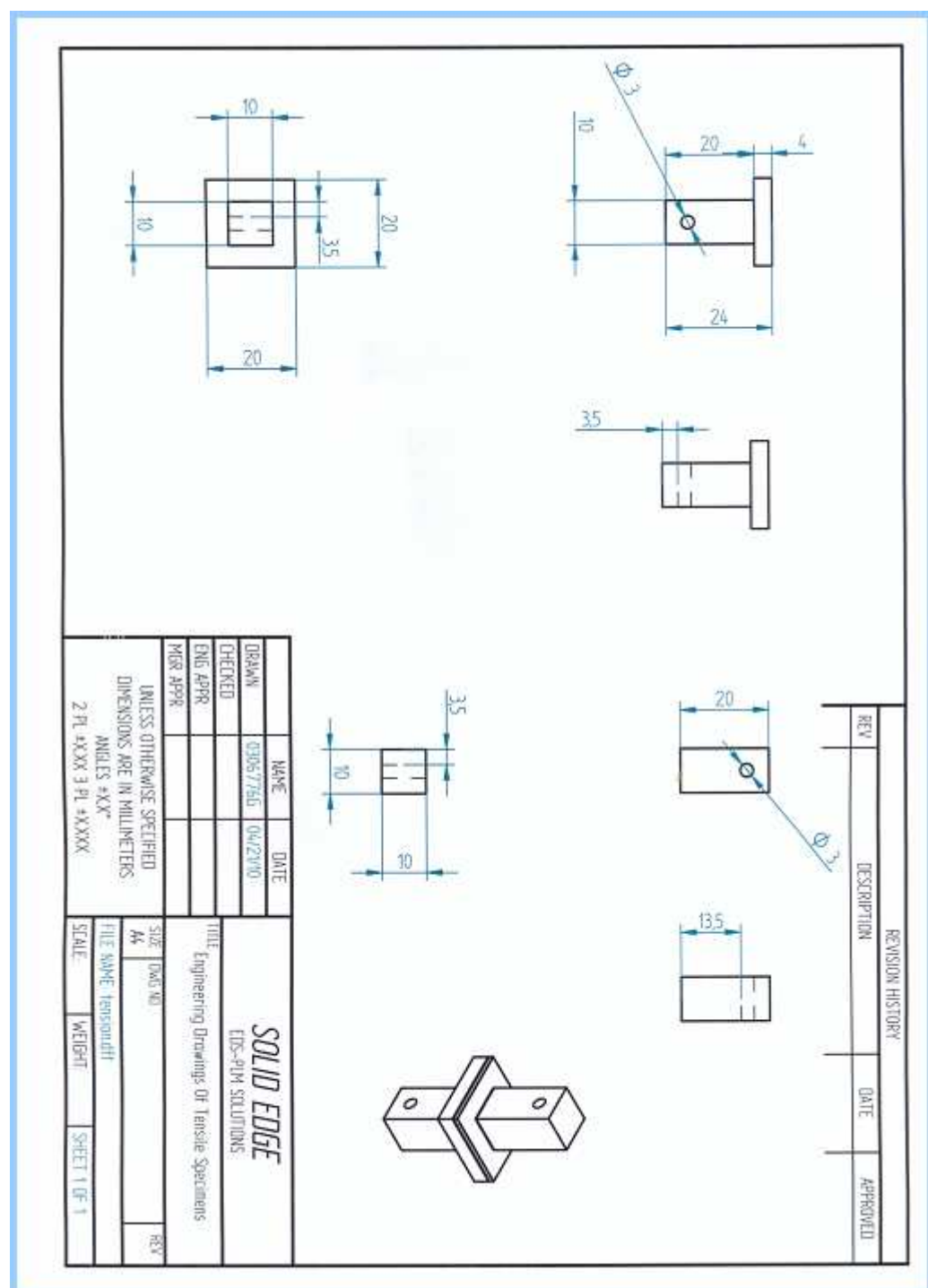


Figure B.4.2: Tensile adherend jig

B.5. Macro-scale joint bonding

B.5.1. Macro bonding jig



Figure B.5.1: Macro bonding jig

B.6 Experimental results

B.6.1 Shear specimen

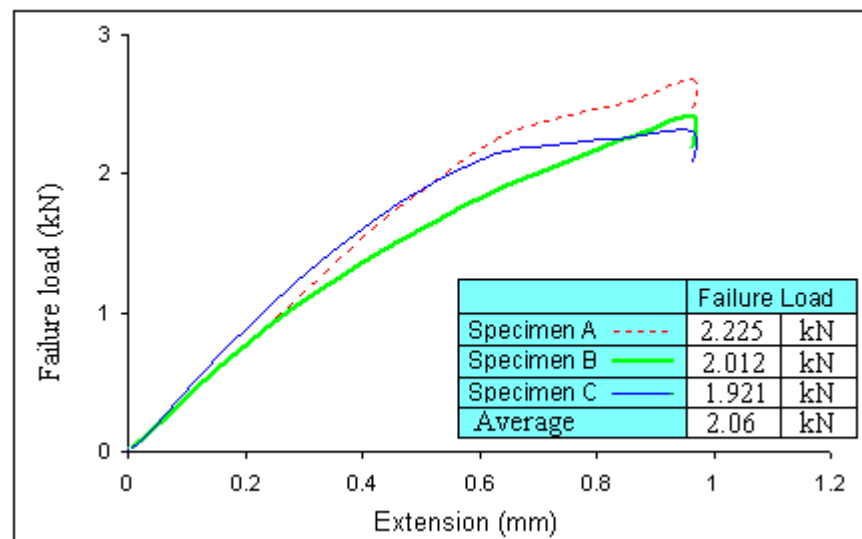


Figure B.6.1.1: Failure load Vs extension curve of LT shear specimen

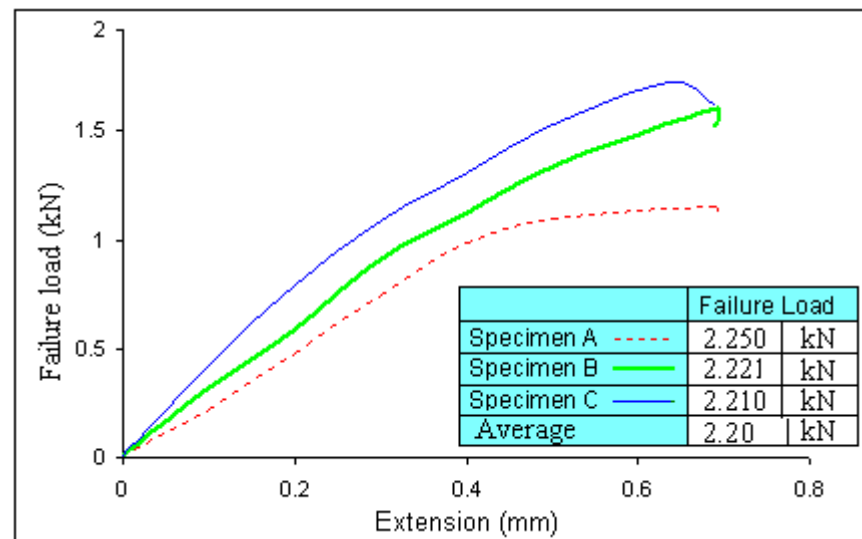


Figure B.6.1.2: Failure load Vs extension curve of RL shear specimen

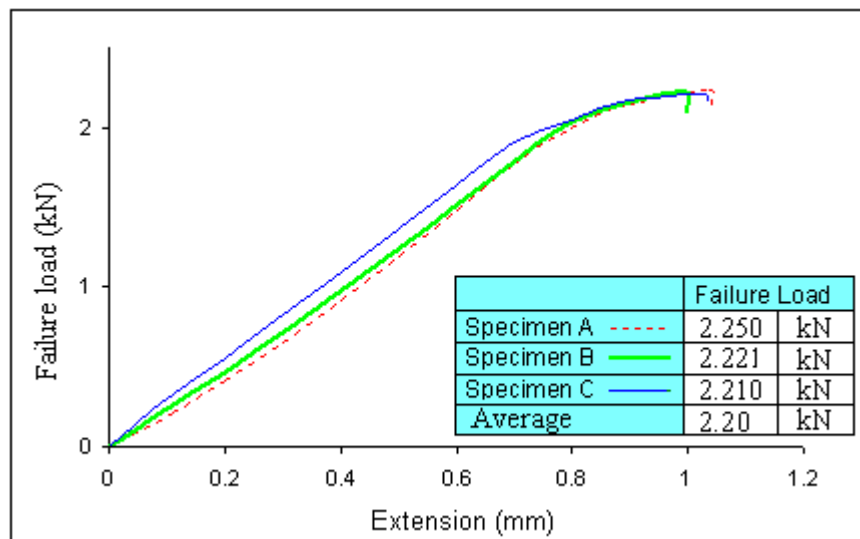


Figure B.6.1.3: Failure load Vs extension curve of WR shear specimen

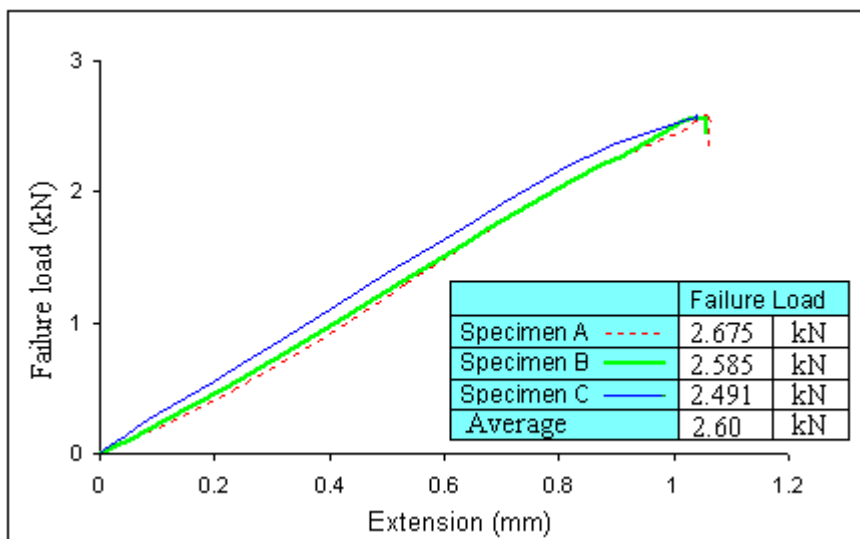


Figure B.6.1.4: Failure load Vs extension curve of IR shear specimen

B.6.2 Tensile specimen

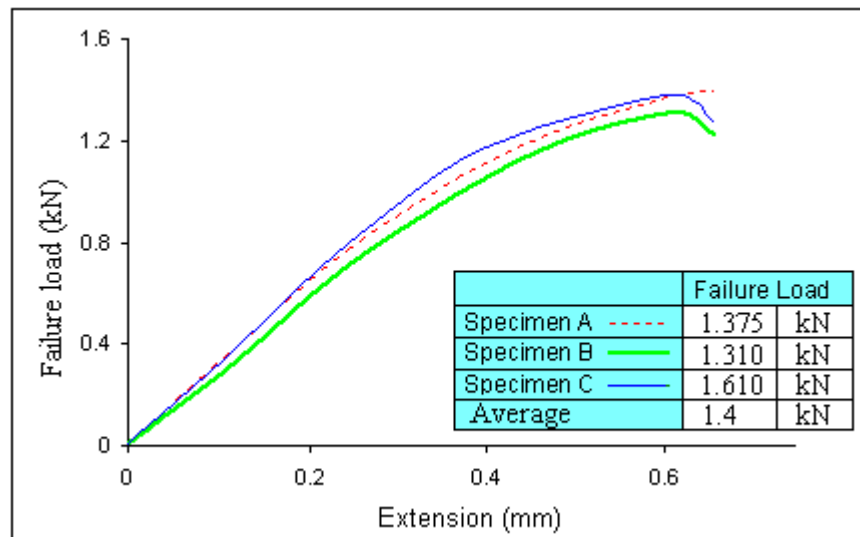


Figure B.6.2.1: Failure load Vs extension curve of LT tensile specimen

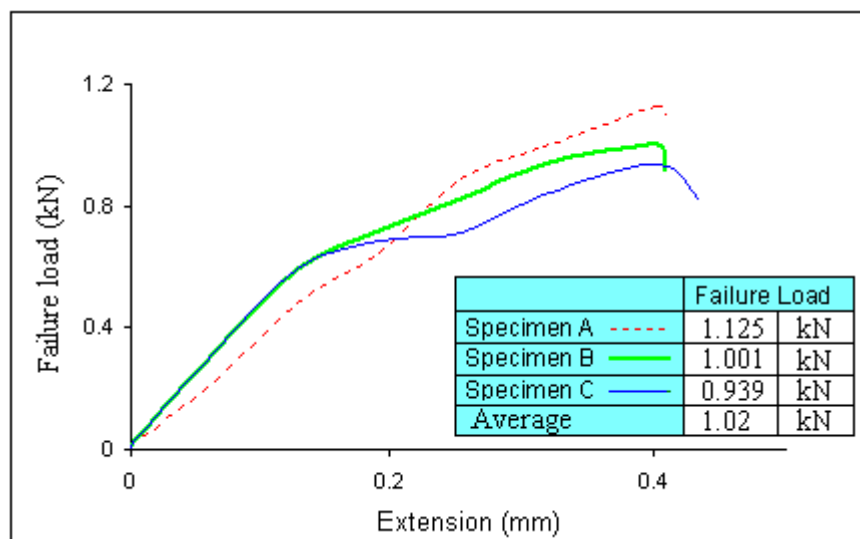


Figure B.6.2.2: Failure load Vs extension curve of RL tensile specimen

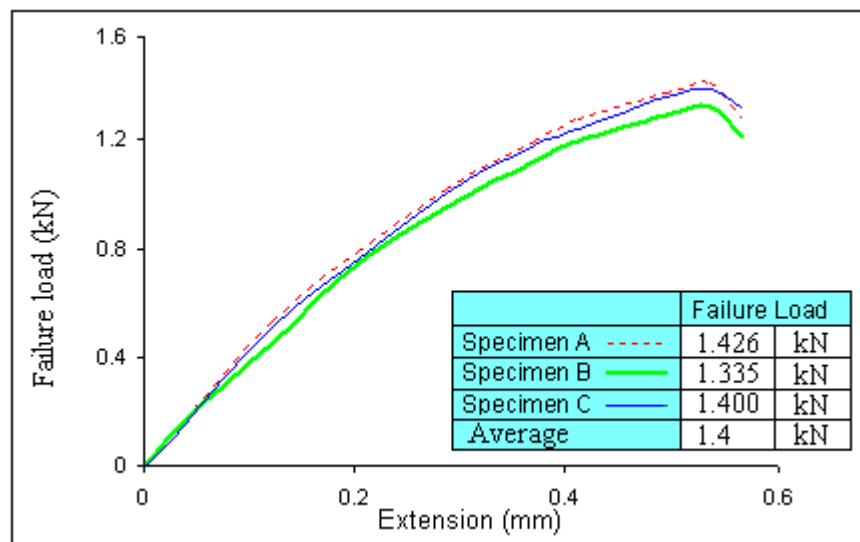


Figure B.6.2.3: Failure load Vs extension curve of WR tensile specimen

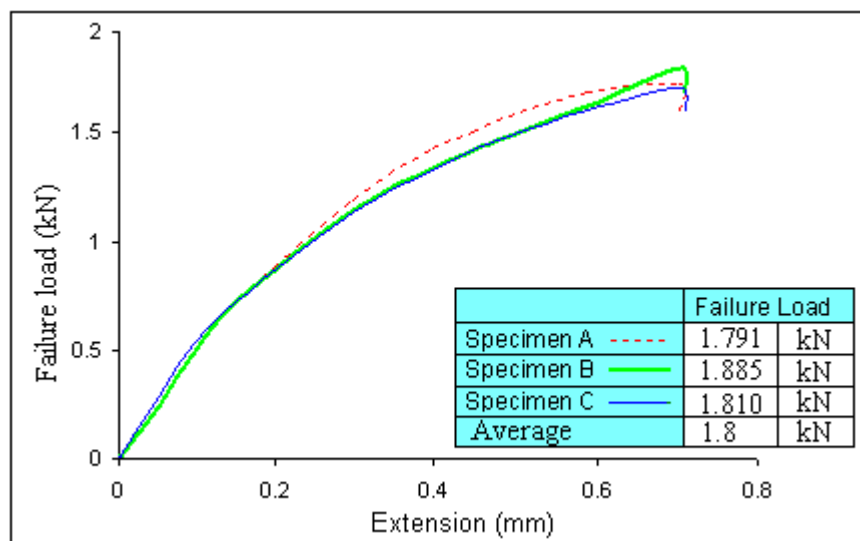


Figure B.6.2.4: Failure load Vs extension curve of IR tensile specimen

Appendix C

Finite Element Analysis

ABAQUS/CAE is an all-purpose finite element analysis tool with enormous range of engineering simulation programs capable of modelling under varying conditions. The FEA based on three distinct stages, preprocessing, simulation and post-processing are shown in Figure 5.1.

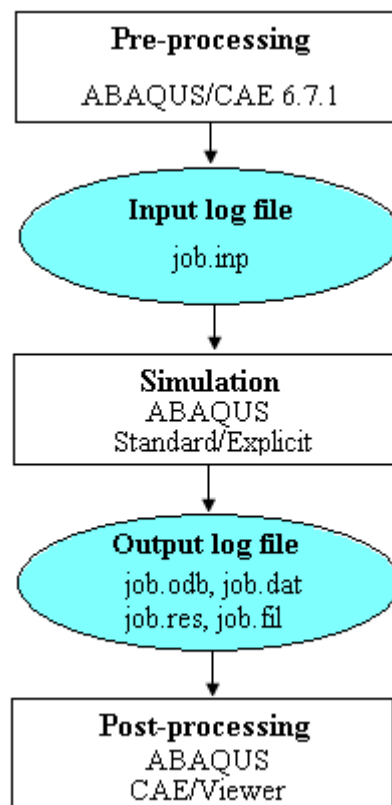


Figure 5.1: Three stages in finite element analysis

In pre-processing, the FE model is created either graphically by using ABAQUS/CAE or through log file. Model log file can be generated directly using text editor by a more experienced user, even though preprocessing with graphical interface is more straight

forward. In simulation, the FE model, which was created in either ABAQUS/CAE or as log file was solved. During simulation running, element displacements are considered from the nodal displacement and finally stresses are calculated from element displacement. The output of simulation in the form of displacement and stresses were then ready to post-processing. Simulation time is varying from job to job; totally depend on the complexity of model and the speed of computer being used. In post-processing, the user could evaluate the simulation results. This evaluation is normally turn out with the interface of visualization module of ABAQUS/CAE. This visualization module scans the binary data and converts into graphical output. ABAQUS/CAE has different option for results displacement, for example colour contour plots, displacement plot, X-Y plot for both stress and displacement. X-Y plot data may also be exported for additional processing by Microsoft Excel.

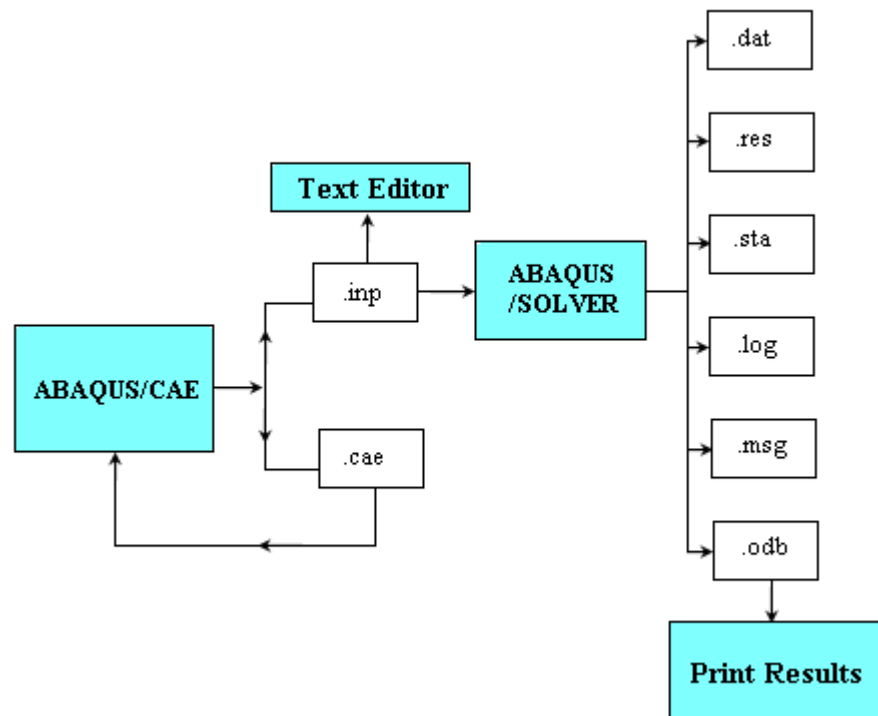


Figure 5.2: ABAQUS file environment

Temporary and permanent files were generated during simulation. The schematic view of ABAQUS file environment is shown in Figure 5.2.

- (.inp) The Input file contains all exact number of instructions.
- (.res) The restart file, ABAQUS itself restart the solution from where it went off from previous simulation.
- (.sta) The status file, contains all record about progress of simulation and nonlinear analysis including steps and number of increments.
- (.log) The log file, contains all record of commands together with CPU processing time.
- (.msg) The message file, contains all record about the progress of simulation.
- (.odb) The output data base file, contain all record read from the visualisation modul

Appendix D

Failure Criteria

Tsai-Wu Failure Criterion [Tsai & Wu, 1971]

Tsai-Wu failure criterion [159] identifies the failure initiation and its growth correctly within the laminate but does not identify the failure modes, such as fibre, matrix, or fibre/matrix delamination as failure mode. Failure is detected in a particular layer of element by element failure; causes the corresponding elements laminate stiffness changes according to material property degradation model. Tsai-Wu criteria, failure occurs when the following criterion is satisfied in any one of the lamina.

$$F = \sum_{i=1}^6 F_i \sigma_i + \sum_{i=1}^6 \sum_{j=1}^6 F_{ij} \sigma_i \sigma_j = 1.0$$

In-plane modes of failure are the main focus here. Let us assume that σ_{11} (Longitudinal), σ_{22} (Transverse), and τ_{12} (In-plane shear) are the in-plane stresses within the lamina and in-plane strength along longitudinal (X_t, X_c), transverse (Y_t, Y_c) and shear S_c with T and C represents tension and compression respectively and F_i, F_{ij} is the tensor strength factor that depends on ultimate stress values, which are expressed as:

$$F(\sigma_{11}, \sigma_{22}, \tau_{12}) = F_1 \sigma_{11} + F_2 \sigma_{22} + F_{11} \sigma_{11}^2 + F_{22} \sigma_{22}^2 + 2F_{12} \sigma_{11} \sigma_{22} + F_{66} \tau_{12}^2 = 1.0$$

$$F_{22} = \frac{1}{Y_t |Y_c|} \quad F_{66} = \frac{1}{S_c^2} \quad F_{12} = -\frac{1}{2} \sqrt{X_t X_c Y_t Y_c}$$

$$F_1 = \frac{1}{X_t} - \frac{1}{X_c} \quad F_2 = \frac{1}{Y_t} - \frac{1}{Y_c} \quad F_{11} = \frac{1}{X_t |X_c|}$$

Hashin Failure Criterion. [Hashin, 1973]

Hashin failure criterion [157] identifies that failure takes place when the failure index exceeds unity for the subsequent failure modes as long as that the materials are elastic [40,145]. Let us assume that σ_{11} (Longitudinal), σ_{22} (Transverse), and τ_{12} (In-plane shear) are the in-plane stresses within the lamina and in-plane strength along longitudinal (X_t, X_c), transverse (Y_t, Y_c) and shear S_c with T and C represents tension and compression respectively [160].

1. Fibre failure:

$$(Tensile) \quad \left(\frac{\sigma_{11}}{X_t} \right)^2 + \left(\frac{\tau_{12}}{S_c} \right)^2 = 1.0 \quad \text{Fibre breakage} \quad (\sigma_{11} \geq 0)$$

$$(Compressive) \quad -\frac{\sigma_{11}}{X_c} = 1.0 \quad \text{Fibre buckling} \quad (\sigma_{11} < 0)$$

2. Matrix failure:

$$(Tensile) \quad \left(\frac{\sigma_{22}}{Y_t} \right)^2 + \left(\frac{\tau_{12}}{S_c} \right)^2 = 1.0 \quad \text{Matrix creaking} \quad (\sigma_{22} \geq 0)$$

$$(Compressive) \quad \left(\frac{\sigma_{22}}{Y_c} \right)^2 + \left(\frac{\tau_{12}}{S_c} \right)^2 = 1.0 \quad \text{Matrix creaking} \quad (\sigma_{22} < 0)$$

Tsai-Hill failure criterion [161]:

Failure takes place within uni-directional laminae when the calculated value equals, or exceeds 1.

$$\left(\frac{\sigma_{11}}{X_t} \right)^2 + \left(\frac{\sigma_{22}}{X_c} \right)^2 - \left(\frac{\sigma_{11} \cdot \sigma_{22}}{X_t^2} \right) + \left(\frac{\tau_{12}}{S_c} \right)^2 \geq 1$$

Where X_t, X_c, S_c are the tensile, compressive and shear strength of lamina.

Principal stresses failure criterion:

Failure takes place in any isotropic material like an adhesive, coating resin and matrix resin, when the maximum in plane principal stress is greater than the material's yield stress.

$$SP1,2 = \frac{(\sigma_{11} + \sigma_{22})}{2} \pm \sqrt{\frac{(\sigma_{11} - \sigma_{22})^2}{2} + \tau_{12}^2} \geq S_y$$

Maximum Stresses failure criterion:

Maximum stress failure criterion has been used for isotropic material failure [162] without the interaction of other stress components. Failure takes place when any of the stress components reaches its corresponding limits. i.e.

$$|\sigma_{11}| \geq X_t \text{ or } X_c$$

$$|\sigma_{22}| \geq Y_t \text{ or } Y_c$$

$$|\tau_{12}| \geq S_c$$

